CREEP OF STRUCTURES

UNDER NON-ISOTHERMAL CONDITIONS

by

M. H. Walter

A thesis submitted to the

University of Leicester for the degree

of Doctor of Philosophy

JUNE 1976

ProQuest LLC
789 East Eisenhower Parkway
P.O. Box 1346
Ann Arbor, MI 48106-1346

X-75-300994-2

Acknowledgements

Throughout the work reported in this thesis I was guided and encouraged by my supervisor, Dr. Alan Ponter. I wish to thank for their invaluable support in the ways indicated, the following:

Colin Morrison and Walter Topliss for assistance with the experimental work executed in the Department of Engineering Creep Laboratory,

The staff of the Department of Engineering Workshop for manufacturing the experimental equipment and test specimens,

Philip Brown for his assistance with the computing work,

John Pearson and Helen Sheppard for the photographs and typescript presented in this thesis, and finally to my wife, Jill, for her support and encouragement over the past four years.

The author acknowledges the assistance of the Science Research Council.

M.H.Walter
June 1976

Summary

Although there has been extensive investigation of the creep behaviour of structures subjected to steady loads and isothermal conditions, the behaviour when temperatures vary both spatially and with time has received relatively little attention. Numerical solutions are extremely difficult to produce for time varying stress and appropriate constitutive relationships have yet to be evolved.

The thesis is divided into two sections both of which are concerned with structural creep behaviour under time-constant applied loads:

In the first section the behaviour of a few simple structures are investigated for spatially varying temperature fields which remain constant in time. Adopting an appropriate form of Norton's constitutive relationship it is shown that the stationary deformation of the structure may be related to a single reference material test conducted at a reference stress and a reference temperature, which is independent of material constants, thereby providing a generalisation of the reference stress technique used for isothermal conditions. Experiments on a simple beam structure are described which confirm that a good correlation between the structural behaviour and uniaxial reference test behaviour exists. In all cases considered the reference temperature remains close to the lowest temperature in the structure indicating that locally high temperatures may sometimes be tolerated without excessive structural deformation.

In the second section the creep behaviour of a parallel two-bar structure and a uniform plate subjected to cyclic histories of temperature is analysed by means of a method of structural analysis which arises from certain bounding theorems. It is shown that these bounding theorems can describe thermal-creep interaction extremely well and general modes of creep behaviour are discernable when the non-linear viscous, strain-hardening or Bailey-Orowan constitutive relationships are adopted.

Deformation maps that relate structural behaviour to a material parameter β are described and in certain circumstances a reference stress may be defined which is independent of other material parameters. This result indicates that a reference stress approach is applicable to variable temperature problems, but that the reference value depends upon the range of values of this quantity β. In order to substantiate the theoretical assumptions a preliminary experimental investigation of the two-bar structure subjected to cyclic histories of temperature is described. Tests using aluminium specimens indicate that a residual stress field is set up that varies quite slowly in time and remains effectively constant after a few cycles. It is found that the strain-hardening constitutive relationship provides a best fit to the structural behaviour.

Contents

Chapter 1

Description of the Contents of the Thesis

Some elements of power plant components as well as many other structures are subjected to the application of some form of loading cycle during operation. This may take the form of thermal loads, a variation of imposed forces and displacements or a combination of these. The interaction between the non-linear creep response of the material and the presence of both spatially and time varying temperature fields is a problem the analysis of which remains amongst the more intractable problems of structural mechanics. Temperature enters into the problem at a material level by producing temperature dependent changes in material behaviour and at a structural level by thermal expansions causing incompatible volume changes which in turn produce thermal stress. Either one or both of these effects are ignored in many of published creep analyses and the relevance of such calculations remains difficult to assess in general terms.

In this thesis the results of a theoretical and experimental study on the creep of structures subjected to spatially- and time-varying temperature fields are reported. Attention is confined to problems with steady applied loads and it is assumed that strains due to time-independent plastic deformation are small. Where calculations are given the material properties, unless stated otherwise, are those applicable to commercially pure aluminium, the material used in the experimental tests. The choice of this material was motivated by the need to provide a reasonably realistic and representative material model of some aspects of the creep behaviour of structural steels at elevated temperatures without recourse to high temperature testing and the associated problems usually incurred. The stress-strain curve for aluminium at and above room temperature is very similar to those of some steels at elevated temperatures and for this reason, besides being relatively inexpensive and easily available, has

been used extensively by the Creep Laboratory in creep tests.

In Chapter 2, a description of the numerous approaches to the problem of creep in metallic structures is given. Both micro- and macro-aspects are examined in order to illustrate the complex nature of creep deformation processes. The creep constitutive equations adopted in this thesis and the reasons for their adoption are also given.

Chapter 3 is concerned with the role of stationary state solutions in the analysis of creeping structures and the manner in which time constant temperature gradients modify the isothermal stress distributions and deformations. An alternative method of obtaining approximate stationary solutions is also described.

The development over recent years of the reference stress technique for estimating deformation of creeping structures is reviewed in Chapter 4 together with methods of obtaining approximate reference values. Adopting an appropriate form of Norton's law it is shown that the stationary solutions to structures with time constant temperature gradients can be related to a material reference test, conducted at a reference stress and a reference temperature which is independent of the material constants. It is shown that solutions using an approximate method may be similarly expressed. A sequence of experiments on a simple beam structure, Chapter 5, indicates that the correlation between structural behaviour and material tests can provide an acceptable design method.

Chapter 6 attempts to shed some light on the various important aspects of thermal-creep interaction for cyclic histories of temperature by means of a method of structural analysis which arises from certain bounding theorems. In a number of papers (1,2,3) a theory was derived for a non-linear viscous material which allows the evaluation of upper and lower bounds on the energy dissipated in a cyclically loaded structure. These solutions correspond to the exact solution when the cycle time is either very short (upper bound) or very long (lower bound) compared with a

characteristic time scale of the average deformation rate. This reference time scale may be taken as the time for the creep strain, in the steady state, to be equal to the elastic strain at either an average or maximum stress in the structure (1). Consideration of typical time scales indicates that in most applications cycle time may be considered to be very short and hence the upper bound solution may be expected to provide a representative and realistic solution which closely approximates the actual solution. A full description of these arguments may be found in the references cited above.

In Chapter 7 the solutions of Chapter 6 for a two-bar structure and a thick plate are presented in the form of deformation maps. A material parameter β is introduced in terms of which a reference stress may be defined which is independent of other material parameters. This result indicates that a reference stress approach can be used for cyclically loaded creeping structures provided the appropriate value of β can be evaluated.

In order to confirm the validity of the concepts previously discussed, Chapter 8 describes the experimental simulation of the two-bar model and the results compared with theory. A full description of the design and development of the test rig is given in Chapter 10.

Finally, the thesis is concluded in Chapter 9 with a discussion of the theoretical and experimental results contained therein and suggestions for further research.

Chapter 2

Creep Deformation of Metallic Structures

2.1. The Creep Curve.

Since the recognition of creep as a problem in the design of engineering components the uniaxial creep test has been, and is likely to remain, the most important means of providing creep data. The information gained from this test reveals, in a simplified way, how a given material will act under different combinations of loading and temperature. Most frequently the creep test is performed at constant temperature and constant load. Although the measurement of creep resistance is quite simple in theory, in practice it requires considerable laboratory equipment.

Deformation data is usually presented in terms of a strain, measured over a gauge length, at various times. This gives a creep curve which generally takes the form shown schematically in Figure 2.1(a). The essential features may be summarised as consisting of a number of stages: an instantaneous extension; a transient (or primary) creep of decreasing rate; a steady-state (or secondary) creep, approximately linear with time; and an accelerating (tertiary) stage leading up to final fracture. The increasing rate of deformation in the third stage is partly a geometric effect not a material property. When constant stress, in contrast to constant load, tests are performed it is frequently found that no region of accelerated creep rate occurs and the curve remains approximately linear with time to fracture, Figure 2.1(b). Accelerated creep is found, however, in constant stress tests where metallurgical changes occur in the metal.

The degree to which the regions of the creep curve are distinguishable depends strongly on the applied stress, the temperature and the duration of the test. The strain represented by Σ_o occurs practically instantaneously

on application of load. Even though the applied stress may be well below the yield stress of the material, not all the instantaneous strain is recoverable on removal of load. The total strain consists of a recoverable strain (elastic), a strain recoverable with time (anelastic) and a non-recoverable strain (plastic).

Primary creep is a period of predominantly transient creep in which the creep resistance of the material increases by virtue of its own deformation. This strain-hardening is due to the increase in dislocation density increasing the flow stress of the material. Secondary creep is a period of nearly constant creep rate which results from a balance between the competing processes of strain-hardening and recovery. Recovery is the stress activated or thermal activated process by which a material may revert to a strain free state. The average value of the creep rate during secondary creep is termed the minimum creep rate. Third stage or tertiary creep is a region of rapidly increasing creep rate leading to fracture. Of the many analytical and experimental theories developed to explain the factors controlling tertiary creep, few have produced any general conclusions. Of particular note is the work of Nemy and Rhines[4], and Hoff[5] who investigated the two most possible reasons for the existence of a tertiary stage; namely, a change in the structure of the metal itself, leading to a change in its response to loading, and secondly, a reduction in the cross-section of the metal resulting in a higher applied stress.

2.2. Metallurgical Aspects of Creep.

The phenomenon of creep deformation is due to several metallurgical processes, involving dislocation movement, vacancy diffusion and void formation. These processes are assisted by the thermal excitation of atoms aiding the movement of imperfections responsible for plastic flow.

The effect of the thermal agitation of atoms on the process of creep can be simply illustrated by consideration of a metal undergoing deformation. During elastic deformation the applied stress is in effect dilating the metal lattice; during plastic flow the metal lattice of groups of atoms become highly distorted and the movement of dislocations and imperfections becomes more difficult, since the glide planes on which dislocations move are not continuous through the material. Dislocations become 'piled-up' at these barriers and the stress for continued plastic flow increases in consequence. However, if thermal energy were available to aid an imperfection to overcome a barrier, additional plastic deformation would occur. Since the transfer of thermal energy from atom to atom is non-uniform, the laws of probability determine whether or not a dislocation is given sufficient additional energy for motion to occur. This type of deformation is, therefore, time-dependent.

Creep deformation, despite being a thermally-activated process, can occur over the whole temperature range of the metallic solid state. For metals commonly used in engineering construction, creep is significant only at temperatures above $0.3\theta_{MP}$ where θ_{MP} is the melting temperature in degrees Kelvin of the basic metal. However, for some metals, aluminium and lead are excellent examples, significant creep can occur at room temperature. The creep behaviour is affected strongly by temperature and depends particularly on the ratio of the test temperature to the melting temperature of the metal or alloy. Thus room temperature may be a relatively low temperature for the creep of steel but a high temperature for creep in lead. For a constant θ/θ_{MP} ratio - that is, the same homologous temperature - Andrade[6] found that it is possible to obtain similar creep curves for steel and lead by properly adjusting the applied stress. It is sufficient at this point to realize that the applicability of creep-time relations that define the creep curve should be discussed in terms of the homologous temperature.

2.2.1. Logarithmic Creep ($0 - 0.3\theta_{MP}$)

Creep is only possible because obstacles to deformation can be overcome by the combined action of thermal agitation and stress. At the lower end of the temperature scale recovery processes which are not thermally activated play important roles. Logarithmic creep occurs at low temperatures and stresses and is believed to be a true exhaustion process in which the rate determining step is the activation energy to move a dislocation. On the initial application of stress, the dislocations with the lowest activation energy move first to produce an initial creep strain. As these easy-to-move dislocations are exhausted, creep can only continue by the movement of dislocations of higher activation energy. Therefore, the activation energy for the process continuously increases, and the creep rate decreases. Theoretical treatments of exhaustion creep that result in a logarithmic equation have been proposed by Mott and Nabarro[7], Cottrell[8], and McLean[9].

Deviations from the logarithmic form occur towards $0.3\theta_{MP}$ where the creep rate declines less rapidly with time than the logarithmic function suggests. Evidently some recovery which is probably due to cross slip takes place and partly offsets the strain-hardening.

2.2.2. Recovery Creep ($0.3 - 0.9\theta_{MP}$)

At these higher temperatures the increased thermal activation allows a continual recovery of the material from the strain-hardened states encountered in the lower temperature logarithmic creep range. There are two types of theory which have been used to describe creep deformation in the recovery range and both types are mainly concerned with steady state creep. One theory is a direct application of reaction rate theory to some slip process that is deemed to be the rate controlling event[10] and

the other [11,12,13] assumes that creep deformation is the result of strain-hardening being continuously annealed out by recovery mechanisms. According to this theory, in the steady state creep condition, strain-hardening must be exactly balanced by recovery to maintain a constant mechanical state in which the flow stress σ remains invariant with time. This can be stated in mathematical terms by

$$d\sigma = \left(\frac{\partial\sigma}{\partial\Sigma}\right) d\Sigma + \left(\frac{\partial\sigma}{\partial t}\right) dt = 0 , \qquad (2.1)$$

where

$$\frac{d\Sigma}{dt} = \frac{Q}{H} . \qquad (2.2)$$

In this expression Q is the rate of recovery given by

$$Q = - \frac{\partial\sigma}{\partial t} ,$$

and H is the strain-hardening coefficient given by

$$H = \frac{\partial\sigma}{\partial\Sigma} .$$

Expression 2.1 , commonly known as the Bailey-Orowan equation, has been tested experimentally by Mitra and McLean[13] on aluminium and nickel specimens. The results support the recovery theory against a slip type theory provided the strain-hardening coefficient was measured on creep tested specimens. In addition it was also shown that the strain-hardening coefficient increases several fold during primary creep and that the stress sensitivity of creep rate is mainly due to the influence of stress on the rate of recovery, which itself is understandable in terms of dislocation network theory.

The steady state region of deformation is normally observed only at or above $0.4\theta_{MP}$; at lower temperatures the creep rate continuously declines. At higher temperatures there is full recovery because climb by vacancy diffusion becomes possible, edge dislocations can also be eliminated at a perceptible rate and a steady state of deformation is reached when strain-hardening and recovery become equal in rate.

2.2.3. Diffusion Creep (0.9 - $1\theta_{MP}$)

If a polycrystalline aggregate is subjected to a small tensile stress at elevated temperatures, deformation is often achieved by the stress directed diffusion of vacancies. The process is known as diffusion or Nabarro-Herring[7,14] creep.

During deformation, high angle grain boundaries that are normal to the stress axis emit vacancies, whereas boundaries that are parallel to this axis absorb vacancies, thereby achieving creep strain in a direction parallel to the stress axis. The creep rate can be calculated absolutely since the parameters involved, namely the diffusion coefficient, the grain size and the atomic size, are known quantities. McLean states that diffusion creep rate is a linear function of the applied stress, unlike dislocation creep at high temperature which is much more sensitive to stress. Diffusion creep therefore predominates over dislocation creep at very low stresses and consequently, it is only observed near the melting point, since at very low stress a high temperature is needed to cause a measurable creep rate.

2.3. Phenomenological Approach to Creep Deformation.

The physical theories of creep can in many cases give a qualitative explanation of observed behaviour, but it is impossible to expect that a quantitative description can be successfully achieved by means of physical models which are always to some degree phenomenological. Consequently the mechanics of creep are not usually based upon creep expressions derived from metal physics. Nonetheless, an understanding of microscopic material behaviour is useful in ensuring that simplified methods are used in the correct context.

The phenomenological approach to the creep deformation of metals has received considerable attention and the relevant literature is extensive.

Many excellent articles have been written including those by Van Leeuwen[15], Finnie[16], Marriott[17] and Kennedy[18]. In the following sections a number of creep theories are given. It is not intended to comment in detail on individual theories but simply to draw attention to certain significant features of the group as a whole.

2.3.1. Creep Laws for Constant Stress.

A tensile specimen under constant stress deforms in a manner that may be described by a general function of the form

$$\varepsilon = f(\sigma,t,\theta) \ . \qquad (2.3)$$

In a phenomenological approach a useful first approximation is to re-express this function by separating variables such that

$$\varepsilon = f_1(\sigma).f_2(t).f_3(\theta) \ . \qquad (2.4)$$

The separation of the stress and time functions, $f_1(\sigma)$ and $f_2(t)$ has been implicit in most creep theories and appears to be generally accepted.

(a) Stress Function $f_1(\sigma)$:

The most commonly used forms of $f_1(\sigma)$ are given below.

Norton[19]	$f_1(\sigma) = k_1\sigma^n$
McVetty[20]	$f_1(\sigma) = k_2 \sinh(\sigma/\sigma_o)$
Soderberg[21]	$f_1(\sigma) = k_3[\exp(\sigma/\sigma_o) - 1]$
Dorn[22]	$f_1(\sigma) = k_4 \exp(\sigma/\sigma_o)$
Garofalo[23]	$f_1(\sigma) = k_5[\sinh(\sigma/\sigma_o)]^n$

where k_i are material constants.

The most extensive treatment of stress dependence appears to be confined to the secondary creep range. Dorn has shown that at high stress levels the

exponential function provides a best fit to experimental data whilst at lower levels Norton's law provides a closer approximation. Leckie et. al.[24] have shown experimentally that when constant temperature uniaxial creep data is plotted as a log stress against log steady state strain rate the linear region defined by Norton's law is separated from the region defined by Dorn's expression by a stress of magnitude $n/(n+1)\ \bar{\sigma}_y$ where $\bar{\sigma}_y$ is the yield stress of the material. Garofalo's expression is proposed to cover both stress regimes, but in view of the simplicity of Norton's power law and its homogeneity with stress, it is less often used. Further, for proportional load changes, Norton's law provides stress distributions that are independent of the magnitude of load.

(b) Time Function $f_2(t)$:

The task of describing the time dependence of creep in a material displaying a high degree of structural change with time is difficult except by extensive curve fitting procedures. Used with care and within the context of their derivation the following time functions have been found of use:

Bailey[25]	$f_2(t) = B_1\, t^m \quad 1/3 < m < 1/2$
Andrade[6]	$f_2(t) = (1 + B_2 t^{1/3})[\exp(B_3 t) - 1]$
McVetty[20]	$f_2(t) = B_4[1 - \exp(-B_5 t)] + B_6 t$

where B_i are constants for a given stress and temperature.

(c) Temperature Function $f_3(\theta)$:

Experimental evidence strongly indicates that a temperature function of the form

$$f_3(\theta) = C \exp(-\Delta H/R\theta)$$

can provide an adequate description of the variation of creep behaviour

with temperature. In this expression C is a constant, R is the universal gas constant and ΔH is the activation energy for the controlling creep process. Since creep involves thermally activated processes changes in ΔH are usually associated with changes in the creep mechanisms. For most metals at temperatures in the range 0.2 to $0.5\theta_{MP}$, ΔH shows some dependence on both stress and temperature, although in practice this variation is of the order of 20 per cent of the value for temperatures above $0.5\theta_{MP}$ where ΔH correlates closely with the activation energy for self-diffusion. Below $0.2\theta_{MP}$ thermally activated creep mechanisms become less rate controlling and ΔH rapidly declines. Some typical values of ΔH in the range $0.2 - 0.5\theta_{MP}$ are given in Table 2.1. Although there is a wide variation in values of ΔH for pure metals, the variation amongst different alloys of the same base metal is usually small for temperatures greater than $0.4\theta_{MP}$.

In this thesis, as stated earlier, a series of experiments conducted on pure aluminium specimens will be described. Therefore to assure continuity all theoretical calculations, unless stated otherwise, assume material parameters which are consistent with this material. An extensive investigation by Sherby[26] et. al. into the variation of the activation energy with temperature for pure aluminium provides valuable information on this material. His results are given graphically in Figure 2.2 from which it can be seen that for $0.25\theta_{MP} \leqslant \theta \leqslant 0.45\theta_{MP}$, ΔH is approximately 113 kJ/mole and for $\theta > 0.45\theta_{MP}$, ΔH equals 140 kJ/mole.

(d) Constitutive Relationship.

In the following chapters it will be assumed that the constitutive relationship for constant stress uniaxial creep is given by,

$$\frac{\varepsilon(t)}{\varepsilon_o} = \left[\frac{\sigma}{\sigma_o}\right]^n \exp\left[\frac{\Delta H}{R}\left(\frac{1}{\theta_o} - \frac{1}{\theta}\right)\right]\left[\frac{t}{t_o}\right]^m \qquad (2.5)$$

where ε_o is the creep strain resulting from a stress σ_o at temperature θ_o and t_o is some time measure.

Alternatively equation 2.5 may be re-expressed as

$$\varepsilon(t) = k_o \sigma^n \exp(-\Delta H/R\theta).t^m \qquad (2.6)$$

where

$$k_o = \frac{\varepsilon_o}{\sigma_o^n} \exp(\Delta H/R\theta_o).\left[\frac{1}{t_o^m}\right].$$

The steady state creep rate $d\varepsilon/d(t^m)$ may be written as either

$$\dot{\varepsilon} = k\, \sigma^n \exp(-\Delta H/R\theta) \qquad (2.7)$$

or

$$\frac{\dot{\varepsilon}}{\dot{\varepsilon}_o} = \left[\frac{\sigma}{\sigma_o}\right]^n \exp\left[\frac{\Delta H}{R}\left(\frac{1}{\theta_o} - \frac{1}{\theta}\right)\right] \qquad (2.8)$$

2.3.2. Creep Laws for Time Varying Stress

Several proposals have been made to generalise equation (2.5). The two most widely used hypothetical material models are the time-hardening and strain-hardening laws. They represent idealized material behaviour and ignore such effects as creep hesitation and recovery. However they do provide a useful insight into real material behaviour and within their limits can provide useful information on structural creep behaviour. Their mathematical forms for isothermal conditions are:

(a) The time hardening law.

$$\frac{\dot{\varepsilon}_{ij}}{\varepsilon_o} = \frac{3}{2} m \frac{\{\sigma_e(t)\}^{n-1}}{\sigma_o^n} s_{ij}(t) \frac{t^{m-1}}{t_o^m} \qquad (2.9)$$

(b) The strain hardening law.

$$\frac{\dot{\varepsilon}_{ij}(t)}{\varepsilon_o} = \frac{3}{2} m\{\sigma_e(t)\}^{(n-m)/m} \left\{\frac{\varepsilon_o}{\varepsilon_e(t)}\right\}^{(1-m)/m} s_{ij}(t) \qquad (2.10)$$

where s_{ij} is the stress deviator, and

$$\{\sigma_e(t)\}^2 = \frac{3}{2} s_{ij}(t)\, s_{ij}(t)$$

$$\{\varepsilon_e(t)\}^2 = \frac{2}{3} \varepsilon_{ij}(t)\, \varepsilon_{ij}(t)$$

2.4. Creep Deformation of Structures.

The derivation of the mechanical equations of creep is a highly complicated process. Various generalizations of the basic equations are readily realized but the use of complex equations increases the difficulty of determining the coefficients or functions they contain from the usual limited experimental data. It then becomes difficult to extract any detailed or comprehensible qualitative pictures or to deduce any practical conclusions that are of use in design.

Structural analysis using constitutive relationships that closely fit observed material behaviour consists essentially of the solution of a set of non-linear differential equations with non-constant coefficients. Several techniques of solution are now well established [27,28]. However the material model adopted is limited in several respects. Firstly, plastic and creep effects can be expected to interact and initial prestraining can be expected to influence the subsequent creep performance of the material. Secondly there is no hypothetical constitutive creep relationship that adequately predicts behaviour due to time varying stress[29]. Anisotropic behaviour and the Bauschinger effect are frequently neglected in material models.

Although computing power is available to permit the step-wise integration (with respect to time) of such problems the lack of adequate constitutive laws leaves such solutions open to question.

Several workers[30,31,32] have approached the problem from a different direction. A simple material model was initially adopted and structural behaviour for the hypothetical material then examined to determine what parameters are important and what creep tests are required to enable realistic but admittedly approximate predictions of structural behaviour to be made. A related field has been the derivation and application of energy theorems for structures composed of certain material models[33,34,35,36,37]. Some of these theorems are basically extensions of the extremum principle for elastic continua[38] and have been progressivly extended to encompass a wider class of material models and more general classes of loading.

2.4.1. Deformation due to Secondary Creep.

It has been observed[34] that a suitable simplification to the estimation of the creep deformation of structures subjected to steady loads is that both elastic and primary creep deformations are small compared with secondary creep deformations. Hoff[39] considered secondary creep in the absence of elastic effects and argued that this was justified for structures in which the creep strain was of the order of 1% since the maximum elastic strain was of the order of 0.1% . The stress distribution can then be considered invariant with time and the well known theorems of minimum total energy and minimum complementary energy can be applied as if to a non-linear elastic material to obtain bounds on the energy dissipation in the structure.

A uniaxial creep law of the form

$$\dot{\varepsilon} = k\,\sigma^{n} \qquad (2.11)$$

permits useful theoretical simplification and in many situations a precise knowledge of n is not required. Calladine and Drucker[33,40] showed that the energy dissipation in a minimum weight structure can be expressed

in a form invariant with n and that little variation with n may occur "in spite of departure from the minimum condition". However, Calladine[41] obtained solutions to a uniformly stretched plate containing a central hole and concluded that there exists an approximately linear relationship between energy dissipation rate and 1/n , and between stress concentration factor and 1/n . Therefore for complex structures where only the elastic, (n=1) , and plastic (n=∞) solutions are known approximate solutions can be found for a structure composed of a material for which $1 < n < \infty$.

Anderson et al[30] and Marriott and Leckie[31] considered the deformation rate of beams composed of a material where n was itself some function of stress, and suggested that the assumption of a creep law of the form given by equation (2.5) would allow sufficiently accurate estimation of the deformation rate providing the creep test was performed at a "representative stress", i.e. providing the creep test data was obtained at a suitable level the variation of n with σ is not important in practice.

The work of Mackenzie[42] and later that of Sim[43] demonstrated that the creep deformation rate of various structures can be estimated from the creep data obtained from a single creep test at a 'reference stress' without precise knowledge of the stress index n . This work will be further discussed in Chapter 4.

The concept of a reference stress based on the energy dissipated in the stationary state has been usefully extended by Leckie[44] and Williams[45]

The outcome of these ideas has been a procedure for obtaining an acceptable estimation of structural performance from a minimum of information on the material behaviour. In the above references only isothermal conditions have been considered whereas in most engineering structures few truly isothermal conditions are present.

2.4.2. Creep due to Variable Loading.

The lack of adequate constitutive relationships for time varying stress reduce considerably the worth of any calculations for variable loading. However many situations involving variable loading are periodic and as such afford some simplification of the problem.

Ponter[1,37] has derived work bounds for structures composed of time-hardening Maxwell material and subjected to variable loading. The theorems provide a generalization to the theorems derived by Martin[46] and Leckie and Martin.[34] The bounds provide a measure of the stress re-distribution occurring and are therefore indicative of situations where a reference stress approach may be used with confidence.

Bounds[2] computed on the energy dissipation when the material has attained a cyclic state provide two extreme states when the cycle time is either large or small compared with a characteristic time of the material. Recently Ponter and Williams have derived sufficient conditions that the bound will be optimal with respect to the stress field, the computation of which involves a structural problem comparable in complexity with the steady state solutions.

In situations where the effects of stress redistribution are found to be small or a design based on an upper bound remains acceptable, Williams[45] states that the time-hardening result can be applied to structures composed of materials with related constitutive relationships whose creep law for time varying stress is unknown, by applying a weighting factor obtained from a single cyclic stress creep test.

When stress redistribution effects are known to be significant and an elastic/creep calculation is required, a weighted time-hardening calculation is employed[45]. As before, the weighting factors are obtained from a single cyclic creep test. The creep law for time varying stress is not required and difficulties frequently experienced when other hypothetical creep laws are used are avoided.

Metal	Creep Activation Energy (kJ/mole)
Aluminium.	113.1
Al-1.6% Mg Alloy.	149.7
0.05% C.Steel.	256.2
1.15% C.Steel.	257.8
Mo-Stainless Steel.	314.1
Fe-27.8% Al Alloy.	276.3
Ni-20% Cr-23% Ti-1.5% Al Alloy.	347.5-523.4

Table 2.1. Creep activation energies for some metals

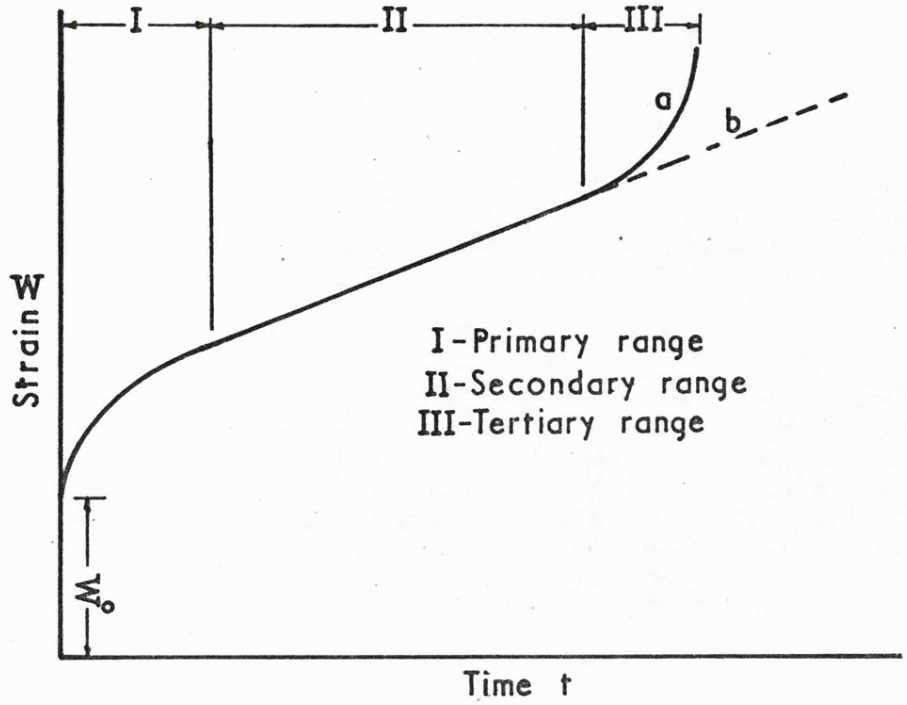

Fig 2·1 A typical creep curve

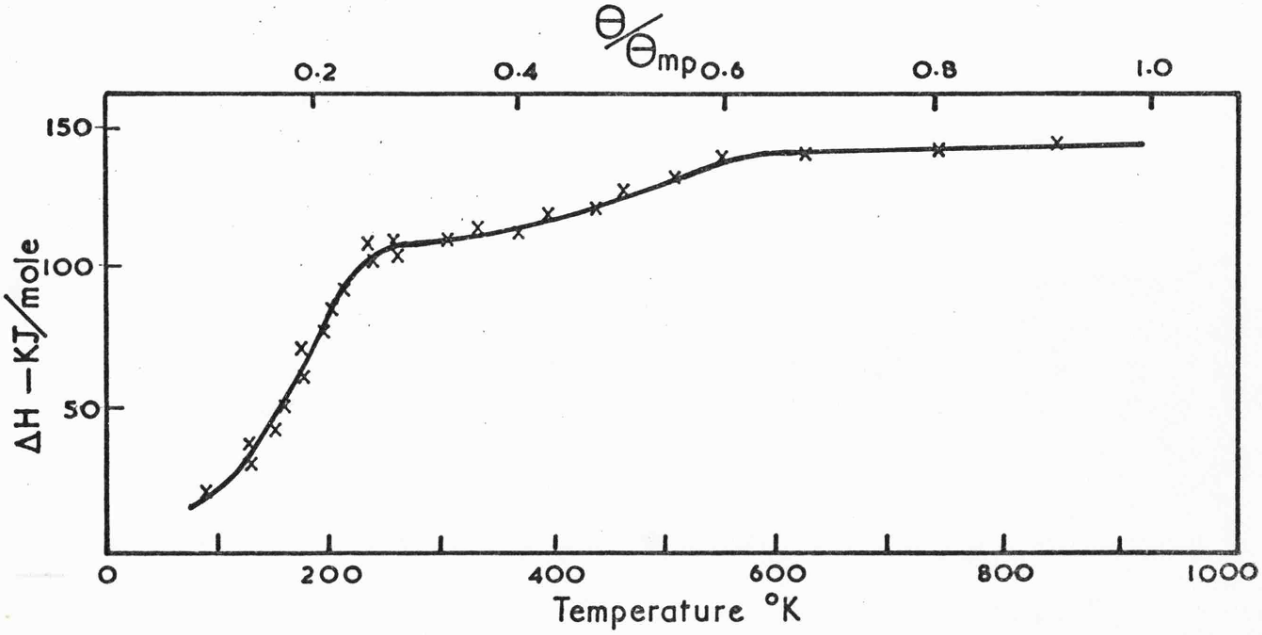

Fig 2·2 Variation of creep activation energy with temperature for aluminium

Chapter 3

Stationary Creep of Structures Subjected to Time-Independent Temperature Gradients

3.1. Introduction.

The stationary state analysis has assumed a major role in the solution of creep problems and there has been much interest shown in the properties of stationary state solutions. However it is noticeable that although there exist numerous stationary state solutions to a variety of structures they are virtually all concerned with isothermal conditions.

In this chapter the effect of spatially varying temperatures on the stationary stress distributions and deformations of some sample structures will be shown. It is found that even quite small temperature gradients have a considerable effect on the stress distributions and that many features of isothermal creep are greatly influenced. Leckie and Ponter,[35] and Ponter[36] have shown that the plastic limit solution can provide a tolerable upper bound on deformation for isothermal conditions. Where temperature gradients are present this solution does not provide an acceptable estimate for $n < 11$ but always provides the asymptotic solution as $n \to \infty$. Therefore, for these cases a plastic solution is defined corresponding to a yield stress dependent on both temperature and stress index. This solution provides an intermediate plastic solution which the actual solution approaches for moderate values of n.

The influence of stress redistribution on structural deformation and the relevance of the stationary state analysis will be discussed.

Solutions are given to three sample problems: a beam under pure bending, a parallel two-bar structure and a propped cantilever beam.

3.2. Stress Redistribution due to Steady Loading.

Hoff[39] considered stress redistribution in a structure composed of a Maxwell material undergoing secondary creep and showed that the stress field in the structure asymptotes to a steady-state. This result was generalised by Hult[47] to embrace much more complex creep laws such as those given by equations 2.9 and 2.10. He termed the stress field that is approached asymptotically, the stationary state. At the stationary state, the elastic strains remain constant in time and make no contribution to the subsequent strain rates. The total deformation is made up of an initial elastic deformation, deformation accumulated in the stress redistribution process and deformation at the stationary state. The effect of stress redistribution is that the total deformation is in excess of that which is obtained if the elastic and stationary-state deformations were simply added (Figure 3.1).

Several attempts have been made to estimate the additional deformation due to stress redistribution. Marriott and Leckie[31] made some critical creep calculations on a variety of simple structures under isothermal conditions. They concentrated on the time-hardening constitutive law and although they recognised that it is physically the least realistic of the available creep laws they were able to show that the 'energy' consumed by a structure in changing over from an initial stress distribution to the stationary state stress distribution is small compared to the elastic energy of the structure or at worst of the same order of magnitude. They also showed that for the structures studied the overall creep deformation did not differ significantly and the stress histories were also similar, for both the time-hardening and strain-hardening laws. The work of Marriott and Leckie[31] has been consolidated in general terms by Leckie and Martin[34]. They showed that structures composed of a time-hardening Maxwell material converge monotonically to the stationary state which is

also that for which energy dissipation rate is a minimum, a result consistent with the theorem of minimum complementary energy. Leckie and Martin were able to show that at large times the total work done by the external forces can be bounded from above by the expression

$$\int_o^t \dot{P}U dt < (n+2)(E^s - E^o) + \int_o^t d\tau \int_V k \sigma_s^{n+1} f(\tau) dV \qquad (3.1)$$

In this relationship, E^s is the elastic internal energy associated with the stationary stress σ_s, E^o is the internal elastic energy on first loading, and the double integral is the creep energy-dissipation corresponding to the stationary stress solution. Consequently the term $(n+2)(E^s - E^o)$ represents an upper bound of the additional energy dissipated during stress redistribution. They obtained values of $(E^s - E^o)/E^o$ for different structures and concluded that the energy dissipation due to stress redistribution was of the same order as the initial elastic strain energy and consequently the assumption by many workers that redistribution effects can be neglected is largely justified.

Stress redistribution in the presence of non-uniform temperature distributions has been investigated by Barnes et al[48]. They simulated experimentally the stress redistribution occurring in a simple redundant structure comprising of three parallel bars joined at their ends by rigid members. Redistribution of load was observed for several initial stress distributions and temperature differences. The authors concluded that the fully redistributed stresses were always more uniform than the initial thermal stresses appropriate to the same temperature difference, the final states of stress were insensitive to the initial stress states, and that the strain-hardening constitutive relationship provided useful descriptions of stress and strain histories during redistribution.

In most circumstances stress redistribution effects are small, the additional deformation being of the order of the initial elastic deformation, and therefore can be neglected in design.

In many design situations the stationary state solution may be difficult to obtain or even unobtainable but an approximate solution such as the plastic limit state may well be available. Leckie and Ponter[49] have extended many of the theorems of perfect plasticity and their corollaries to include the effects of creep. They computed upper bounds on deformation by making use of the limit state solutions and showed that the bounds so obtained can be acceptable and of use to the designer.

3.3. Stress Redistribution Times.

For design purposes the time to attain the stationary state is seldom required to be known with extreme accuracy, only whether the redistribution time is large compared with the period of component loading.

Calladine[50], on the basis of certain simple calculations, proposed that since the stationary state is approached asymptotically the stress redistribution time be given by the time required for

$$\sigma(t_{10}) - \sigma_s = (\hat{\sigma}-\sigma_s)/10$$

where t_{10} is the time required, σ_s is the stationary stress and $\hat{\sigma}$ is the initial elastic stress.

The approximate relationship quantifying t_{10} derived by Calladine is

$$t_{10} = \frac{2.3}{n} t^*$$

where t^* is the time taken for the creep strain to be equal to the elastic strain when maintained at a constant stress of magnitude equal to the stationary state value.

The above expression is claimed to give an overestimate of the stress redistribution time for larger values of n and the quotient $(\hat{\sigma} - \sigma_s)/\sigma_s$.

Values of nt_{10}/t^* for different structures have been obtained by Sim[43]. He compared these results with 2.3 and showed that they were in close agreement for the range of structures considered with the exception of thick shells subjected to internal pressure where the value of nt_{10}/t^* can rise to 7.9.

Calladine's formula is applicable to any structure but requires a knowledge of both the initial elastic stress distribution and the stationary state stress distribution together with creep data from a test at the appropriate stress level.

Bill and Mackenzie[51] expressed the stress redistribution time in terms of the ratio of creep strain at time t_{10}, due to some reference stress σ_R, to the corresponding elastic strain. They showed that by a suitable choice of σ_R their measure of stress redistribution time could be made sensibly independent of n. They also observed that the values of σ_R obtained did not differ significantly from reference stresses obtained for estimating deformation due to stationary creep. Thus providing t_{10} is known for one value of n it should be possible to make acceptable estimates of t_{10} for other values of n.

Both Bill and Mackenzie, and Calladine were concerned with stress redistribution times in structures composed of time-hardening material. Marriott and Leckie[31] report that redistribution times for structures composed of strain-hardening material are significantly longer than corresponding values for a time-hardening material. Some recent results by Williams[45] also support this. These results are not unexpected, since structures composed of material obeying creep laws other than time-hardening, will be stiffer in the sense that stress redistribution effects, when considered from the micro-structure aspect, will increase the state variables of the material at a faster rate than would occur at the stationary state. A structure composed of a time-hardening material is not affected by stress redistribution effects in the same manner since by

definition it is only dependent on time. The structure will therefore have no memory of the redistribution process.

Some recent work by Megahed[52] using the time-hardening law has shown that for a two-bar structure similar to that considered by Williams under isothermal conditions, Calladine's method provides a conservative estimate of t_{10} for $n > 3$. For non-isothermal conditions with a step change in load and temperature occurring simultaneously, results obtained by step-by-step calculations indicate that redistribution times are considerably longer than those predicted by Calladine. In comparison, much smaller values are calculated for a step change in load on the fully redistributed non-isothermal structure.

It may be argued heuristically that in a structure where changes in load and temperature occur simultaneously the interaction between the applied and thermal stresses may be expected to produce values of t_{10} greater than those for a fully-redistributed non-isothermal structure subjected to an equivalent load change where the only effect of temperature is to produce a 'softening' of the material.

The general effect of a temperature field on a fully-redistributed non-isothermal structure is to decrease the redistribution time for further loading in the sense that since creep is highly temperature dependent local creep strains may be accumulated at a greater rate thereby modifying the stress distribution.

From the review given it can be seen that stress redistribution times can be very dependent upon the constitutive equation for time varying stress and since no satisfactory generalisation of equation 2.5 is available at present, the only method of obtaining such times is by experiment.

3.4. Stationary State Creep of Some Simple Structures.

This section is concerned with creep; elastic, and time-independent plastic deformations are not considered. Stress distributions are therefore stationary (steady-state) distributions. The constitutive relationship 2.7 is adopted and in the solutions presented the activation energy for creep, ΔH, was taken as 113 KJ/mole with the lowest temperature in each example, θ_1, being 300°K. (ΔH correlates with θ_1, for pure aluminium.)

It may be noted that many calculations were performed using different values of both ΔH and θ, and it was found that the principal features of the solutions are relatively independent of these quantities.

The complete solutions to the three examples are given in Section 10.3.

(a) Beam in Pure Bending

A uniform beam of rectangular cross-section, width b and depth d, is subjected to constant end moments M and a linear temperature gradient through the depth. (A situation that occurs if the beam sides are insulated.) At any section distance y from the lower edge the temperature is given by

$$\theta(y) = \left[(\theta_2-\theta_1)\,\frac{y}{d} + \theta_1\right] ,$$

where θ_2 and θ_1 are the temperatures at the upper and lower surfaces respectively.

The axial strain $\varepsilon(y)$ at a distance y from the lower surface is

$$\varepsilon(y) = \kappa(y+\phi d) ,$$

and

$$\dot{\varepsilon}(y) = \dot{\kappa}(y+\phi d) ,$$

where κ denotes the curvature of the centroidal axis.

The stationary state moment-curvature rate relationship may be expressed

$$\dot{\kappa} = \frac{k}{d}\left[\frac{2M}{bd^2}\right]^n I_B \qquad (3.2)$$

where I_B is evaluated from conditions of equilibrium and compatibility:

$$I_B = \left\{ 2 \int_o^1 (x+\phi)^{1/n}\, x \exp[\Delta H/nR\theta(x)]\, dx \right\}^{-n} ,$$

and $x = y/d$.

The stationary stress distribution depends upon the activation energy, the temperature difference $(\theta_2-\theta_1)$, and the stress index n ;

$$\sigma(x) = \left[(x+\phi) I_b \exp(\Delta H/R\theta(x))\right]^{1/n} \left[\frac{2M}{bd^2}\right] . \qquad (3.3)$$

The other variables $\dot{\varepsilon}_o$, σ_o and θ_o only affect the curvature rate.

In Figure 3.4 the stationary stress distributions for isothermal conditions are shown for $1 \leqslant n \leqslant 11$. Two well known features are immediately evident; the variation between the $n = 1$ solution (analogous to the linear elastic case) and the $n \to \infty$ solution (analogous to the rigid perfectly plastic case) for intermediate values of n and the existence of two points symmetrically placed about the neutral axis where the stresses vary only slightly with n . These positions were referred to by Marriott and Leckie[31] as 'skeletal' points and their associated stresses as 'skeletal' stresses. These will be further discussed in the following chapter.

In Fig.3.5 the stress distributions are shown for a temperature difference $(\theta_2-\theta_1) = 12°K$. It can be seen that for this fairly small temperature difference the isothermal picture has been substantially disturbed. No clearly defined skeletal points are present and the transition from $n = 1$ to $n = 11$ possesses entirely different characteristics to the isothermal case. The $n = 1$ case remains analogous to a linear elastic solution but with a Young's Modulus which varies through the depth of the

beam (i.e. with temperature). For larger values of n the solution asymptotes to the homogeneous perfectly plastic solution (shown as a broken line). This can be seen by rearranging equation 2.8 into the form

$$\left|\frac{\sigma}{\sigma_o}\right| = \left|\frac{\dot{\varepsilon}}{\dot{\varepsilon}_o}\right|^{1/n} \exp\left[\frac{\Delta H}{nR}\left(\frac{1}{\theta} - \frac{1}{\theta_o}\right)\right] . \qquad (3.4)$$

As $n \to \infty$, provided kinematic conditions demand that $\dot{\varepsilon}/\dot{\varepsilon}_o$ remains finite, then $\sigma/\sigma_o \to 1$, the condition associated with the perfectly plastic solution. Thus the variation of stress with creep index spans the range between a non-homogeneous linear elastic solution and the homogeneous rigid perfectly plastic solution.

In Fig.3.6 the stress distributions for a much larger temperature difference $(\theta_2-\theta_1) = 60°K$ are presented. The $n = 1$ case can be seen to be highly variable especially near the cooler side, and for $n = 11$ the solution differs considerably from the $n \to \infty$ case, whereas for isothermal conditions the $n = 11$ and $n \to \infty$ solutions are virtually identical. For even larger temperatures differences the difference between these two solutions becomes more marked. The reason for this is that for large temperature differences the exponential term in equation 3.4 has not become constant at $n = 11$ although the first term $(\dot{\varepsilon}/\dot{\varepsilon}_o)^{1/n}$ closely approaches unity. This suggests an intermediate stress profile of the form

$$\left|\frac{\sigma}{\sigma_o}\right| = \exp\left[\frac{\Delta H}{nR}\left(\frac{1}{\theta} - \frac{1}{\theta_o}\right)\right] \qquad (3.5)$$

which corresponds to a plastic solution with a spatially varying yield stress dependent upon n. The stress profile obtained from equation 3.5 is shown as a broken line in Fig.3.6 and is seen to closely approximate the solution for $n = 11$. This 'plastic' solution will be further discussed in section 3.5.

Calladine[53] investigated means of estimating the maximum stress in a structure without performing a non-linear analysis. He observed that there existed, for a variety of simple structures under isothermal conditions,

a linear relationship between the maximum stress and the reciprocal of the stress index. Therefore, providing the $n = 1$ and $n \to \infty$ solutions are obtainable, the maximum stress for intermediate values of n can be gained from a linear interpolation between these two solutions. In Fig.3.7 the maximum stress, which is always compressive is plotted against $1/n$ for a range of values of $(\theta_2-\theta_1)$. It can clearly be seen that a linear interpolation between the $n = 1$, non-homogeneous linear elastic solution and the $n \to \infty$ solution is liable to be considerably in error since the variation is far from linear except for the isothermal solution. However for this structure a linear interpolation provides a conservative estimate of the maximum stresses occurring. From Fig.3.8 it is seen that whereas the maximum compressive stress shows a monotonic change with increasing θ_2 the maximum tensile stress achieves a minimum value at a small value of θ_2 and again Calladine's linear interpolation provides a conservative result.

(b) Two-bar Structure.

Consider the two-bar structure shown in Fig.3.2. It was argued in reference (45) that this structure was representative in some respects of many simple structures. In the example chosen the bar lengths are in the ratio of 4:1 and have equal cross-sectional areas.

Using the constitutive relationship 2.7, and from considerations of equilibrium and compatibility of displacements, the stress in each bar was evaluated for a range of values of n and a range of values of the temperature difference $(\theta_2-\theta_1)°K$ where θ_2 and θ_1 are the temperatures of the longer and shorter bar respectively.

In Fig.3.9 the variation of maximum stress with $1/n$ for three cases is presented and as expected, always occur in the shorter bar. It can be readily seen that when isothermal conditions prevail the maximum deviation

of the solution from a straight line is at most 2% and Calladine's linear interpolation provides good predictions over the range of n. For a small change in temperatures $(\theta_2-\theta_1) = 10°K$ it is seen that a linear interpolation would be much in error. This deviation increases rapidly with an increasing temperature difference. The $n = 1$ cases still remain analogous to linear elastic solutions, but as in the beam problem, having Young's moduli varying as a function of the temperature difference. As expected, for large values of n the solutions tend toward the homogeneous, rigid/perfectly plastic solution. In the extreme cases where the temperature differences are so large as to make the stiffness of the hotter bar small, the structure appears to behave as a single bar at the lower temperature. Even in this case the solution will asymptote to the homogeneous plastic solution as $n \to \infty$ but its approach occurs at very large values of n.

When the shorter bar is at the higher temperature the variation of maximum stress with $1/n$, Fig.3.10, does not show a monotonic change with increasing temperature. However in both cases a linear interpolation provides a non-conservative result.

This change in behaviour may be more easily understood from consideration of Fig.3.11 which identifies the interaction between the stationary state stresses derived from equilibrium and compatibility conditions. Line S_1S_2 represents stationary state stresses obtained from the equilibrium condition and any line from the origin represents states of stress which satisfy compatibility. The point of intersection represents allowable states of stress within the structure. The solutions presented are for $n = 3$, but similar solutions may be obtained for other values of n. Any point on the line between S_3 and S_1 represents allowable states of stress for an increasing temperature difference when the higher temperature acts on the longer bar, and similarly any point between S_3 and S_2 represents states of stress when the higher temperature acts on the

shorter bar. Point S_3 represents the isothermal solution.

Within region S_3S_1 the maximum stress occurs on the shorter bar and is always larger than the maximum isothermal stress, i.e. there is a monotonic change in maximum stress with increasing temperature difference. However this is not the case within region S_3S_4 where it is seen that the maximum stress is less than the isothermal value. Between S_3 and S_5 ($\sigma_1=\sigma_2=P/2A$) the maximum stress occurs on the hotter bar. At S_5 both bars carry equal loads although the temperature of the shorter bar is 7.4°K higher than the longer bar. Further increase in temperature increases the stress on the shorter bar but this stress does not equal the maximum isothermal value (0.6 P/A) until the temperature difference 15.3°K is reached (point S_4). Within region S_4S_2 increasing temperature difference again provides a monotonic change in maximum stress.

For a two-bar structure with bars of equal length points S_3 and S_5 coincide and the maximum stress always changes monotonically with increasing temperature difference.

(c) Propped Cantilever Subjected to Central Load.

The geometric configuration is shown in Fig.3.3. A uniform rectangular section beam of length ℓ is simply supported at one end and encastré at the other with a point load acting laterally at the centre of span. A linearly varying temperature distribution has its maximum value at the encastré end and the temperature is assumed to be constant through any section.

A moment/curvature rate relationship consistent with equation 2.7 is given by

$$\frac{\dot{\kappa}}{\dot{\kappa}_o} = \left(\frac{M}{M_o}\right)^n \exp\left[\frac{\Delta H}{R}\left(\frac{1}{\theta_o} - \frac{1}{\theta}\right)\right] \qquad (3.6)$$

The problem was solved numerically using a virtual work method which is described in Section 10.3. As the problem involves only a single redundancy, the moment distribution is of the form

$$M(x) = Pm_1 + Fm_2$$

where m_1 denotes the moment due to a unit central load acting upon a simply supported beam and m_2 the reactive bending moment due to a unit load acting at the tip of a cantilever of length ℓ .

The variation of bending moment with temperature and n may be adequately described by the prop reaction F . In Fig.3.12 variation of F/P with $1/n$ is shown for a range of values of the temperature gradient $(\theta_2-\theta_1)/\theta_1$ where θ_2 and θ_1 are the temperatures at the encastre end and simply supported end respectively. The observed behaviour shows similar tendencies to that exhibited by both the beam and two-bar structure. It is seen that for all values of θ_2 , as n becomes large, F/P asymptotes toward the limit $n \to \infty$ corresponding to the homogeneous perfectly plastic case. For the larger values of θ_2 , the $n \to \infty$ solution is only approached for very large values of $n > 20$, whereas for smaller values of θ_2 the approach is more gradual.

The effect of an increase in temperature difference on the $n = 1$ solution is to decrease the stiffness of the encastre end and $F/P \to 0.5$, the simply supported case. As in the previous examples the variation of F/P is far from linear and a linear interpolation of F/P with $1/n$ is clearly non-conservative.

3.5. An Upper Bound on Stationary State Solutions.

Where analytical solutions are not easily obtainable Ponter and Leckie[49] have discussed the application of energy methods to provide bounds on the deformation of isothermal creeping structures. It was shown that a tolerable upper bound on deformation could be obtained from knowledge of the plastic limit state solution and in this section the effect of spatially varying temperatures on these solutions will be discussed. The theory (35,54) remains formally unaltered but as has been shown in

the beam example the use of the limit state solution $(n \to \infty)$ does not provide an acceptably accurate estimate of the stress distribution for values of $n \lesssim 11$ when non-isothermal conditions are present. A 'plastic' solution corresponding to a yield stress dependent upon both temperature and stress index will be defined that provides an intermediate plastic solution which the stationary state solution approaches for moderate values of n.

3.5.1. Energy Theorem.

On the basis of the assumed properties of the material it has been deduced[35] that the contribution of the plastic strains to the deformed shape of a structure are likely to be small provided the loading is kept below the value $n/(n+1)$ of the limit load P_L.

Assume a body of volume V and surface S subjected to applied load P_i over part of the surface S_T and zero displacements over the remainder. In the stationary state the displacement rates of the body may be found directly by assuming $\dot{\varepsilon}$, and may be bounded from above by

$$\int_{S_T} P_i \dot{U}_i \, dS \leq \int_V \dot{D}^c(\sigma^*_{ij}) \, dV \qquad (3.7)$$

where $\dot{D}^c(\sigma)$ denotes the rate of creep energy dissipation associated with the stress σ.

The stress field σ^*_{ij} may be any equilibrium stress field in equilibrium with P_i which satisfies the yield condition

$$f\left(\frac{n}{(n+1)} \sigma^*_{ij}\right) < 0 \, . \qquad (3.8)$$

Note that the restriction (3.8) requires σ^*_{ij} to lie within a surface geometrically similar to the yield surface in stress space and scaled by a factor $n/(n+1)$.

Corresponding to a given P_i, a plastic limit load P_i^L exists where

$P_i = \bar{\lambda} P_i^L$. The conditions of inequality (3.8) are then satisfied by $\sigma_{ij}^* = \bar{\lambda}\sigma_{ij}^L$ provided $\bar{\lambda} < n/(n+1)$, where σ_{ij}^L denotes the limit stress state at plastic collapse.

For a structure where all points of the structure are at a state of plastic yield at collapse, $\bar{\lambda}\sigma^L$ remains on a surface of constant $\dot{D}^c$ and

$$\int_{S_T} P_i \dot{U}_i \leqslant V \dot{D}_c(\bar{\lambda}\bar{\sigma}_y) \qquad (3.9)$$

where $\bar{\sigma}_y$ denotes the uniaxial yield stress.

Thus inequality (3.9) provides a bound on the total energy dissipation rate in terms of the limit load and data from a single uniaxial test, a result which provides a simple calculation to allow a conservative estimate of structural creep deformation. Comparison of these estimates with theory and experiment are to be found in references (45) and (49). The accuracy of these simple estimates are greatest for larger values of n where the creep solution closely approximates the limit state solution.

3.5.2. Application to Beam under Flexure.

It was shown in Fig.3.4 that the perfectly plastic solution provides a limit state on the stress distribution and closely approximates the n = 11 case. In this particular case the bound on curvature rate, $\dot{\kappa}_L$, provided by inequality (3.9) overestimates the exact value $\dot{\kappa}$ by at most 26% in the range $3 \leqslant n \leqslant 11$. Such a discrepancy in curvature rate corresponds to a change in applied moment of at most 8% , or , alternatively, a change in depth of the beam of 4% .

For non-isothermal conditions, Fig.3.5, it was seen that the approach to the limit state solution only occurs at large values of $n > 11$. It was suggested that an intermediate plastic state equation (3.5) provides a better approximation of the stress distributions for $n \leqslant 11$. The stress profiles corresponding to this plastic solution are shown in Fig.3.13 and are seen to closely approximate the actual stresses. The bound formed by

substituting this solution into inequality (3.9) gives a moment-curvature rate relationship of the form

$$\dot{\kappa} \leq \frac{k}{d}\left(\frac{2M}{bd^2}\right)^n I_B^U , \qquad (3.10)$$

where $$I_B^U = \frac{\int_0^1 \exp[\Delta H/nR\theta(x)]dx}{2^n\left\{\int_0^1 x.\exp[\Delta H/nR\theta(x)]dx - \int_0^{\phi} x.\exp[\Delta H/nR\theta(x)]dx\right\}^{n+1}}$$

In Table 3.1 a comparison is made of the curvature rates obtained from the intermediate plastic solution with those obtained from the exact stationary state solution for $\theta_2 = 360°K$. A similar comparison of the bound given by the plastic solution using a constant yield stress and temperatures through the depth is also included. The intermediate plastic solution clearly provides a close estimate of the exact deformation but it is more difficult to obtain than the limit state solution. However, it does provide a reasonably accurate bound on non-isothermal structural behaviour for this problem. The application to more complex structures requires to be investigated.

n	$\frac{\dot{\kappa}_1}{\dot{\kappa}}$	$\frac{\dot{\kappa}_L}{\dot{\kappa}}$
1	2.25	23.2
3	1.55	14.5
5	1.40	14.2
7	1.36	14.0
9	1.33	13.7
11	1.30	13.6

$\dot{\kappa}$: Exact Solution.

$\dot{\kappa}_1$: Intermediate Plastic Solution.

$\dot{\kappa}_L$: Limit State Solution.

Table 3.1

Comparison of Curvature Rates for $\theta_2 = 360°K$

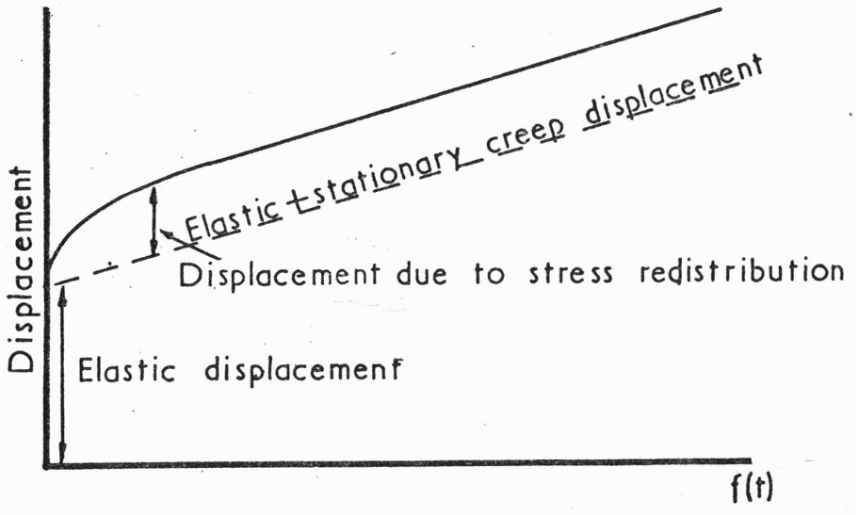

Fig 3·1 Effect of stress redistribution

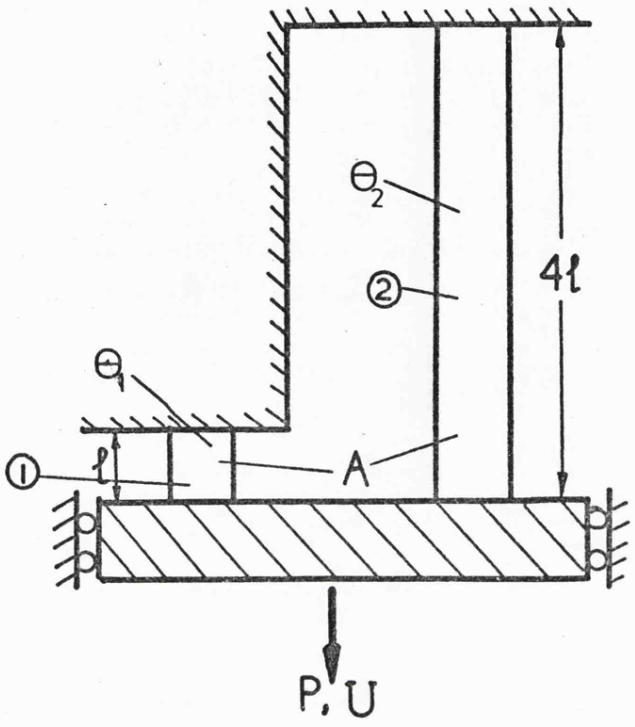

Fig 3·2 Two-bar structure

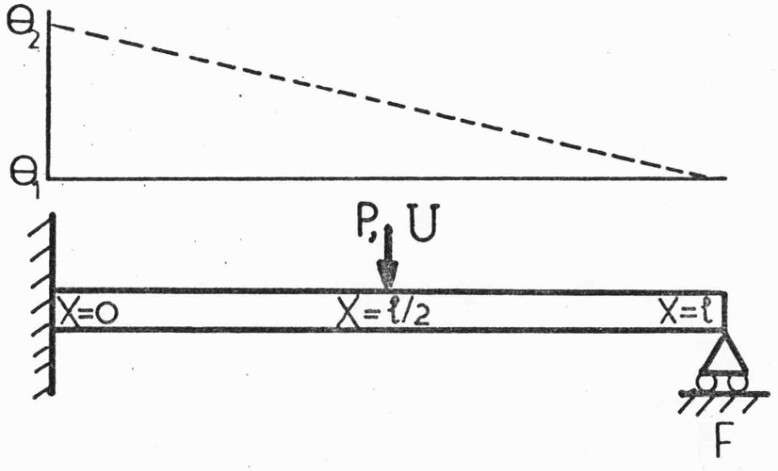

Fig 3·3 Propped cantilever

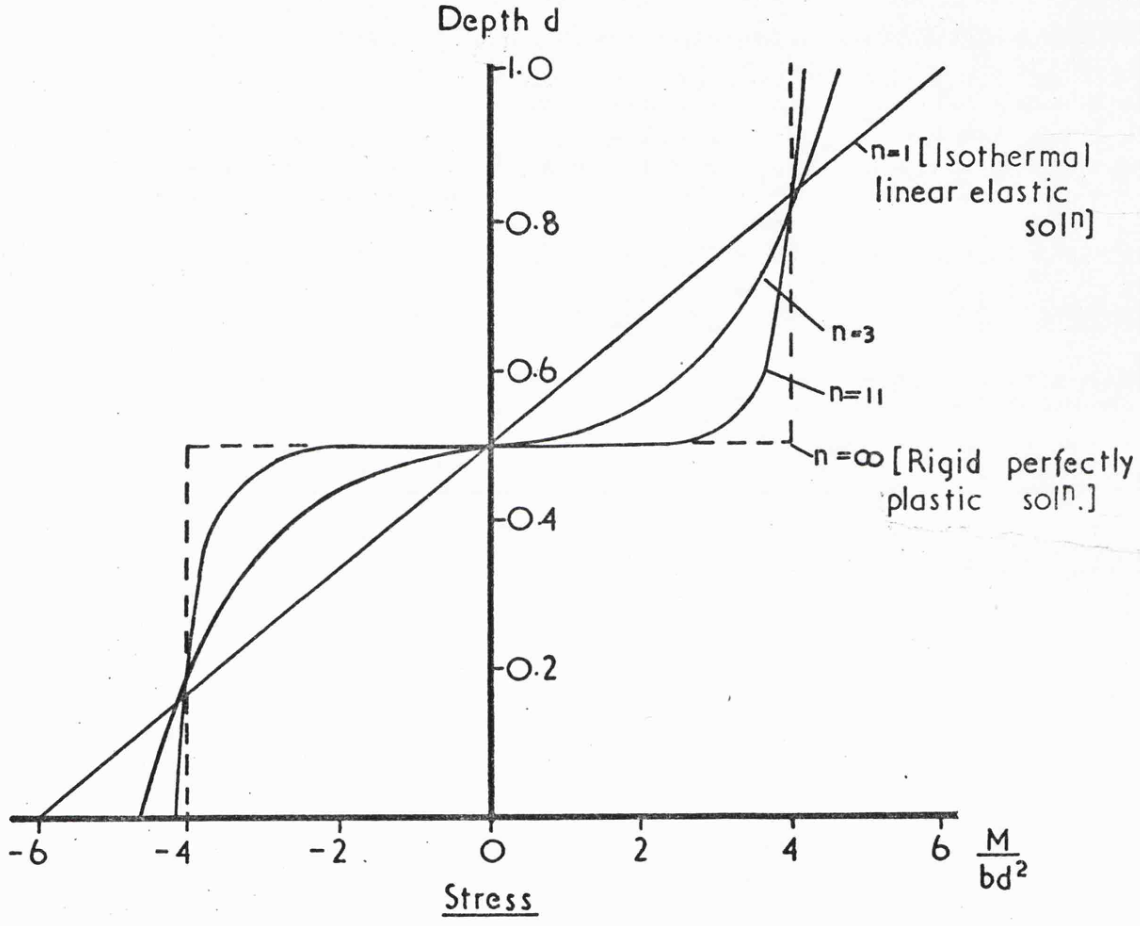

Fig3·4 Stress distributions for isothermal conditions

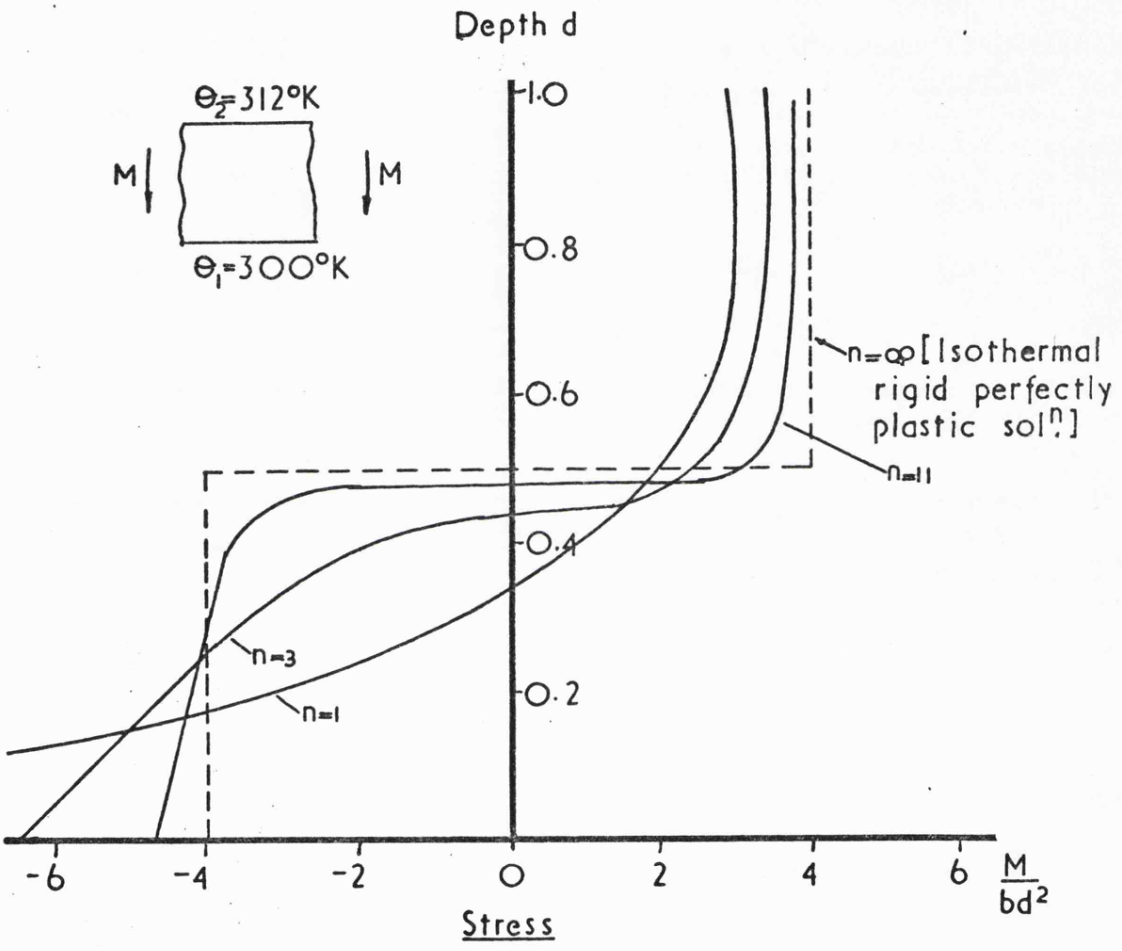

Fig 3·5 Stress distributions for non-isothermal conditions

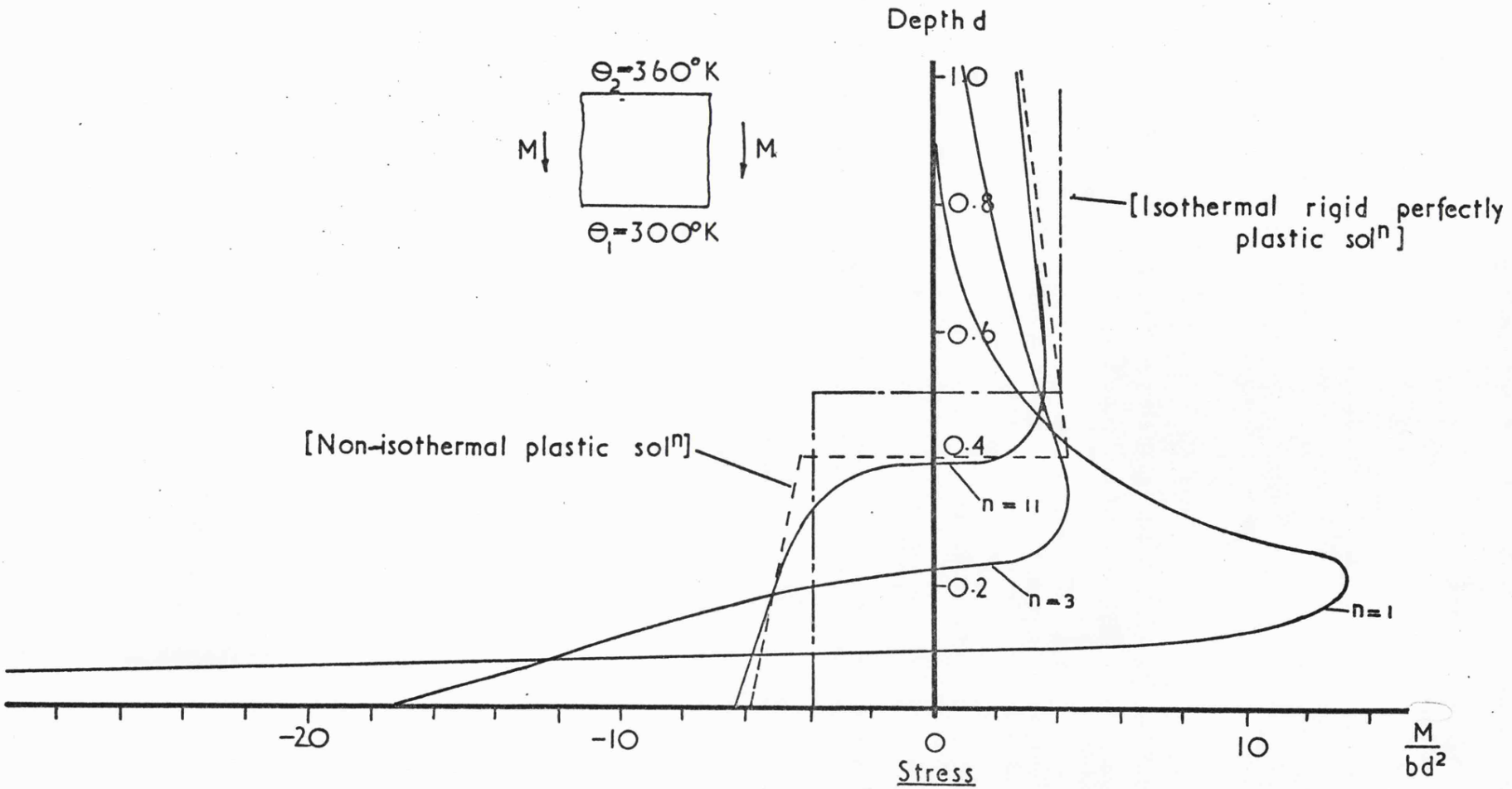

Fig 3·6 Stress distributions for non-isothermal conditions

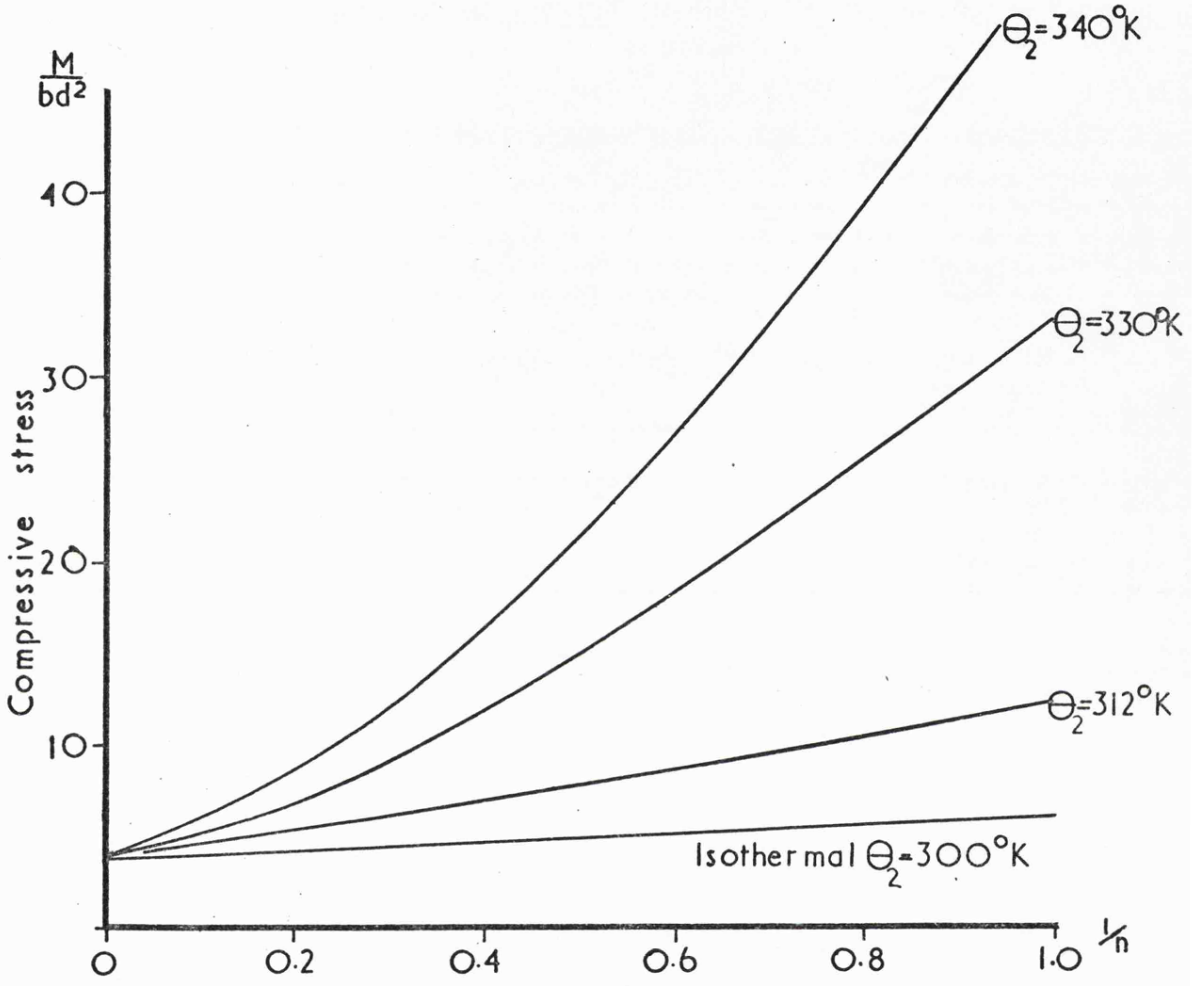

Fig 3·7 Variation of maximum bending stress with 1/n

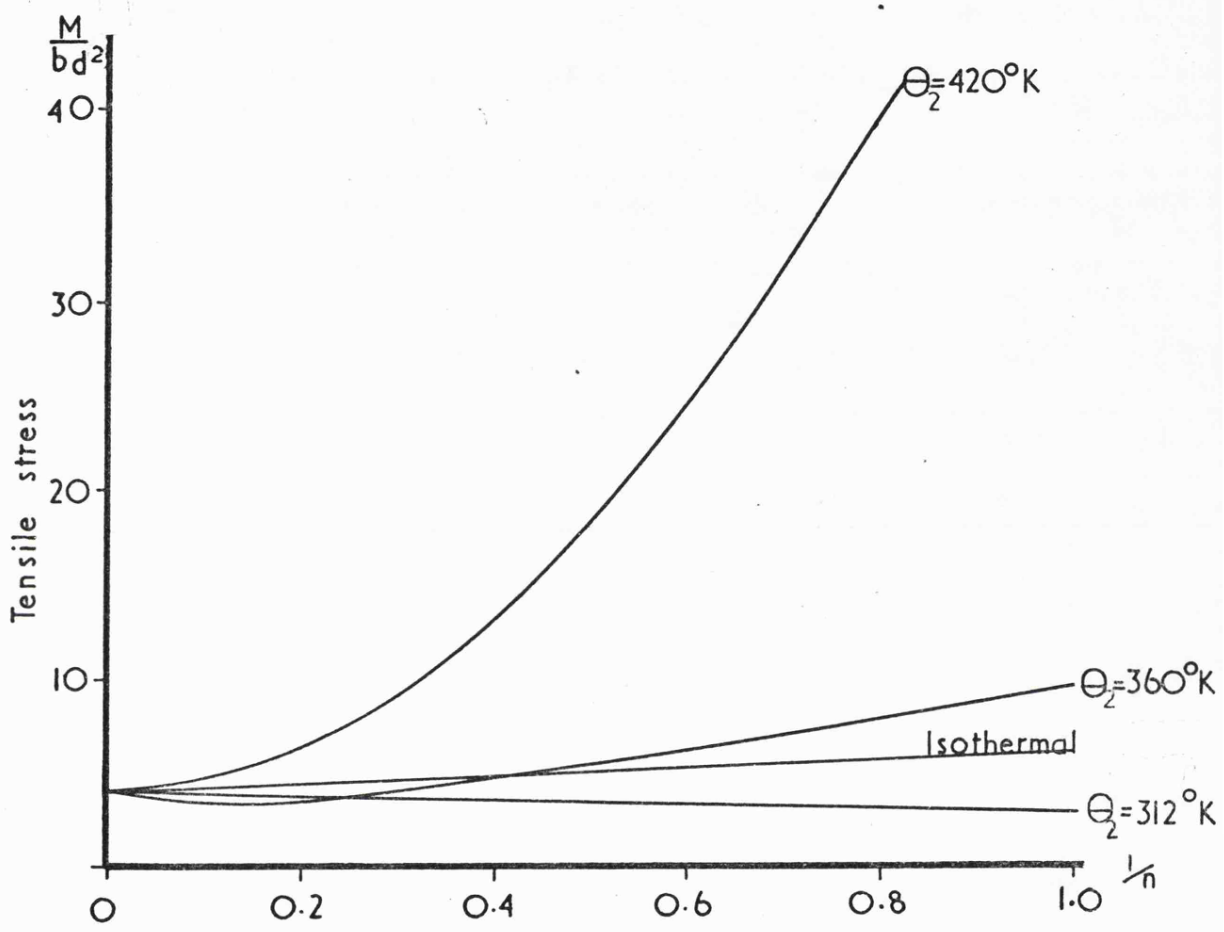

Fig3·8 Variation of maximum tensile bending stress with 1/n

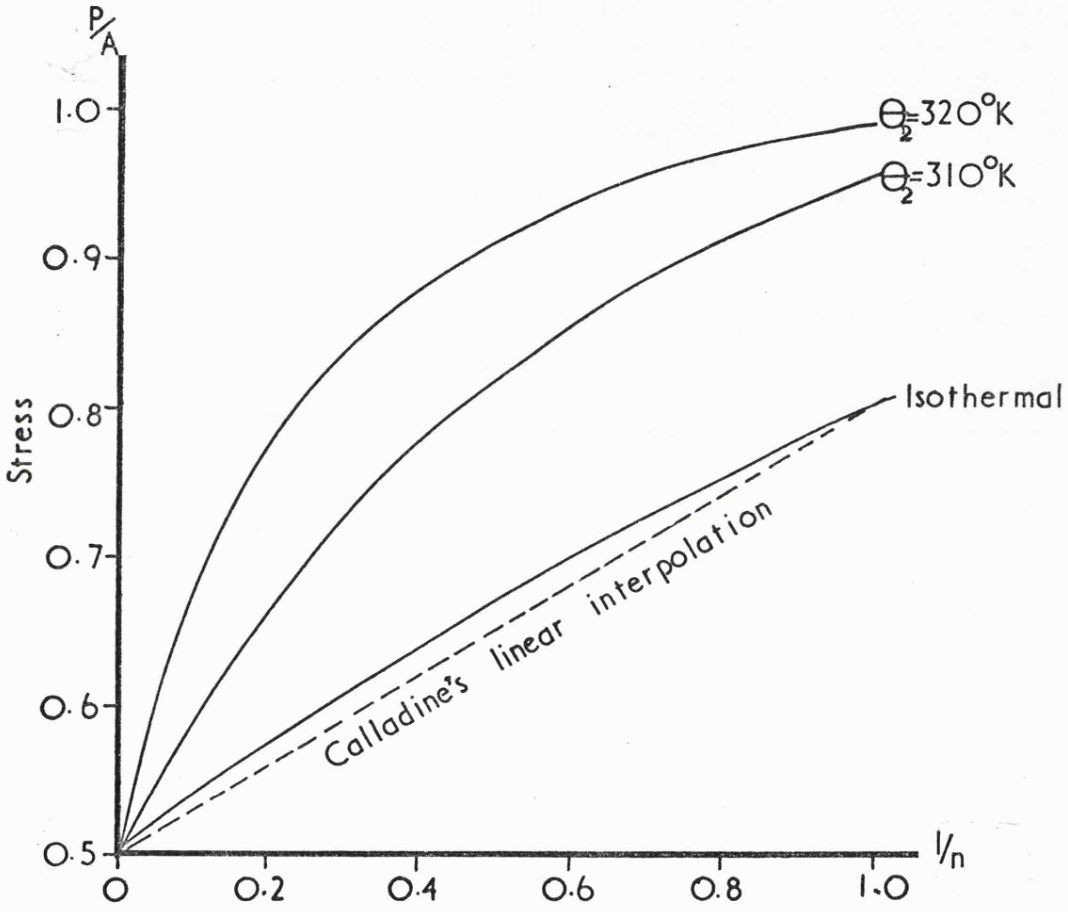

Fig 3.9 Variation of maximum stress with 1/n for the two-bar structure with the higher temperature on the longer bar

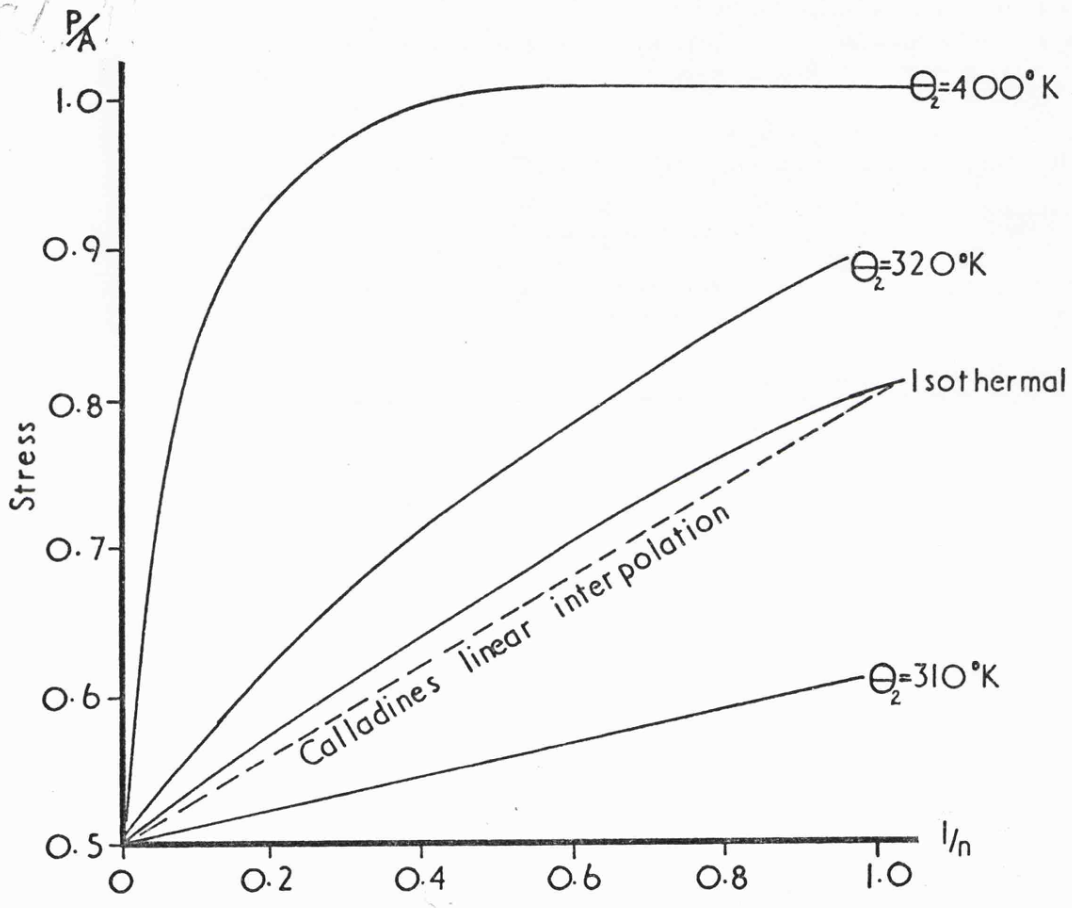

Fig 3·10 Variation of maximum stress with 1/n for the two bar structure with the higher temperature on the shorter bar

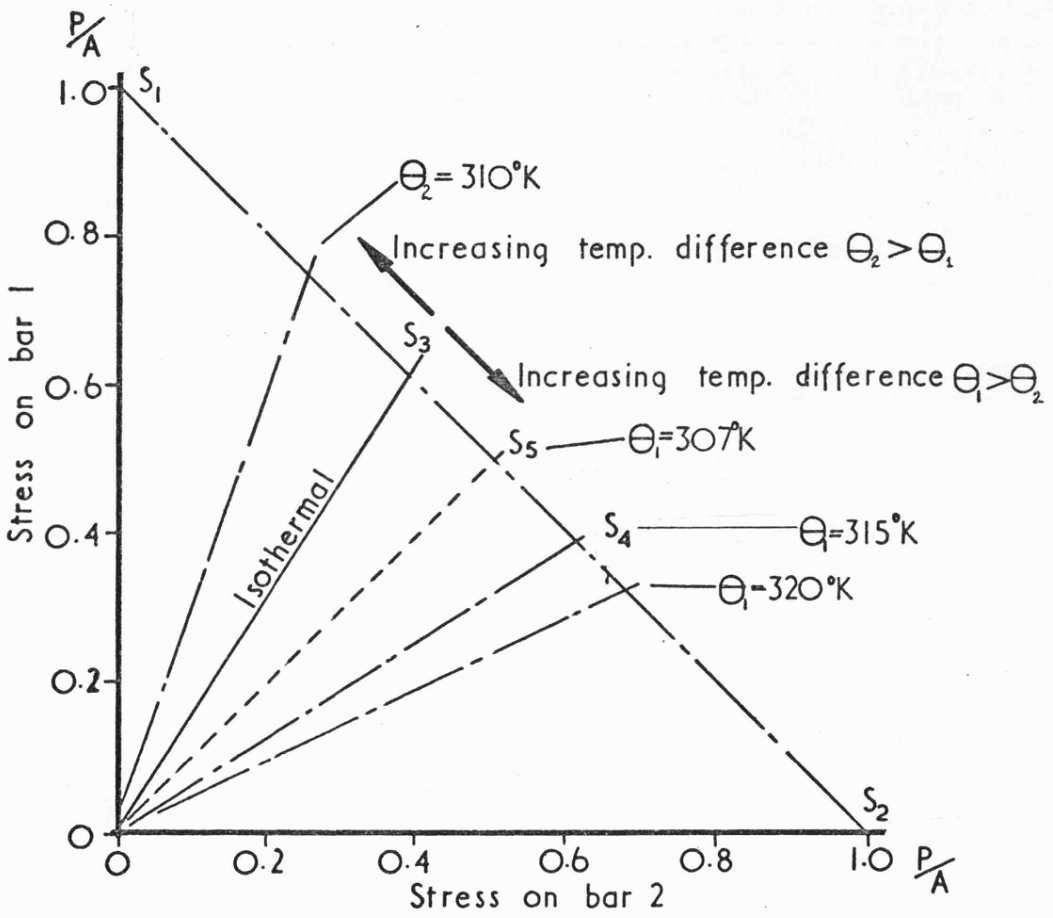

Fig 3·11 Stationary state stress regimes for the two-bar structure

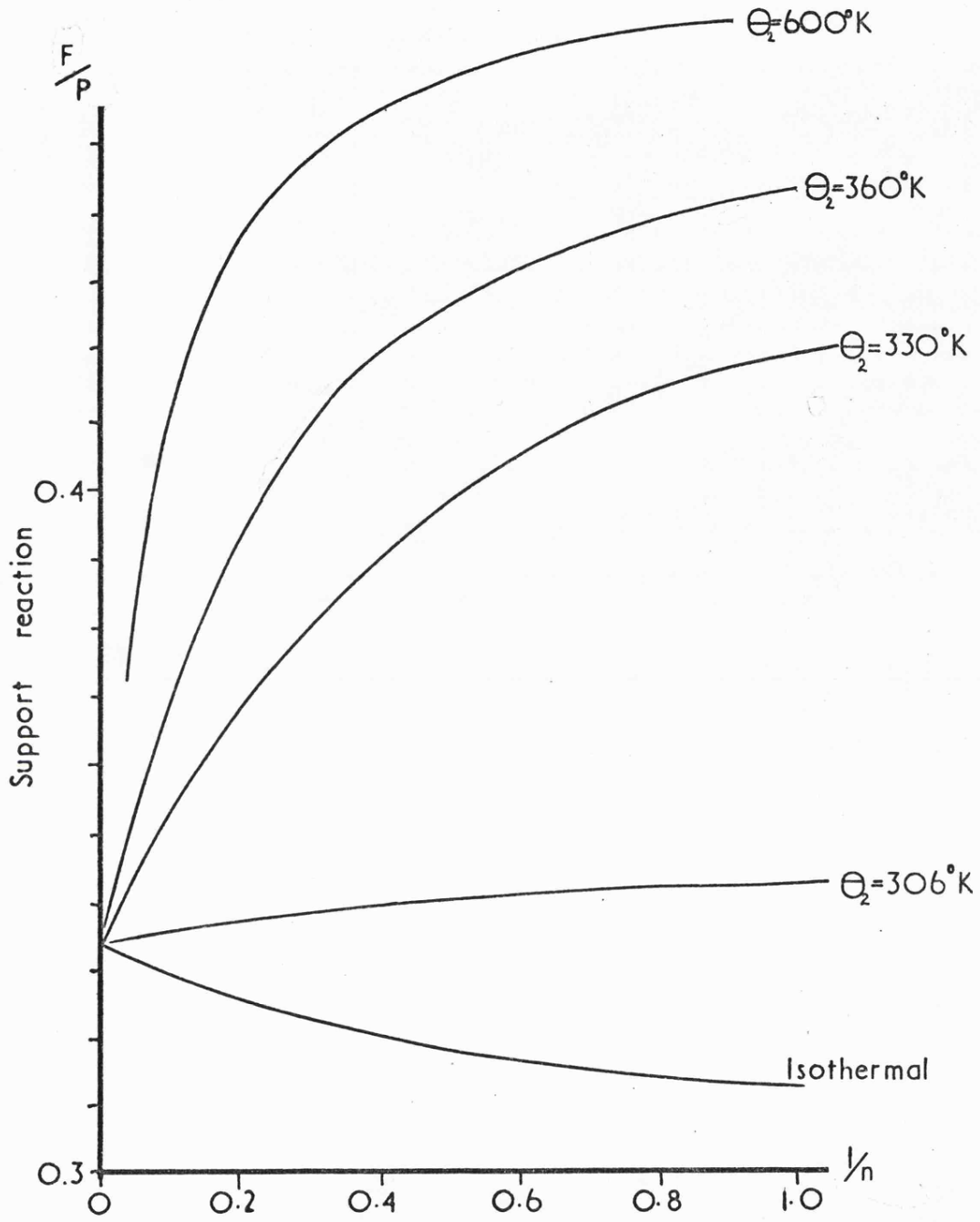

Fig 3·12 Variation of support reaction with 1/n for the propped cantilever with linear temperature gradient

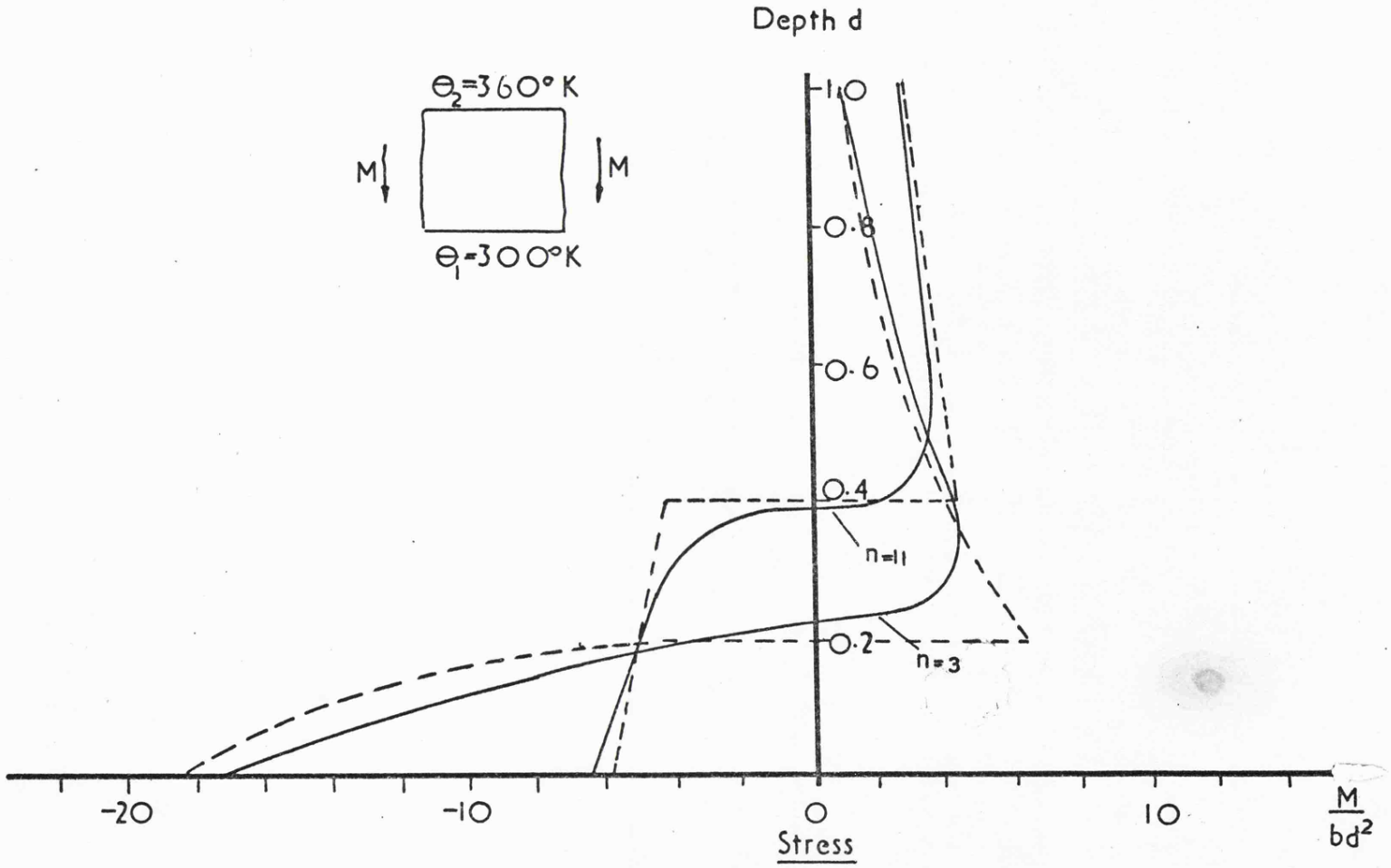

Fig 3·13 Comparison of exact and non-isothermal plastic stationary stress distributions

Chapter 4

A Reference Stress-Reference Temperature Technique for Structures Subjected to Steady Loads

4.1. Introduction

In creep design one major problem is the lack of precise knowledge of material behaviour at temperature and under long term loading. An attractive means of directly utilizing experimental creep data in conjunction with an analytical treatment of a design problem is to use a reference stress technique. This technique is based on the observation that it is often possible, using traditional analytical procedures in conjunction with a power function constitutive equation, to determine a stress at which the creep rates obtained from a tensile test will be proportional to component displacement rates. Such an approach avoids the need for defining the details of material behaviour since this would be included in the tensile creep data. The reference stress also guides the experimental work by indicating in what stress range the tests are to be performed.

In this chapter a reference stress technique originally proposed by Mackenzie[42] will be extended to include the effects of non-uniform temperature distributions. It will be shown that under isothermal conditions there is a single reference stress which has an associated creep deformation in proportion to the deformation occurring in a structure at stationary state conditions. Since the reference stress is based on the stress and strain rate distributions at the stationary state it may be expected that the reference stress is unaffected by an initial temperature gradient in the structure. However, stationary creep rates are strongly dependent on temperature and the specification of only a reference stress provides insufficient information where spatially varying temperature distributions are present. The question arises as to at what temperature should a creep

test be conducted so as to be able to predict correctly the stationary state behaviour of the structure according to a reference stress approach. In section 4.3 a reference temperature technique is defined and applied to some simple structures subjected to steady loads and spatially varying temperature fields. The technique is also applied to the modified limit state solution previously discussed in Chapter 3, and it will be shown that the reference values obtained provide an acceptable bound on structural behaviour for design purposes.

In the following section the development of 'exact' and approximate methods of obtaining reference stresses are discussed. The reference stress technique has been discussed in many papers and different structures are treated, e.g. Söderberg[21], Anderson et al[30], Mackenzie, Sim[43] and Marriott[55]. It is the intention of this section to include some of the information to be found in these references and to review the additional literature subsequently published.

4.2. The Development of Reference Stress Techniques.

4.2.1. Exact Reference Stress Techniques.

Söderberg[21] in 1941 made an early attempt to relate component behaviour to the behaviour of a single tensile test. From a steady state analysis of creep in thick tubes subjected to internal pressure, P', he calculated a reference stress given by

$$\sigma_R = 0.87 \frac{r_m}{h} P' , \qquad (4.1)$$

where r_m denotes mean radius and h wall thickness.

The corresponding deformation is given by

$$\varepsilon_m = 0.87\, \varepsilon(\sigma_R) \qquad (4.2)$$

where $\varepsilon(\sigma_R)$ is the creep strain in a tensile test at a stress of σ_R and

ε_m is the creep strain at the mean radius.

Another early use of a reference test was in the approximate solution of transient creep in beam sections made of polymeric material[56]. This Schulte achieved by noting a point within the cross-section at which elastic and stationary stresses were coincident. By assuming constant stress at this point, and performing a creep test at that stress it was possible to make accurate predictions of beam deflections.

The first paper to treat the reference stress as a general principle was the contribution by Anderson et al[30] in 1962. They considered the deformation rate of beams composed of a material where the stress index n was itself some function of stress and suggested that a sufficiently accurate estimation of deformation rate could be obtained from a creep test at a 'representative stress'. In other words, providing the creep test data was obtained at a suitable stress level the variation of n with σ was not important in practice.

Marriott and Leckie[31] defined points in a structure where the stresses are almost invariant with time as 'skeletal points' and their associated stresses as 'skeletal stresses'. They argued that since the stationary state deformation rate in the structure was directly proportional to the stationary creep strain rate at any point in the structure, an acceptable estimate of the creep deformation would be obtainable from creep data derived from a creep test at the 'skeletal stress'. This idea is similar to that of Anderson et al since in both cases the 'skeletal stress' and 'representative stress' were obtained by inspection. For the structures considered by Marriott and Leckie deformation due to redistribution of stress was small, and the approximate deformation given by adding the stationary state deformation, obtained from a test at the 'skeletal stress', to the initial elastic deformation.

Mackenzie[42] has devised a more systematic method of extracting an appropriate 'reference stress' from consideration of the normalised

deformation rate in the stationary state. He considered a selection of standard structures and assuming a Norton type creep law, compared the deformation rate for some value of n to the corresponding rate for $n = 1$. He was then able to find a 'reference stress' such that the normalised deformation rate was equal to unity. For these structures it was found that a suitable choice of reference stress allowed the stationary state deformation rate of a structure to be predicted within approximately 10 per cent using only the data from a single tensile test. Mackenzie gives a physical interpretation to his method by noting that the position of the 'skeletal point' coincides with the position at which the stress in the stationary state is independent of the value of n and therefore the reference stress technique should give acceptable estimations of deformation for structures composed of materials where n is stress dependent. This is consistent with the observations of Calladine and Drucker[33] mentioned previously in Chapter 2.

A serious limitation to Mackenzie's technique is that it is limited to structures for which analytical expressions for stationary state deformation rates are available whereas for many structures of practical interest such solutions are unobtainable. Fortunately, as will be shown later, the extension of this technique to include some of the theorems of plasticity is reasonably straightforward.

Leckie[44] improved the method of obtaining the reference stress suggested by Mackenzie and showed that by equating the initial elastic strain energy and the energy dissipated in the stationary state for the particular structure with the corresponding quantities for a uniaxial tensile specimen the value of the reference stress can be determined. This method can be illustrated by considering the classic example of a beam of rectangular section under flexure. The moment-curvature expression is given by

$$\kappa = \kappa_e + \left(\frac{2n+1}{n}\right)^n 2^{n+1} \left(\frac{k}{b^n d^{2n+1}}\right) M^n \quad f_2(t) \tag{4.3}$$

assuming that terms due to stress redistribution can be neglected.

Leckie has shown that it is convenient to express the above results in terms of a single uniaxial specimen of volume ψbd and subjected to a stress

$$\sigma_R = \frac{\phi M}{bd^2} , \tag{4.4}$$

then the corresponding strain is

$$\epsilon_R = \frac{\phi M}{Ebd^3} + k\left(\frac{\phi M}{bd^3}\right)^n f(t) \tag{4.5}$$

An energy balance per unit length of beam is given by

$$\psi bd\sigma_R\epsilon_R = M\kappa \tag{4.6}$$

Equating the elastic and creep energy components of the structure, and uniaxial specimen yields

$$\phi = \left[\frac{2n+1}{n}\right]^{n/(n+1)} \frac{2}{3^{1/(n-1)}} , \quad \psi = \frac{12}{\phi^2} \tag{4.7}$$

From these results the expression for κ becomes

$$\kappa = \frac{12}{\phi d} \epsilon_R \tag{4.8}$$

The curvature κ is obtained from the above expression by finding the strain ϵ_R associated with the stress σ_R. For a given value of n, ϕ can be calculated from equation (4.7) and the corresponding tensile test conducted at the stress given by equation (4.4). The value of ϕ for the beam is almost independent of n and an exact knowledge of n is not required if ϕ is assumed to be 4.1 .

A method for deriving reference stresses from numerical solutions has been devised by Sim[43] and is as follows:

Any creep deflection U can be expressed as

$$U = U(k\sigma^{n}\ ,\ \text{dimensions})\ f_2(t) \tag{4.9}$$

This expression can be non-dimensionalised by

$$U = (k\sigma'^{n})\ .\ f_2(t)\ .\ g(\text{dimensions})\ .\ \bar{U}\left[\left(\frac{\sigma}{\sigma'}\right)^{n}\right], \tag{4.10}$$

where $\bar{U}$ is a function of loading and linear dimensions, $f_2(t)$ is a time function for the creep curve and g is purely a function of dimensions. The function $\bar{U}\left[\left(\frac{\sigma}{\sigma'}\right)^{n}\right]$ is a non-dimensional deflection to be determined by the numerical analysis.

In general $\bar{U}$ varies with n and the degree of variation differs according to σ'. When plotted on semi-log paper the variation of $\bar{U}$ with n is approximately linear and the particular value of σ' which results in zero slope is the desired reference stress σ_R since the deflection $\bar{U}$ will then be insensitive to n. Only two computations are required to find σ_R. Putting

$$\sigma_R = \phi'\ \sigma' \tag{4.11}$$

where ϕ' is some ratio to be determined. Substitute from (4.11) to (4.10) noting that $\bar{U}$ is an n-degree homogeneous function of σ

$$\bar{U}\left[\left(\frac{\sigma}{\sigma'}\right)^{n}\right] = \phi'^{n}\ \bar{U}\left[\left(\frac{\sigma}{\sigma_R}\right)^{n}\right]. \tag{4.12}$$

By computing $\bar{U}(\sigma/\sigma')^{n}$ using an arbitrary choice of σ', Sim chose two values of n, for example n_1 and n_2, and equated

$$\bar{U}[(\sigma/\sigma_R)^{n_1}] = \bar{U}[(\sigma/\sigma_R)^{n_2}]\ . \tag{4.13}$$

This equality gives

$$\phi' = \{\bar{U}[(\sigma/\sigma')^{n_2}]/\bar{U}[(\sigma/\sigma')^{n_1}]\}^{1/(n_2-n_1)}. \tag{4.14}$$

Sim found that reference stresses that are least sensitive to n can be calculated by equating non-dimensional deflections for two n-values

other than $n = 1$. The range of insensitivity of reference stresses calculated in this manner was found to differ from one structure to another but over the range of n, reference values obtained between n equals 3 to 9 were reasonably constant.

In the techniques described references stresses were derived from a constitutive law of the n power form. The main advantage of this form is its relative simplicity in analytical treatment. Since the reference parameters have appeared to be only 'weakly' dependent on n, this behaviour can be taken as an indication of the reference stress being independent of the creep law. The desirability of showing this analytically was pointed out by Marriott[55].

Some work on this has been done by Fairbairn[58], who applied the reference stress obtained from Norton's law to thick-walled tubes in bending, where the tubes were made of materials following different creep laws. For both circular and elliptical section tubes it was shown that a reference stress derived from Norton's law used in conjunction with either exponential or hyperbolic sine forms of creep law produced estimates of bending moments to within 2 per cent of analytically derived values. These results are similar to those obtained by Johnsson[59] who derived a reference stress and scaling factor for a general two-parameter creep law. He demonstrated that for a beam under flexure and a two-bar structure the reference parameters derived from Norton's law are also applicable for a Prandtl[20] or Dorn[22] type creep law and that the resulting errors in deformation rate are within a range fully acceptable from a design point of view. The use of a Norton type creep law to provide a theoretical simplification to more complex creep laws would seem well justified.

The extension of the above techniques to identify reference temperatures for conditions where temperature gradients are present has received little attention. To the author's knowledge, the only attempt to rectify this has

been made by Sim[60]. He has extended his analytical procedure to provide a means of identifying reference temperatures for thick cylinders and spheres subjected to internal pressures and a negative temperature gradient in the radial direction. The only difference in the analysis is caused by the introduction of an exponential temperature term otherwise the procedure remains unaltered. By definition the reference temperatures and reference stresses are located at the same dimensionless radius within the thickness of the wall. No real conclusions may be deduced from this technique since there exists no experimental verification, or application to other structures.

4.2.2. Approximate Estimates of Reference Stresses.

A drawback of the reference stress technique is the effort required to calculate reference values in anything but trivial examples. If an order of magnitude check is only required, even an approximation to the reference stress is as useful as the exact value. Several workers, notably Leckie, Ponter and Sim have shown in their numerous publications that results from the theorems of perfect plasticity can prove useful in determining reference values. It has been proposed that for a structure subjected to an applied load P, a reference stress may be given by the expression

$$\sigma_R = P/P_L \, \bar{\sigma}_y \qquad (4.15)$$

where P_L is the ultimate load for the structure and $\bar{\sigma}_y$ is the yield stress. Sim has shown that the correlation between the reference values obtained using equation (4.15) and those using finite n creep solutions is good for a spinning disc, and a cylinder and sphere under internal pressure. By utilising the results of perfect plasticity, reference stresses can be determined with reasonable accuracy. However, a knowledge

of σ_R is in itself insufficient to allow predictions to be made of structural deformation. As a minimum the dimensionless parameter used by Sim to relate the structural and uniaxial deformation requires to be known and cannot be determined using only the plasticity theorems.

The work conducted by Leckie and Ponter has shown that equation (4.15) may be used in conjunction with the results of a steady-state creep calculation to give an upper bound on structural behaviour.

In addition, by its form, equation (4.15) implies that the results of a short-time (elastic-plastic) test on a structure may be used to predict the long time (elastic-plastic-creep) behaviour of the structure. Such an approach is particularly attractive for structures which because of their asymmetry or other factors are not amenable to analysis. By conducting a short-time test on such a structure and comparing it to the results of a tensile test conducted at a comparable strain rate on a specimen of the structural material the parameters necessary for use in a reference stress approach can be evaluated. Knowing these parameters, the creep deformation of the structure may be predicted if the creep strain-time response associated with the reference stress is known.

Some experimental results that support the above approach have been reported by Sim and Penny[57], Leckie and Ponter[49] and Williams[45] and good agreement between experimental and theoretical predictions found.

4.3. Analyses of Some Simple Structures

4.3.1. Reference Values for Steady Loading.

It has been shown in the preceding sections the manner in which reference stresses have been obtained for structures under isothermal conditions. In the following examples the reference stress approach suggested by Mackenzie[42] will be extended to define reference temperatures. The structures considered are; the classic example of a beam under

flexure, a propped cantilever beam and the creep bending of straight tubes which has recently aroused interest[58].

(a) Beam under Flexure.

The stationary curvature rate-moment relationship for the flexure problem may be written in the form

$$\dot{\kappa} = \frac{k}{d}\left[\frac{2M}{bd^2}\right]^n I_B \tag{4.16}$$

where I_B is given by

$$I_B = \left[\int_0^1 2\,(\phi+x)^{1/n}.x.\exp\{\Delta H/nR\theta(x)\}dx\right]^n \tag{4.17}$$

In the isothermal case I_B reduces to

$$I_B = 2\left[\frac{2n+1}{n}\right]^n / \exp(\Delta H/R\theta_i) \tag{4.18}$$

where θ_i is the constant temperature.

The moment-curvature rate relationship (4.16) may be rewritten

$$\dot{\kappa} = \frac{I_B}{d}\,\dot{\epsilon}(\sigma), \tag{4.19}$$

by direct use of the uniaxial creep strain rate equation with $\sigma = (2M/bd^2)$. Thus the curvature rate may be calculated from the strain rate derived from a uniaxial test conducted at a stress σ providing the stress index n is known. A reference stress that is independent of n requires that the function I_B be also independent. Such a reference stress may be evaluated by introducing a multiplier λ so that equation (4.16) becomes

$$\dot{\kappa} = \frac{k}{d}\left[\frac{2M}{\lambda bd^2}\right]^n (\lambda^n I_B). \tag{4.20}$$

A value of λ may now be found such that $(\lambda^n I_B)$ remains insensitive to n. The exact value of λ depends on the procedure adopted and in the following calculation values of $(\lambda^n I_B)$ are equated for $n = 3$ and

$n = 11$. This gives a value of $\lambda = 0.498$ and a variation of $(\lambda^n I_B)$ with n shown in Table 4.1.

If $\lambda^n I_B = 3.16$ is selected, the mid-surface curvature rate is given by

$$\dot{\kappa} = \frac{3.16}{d}\,\dot{\varepsilon}(\sigma_R), \tag{4.21}$$

where $\dot{\varepsilon}(\sigma_R)$ is the uniaxial creep strain rate corresponding to the reference stress $\sigma_R = 4.01\ M/bd^2$.

This reference stress lies close to the upper bound reference stress of Ponter and Leckie[35,49],

$$\sigma_R = \frac{M}{M_L}\,\bar{\sigma}_y = \frac{4M}{bd^2}\ ,$$

where M_L denotes the limit load corresponding to a homogeneous yield stress $\bar{\sigma}_y$.

The maximum error incurred in selection of either the maximum or minimum value of $\lambda^n I_B$ is of the order of one per cent. Thus for a beam of given dimensions, b and d , and subjected to end moments M , the deformation may be related to the strain rate of a uniaxial test at a stress σ_R by equation (4.21) and the value of $\dot{\kappa}$ obtained will be within one per cent of the actual curvature rate whatever the value of n within the range $3 < n < 11$.

To evaluate the problem when <u>non-isothermal</u> conditions are present it is required that in the limit the non-isothermal solutions reduce to the isothermal case such that the reference temperature obtained equals the isothermal value, θ_i . The method used to determine the reference values assumes a knowledge of the isothermal reference stress.

Under steady state thermal conditions the isothermal reference stress is adopted and

$$\dot{\kappa} = 3.16\,\frac{k}{d}\left[\frac{4.01M}{bd^2}\right]^n \frac{I_B}{3.16(4.01)^n}\ . \tag{4.22}$$

This ensures that under isothermal conditions

$$\frac{I_B}{3.16(4.01)^n} = \exp(-\Delta H/R\theta_i) \quad . \tag{4.23}$$

A 'reference temperature' $\bar{\theta}$ may be defined by

$$\bar{\theta} = \Delta H/R \; \ell n\left[\frac{3.16(4.01)^n}{I_B}\right] \tag{4.24}$$

which is consistent with the isothermal case. However it is found that $\bar{\theta}$ varies as a function of n and clearly this definition of a reference temperature is deficient. A further multiplier μ is introduced which makes $\bar{\theta}$ equal for $n = 3$ and $n = 11$ and

$$\dot{\kappa} = \frac{3.16}{d} k(\mu\sigma_R)^n \exp(-\Delta H/R\theta_R) \tag{4.25}$$

where θ_R is a reference temperature independent of n and defined by

$$\theta_R = \Delta H/R \; \ell n\left[\frac{3.16(4.01\mu)^n}{I_B}\right] \tag{4.26}$$

The curvature rate expression

$$\dot{\kappa} = \frac{3.16}{d} k\left[\frac{4.01\mu M}{bd^2}\right]^n \exp(-\Delta H/R\theta_R) \tag{4.27}$$

may be re-expressed as

$$\dot{\kappa} = \frac{3.16}{d} \dot{\varepsilon}(\mu\sigma_R, \theta_R) \tag{4.28}$$

where $\dot{\varepsilon}(\mu\sigma_R, \theta_R)$ is the uniaxial creep strain rate corresponding to a uniaxial test at a modified isothermal reference stress, $\mu\sigma_R$, and a uniform reference temperature θ_R.

The effectiveness of the above procedure may be judged by evaluating values of $\theta_R(\theta_2, \theta_1)$ at different values of n since by the procedure adopted it is only exact for $n = 3$ and $n = 11$.

The results in Table 4.2 are for a linear temperature gradient through the beam depth and a lower surface temperature $\theta_1 = 300°K$. The creep activation energy is taken as 113 KJ/mole.

It is seen that the values of θ_R are remarkably insensitive to n. As values of θ_R are higher for intermediate values of n a 'conservative' estimate of $\dot{\kappa}$ may be obtained by selection of the maximum value as the reference temperature.

In Fig.4.1 the variation of θ_R with θ_2 is shown and it can be seen that the variation remains close to linear over a range of θ_2. This implies that the position of the reference temperature remains fixed and independent of θ_2. It may be noted that this position is not close to any of the points where the stress profiles approach each other.

In Fig.4.2 the variation of $\mu\sigma_R$ with θ_2 is shown. The value of μ remains reasonably close to unity for quite large temperature differences. For example $\mu = 0.958$ for $(\theta_2-\theta_1) = 120°K$.

(b) Tube under Flexure.

The stationary state curvature rate for a straight tube of circular section subjected to end moments M is given by

$$\dot{\kappa} = \frac{k}{r_o}\left[\frac{M}{4r_o^3}\right]^n \cdot I_T \qquad (4.29)$$

where $2r_o$ is the external diameter,

$$I_T = \left[\int_{z=0}^{z=\pi/2}\int_{r_i/r_o}^{1} \bar{r}^{\frac{2n+1}{n}} (\sin z)^{\frac{n+1}{n}} \exp[\Delta H/nR\theta(\bar{r})]dz d\bar{r}\right]^{-n}, \qquad (4.30)$$

$\bar{r}$ is a dimensionless radius and r_i is the internal radius. The temperature at any point in the surface of the tube is defined by $\theta(\bar{r})$.

A full analysis is given in section 10.3.

For isothermal conditions a reference stress may be obtained by a procedure similar to that for the beam problem and the curvature rate given by

$$\dot{\kappa} = \frac{\lambda^n I_T}{r_o} \dot{\varepsilon}(\sigma_R) \ , \qquad (4.31)$$

where $\sigma_R = \left[\frac{M}{4\lambda r_o^3}\right]$.

The variation of λ and $\lambda^n I_T$ with r_i/r_o is shown in Figs.4.3 and 4.4. For any given value of r_i/r_o the maximum difference in $\lambda^n I_T$ is less than one per cent. Some typical values are shown in Table 4.3.

Figs. 4.3 and 4.4 therefore provide simple design charts for calculating the curvature rate for any thickness of tube using the appropriate tensile data.

Spence has examined the creep bending of curved pipes and used energy methods together with thin shell theory, to obtain lower[63] and upper [64] bounds on curvature rates. He obtained a reference stress σ_{R_s} given by

$$\sigma_{R_s} = 1.019 \frac{M}{r_o^3} (1 - r_i^2/r_o^2)(1 + r_i/r_o)^{-1} \qquad (4.32)$$

In the Fig.4.5 reference values previously obtained are replotted as $\log\left(\frac{\sigma_R r_o^3}{M}\right)$ against r_i/r_o for convenience. The broken line represents Spence's solution. For values of $r_i/r_o > 0.5$ the solutions are equivalent but at lower values they diverge and Spence's solution forms an upper bound. For example at $r_i/r_o = 0.1$, $\sigma_R = 0.75\ M/r_o^3$ and $\sigma_{R_s} = 0.95\ M/r_o^3$.

An upper bound on the reference stress derived from the rigid perfectly plastic solution is given by

$$\sigma_R^u = 0.75 \frac{M}{r_o^3} \left(1 - \frac{r_i}{r_o}\right)^{-1} \qquad (4.33)$$

and provides a solution that closely approximates the exact solution to within 0.5 per cent for all values of r_i/r_o .

In the non-isothermal case with a temperature gradient through the tube the moment-curvature rate may be written

$$\dot{\kappa} = \frac{k\zeta}{r_o} \left[\frac{\mu M}{4\lambda r_o^3}\right]^n \exp(-\Delta H/R\theta_R) \qquad (4.34)$$

where ζ represents the isothermal value of $\lambda^n I_T$ for a given r_i/r_o and

$$\theta_R = \Delta H/R \; \ell n \left[\frac{\zeta \mu^n}{I_T \lambda^n}\right] . \qquad (4.35)$$

such that θ_R is virtually independent of n for $3 \leq n \leq 11$.

For steady heat flow the temperature at radius $\bar{r}$ is given by

$$\theta(\bar{r}) = \theta_2 + \frac{\log(\bar{r}.r_o/r_i)}{\log(r_o/r_i)} \{\theta_1 - \theta_2\} \qquad (4.36)$$

where θ_2 and θ_1 are internal and external temperatures respectively.

Consider, as an example, a tube with $r_i/r_o = 0.5$, $\theta_2 = 350°K$ and $\theta_1 = 300°K$.

The values of λ and ζ are obtained from Figs. 4.3 and 4.4 at $r_i/r_o = 0.5$, (i.e. $\lambda = 0.29$, $\zeta = 1.66$) , and the isothermal reference stress is given by

$$\sigma_R = 0.86 \frac{M}{r_o^3} \qquad (4.37)$$

and

$$\dot{\kappa} = \frac{1.66}{r_o} \dot{\varepsilon}(\sigma_R) . \qquad (4.38)$$

Solution of the problem gives $\mu = 0.94$ and the variation of θ_R with n shown in Table 4.4. If it is assumed that $\theta_R = 311.2°K$, the curvature rate derived from equation 4.34 and the curvature rate derived from

$$\dot{\kappa} = \frac{\zeta}{r_o} \dot{\varepsilon}(\mu\sigma_R, \theta_R), \qquad (4.39)$$

differ by at most 4 per cent.

In Figs. 4.6 and 4.7 the variation of μ and θ_R with r_i/r_o are shown for a range of θ_2. The use of these figures together with the isothermal charts provide the constants to enable the curvature rate to be defined in terms of the reference values for the necessary restricted range of parameters.

In Fig.4.8 the position of the reference temperature is plotted against θ_2 for a range of r_i/r_o. It is seen that whereas in Sim's procedure the reference temperature remains at a fixed position regardless of the magnitude of the temperature gradient, in this method the position varies as some function of θ_2.

(c) Propped Cantilever Beam.

The creep energy dissipation rate for a propped cantilever beam subjected to a point load at the centre of span can be calculated from

$$\dot{D}_c = \int_0^{\ell} M\dot{\kappa}dx \qquad (4.40)$$

where x is the distance along the beam and

$$\dot{\kappa} = k\, M^n \exp(-\Delta H/R\theta(x)) \qquad (4.41)$$

The single redundancy is taken as the prop reaction at the simply supported end and the problem solved for the deflection rate $\dot{U}$ under the applied load by numerical integration. This is fully described in section 10.3.

In the isothermal case computation gives

$$\dot{U} = 0.0468\, \ell^2\, \dot{\kappa}(M_R) \qquad (4.42)$$

where the reference moment M_R is

$$M_R = P\ell/6.757 \qquad (4.43)$$

Equation (4.43) is exact for $n = 3$ and 11, and is approximately 10 per cent conservative on deflection rate for $n = 7$.

The propped cantilever is of rectangular section, width b and depth d, and the above equation can thus be expressed in terms of a reference stress by direct use of

$$\sigma_R = 4.01 \frac{M_R}{bd^2} .$$

Then

$$\dot{U} = 0.148 \frac{\ell^2}{d} \dot{\varepsilon}(\sigma_R) , \qquad (4.44)$$

where

$$\sigma_R = 0.593 \, P\ell/bd^2 .$$

In the problem with a temperature gradient along the propped cantilever, Fig.3.3, reference values may be derived using the same procedure as in the problems already discussed and a deflection rate obtained in the form

$$\dot{U} = 0.0468 \, k\ell^2(\mu M_R)\exp(-\Delta H/R\theta_R) , \qquad (4.45)$$

where

$$\theta_R = \Delta H/R \; \ell n\left[\frac{0.0468\mu^n}{I_{PC}}\right] . \qquad (4.46)$$

The reference stress θ_R reduces to θ_i for isothermal conditions. The displacement rate is given in terms of a uniaxial creep strain rate by

$$\dot{U} = 0.148 \frac{\ell^2}{d} \dot{\varepsilon}(\mu\sigma_R, \theta_R) . \qquad (4.47)$$

providing there is no temperature gradient through the section.

In Table 4.5 the computed results for a propped cantilever with a negative temperature gradient along the beam length, as in Chapter 3, are given. The temperature at the simply supported end is constant at $\theta_1 = 300°K$ and the maximum temperature θ_2 acts at the encastré end.

These values provide deformation rates within 15 per cent of the exact solution and therefore it would appear that this procedure used to determine the reference quantities is less satisfactory for this statically indeterminate beam problem.

4.3.2. Approximate Reference Values.

It has been shown that use of a rigid perfectly plastic solution provides reasonably accurate predictions of stationary state deformation rates for structures under isothermal conditions. However, under non-isothermal conditions this solution provides a highly conservative bound and a closer approximation may be obtained if the yield stress is assumed to be a function of temperature. The function adopted is the intermediate plastic solution previously discussed in Chapter 3,

$$\sigma = \sigma_o \exp \frac{\Delta H}{nR} \left(\frac{1}{\theta} - \frac{1}{\theta_o}\right) . \qquad (4.48)$$

Under isothermal conditions $\sigma = \sigma_o \to \bar{\sigma}_y$.

As in the previous section, reference values will be calculated using the procedure previously adopted for the beam and propped cantilever examples.

(a) Beam under Flexure.

An upper bound on the stationary state curvature rate obtained from a stress function of the form (4.48) is given by

$$\dot{\kappa} \leqslant \frac{k}{d} \left(\frac{M}{bd^2}\right)^n I_B^u \qquad (4.49)$$

where I_B^u is derived from conditions of compatibility and equilibrium (section 10.3).

In the isothermal case

$$I_B^u = 4^{n+1} \exp(-\Delta H/R\theta_i) \qquad (4.50)$$

and

$$\dot{\kappa} \leqslant \frac{4}{d} \dot{\varepsilon}(\sigma_R^u, \theta_i) \qquad (4.51)$$

with

$$\sigma_R^u = \frac{4M}{bd^2} = \frac{M}{M_L}\bar{\sigma}_y \ .$$

In this example the multiplier λ introduced is unity since I_B^u is independent of n .

To evaluate the problem when non-isothermal conditions are present it is required as in the exact analysis, that in the limit the non-isothermal solutions should reduce to the isothermal case such that the reference values obtained are equivalent to the isothermal values. As in the exact solution a further multiplier μ is introduced so that

$$\dot{\kappa} \leqslant \frac{4}{d}\dot{\bar{\varepsilon}}(\mu\sigma_R^u, \theta_R^u) \qquad (4.52)$$

where

$$\theta_R^u = \Delta H/R \ \ell n \left[\frac{4\mu^n}{I_B^u}\right] . \qquad (4.53)$$

The variation of θ_R^u with n is tabulated in Table 4.6 for a range of values of θ_2, and as in the exact solution the percentage variation is small.

In Table 4.7 the reference values obtained from the above intermediate plastic solution and those of the exact solution (section 4.3) are tabulated. It is seen that the intermediate plastic solution provides a good approximation to the exact reference values.

(b) Propped Cantilever Beam.

The structure is identical to that considered in section 4.3.1. The upper bound inequality (3.9) achieves the form

$$\dot{U} \leqslant k\ell^2 \ (P\ell)^n \ I_{PC}^u \qquad (4.54)$$

where I_{PC}^u is obtained from the creep energy dissipation rate assuming a yield moment of the form

$$M = M_o \exp\left[\frac{\Delta H}{nR}\left(\frac{1}{\theta} - \frac{1}{\theta_o}\right)\right] . \qquad (4.55)$$

In the isothermal case the procedure yields $\lambda = 6.75$ and a variation of $\lambda^n I^u_{PC}$ given in Table 4.8. Inequality (4.54) may be rewritten

$$\dot{U} \leqslant 0.047\ \ell^2\ \dot{\kappa}(M^u_R, \theta_i) \qquad (4.56)$$

where $M_R = \frac{P\ell}{6.75}$ and $\dot{\kappa}(M_R, \theta_i)$ is the creep curvature rate corresponding to a moment M_R and isothermal temperature θ_i .

For a temperature gradient along the length of the propped cantilever the central deflection rate is given by

$$\dot{U} \leqslant 0.047\ \ell^2\ \dot{\kappa}(\mu M^u_R, \theta^u_R) \qquad (4.57)$$

and the variation of μ and θ_R with θ_2 given in Table 4.9.

This table can be compared directly with Table 4.5 where it is seen that the higher reference temperature obtained in the approximate analysis yields a lower μ thereby tending to equalise the creep rates towards those of the exact solution. For $\theta_2 = 420°K$ the difference between the two solutions is approximately 30 per cent.

4.4. Discussion.

The calculations presented show that reference stresses and reference temperatures can be found for structures subjected to temperature gradients. The reference values are however slightly less accurate than those for isothermal conditions. The method adopted in both the 'exact' and approximate solutions require calculation of the isothermal reference stress σ_R . This is then modified by a quantity μ which provides a reduction in σ_R such that at θ_R the normalised creep strains are equal for $n = 3$ and $n = 11$. It is found that the reference temperature is always closer to the minimum temperature and therefore if design were based on the isothermal

reference stress and the maximum temperature, the resulting deformation rate would be highly conservative. A knowledge of the deformation in terms of the reference values clearly provides a considerable advantage over isothermal solutions.

The suggested technique appears to require an exact knowledge of the temperature dependence of creep through the activation energy ΔH, and therefore the reference temperatures obtained are not reference quantities as defined in the true original sense. Numerous calculations were performed with different values of ΔH and θ_1 and it was found that in the examples given, a variation of 30 per cent in ΔH produced a variation in θ_R of less than 4 per cent. It would appear that θ_R is only slightly dependent on ΔH and θ_R can therefore be considered a 'true' reference temperature.

The potentially most useful application of the reference stress/temperature approach is for structures which are subjected to variable loads and temperatures. The advantage of a reference stress/temperature approach in such cases is that the predictions of the creep behaviour of a structure may be based directly on creep strain-time data obtained from a simple test conducted on a specimen of the material loaded by the reference stress, $\mu\sigma_R(t)$, and the reference temperature $\theta_R(t)$. Implicit in such an approach is the recognition that the main uncertainty about predicting the creep behaviour of structures under variable loading is the material creep behaviour. By basing the predictions of the structure's behaviour directly on test data the uncertainties involved in trying to analytically define the material creep behaviour are avoided. The results presented in this chapter may be used for variable load/temperature problems providing ratchetting effects are either avoided or taken into account.

n	$\lambda^n I_B$
3	3.144
5	3.156
7	3.163
9	3.157
11	3.144

Table 4.1

Variation of $\lambda^n I_B$ with n for a beam under flexure

n	θ_R (300)	θ_R (360)	θ_R (420)	θ_R (480)
3	300.0	328.6	351.6	370.9
5	300.0	328.7	352.4	371.8
7	300.0	328.7	352.8	372.4
9	300.0	328.6	352.2	371.6
11	300.0	328.6	351.6	370.9

Table 4.2

Variation of reference temperature with n for a beam with $\theta_1 = 300°K$

n	r_i/r_o=0.1	r_i/r_o=0.5	r_i/r_o=0.9
3	1.792	1.650	1.382
5	1.807	1.660	1.388
7	1.807	1.660	1.388
9	1.801	1.656	1.386
11	1.792	1.650	1.382

Table 4.3

Variation of $\lambda^n I_T$ with n for a tube of ratio of radii r_i/r_o

n	θ_R °K
3	310.9
5	311.6
7	311.6
9	311.3
11	310.9

Table 4.4

Variation of θ_R with n for the tube with θ_2=350°K and r_i/r_o=0.5

θ_2 °K	μ	θ_R °K
300	1.00	300
360	0.98	337.1
420	0.97	375.3
480	0.95	417.2

Table 4.5

Variation of μ and θ_R with θ_2 for the propped cantilever

n	θ_2=300	θ_2=360	θ_2=420	θ_2=480
3	300	330.3	355.0	373.5
5	300	329.9	356.0	377.3
7	300	329.9	355.7	376.5
9	300	330.1	355.3	374.9
11	300	330.3	355.0	373.5

Table 4.6

Variation of θ_R^u with n for the beam under flexure

θ_2	θ_1	Exact Soln.		Intermediate Soln.	
		$\frac{\mu\sigma_R bd^2}{M}$	θ_R	$\frac{\mu\sigma_R bd^2}{M}$	θ_R
300	300	4.0	300	4.0	300
360	300	4.0	328.6	4.0	330.3
420	300	3.8	351.6	3.9	356.0
480	300	3.6	370.9	3.7	377.3

Table 4.7

Comparison of exact and approximate reference values

n	λ^n
3	0.047
5	0.043
7	0.042
9	0.044
11	0.047

Table 4.8

Variation of $\lambda^n I_{PC}^u$ with n for the propped cantilever under isothermal conditions

θ_2	μ	θ_R^u
300	1	300
360	.98	338.4
420	.93	379.2
480	.88	424.1

Table 4.9

Variation of μ and θ_R^u with θ_2 for the propped cantilever

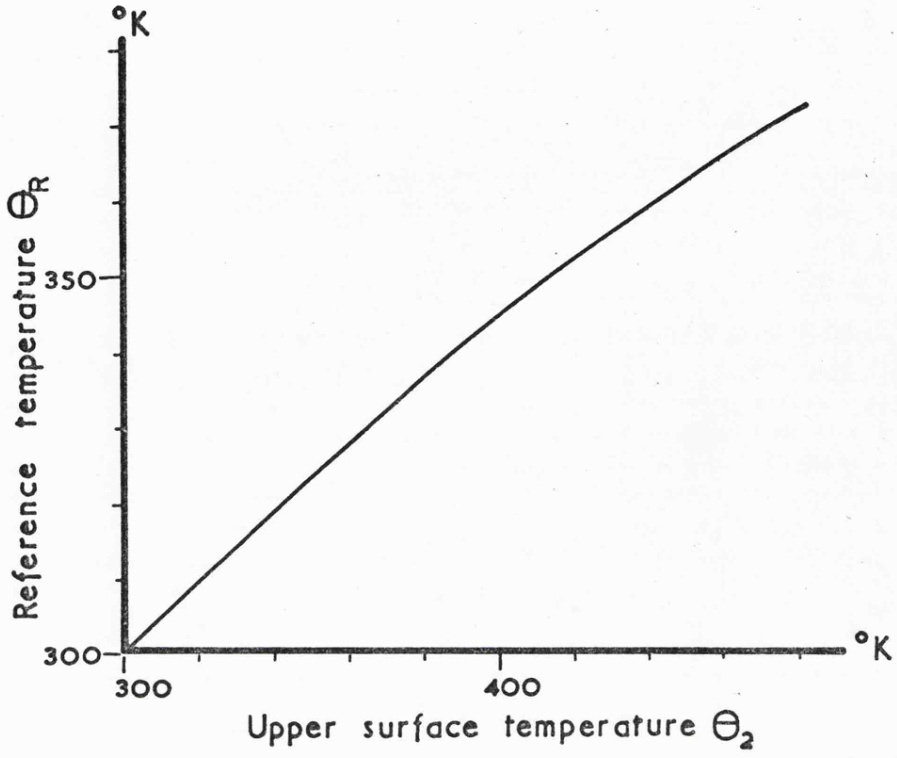

Fig 4.1 Variation of Θ_R with Θ_2 for the beam

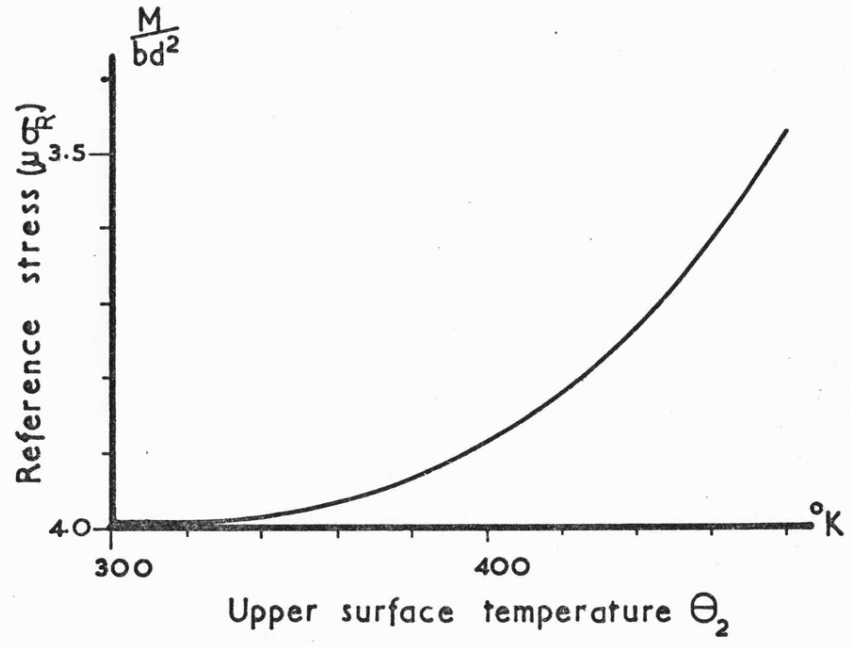

Fig 4.2 Variation of reference stress with Θ_2 for the beam

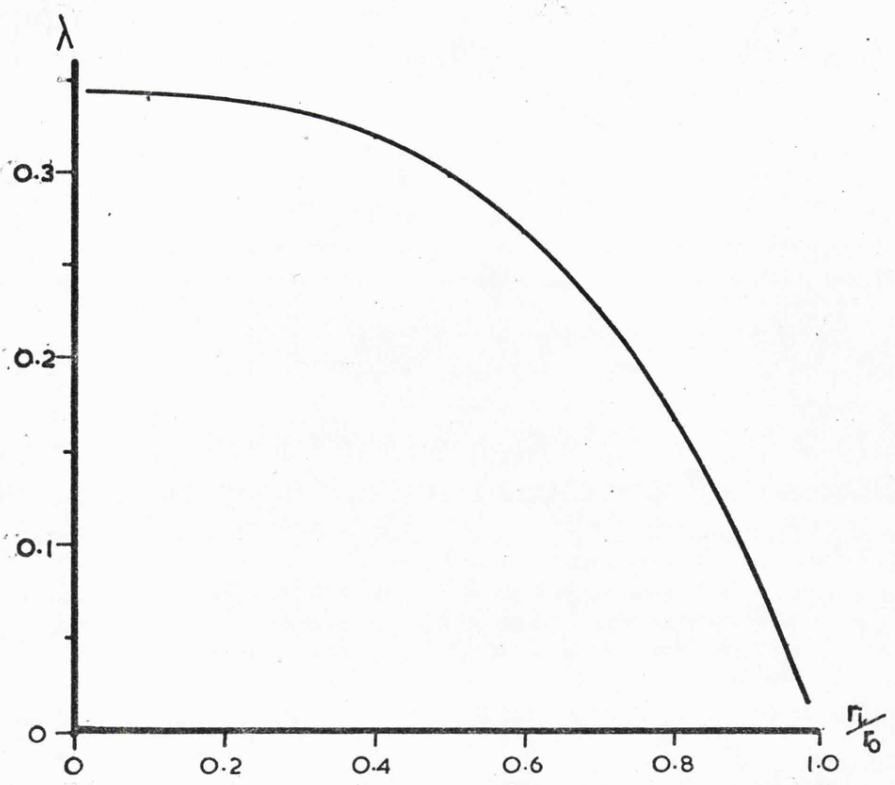

Fig 4.3 Variation of λ with r_i/r_o for a tube

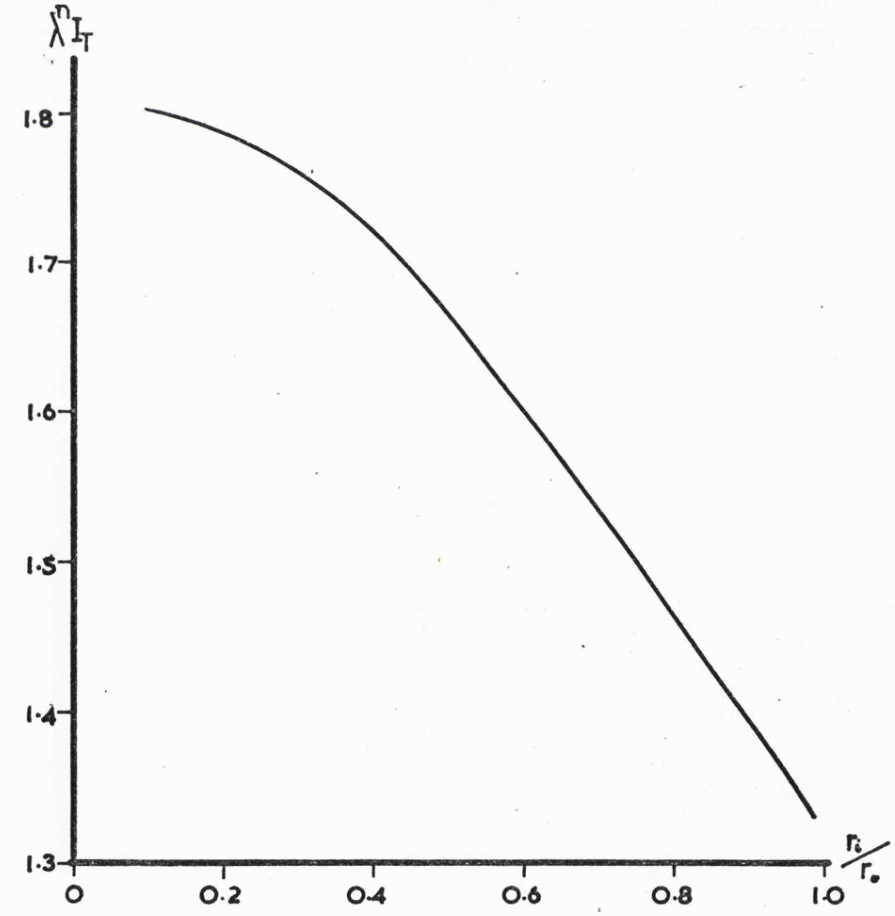

Fig 4.4 Variation of $\lambda^n I_T$ with r_i/r_o for a tube

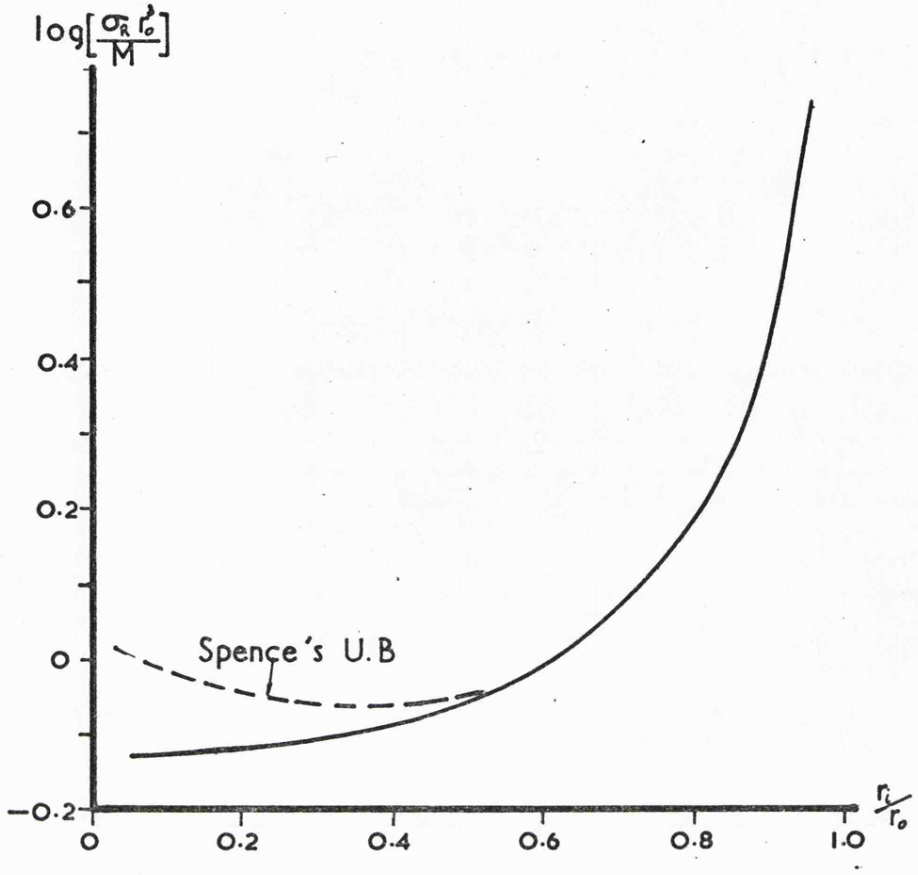

Fig 4.5 Design diagram for a tube under flexure

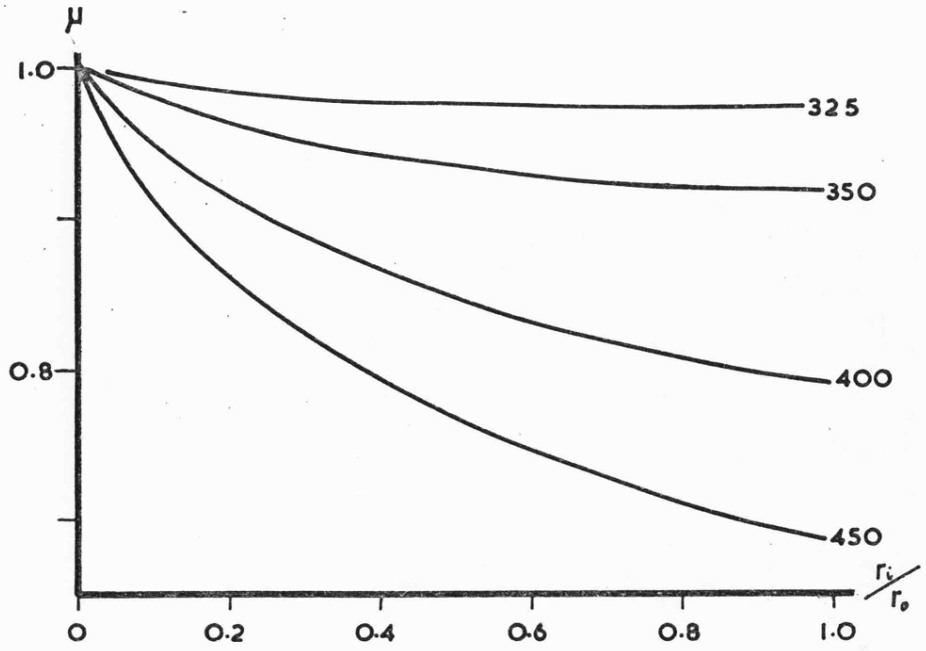

Fig 4.6 Variation of μ with r_i/r_o for a tube under a temperature gradient

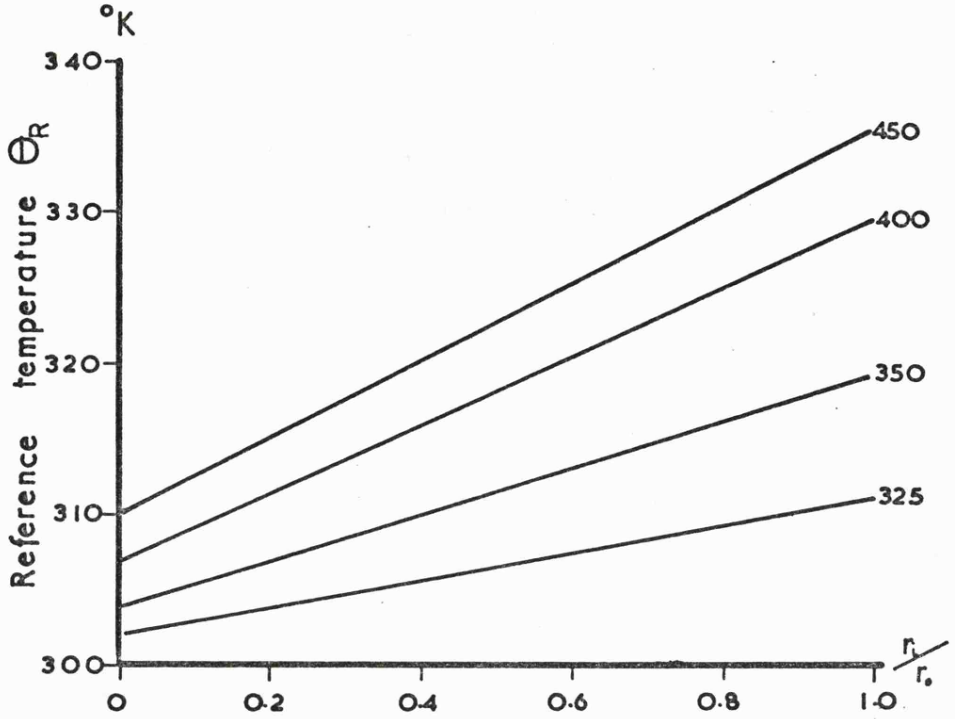

Fig 4.7 Variation of Θ_R with $\frac{r_i}{r_o}$

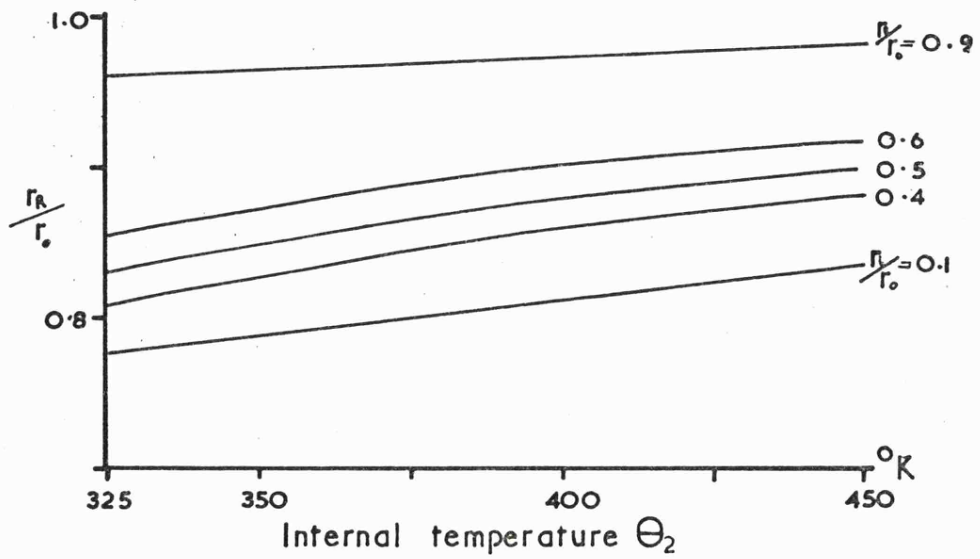

Fig 4.8 Variation of position of Θ_R with Θ_2

Chapter 5

Some Results of Testing a Simple Structure Subjected to a Temperature Gradient and Steady Loads

5.1. Introduction.

To verify the use of the reference stress, reference temperature technique described in Chapter 4, a series of experiments were conducted on propped cantilever beams subjected to constant loads and a temperature gradient. The results are compared with predictions based on uniaxial data obtained at the reference temperature.

Sim and Penny[57] have reported some results on testing pure aluminium beams and circular plates subjected to constant loading during creep. The room temperature test results were compared with predictions based on a reference stress approach and showed close agreement. This is not surprising since the tests were conducted at load levels where the applied loads $P \leq n/(n+1).P_L$ and consequently the influence of plastic strains on the overall deformation was small. This can be illustrated from the results of the tests on beams under flexure where the maximum outer fibre stress was of the order of 15000 lb/in^2 . Since the yield stress of the material is approximately 16000 lb/in^2 the ratio of the maximum applied moment to the moment to cause plastic collapse $M/M_L = 0.63$ and therefore, as $n=4$ for this material at room temperature, the contribution of plastic strains to the overall deformation is likely to be small for $M/M_L < 0.8$.

Leckie and Ponter[49], and Williams[45] have reported tests on pure aluminium and aluminium alloy RR58 portal frames under both steady and variable loads. Reference stresses were derived from a knowledge of the limit state solution and uniaxial tests at the appropriate stress levels were performed. It was shown that the analytically predicted deformation

rates were in close agreement with those gained experimentally even when loads on the structure were > $n/(n+1).P_L$ and large plastic strains were present.

The above tests were all conducted under isothermal conditions and to the author's knowledge there appears to have been no attempts to perform similar experiments on structures where temperature gradients are present. Some experiments on this will now be described.

5.2. Test Rig.

The test rig, Figure 5.1, was constructed of welded steel channel to form a rigid frame. This was mounted on rubber pads to both eliminate any laboratory vibrations and to allow level adjustment. The frame was designed to accommodate beams 12 in . long, 0.25 in . thick by 0.375 in . deep which were the maximum size that could be machined from the material available.

The beam was simply supported at one end by a knife-edge resting on roller bearings which in turn rested on a flat ground surface of a thick supporting plate. This supporting plate was connected to the main frame by adjustable legs to allow fine level adjustment.

The encastre end condition was provided by a split cylindrical stainless steel clamp rigidly bolted to the vertical surface of the main frame. Bolts passing vertically through the clamp held the beam specimen rigid in the mounting. A furnace consisting of two tubular heating elements wound on the clamp provided specimen heating and in order to minimise heat loss the complete unit was encased in an asbestos insulating jacket.

The vertical loads at the centre of the beam length were applied by a weight hanger system. Dead weights were lowered onto a loading stirrup by a screw jack driven by a constant speed electric motor. The weights were supported by a hollow cylinder attached to the top of the screw jack.

The inside of the cylinder was such that the load stirrup and disk could hang inside it with the weights supported above the disk. Therefore when the cylinder was lowered, the weights were left on the load disk. The load could be removed in the same way. This system gave a constant and repeatable rate of loading. The furnace temperature was controlled by a Eurotherm Temperature Controller Unit using a thermocouple as a sensor. The Chromel/Alumel thermocouple was 'peened' into the surface of the beam at the clamped support. Using this system temperature was maintained to within $\pm \frac{1}{2}°C$ of the set value. Additional thermocouples placed at discrete points along the beam allowed continuous monitoring of the beam temperature.

Measurements were made of the central vertical deflection and the vertical deflection at the knife edge by L.V.D.T's (Linear Variable Differential Transformers) with a resolution of 5×10^{-5} in.

5.3. Description of Tests.

5.3.1. Specimens.

The beam specimens were machined from commercially pure aluminium sheet in half-hard condition with the direction of rolling along the longitudinal axis. The choice of material has been discussed previously and the uniaxial tensile test results are given in Chapter 10 section 10.2.

5.3.2. Test Temperature.

The beam was held at a constant temperature of $150°C$ at the encastre end with a temperature distribution of an exponential form, Figure 5.2 occurring along the beam length. Variation of temperature with time was better than $\pm \frac{1}{2}°C$ and the temperature difference across any section was negligible.

The criteria used in evaluating a suitable maximum temperature were that for the form of temperature gradient obtained, the value of the temperature at any point along the beam length was sufficiently high to ensure that a true steady state creep rate was achieved since at room temperature the material exhibits logarithmic creep but also that the temperature was not so high that the problems usually associated with high temperature creep testing occurred. Also within the range 100 - 150°C the creep activation energy for pure aluminium is reasonably constant although as was shown earlier the reference values are reasonably insensitive to ΔH .

5.3.3. Limit Load Tests.

Limit load tests were conducted after allowing the beams to 'soak' for approximately twenty-four hours at temperature for steady state conditions to be attained. The limit load was determined by applying a monotonically increasing load P to the weight hanger. The central deflection and the deflection at the knife edge were measured for each increment of load. The whole test was only of a few minutes duration ensuring that the beam behaviour was sensibly time-independent.

A series of six limit load tests were performed. A typical load/central deflection curve is shown in Figure 5.3 from which it is seen that the limit load, P_L , is approximately 73 lb. The vertical deflection at the knife edge was 10^{-3} in. and this 'settlement' was not considered further.

5.3.4. Creep Tests.

A number of creep tests at constant load were performed at a sequence of values of P/P_L . Each beam, as in the limit load tests, was given a twenty-four hour temperature 'soak' before the commencement of a test. Test duration was typically 800 hours.

The central deflection-time curve shown in Figure 5.4 was obtained from a test at $P/P_L = 0.7$. Normally the region of constant creep rate was achieved approximately 200 hours after the commencement of the test and the average displacement rates measured within the interval 350 - 550 hours. The resulting average displacement rates-load curve is shown plotted on log-log axes in Figure 5.5 as the unbroken line. The broken line curve in the above figure was obtained from a limited number of room temperature tests conducted during the test rig development stage and is shown for comparison.

5.4. Reference Values.

Since the temperature gradient along the beam length in the experiments does not comply with the linear gradient assumed in the example of Chapter 4 relevant calculations were performed to evaluate the reference values.

The reference temperature obtained from a stationary state analysis for the experimental temperature gradient and assuming $\Delta H = 113$ kJ/mole is 100°C . A twenty-five per variation in ΔH either side of this value changed the reference temperature by $\pm$.2 per cent.

By a similar analysis to that given for the theoretical example the central deflection rate $\dot{U}$ may be expressed in terms of a uniaxial strain rate by

$$\dot{U} = \frac{0.148\ell^2}{d} \dot{\varepsilon}(\sigma_R, \theta_R)$$

where $\ell = 9$ in. , $d = 0.375$ in., σ_R is related to the applied load by

$$\sigma_R = 0.600 \frac{P\ell}{bd^2} ,$$

and $b = 0.25$ in .

Similarly an upper bound on deflection rate is obtained using the intermediate plastic solution and is given by

$$\dot{U}^u = \frac{0.191\,\ell^2}{d}\,\dot{\varepsilon}(\sigma_R^u, \theta_R^u)$$

where $\sigma_R^u = 0.64\,\frac{P\ell}{bd^2}$ and $\theta_R^u = 101°C$.

5.5. Discussion of the Results.

The displacement rates obtained from the reference values and the uniaxial data (section 10.2) are virtually indistinguishable for the above two solutions so no attempt to discuss the results in individual terms will be made.

The results obtained from the reference approach are shown by crosses on Fig.5.5 for both the room temperature and 150°C displacement rate-load curves. Both these curves are remarkedly free from scatter with the exception of one result which was discarded. The transition of the curves from a virtual straight line at lower loads to a more rapidly rising curve is seen to occur at $P = n/(n+1)P_L$ as predicted by Leckie and Ponter. The agreement between the experimental results and the analytical predictions is good for this simple structure but whether a similar result would be achieved for more complex structures remains to be investigated. From comparison of the isothermal and non-isothermal curves it would appear that the reference stress, reference temperature approach is capable of providing good predictions on stationary state displacement rates to a similar degree of accuracy as for isothermal conditions.

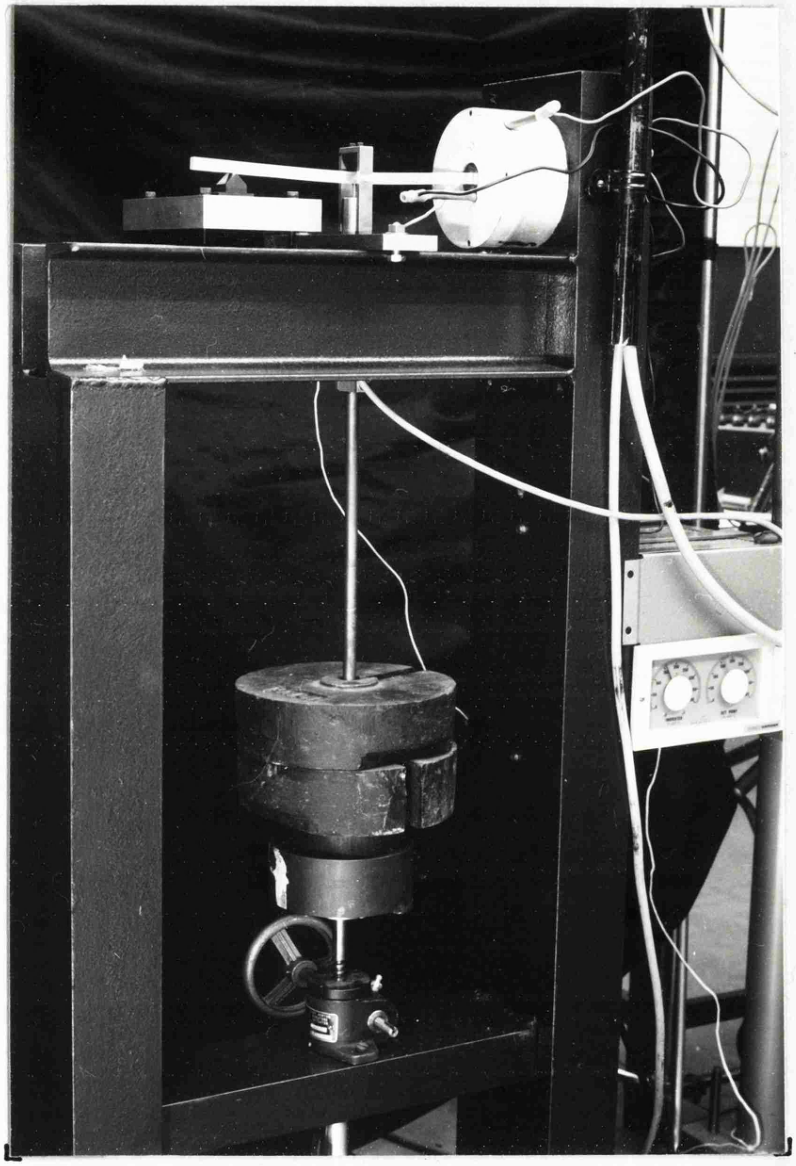

Fig 5.1 Photograph of test rig

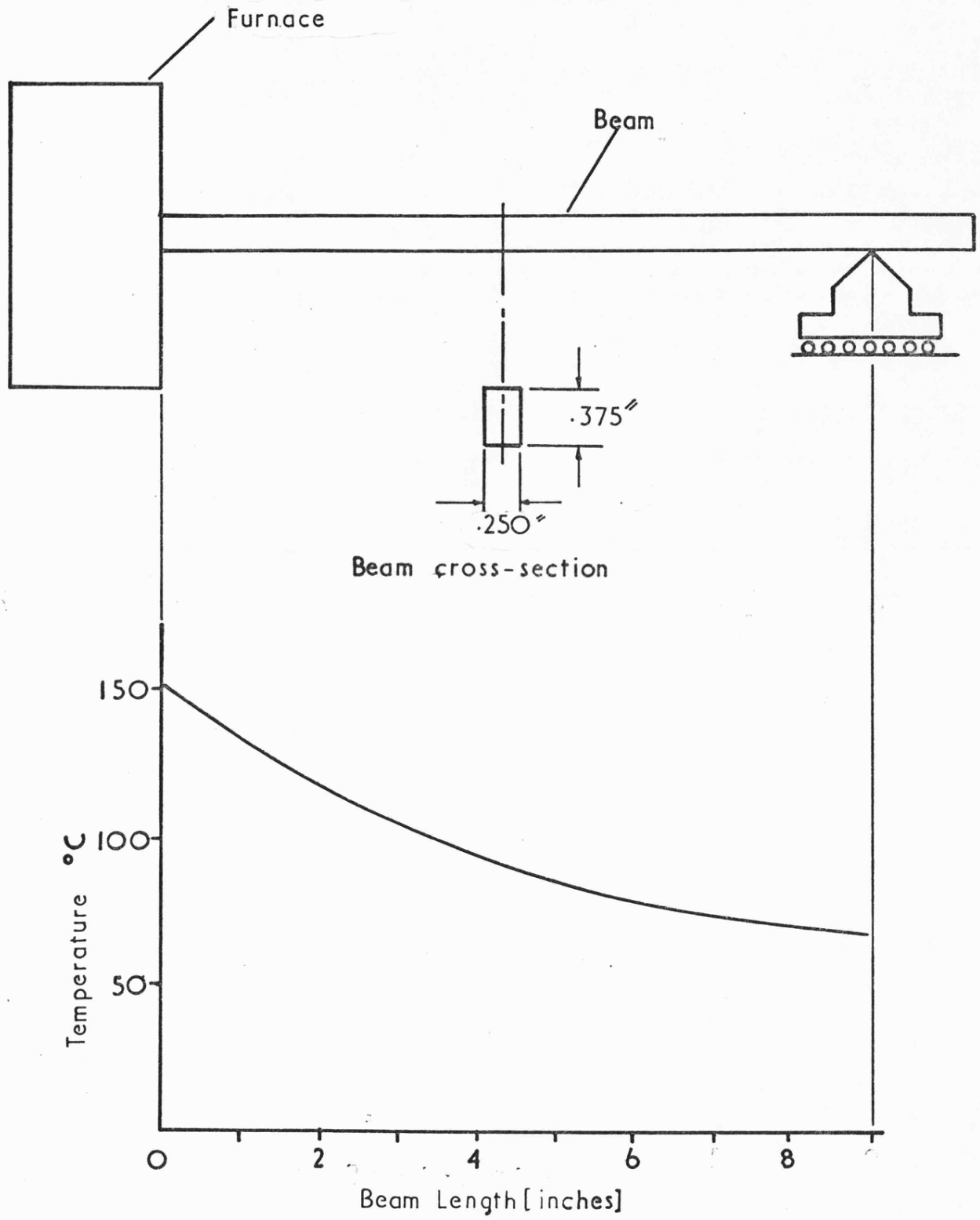

Fig 5.2 Temperature gradient on the propped cantilever

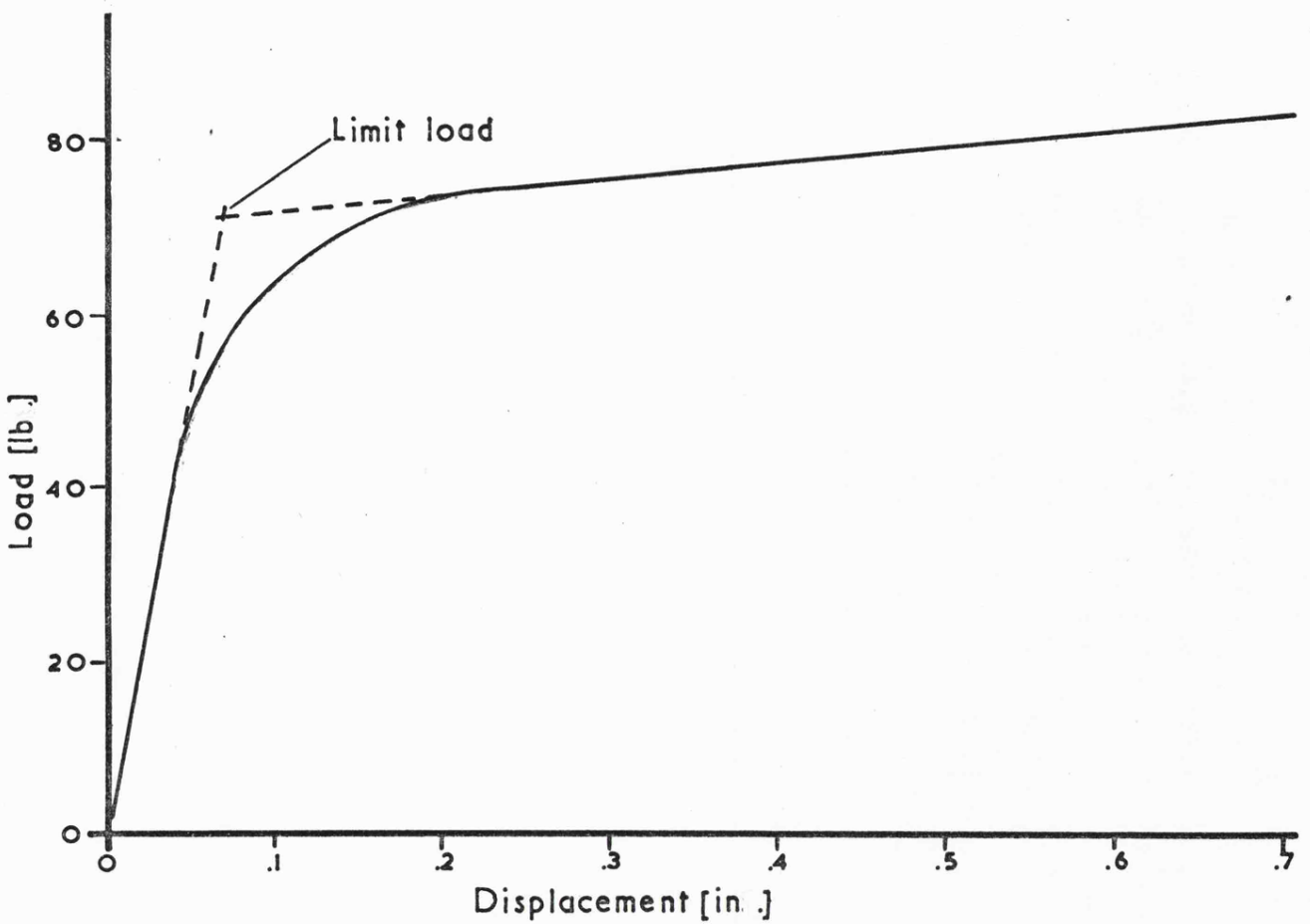

Fig 5.3 Limit load test

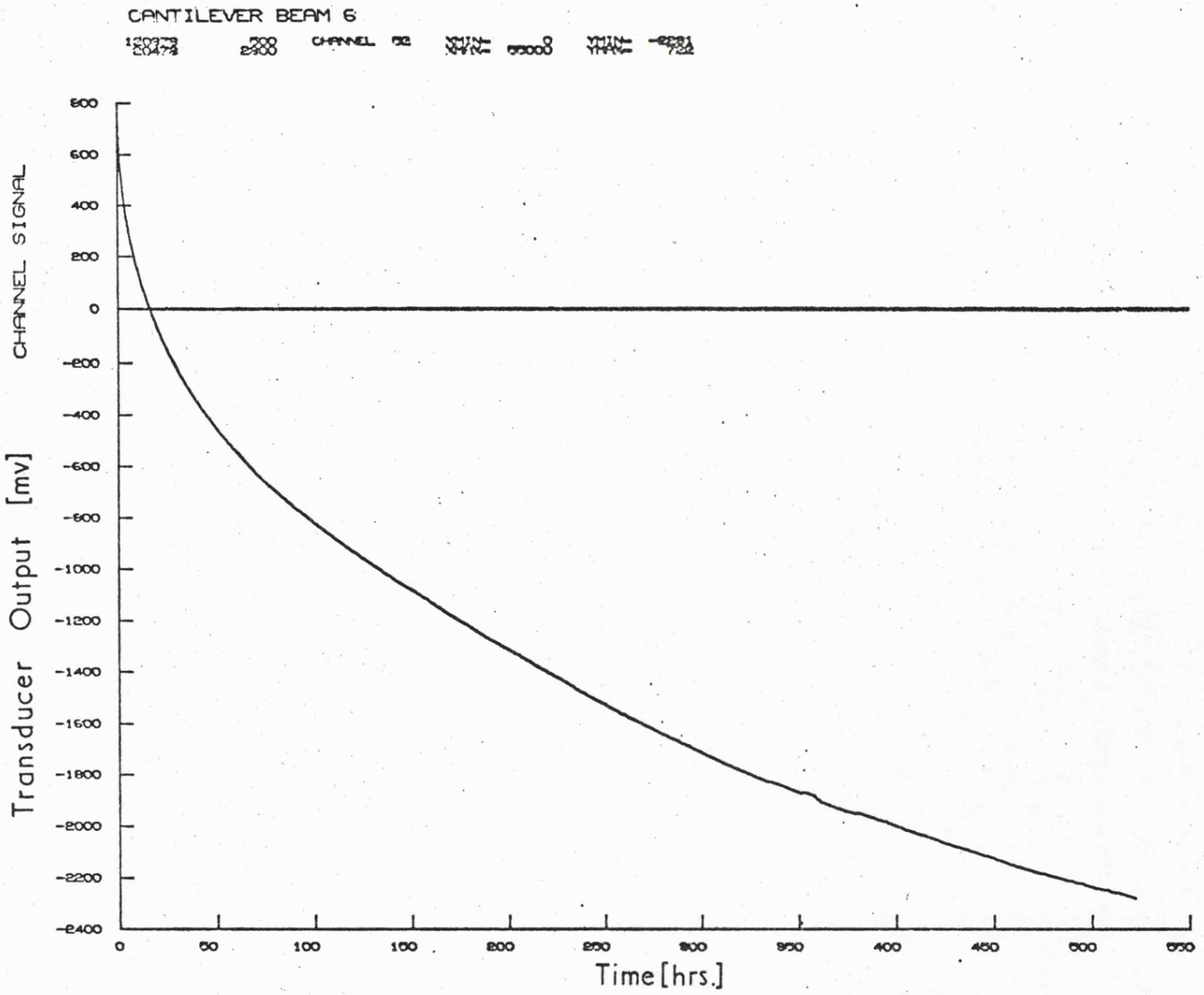

Fig 5.4 Central deflection–time plot for P/R= 0.7

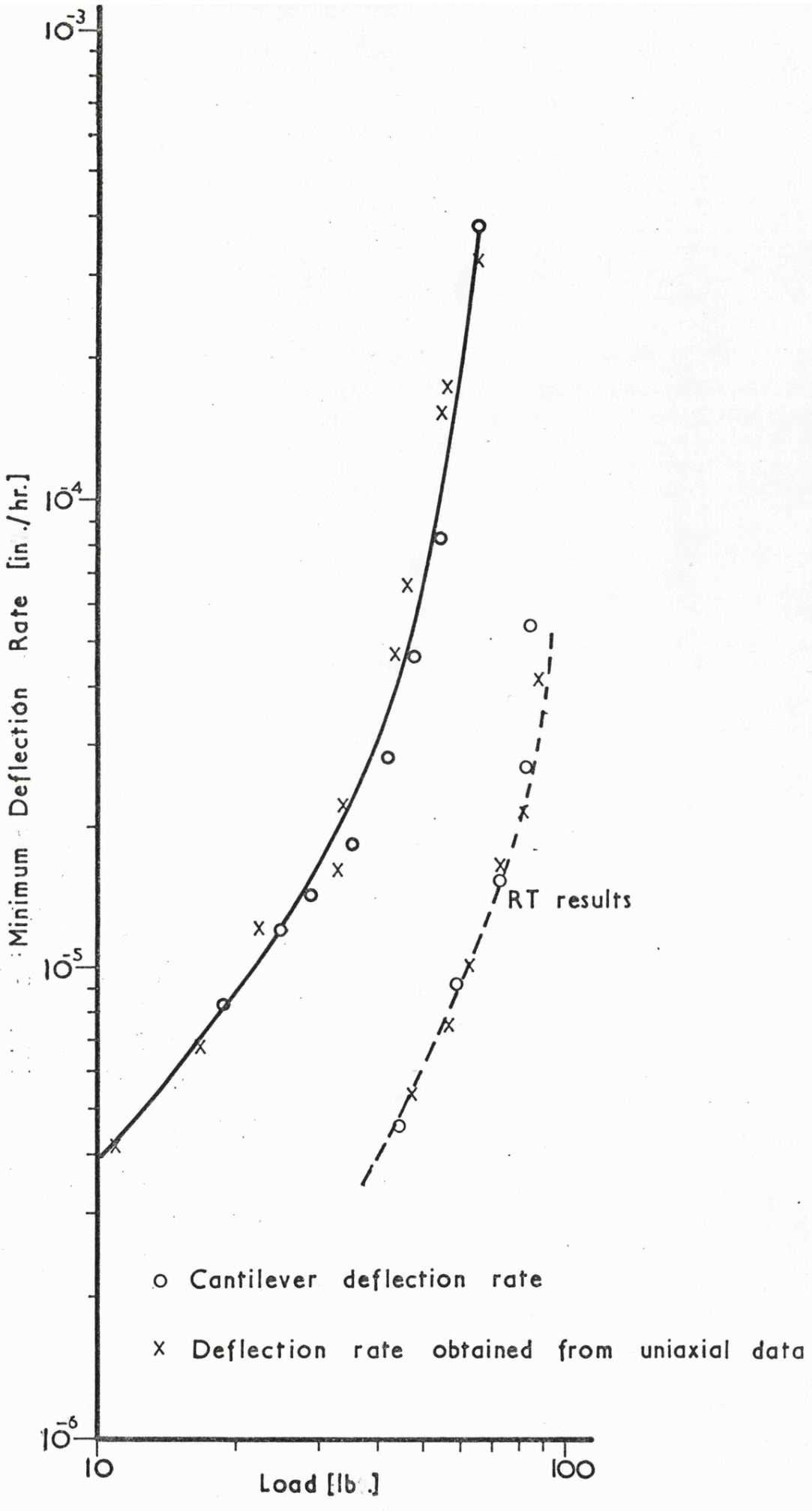

Fig 5.5 Log minimum deflection-rate against log load

Chapter 6

Creep of Structures Subjected to Cyclic Temperatures

6.1. Introduction.

Many structural components subjected to both thermal and mechanical loading in addition usually suffer time-independent deformations which may or may not be excessive. However the interaction between the non-linear creep response of the material and the presence of varying temperature fields is a problem the analysis of which remains amongst the more intractable problems of structural mechanics.

In principle methods of calculation are available which can be used to determine stress and strain histories in time-dependent structures subjected to variable loading when isothermal conditions are present. Unfortunately the lack of realistic constitutive equations for time-varying stress limit these methods to problems of steady loading. It has been shown that for structures subjected to steady loads and temperature distributions the reference stress/temperature concept can be particularly useful in predicting structural behaviour. This concept may also be used to estimate deformation for proportional loading providing stress redistribution effects are small. A relevant theoretical study has been reported by Ponter[37] who has obtained bounds on the creep energy dissipation when the structure is composed of time-hardening material. The bounds are extremely useful in determining whether stress redistribution effects are significant. If the bounds show that stress redistribution effects are small then the use of the reference stress technique is justified, but when stress redistribution effects become prominent then another procedure is necessary for a more general class of materials. Williams[45] has proposed a method of solution for estimating creep deformation due to proportional cyclic loading. The method relies

on the use of an equivalent steady stress obtained from a cyclic stress creep test and the creep law for time-varying stress is therefore not required.

Solutions to the problem when both variable load and temperature histories are present is virtually impossible and it is quite possible that in the event of realistic constitutive relationships becoming available it would not be easy to use in computer calculations. Many situations involving variable loading are periodic and as such afford some simplification of the problem. Calculations have been performed for a thick tube subjected to cyclic histories of pressure and temperature, by Frederick, Chubb and Bromley[65]. The value of such calculations depends upon the adequacy of the constitutive equation for time-varying stress.

Some theoretical results, recently derived by Ponter[66], may provide a more detailed understanding of thermal/creep interaction. He considered a structure composed of an elastic/time hardening/creeping/plastic material which was subjected to a history of applied loading, applied displacement and inelastic strain. A number of theoretical results were derived which included bounds on the energy dissipated by the material in the formation of inelastic (creep and plastic) strains for load levels below the plastic shake-down limit. The analysis indicated that under cyclic histories of load the bounds provided two extreme modes of behaviour involving the creep energy dissipation associated with two equilibrium historiesof stress. The bounding solutions are relatively simple to compute and are such that the time integration of the material behaviour is effectively uncoupled from the solution of the spatial continuum problem. Examples of the application of these bounds to some simple structures and comparisons with experiments are discussed in (2,49).

The two equilibrium histories of stress correspond to the actual behaviour of the structure when the cycle time is considered to be very long or very short compared with a characteristic time of the material at some mean

stress level. These two stress distributions give the asymptotic stress histories and provide the corresponding average displacement rates of the structure. The bounds will be discussed in more detail in section 6.3 but it may be mentioned in passing that consideration of time scales involved in many practical creep problems[45,51] indicate that cycle times are generally very short compared with characteristic material times and the upper bound solution is likely to approximate the true state of affairs. Therefore the two stress histories given by this theory and the corresponding displacements they predict are likely to provide a strong indication of the behaviour of the structure for finite cycle times and indicate the relative importance of the various phenomena involved.

In the following section stress redistribution due to cyclic loading will be briefly discussed followed by a section describing the energy dissipation bounds in detail. It will then be shown that the pertinent phenomenon which occurs due to variable cyclic temperature may be exhibited by computing bounding solutions to two structural problems. These will be discussed under specific load and temperature histories that illustrate simple patterns of behaviour. In Chapter 7 these patterns of behaviour will be incorporated into design charts for the problems under generalised temperature histories. The first problem investigated is the parallel two-bar structure, subjected to constant applied loads and a variable temperature history. This structure is perhaps the simplest redundant structure imaginable and was chosen for the following reasons: in reference (48) it was argued that this structure was representative in some respects of many simple structures, severe thermal ratchetting effects are produced by small temperature changes and since it is a simple structure that illustrates thermal creep interactions particularly well, has been simulated experimentally. Details of the experimental test rig and test results are given in Chapters 8 and 10.

The second problem is technologically more interesting; the creep of a plate subjected to constant biaxial loads and surface temperatures that vary in time. Some aspects of this problem have already been considered by Ponter and Leckie[3].

6.2. Stress Redistribution due to Cyclic Loading.

A steady state of cyclic stress is defined as a state in which the stresses before and after the application of a loading cycle are the same, i.e. the repeated application of a loading cycle produces no net change in stress. Frederick and Armstrong[67] demonstrated that a body composed of elastic-perfectly plastic or elastic-creeping material whose strain rate is given by

$$\frac{\dot{\varepsilon}_{ij}}{\dot{\varepsilon}_o} = \frac{3}{2} \frac{\{\sigma_e(t)\}^{n-1}}{\sigma_o^n} s_{ij}(t) \qquad (6.1)$$

and subjected to cyclic loading approached a cyclic history of stress as time increased, although they were unable to characterise this cyclic state more specifically. Martin and Williams[68] discussed the existence of an extremum principle for structures composed of a time-dependent stable dissipative material subjected to cyclic loading and were able to show that such a principle provides alternative arguments to establish the convergence to a unique state of stress.

Ponter[37] provides an extension to the theorem of Frederick and Armstrong to structures composed of materials whose creep law is of the form

$$\frac{\dot{\varepsilon}_{ij}}{\dot{\varepsilon}_o} = \frac{3}{2} \frac{\{\sigma_e(t)\}^{n-1}}{\sigma_o^n} s_{ij}(t)\ f\left(\frac{t}{t_o}\right) \qquad (6.2)$$

provided such a state of stress exists.

It has been shown that under conditions of steady loading creeping structures suffer stress redistribution until the stationary state is attained. The convergence to the cyclic state of stress is analogous to

the stress redistribution process and the cyclic state corresponds directly to the stationary state under steady loading. Since the stationary state is associated with the minimum energy dissipation rate it may be assumed that the cyclic state similarly minimises the energy dissipation rate per cycle. However, Martin and Williams[68] have shown that the functional that is minimised is not the energy dissipation per cycle but a weighted integral of this quantity, of which they were unable to provide any physical interpretation.

6.3. Energy Dissipation Bounds for Cyclic Loading.

The theorems described in this section are due to Ponter[1,2,36,37] and are based on a material model which was described briefly in Chapter 3.

Consider a body with volume V and surfaces S. The surface is subjected to applied loads $P_i(x_k,t)$ over part S_T, and applied displacements $U_i(x_k,t)$ over the remainder, S_u. Within the volume a state of stress exists which has the value of $\rho_{ij}(x_k,o)$ at time $t = 0$. A known history of inelastic strains $\Delta_{ij}(x_k,t)$ are induced by a temperature field $\theta(x_k,t)$ or by some other externally applied agencies.

The strains induced in the body are assumed to be sufficiently small for the classical assumptions of infinitesimal continuum mechanics to remain valid. The total strain accumulated at time t, $\Sigma_{ij}(t)$, consists of four components,

$$\Sigma_{ij} = e_{ij} + \varepsilon_{ij} + p_{ij} + \Delta_{ij}, \tag{6.3}$$

where e_{ij}, ε_{ij} and p_{ij} denote the elastic, creep and plastic strains respectively.

The elastic component, e_{ij}, is related to the stress by a general linear relationship,

$$e_{ij} = C_{ijk\ell}\,\sigma_{k\ell}, \tag{6.4}$$

where $C_{ijk\ell}$ denotes the elastic constant tensor which is positive-

definite and fully symmetric.

The creep strains are given by

$$\dot{\varepsilon}_{ij} = \frac{\partial}{\partial \sigma_{ij}} \left\{ \frac{\bar{\Phi}^{n+1}(\sigma_{k\ell})}{n+1} \right\} \frac{\dot{\varepsilon}_o}{\sigma_o^n} \tag{6.5}$$

where $\bar{\Phi}$ denotes a homogeneous function of degree one in $\sigma_{k\ell}$, and $\dot{\varepsilon}_o$ denotes a uniaxial creep strain rate corresponding to the uniaxial constant stress σ_o . The rate of creep energy dissipation, $\dot{D}^c$, is given by

$$\dot{D}^c = \sigma_{ij}\dot{\varepsilon}_{ij} = \bar{\Phi}^{n+1}(\sigma_{k\ell}) \frac{\dot{\varepsilon}_o}{\sigma_o^n} \tag{6.6}$$

The plastic strains p_{ij} are given by a perfectly plastic model associated with a convex yield function $f(\sigma_{k\ell}) = 0$,

$$\dot{p}_{ij} = \dot{\mu} \frac{\partial f}{\partial \sigma_{ij}} \quad , \; f = 0 \; , \; \dot{\sigma}_{ij} \frac{\partial f}{\partial \sigma_{ij}} = 0$$

$$\dot{p}_{ij} = 0 \qquad , \; f \leqslant 0 \; , \; \dot{\sigma}_{ij} \frac{\partial f}{\partial \sigma_{ij}} < 0 \tag{6.7}$$

As in the previous chapters the functional dependence of $\varepsilon_o(t)$ upon θ assumes the form

$$\frac{\dot{\varepsilon}_o(t)}{\sigma_o^n} = k \exp\{-\Delta H/R\theta(t)\}$$

The linear elastic stress distribution for the stated problem is denoted by $\hat{\sigma}_{ij}$ and a related stress history σ^*_{ij} is defined by

$$\sigma^*_{ij}(x_k,t) = \hat{\sigma}_{ij}(x_k,t) + \bar{\rho}_{ij}(x_k) \tag{6.8}$$

where $\bar{\rho}_{ij}$ denotes an arbitrary time constant residual stress field in equilibrium with zero applied loads on S_T . The stress history may be recognised as that associated with the lower bound shakedown theorems.

The energy dissipated due to the formation of inelastic strains within the time $0 \leqslant t \leqslant \Delta t$ is given by

$$W_o^{'\Delta t} = \int_o^{\Delta t} \int_V \sigma_{ij}(\mathring{\Sigma}_{ij} - \dot{e}_{ij}) dV dt \tag{6.9}$$

where $W_o^{'\Delta t}$ denotes a work quantity associated purely with inelastic strains.

Ponter[37] has shown that upper and lower bounds on the quantity $W_o^{'\Delta t}$ are given by

$$\int_o^{\Delta t} \int_V \dot{D}^c(\sigma_{ij}^s) dV dt \leq W_o^{'\Delta t} \leq (n+1)\{E(o) - E(\Delta t)\} + \int_o^{\Delta t} \int_V \dot{D}^c(\sigma_{ij}^*) dV dt. \tag{6.10}$$

The stationary state creep solution σ_{ij}^s is defined as the solution to the stated problem under the assumption $e_{ij} = p_{ij} = \Delta_{ij} = 0$ and $U_i = 0$ on S_u. Therefore σ_{ij}^s provides the purely viscous solution with rigid supports ($U_i = 0$). The temperature field enters into the problem only through the functional dependence of $\dot{\varepsilon}_o$ upon θ.

The total complementary elastic strain energy quantity, $E(t)$, is defined as

$$E(t) = \frac{1}{2} \int_V C_{ijk\ell}(\rho_{ij}(t) - \bar{\rho}_{ij})(\rho_{k\ell}(t) - \bar{\rho}_{k\ell}) dV \tag{6.11}$$

where $\rho_{ij}(t) = \sigma_{ij}(t) - \hat{\sigma}_{ij}(t)$, the instantaneous residual stress field. The quantity $E(o)$ is known if at $t = 0$ the structure is in the unstressed state and $E(t)$ may be removed without violating the inequality.

When the structure is subjected to cyclic loads, i.e. P_i, U_i and θ are all cyclic with period Δt, it was shown in (1) that the stress distribution asymptotes to a cyclic state (provided such a state exists) with period Δt and that the total inelastic and elastic work (excluding the work done by the thermal strain Δ_{ij}) may be bounded by the creep energy dissipation associated with σ_{ij}^* and σ_{ij}^s

$$W^L = \int_o^{\Delta t} \int_V \dot{D}^c(\sigma_{ij}^s) dV dt \leq W_o^{\Delta t} \leq \int_o^{\Delta t} \int_V \dot{D}_c(\sigma_{ij}^*) dV dt = W^u \tag{6.12}$$

where $W_o^{\Delta t}$ denotes the total work done by the applied loads minus the work

done by thermally induced strains

$$W_o^{\Delta t} = \int_o^{\Delta t} \int_V \sigma_{ij}(\dot{\Sigma}_{ij} - \dot{\Delta}_{ij}) dV dt = \int_o^{\Delta t} \int_{S_T} P_i \dot{U}_i dS dt \qquad (6.13)$$

As the work depends upon the magnitude of the stress and not the sign, the difference between the two bounds provides a measure of the average deviation of the stress from σ_{ij}^s , the purely viscous solution.

The stress distributions are subject to the yield conditions[49],

$$f(\sigma_{ij}^s) \leqslant 0 \quad \text{and} \quad \left(f\left\{\frac{n+1}{n}\right\} \cdot \sigma_{ij}^*\right) \leqslant 0. \qquad (6.14)$$

The latter condition implies that the upper bound may be evaluated provided the applied loads $P_i(t)$ are such that $\left(\frac{n+1}{n}\right) P_i(t)$ does not cause incremental plastic collapse whereas the lower bound may be computed provided $P_i(t)$ does not cause instantaneous plastic collapse.

Ponter, on the computation of optimal upper bounds, has shown that the residual stress field $\bar{\rho}_{ij}$ which minimized the upper bound W^u made the accumulated creep strain over a cycle

$$\Delta^u \varepsilon_{ij} = \int_o^{\Delta t} \dot{\varepsilon}_{ij} dt \ , \qquad (6.15)$$

kinematically admissable, and was uniquely defined by this condition. The optimal stress field $\bar{\rho}_{ij}$ so formed provides a displacement field ΔU_i^u from $\Delta^u \varepsilon_{ij}$ which may be interpreted as the asymptotic state which occurs when the cycle time Δt is small compared with a characteristic time of the material (which may be defined as the time to accumulate creep strain equal to the elastic strain at a mean stress (1,39)) . The displacement field associated with the optimal upper bound can be interpreted as the limiting case as the cycle time tends to zero. Under such circumstances the creep strains accumulated over a cycle are small compared with the changes in elastic strains, and stress redistribution is therefore occurring continuously with the result that any consequent ratchetting effects are

maximised[1].

On the other hand, the lower bound solution, σ^{s}_{ij}, provides, by definition, a kinematically admissible strain rate field $\dot{\varepsilon}^{s}_{ij}(\sigma_{k\ell})$ from which can be derived a displacement rate field $\Delta^{s}\dot{U}_{i}$ and the corresponding displacement $\Delta^{L}U_{i}$ accumulated over a cycle. This solution corresponds to a situation when the cycle time is very long and perturbations due to changes in thermal loading and changes in elastic strains make a negligible contribution to the total deformation of the body. The implications are that stress redistribution is occurring for only a small part of the time and stress redistribution effects are correspondingly small.

The plastic strains enter into the problem merely as yield restraints upon the stress fields and the analysis will indicate the range of loading for which plastic straining will occur. In general a stress history of the form σ^{*}_{ij} is possible providing the loads are less than $n/(n+1)$ of a plastic shakedown state as the experimental investigation of Williams[45] tended to confirm.

The two solutions σ^{*}_{ij} and σ^{s}_{ij} provide bounds which describe extreme modes of behaviour which may occur in the sense signified by inequality (6.12). The relative values of the upper and lower bounds on the work indicate the sensitivity of the structure to cycle time and the corresponding displacement fields indicate the two extremes of structural behaviour. The lower bound solution corresponds to the most widely used solution for this type of problem and can be seen to always underestimate the energy dissipated within the body. Conclusions reached by Williams and Leckie[32] tend to indicate that the upper bound solution may be expected to closely approximate the actual behaviour for many structures, as typical cycle times are short compared with the total lifetime of the structure.

6.4. The Analysis of Example Problems.

In the following problems the material properties chosen are those of a typical 816-type stainless steel. The relevant values are listed in Table 6.1. In practice several materials may have similar time-independent properties but with differing values of the stress index. Therefore all results were obtained for $n = 3$, 7 and 11 with the intention of providing as many aspects of thermal creep interaction as possible within the limits of the theory.

Unless otherwise specified all results are normalised with respect to the maximum thermo-elastic stresses and a mean temperature θ_m defined in the text.

6.4.1. The Two-bar Structure Problem.

The two-bar structure shown in Fig.6.1 has bars of equal length and equal cross sectional area which are restrained to remain of equal length. A steady load P is applied and the bars subjected to a cyclic history of temperature.

The temperature history chosen is shown in Fig.6.2 where bar 1 is maintained at a constant mean temperature θ_c while bar 2 is subjected to a variable temperature which fluctuates between the limits $\theta_c \pm \Delta\theta$. Changes in temperature are considered to take place sufficiently slowly for thermal transients to be negligible.

Assuming each bar to be unit cross-sectional area, the stress distribution σ^*_{ij} for the upper bound assuming zero plasticity effects is given by

$$\sigma^*_i = \frac{P}{2} \pm \sigma^\theta_i \pm \rho \qquad i = 1,2 \tag{6.16}$$

where σ^θ_i is the isotropic thermo-elastic stress due to thermal expansion alone.

For the upper bound it is required that the creep rates of each bar,

$\dot{\varepsilon}_1$ and $\dot{\varepsilon}_2$, shall be kinematically admissable when integrated over a cycle of stress history. The accumulated displacement per cycle is then

$$\Delta U^u = \ell \int_0^{\Delta t} \dot{\varepsilon}(\sigma_1^*)dt = \ell \int_0^{\Delta t} \dot{\varepsilon}(\sigma_2^*)dt \qquad (6.17)$$

The residual stress ρ is determined from equation 6.17 in terms of ΔU^u as P and σ^θ are known. The solution is then obtained by solving the compatibility condition by a Newton-Raphson procedure.

The lower bound stress distribution is simply the stationary state solution for the temperature distribution in each part of the cycle. The corresponding displacement per cycle is given by

$$\Delta U^L = \ell \int_0^{\Delta t} \dot{\varepsilon}(\sigma_1^s)dt = \ell \int_0^{\Delta t} \dot{\varepsilon}(\sigma_2^s)dt \qquad (6.18)$$

6.4.2. Solutions to the Two-bar Structure.

The fixed temperature θ_c was taken as $800°K$ and in the first set of bounds increments of temperature $\Delta\theta$ were selected to give the ratio of the thermo-elastic stress to the yield stress, $\sigma^\theta/\bar{\sigma}_y$, a range of values.

In the first set of calculations the applied load was maintained steady at $P = 1\bar{\sigma}_y$ (assuming each bar to be of unit area) and the effects of temperature upon the material properties removed by identifying $\Delta H = 0$. The ratio of the upper to the lower work bounds and corresponding ratio of displacements are shown in Table 6.2 for a sequence of values of $\Delta\theta$ for $n = 3$, 7 and 11 . For any given value of n , the ratio of the work bounds and the ratio of displacements increase rapidly with increasing $\Delta\theta$. For example at $\Delta\theta = 40°K$, $\sigma^\theta = 0.2\ P$ the difference in the work bounds corresponds to a change in the applied load of 20 , 30 and 35 per cent for $n = 3$, 7 and 11 respectively. The difference between the work bounds corresponds to the energy dissipation due to the effects of thermal ratchetting and therefore this solution predicts an increase in thermal ratchetting if either n or $\Delta\theta$, or both of these increase.

The calculations were repeated including the effects of temperature on material behaviour. The resulting work and displacement ratios are given in Table 6.3. It can be readily seen that this set of solutions possess entirely different characteristics to those obtained for $\Delta H = 0$. In this case the bounds lie reasonably close together and do not show a monotonic change with increasing $\Delta\theta$. For $n = 3$ the ratio of the work bounds are close to unity for all values of $\Delta\theta$, and for $n = 7$ the bounds achieve a maximum value then decrease. These results clearly show an effect of the stress index on structural behaviour. This will be more easily seen in Chapter 7.

The reason for the marked change in behaviour that occurs between the two sets of solutions can be explained in terms of the stress histories. In Fig.6.7 the stress histories are presented for $\Delta H = 0$ and $\Delta H = 342$ KJ/mole with $n = 7$ and $\Delta\theta = 30°K$. The upper bound σ^*_{ij} appears as full lines and the lower bound σ^s_{ij} as broken lines. In this example the equivalent applied stress is approximately four times larger than the thermal stress.

When $\Delta H = 0$ it can be seen that whereas the upper bound stress history is dependent on the temperature history, the lower bound solution is directly related to the magnitude of the applied load only. The stress histories do not approach each other during any part of the cycle and consequently since the lower bound solution provides the absolute minimum energy dissipation for any equilibrium stress field, the upper bound predicts large thermal ratchetting effects. However, when $\Delta H \neq 0$ the stress distributions lie close together during the first part of the cycle when the higher temperature acts. During the second part of the cycle they are distinctly different. In the lower bound solution compatibility conditions demand that both bars remain of equal length during each part of the cycle and as creep rates are exponentially related to temperature, (i.e. small changes in temperature cause large changes in creep rates) this condition can only be

satisfied by the maximum stress occurring on the cooler bar during each part of the cycle. Consequently as the creep rates are higher during the first part of the cycle the total deformation is dominated by the deformation accumulated during this period. The optimal upper bound involves a residual stress field that minimises the energy dissipation and since most energy dissipation occurs during this dominant period the upper bound stress distribution approaches that of the lower bound. Therefore the inclusion of the variation of material behaviour with temperature in the problem appears to reduce the statical indeterminancy caused by thermal expansion and thus provide a reduction in thermal ratchetting effects.

In order to provide some simplification of the problem a fixed thermal history is considered. The lower bound solutions are then dependent only upon the magnitude of the applied loads and similarly the upper bound is dependent on the ratio of the applied loads to the thermal load.

Both the values of the work bounds in inequality 6.12 and the corresponding displacements per cycle ΔU^u and ΔU^L were computed for a sequence of values of P and n. The results are normalised with respect to $W(\sigma^\theta, \theta_m)$ and $\Delta U(\sigma^\theta, \theta_m)$ the work and displacements computed on the assumption that the thermal stress σ^θ and temperature θ_m occur on both bars during a cycle. The mean temperature θ_m is defined by

$$\exp\{-\Delta H/R\theta_m\} = \tfrac{1}{2}[\exp\{-2\Delta H/R(2\theta_c+\Delta\theta)\} + \exp\{-2\Delta H/R(2\theta_c-\Delta\theta)\}.$$

The results for $\Delta\theta = 47°K$, $\sigma^\theta = 0.25\,\bar{\sigma}_y$ and $\theta_c = 800°K$ are presented in Figs. 6.8 to 6.13 as the full lines. The dashed lines correspond to the solutions for $\Delta H = 0$. The solutions for $\Delta H \neq 0$ indicate that for any given value of the applied load the differences between the bounds increase with increasing n. The corresponding displacements show a marked change with the value of n; for $n = 3$ the upper bound displacement is always less than that of the lower bound whilst for

$n = 7$ or 11 the upper bound predicts the larger displacement. However the results show that for all values of n similar features are exhibited; at large values of P the differences between the bounds become small and in the limit are zero. At lower values, the bounds rapidly diverge and the upper work bound tends towards the value associated with zero displacement per cycle, although the lower bound predicts a non-zero positive displacement at this value of the applied load. The upper work bound then increases with further decreases in load and the corresponding displacements are non-zero and negative. In this region the thermal-creep interaction produces a net reduction in the lengths of the bars.

The effects of thermal creep interaction can be seen more clearly from the stress histories presented in Fig.6.14 for $n = 7$. The upper bound σ^{*}_{ij} appears as the full lines, the lower bound σ^{s}_{ij} as the broken lines and the thermo-elastic solution as the chain lines. At large values of the applied load, thermal ratchetting has little effect on the overall creep deformation and the stress histories predicted from the two bounds coincide. In this region 96 per cent of the total energy dissipation and total deformation occurs during the first part of the cycle when the creep rates are higher.

The stress history shown in Fig.6.14a corresponds to a work ratio of 1.03 and a displacement ratio of 1.002. Even though the thermo-elastic stress is approximately 30 per cent of the applied stress only 3 per cent of the energy dissipation is associated with thermal ratchetting. In this solution the thermo-elastic stress history is close to the lower bound solution during the second period of the cycle but since kinematic conditions demand that the corresponding creep strain rates when integrated over a cycle produce the same deformation in each bar the resulting residual stress field removes part of the load from the most severely loaded member during the first part of the cycle and increases the severity on the higher loaded bar during the second part of the cycle. Most of the increased statical

indeterminancy due to thermal expansion is offset by the rapid variation of material behaviour with temperature and the total energy dissipation and deformation continue to be dominated by the energy dissipation and deformation occurring in the first part of the cycle but to a slightly lesser degree.

When the bounds are reasonably close together the characteristic feature of the problem appears to be a period of high stress on the bar at constant temperature when the higher temperature acts followed by a period of high stress on the opposite bar when the cooler temperature acts.

As the applied load decreases the thermal ratchetting effect becomes more dominant. The stress histories do not approach each other during any part of cycle and stress on the cooler bars continues to increase. Likewise the contribution to the total energy dissipation and the total deformation from the second part of the cycle continues to increase. It is seen from Figs. 6.14b and 6.14c that as P decreases the stress on bar 1 eventually becomes compressive. At $P = 0.5\ \bar{\sigma}_y$ the total energy dissipation becomes dominated by the energy dissipation of the cooler bar during the second part of the cycle and the overall deformation becomes small. In Fig.6.15 the stress histories that correspond to zero displacement per cycle are shown. The stress on bar 1 coincides with the thermo-elastic solution and the stress on bar 2 is compressive during the first part of the cycle. The strain rates corresponding to these stress histories when integrated over a cycle give rise to equal and opposite displacements on each bar during the first and second half of the cycle. The energy dissipation is associated with thermal cycling alone.

6.4.3. The Plate Problem.

Consider the problem of a plate, Fig.6.3 of thickness $2h$ subjected to a uniform state of mean stress (p_x , p_y) with respect to a fixed axis in the plane of the plate's central surface, which result from a stress field $\sigma_x(z) , \sigma_y(z)$ through the plate thickness.

The plate is subjected to a cyclic varying temperature field which has the form shown in Fig.6.4 where the lower side of plate $z = - h$ is at a temperature $\theta_1(t)$ and the upper side $z = h$ at a temperature $\theta_2(t)$. As in the previous example changes in temperature are considered to take place sufficiently slowly for thermal transients to be negligible, so that the temperature distribution through the plate is linear and given by

$$\theta(z,t) = \left(\frac{\theta_1 + \theta_2}{2}\right) + \left(\frac{\theta_1 - \theta_2}{2}\right) \frac{z}{h}$$

It is assumed that the surfaces x = constant and y = constant suffer only rigid body displacement and thereby simulate the condition which occurs, for example, in a thin walled tube under internal or external pressure $(p_x = 2p_y)$ or a sphere under internal or external pressure $(p_x = p_y)$.

The stress distribution σ^*_{ij} for the upper bound can be written

$$\sigma^*_x = p_x + \sigma^\theta_x + \rho_x$$

$$\sigma_y = p_y + \sigma^\theta_y + \rho_y \qquad (6.19)$$

where σ^θ_x and σ^θ_y are the thermo-elastic stresses in the x and y directions, and equilibrium of the residual stress field (ρ_x , ρ_y) require that

$$\int_{-h}^{h} \rho_x \, dz = \int_{-h}^{h} \rho_y \, dz = 0 . \qquad (6.20)$$

The creep strain component is assumed to obey a Von Mises flow rule obtained by substituting

$$\bar{\phi}(\sigma_{ij}) = \left(\frac{3}{2} s_{ij}s_{ij}\right)^{\frac{1}{2}}$$

into equation 6.5 to obtain

$$\dot{\varepsilon}_{ij} = \frac{3}{2} k \left(\frac{3}{2} s_{k\ell}s_{k\ell}\right)^{\frac{n-1}{2}} s_{ij} \exp(-\Delta H/R\theta) \qquad (6.21)$$

where

$$s_{ij} = \sigma_{ij} - \frac{1}{3}\delta_{ij}\sigma_{kk}$$

The creep strain rates in the x and y directions are therefore given by

$$\dot{\varepsilon}_x = \frac{k}{2} (\sigma_x^2 - \sigma_x\sigma_y + \sigma_y^2)^{\frac{n-1}{2}} (2\sigma_x - \sigma_y)\exp(-\Delta H/R\theta)$$

$$\dot{\varepsilon}_y = \frac{k}{2} (\sigma_y^2 - \sigma_x\sigma_y + \sigma_x^2)^{\frac{n-1}{2}} (2\sigma_x - \sigma_y)\exp(-\Delta H/R\theta) \qquad (6.22)$$

The upper work bound requires that $\dot{\varepsilon}_x$ and $\dot{\varepsilon}_y$ shall be kinematically admissable when integrated over a cycle of stress history. If ΔU_x^u and ΔU_y^u denote the accumulated displacements per unit width of plate then;

$$\Delta U_x^u = \int_0^{\Delta t} \dot{\varepsilon}_x(\sigma_x^*, \sigma_y^*)dt \qquad (6.23)$$

$$\Delta U_y^u = \int_0^{\Delta t} \dot{\varepsilon}_y(\sigma_x^*, \sigma_y^*)dt \qquad (6.24)$$

These two equations determine $\rho_x(z)$ and $\rho_y(z)$ in terms of ΔU_x^u and ΔU_y^u as σ_x^θ , σ_y^θ , p_x and p_y are known.

The procedure adopted for the solution to the problem was as follows: For selected values of ΔU_x^u and ΔU_y^u equations 6.23 and 6.24 were solved for $\rho_x + p_x$ and $\rho_y + p_y$ at a sequence of stations through the plate thickness, by a Newton-Raphson procedure. The value of p_x and p_y were then found by integration of the computed values, making use of the residual stress field equilibrium equations 6.20 .

In terms of the temperature history a mean temperature θ_m is defined as

$$\exp(-\Delta H/R\theta_m) = \frac{1}{2}[\exp(2\Delta H/R(\theta_{11}+\theta_{21})) + \exp(2\Delta H/R(\theta_{12}+\theta_{22}))]$$

The mean temperature is the constant temperature which produces the same accumulated strain per cycle as the temperature history on the central surface $z = 0$.

6.4.4. The Plate Solutions.

Bree[69,70] in a study on nuclear reactor fuel can problems has obtained approximate criteria for the onset of ratchetting and plastic cycling in thin-walled tubes and shells subjected to constant internal pressure P^R and variable temperature $\Delta\theta$ between the inner and outer walls. In the absence of creep the stress strain law was assumed to have the form shown in Fig.6.5 where $\bar{\sigma}_y$ is the yield stress. This simple uniaxial stress model of the fuel can was used in the case of non-work hardening to provide the resulting strain behaviour presented in Fig.6.6 that is solely dependent on the stress regimes. In this diagram the axes are defined by

$$p_x = \frac{P^R}{d} \quad \text{and} \quad \sigma^\theta .$$

For loading histories that fall within the area marked E the response of the structure is purely elastic. For operating conditions in the area P_1 certain parts of the structure suffer alternating plasticity and in regions S_1 and S_2 the response of the structure is purely elastic after initial yielding during the first cycle of load application. This condition is referred to as the shakedown condition and whilst S_1 and S_2 both define operating conditions for shakedown, the permanent residual stress groups in each area differ from one another. The lines $\sigma^\theta = 2\bar{\sigma}_y$ and $p_x + \sigma^\theta/4 = \bar{\sigma}_y$ define the shakedown limit.

In the first set of solutions the temperature history is the same as used by Ponter and Leckie[3] where

$$\theta_{11} = \theta_{12} = \theta_{21} = 723°K \ , \quad \theta_{22} = 856°K$$

and the maximum thermo-elastic stress $\sigma^{\theta} = \bar{\sigma}_y$.

Work bounds and associated displacements per cycle ΔU_x^u and ΔU_x^L were computed for a sequence of values of p_x assuming $\Delta U_y = 0$. The sequence of values of p_x corresponds to the line OO' in Fig.6.6. As the shakedown solution corresponds to the largest load for which a solution of the form σ_{ij}^* exists for $f(\sigma_{ij}^*) < 0$, the upper bound may be computed only within a region formed by the shakedown limit surface scaled by a factor $n/n+1$. This is shown for an arbitrary n as the broken line in Fig.6.6. The results were normalised with respect to $W(\sigma^{\theta},\theta_m)$ and $\Delta U_x(\sigma^{\theta},\theta_m)$ the work and displacements computed on the assumption that the stress σ^{θ} and temperature θ_m occur through the thickness of the plate during a complete cycle.

The non-dimensional work bounds are shown in Figs.6.16, 6.17 and 6.18 and the associated displacements in Figs. 6.19, 6.20 and 6.21 for values of the stress index equal to 3 , 7 and 11 respectively. The results derived for $n = 7$ duplicate the results obtained by Ponter and Leckie. The assumption that the value of the stress index remains constant over this temperature range provides a simplification of the problem since in practice the stress index appears to be highly sensitive to temperature. A necessary precaution in predicting the structural response to the applied loads is to, in addition, investigate the behaviour for the two extreme values of n usually encountered in engineering materials i.e. $n = 3$ and $n = 11$. This clearly provides a complete spectrum of behaviour that can be predicted within the sense signified by the bounding solution.

It is seen that the bounding solutions to the plate problem exhibit similar features to those obtained to the two-bar structure. At larger values of p_x and for all values of n the difference between the work bounds becomes small. As the stress index increases the difference

between the bounds also increases, thus the percentage of the total energy dissipation that is associated with thermal ratchetting effects also increases. The stress distribution of p_x and p_y corresponding to $p_x = 0.64$ are shown in Figs.6.22, 6.23 and 6.24 where the upper bound σ^*_{ij} appears as the full lines. An important and distinct feature of these profiles is that they are close to each other during the period when the higher temperature acts and on the cooler side of the plate. At other positions and times the stresses do not approach each other. The reason for this behaviour as in the previous problem is that when the effects of stress redistribution due to the thermal stress are small in comparison to the applied loads the upper and lower work bounds become equal. In the lower bound solution the energy dissipation is dominated by the stresses in this region because of the rapid variation of material behaviour with temperature and consequently the contribution to the total deformation from the first part of the cycle is considerably less than the contribution from the second part of the cycle when the creep rates are higher. The optimal upper bound involves a residual stress field that makes the inelastic energy dissipation a minimum and since most of the energy dissipation occurs during this dominant region and time the stresses may be expected to lie close to the lower bound solution which provides the absolute minimum energy dissipation rate for any equilibrium stress field. It is seen that the stress profiles show a marked sensitivity to the value of the stress index.

For smaller values of p_x the work bounds and associated displacements, as in the two-bar problem, diverge and the upper work bound tends towards a value associated with the thermal cycling alone. The stress profiles corresponding to a small value of the applied load, $p_x = 0.2\,\sigma^\theta$, are shown in Figs.6.25, 6.26 and 6.27 for $n = 3$, 7 and 11 respectively. For $n = 3$ the ratio of the work bounds is approximately 4 and the upper and lower bound stress profiles still show a tendency to follow one another

during the hotter part of the cycle. However as n increases the two stress histories diverge and do not approach each other for any part of the cycle. Therefore there exists no dominant time interval during which the majority of the deformation can be accumulated. In this region the thermal load is large compared with the applied load and the deformation becomes dominated by the deformation associated with the thermal stress field. As the applied load approaches zero the displacements per cycle derived from the lower work bound also approach zero, but in the upper bound case, zero displacement corresponds to a small non-zero value of p_x. At this value the upper work bound attains a minimum value. Further decrease in the applied load increases the energy dissipation and the displacement per cycle becomes negative. At $p_x = 0$ the upper work bound equals the energy dissipation associated with thermal cycling alone.

In the two-bar problem the effect on the work bounds of neglecting the variation of material behaviour with temperature indicated that large ratchetting effects occur. Similarly, to assess the effect in this problem the calculations were repeated with $\Delta H = 0$. The thermal expansion terms were included and the creep rate scaled so that

$$k = \exp(-\Delta H/R\theta_m)$$

The resulting work and displacement bounds are shown as dotted lines in Figs.6.16 to 6.21. The difference between the upper and lower work bounds is again seen to have increased considerably for any given value of n. The reason for this increased ratchetting effect may be understood from the stress histories involved which are shown in Fig.6.28, for $n = 3$ and $p_x = 0.6\ \sigma^{\theta}$. The upper bound solution appears as a full line. As no thermal softening effects are included there exists no dominant time interval or locations and the stress histories do not approach each other for any part of the cycle. As in the two-bar problem the effect of thermal softening appears therefore to reduce the statical indeterminancy

of the structure and thus reduce the ratchetting effects. The exclusion of thermal softening results in very non-conservative displacement predictions and erroneous stress histories.

The preceding solutions to the plate problem have been obtained under conditions of plane strain. In order to gain an overall assessment of the structural behaviour under some arbitrary load system the effects of various applied stress systems (p_x, p_y) were investigated. Contours of constant work W^u and W^L were computed for an arbitrary work value of $W/W(\sigma^\theta, \theta_m) = 3 \times 10^{-3}$. Contours corresponding to this value are shown in Fig.6.29 for $n = 3$ and 11. The lower work bound in each case forms an ellipsoidal curve symmetrically placed about the line $p_x = p_y$. In addition the major and minor axes intersect at $p_x = p_y = 0$ and in the limit the work contour $W^L = 0$ reduces to this point. The upper bound contour on the other hand exhibits a sensitivity to the sign of the applied stress resultant. It was shown for $\Delta U_y = 0$ that the work value was non-zero and positive for zero displacement per cycle. The calculations reveal that zero displacements and hence minimum energy dissipation correspond to a positive applied load shown as point P for the three values of n. It may be noted that the values of $p_x = p_y$ at point P differ for each value of n. The displacements corresponding to the work contours are shown in Fig.6.30. The contour corresponding to the lower work bounds in each case forms an ellipsoidal curve symmetric about both $\Delta U_y = \Delta U_x$ and $\Delta U_y = -\Delta U_x$, and the upper bound contour forms a closed curve symmetrically placed about $\Delta U_y = \Delta U_x$. The reason for the lower bound solution providing displacements greater than those of the upper bound solution may be explained simply by the fact that since the magnitude of any stress system is greater for any given work quantity in the lower bound case and there is no energy dissipation associated with thermal ratchetting effects, the displacements must therefore be correspondingly higher.

If the work bounds alone are considered the most severe difference between the upper and lower bound stress resultant occurs when $p_x = p_y \leqslant 0$. However, in terms of the displacements the most severe situation occurs when $p_y = -p_x$ for both $p_x < 0$ and $p_x > 0$. The displacement vectors are in the same direction as the applied stress vectors and it can be seen that the most severe stress situation in terms of the work quantities produces the least severe situation in terms of displacements.

It must be remembered that the diagrams represent contours of constant non-dimensional quantities and the absolute values are dependent on n and in these circumstances it is difficult to distinguish between individual features corresponding to any given value of n.

6.5. Discussion.

The solutions presented for the plate problem have shown that many of the features observed in the two-bar structure also pertain to this problem. It has been shown[1] that the upper bound solution probably corresponds to the actual solution that occurs in practice in cases of variable loading under isothermal conditions. This may also be true of cyclic temperature conditions although no formal proof is offered and the exact conditions when this may be assumed remains open to question.

It has been shown that the deviation of the upper bound from the steady state lower bound solution is sufficiently pronounced to require inclusion in design calculations and that the lower bound is clearly non-conservative. If the effects of temperature on material behaviour is excluded the resulting solutions produce highly non-conservative displacements and erroneous stress histories.

The upper bound solution provides a clear picture of the variation of stress during the cycle and the characteristic feature of the plate problem appears to be a period of high stress at a lower temperature followed by a

lower stress at the higher temperature. The two-bar structure represents a more severely loaded structure and from the results it is difficult to identify a characteristic feature. This will be discussed further in Chapter 7.

The final aspect is the variation of the bounds with the value of the stress index. Distinct behaviour patterns dependent on n have been shown and therefore unless, under such situations, prediction of structural behaviour that is independent of n can be found, a knowledge of the exact value is required.

Youngs Modulus	2×10^7 lb/in^2
Poisso ns' Ratio	0.3
Yield Stress	2.1×10^3 lb/in^2
Coefficient of Expansion	3.3×10^{-7}/°K
Creep Activation Energy	342 KJ/mole

Table 6.1

Material Properties of 816-type Stainless Steel

n = 3

$\Delta\theta$	$\Delta U^u/\Delta U^L$	W^u/W^L
0	1.000	1.000
10	1.033	1.066
20	1.132	1.265
30	1.296	1.602
40	1.527	2.084
50	1.823	2.722
60	2.185	3.527
70	2.613	4.516

n = 7

$\Delta\theta$	$\Delta U^u/\Delta U^L$	W^u/W^L
0	1.000	1.000
10	1.235	1.316
20	1.989	2.366
30	3.422	4.476
40	5.805	8.227
50	9.541	14.535
60	15.192	24.740
70	23.503	40.738

n = 11

$\Delta\theta$	$\Delta U^u/\Delta U^L$	W^u/W^L
0	1.000	1.000
10	1.644	1.785
20	4.090	4.931
30	10.113	13.286
40	23.493	33.336
50	51.426	78.362
60	106.859	174.026
70	212.147	367.718

Table 6.2

Ratio of Bounds for the Two-bar Structure with $\Delta H = 0$

n = 3

$\Delta\theta$	$\Delta U^u/\Delta U^L$	W^u/W^L
0	1.000	1.000
10	1.001	1.001
20	1.001	1.001
30	0.998	1.001
40	0.995	1.001
50	0.993	1.001
60	0.992	1.002
70	0.990	1.002

n = 7

$\Delta\theta$	$\Delta U^u/\Delta U^L$	W^u/W^L
0	1.000	1.000
10	1.048	1.087
20	1.144	1.267
30	1.209	1.409
40	1.216	1.463
50	1.183	1.439
60	1.136	1.372
70	1.093	1.288

n = 11

$\Delta\theta$	$\Delta U^u/\Delta U^L$	W^u/W^L
0	1.000	1.000
10	1.268	1.353
20	1.901	2.241
30	2.649	3.419
40	3.343	4.681
50	3.864	5.829
60	4.151	6.702
70	4.181	7.188

Table 6.3

Ratio of Bounds for the Two-bar Structure with $\Delta H \neq 0$

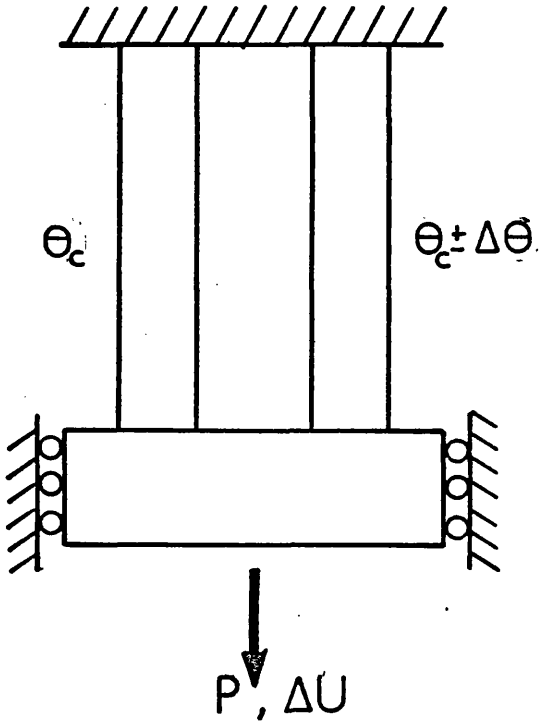

Fig.6.1 Two-bar Structure

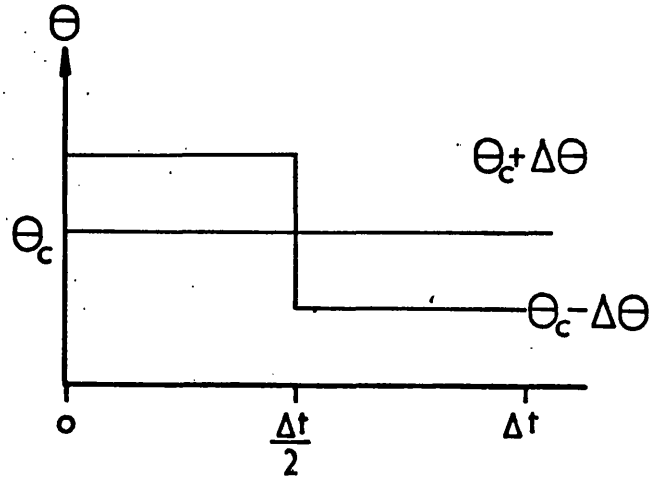

Fig.6.2 Cyclic Temperature History

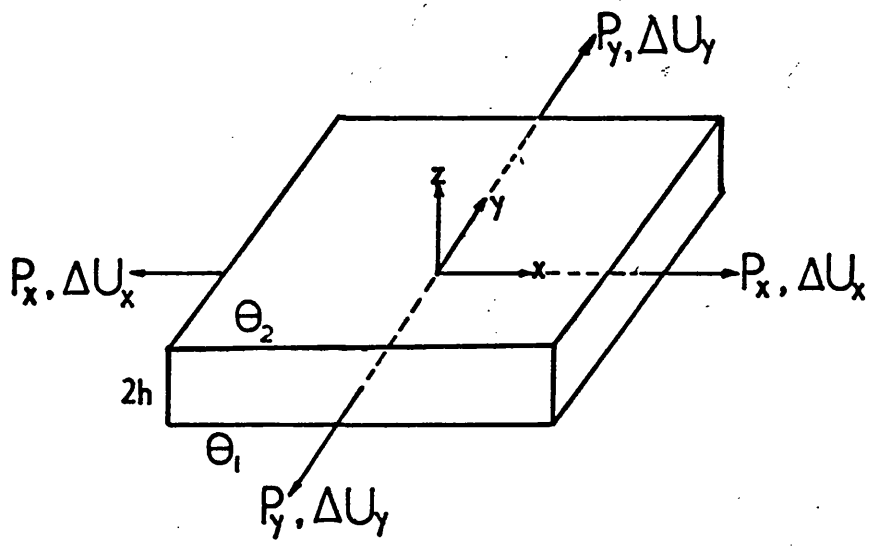

Fig 6.3 Plate Problem

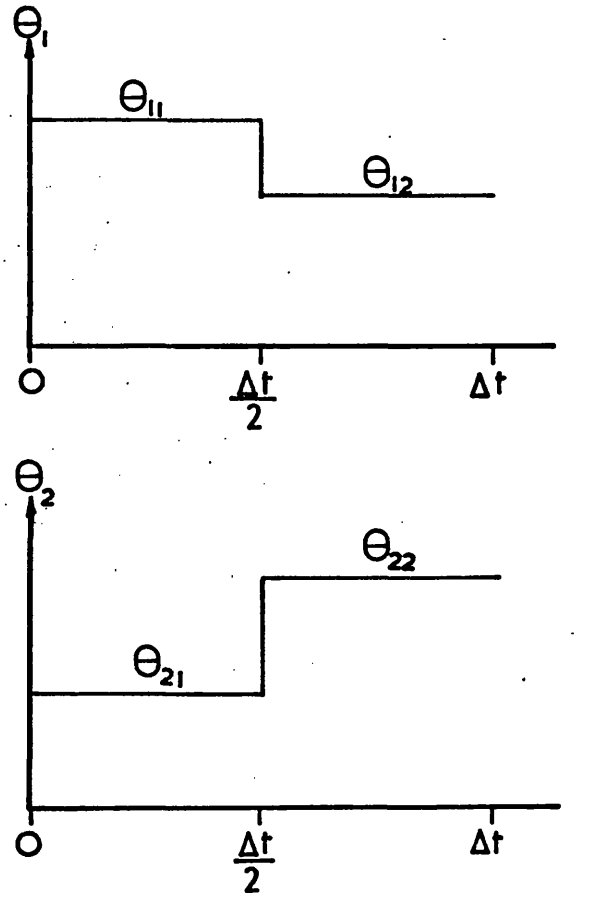

Fig.6.4 Cyclic Temperature History

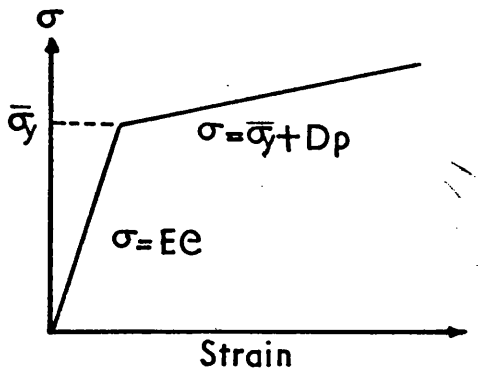

Fig 6.5 Stress-strain Behaviour

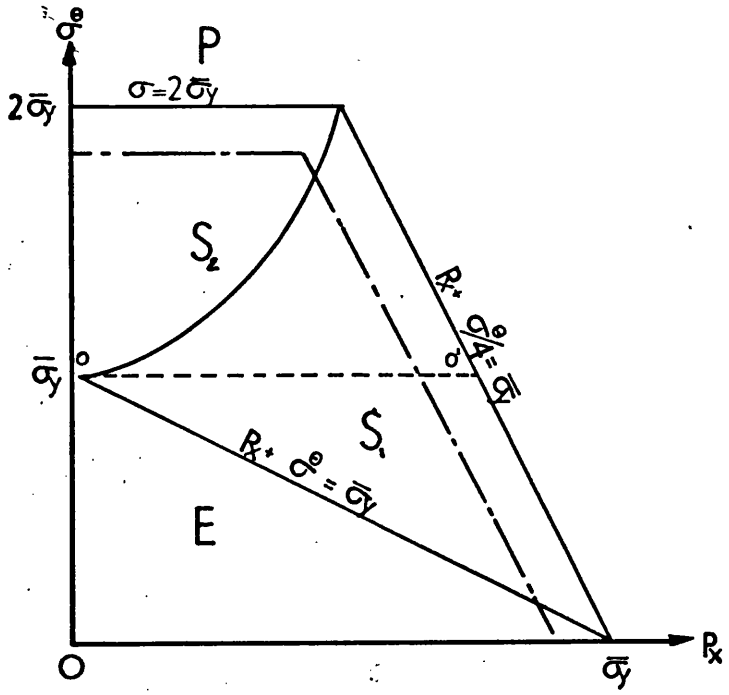

Fig 6.6 Stress Regimes for Non-Work Hardening Material

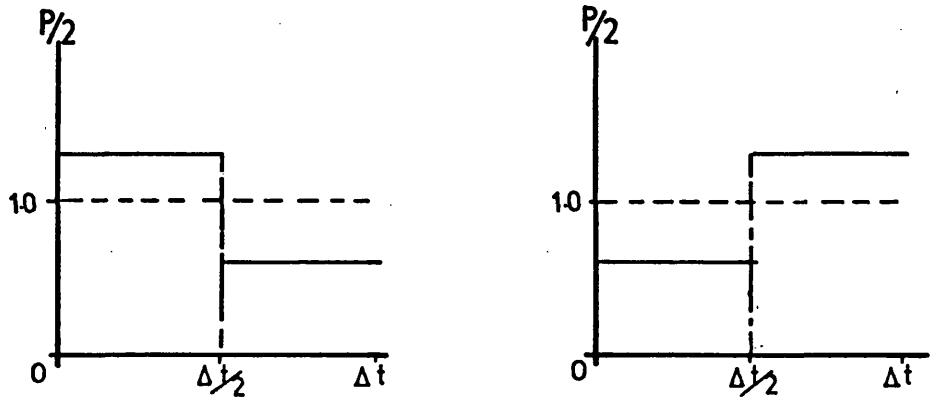

ΔH=O

ΔH≠O

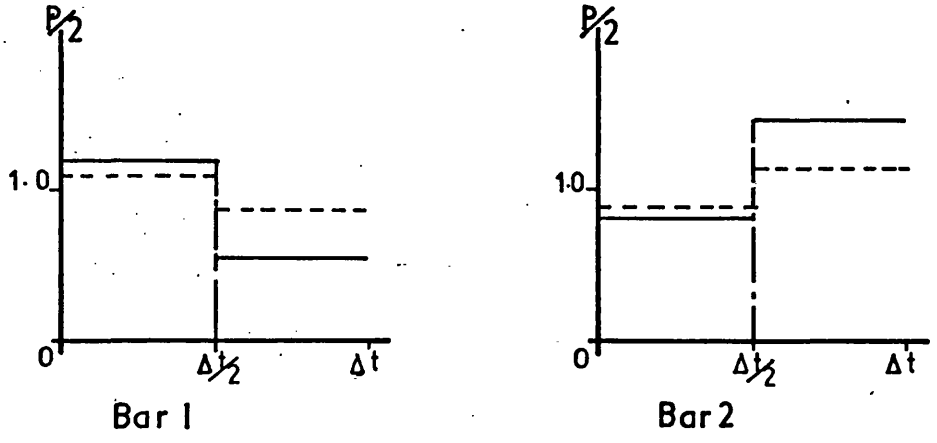

Fig 6·7· Stress histories for $\Delta\Theta = 30^{\circ}K$, $n=7$

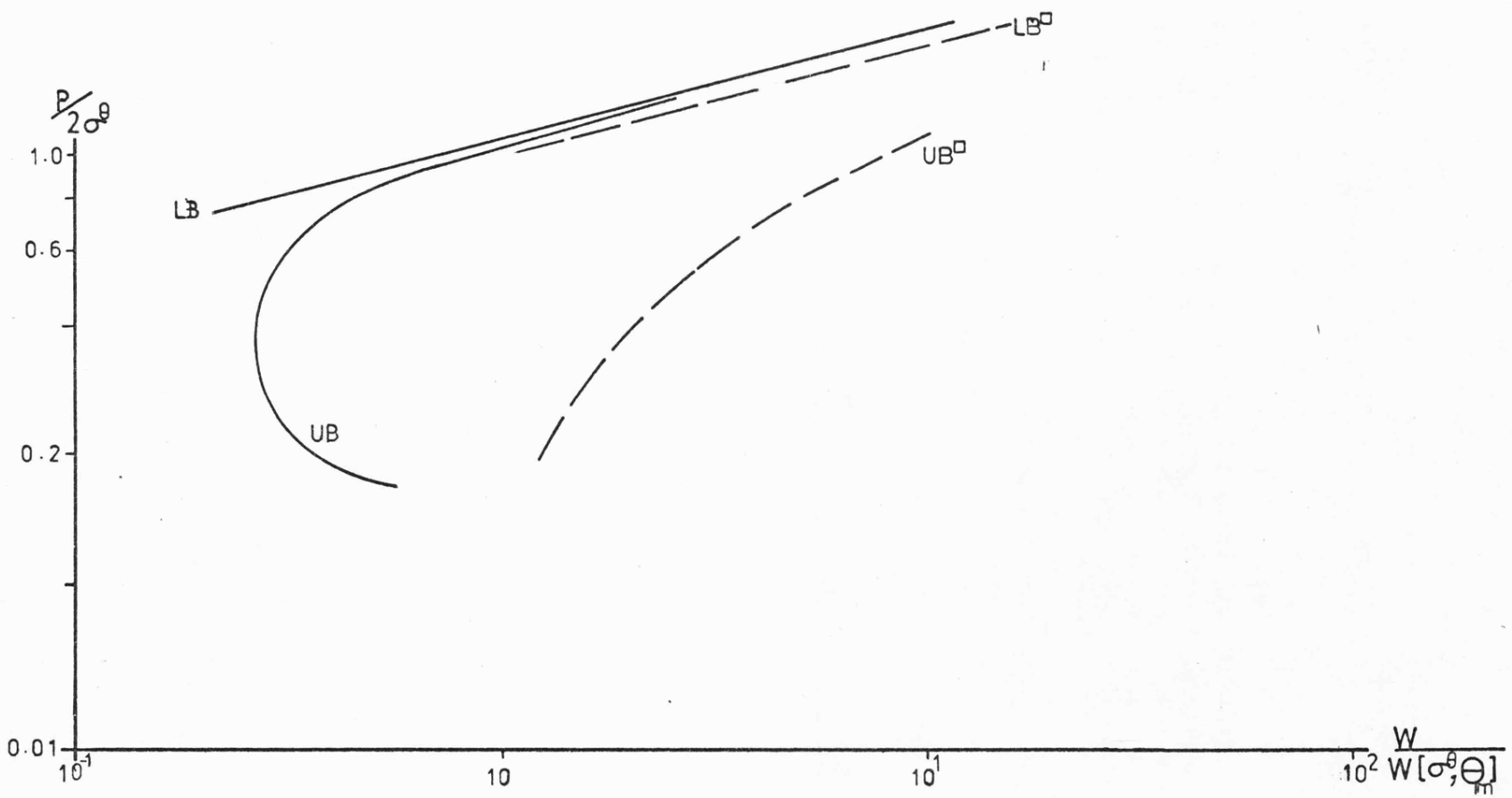

Fig.6.8 Work Bounds [n=3]

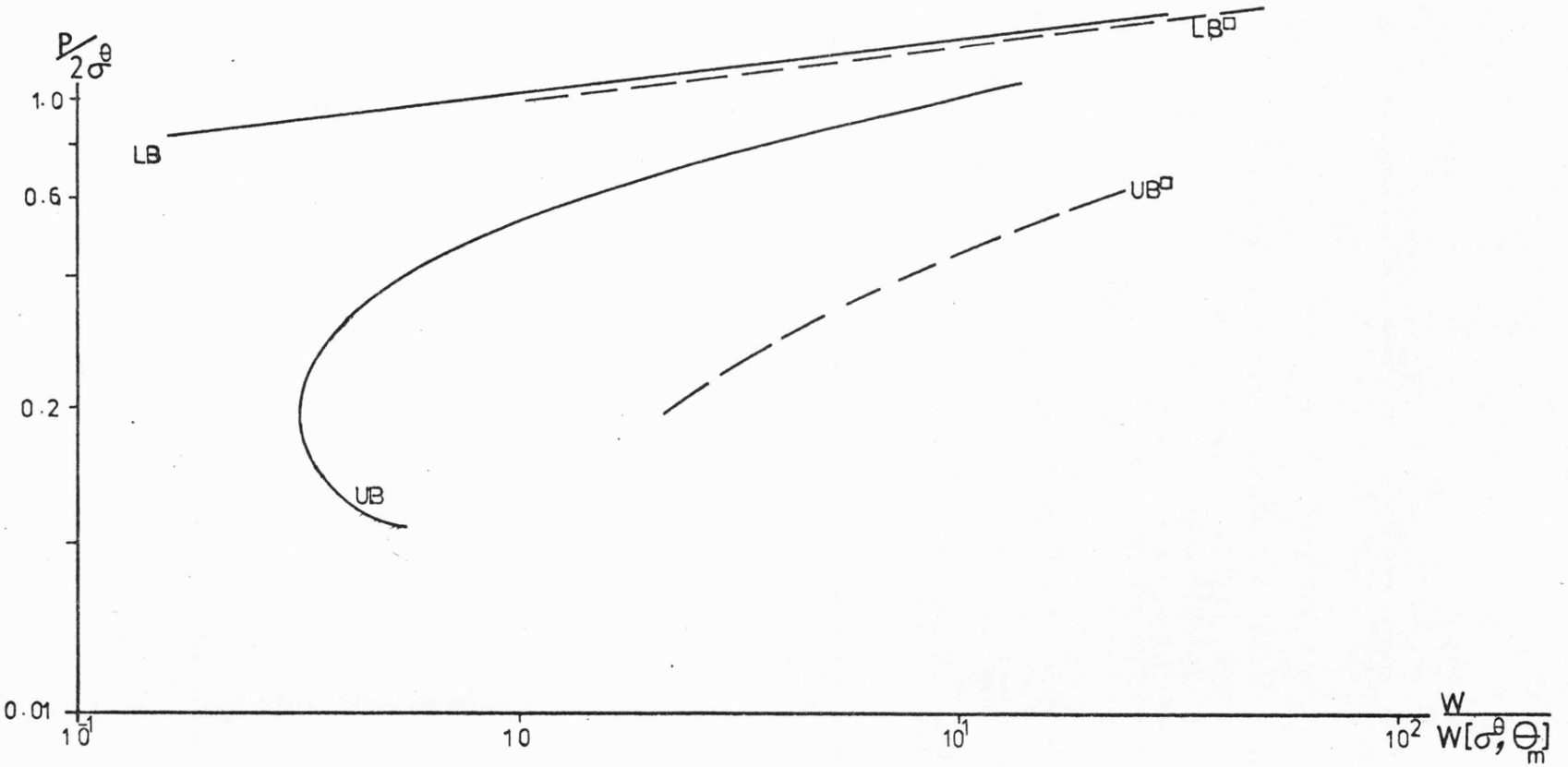

Fig.6.9 Work Bounds [n=7]

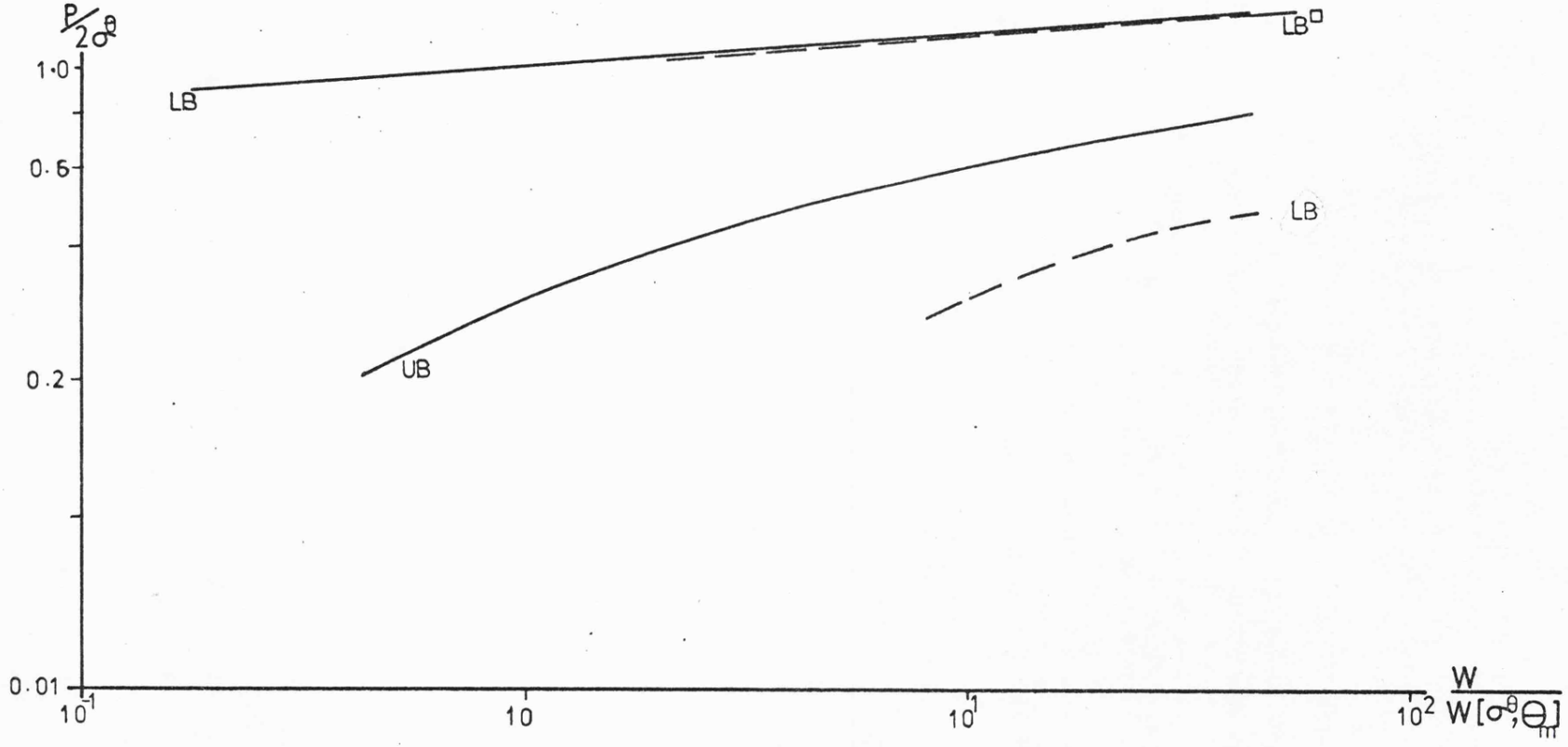

Fig 6·10 Work Bounds [n=11]

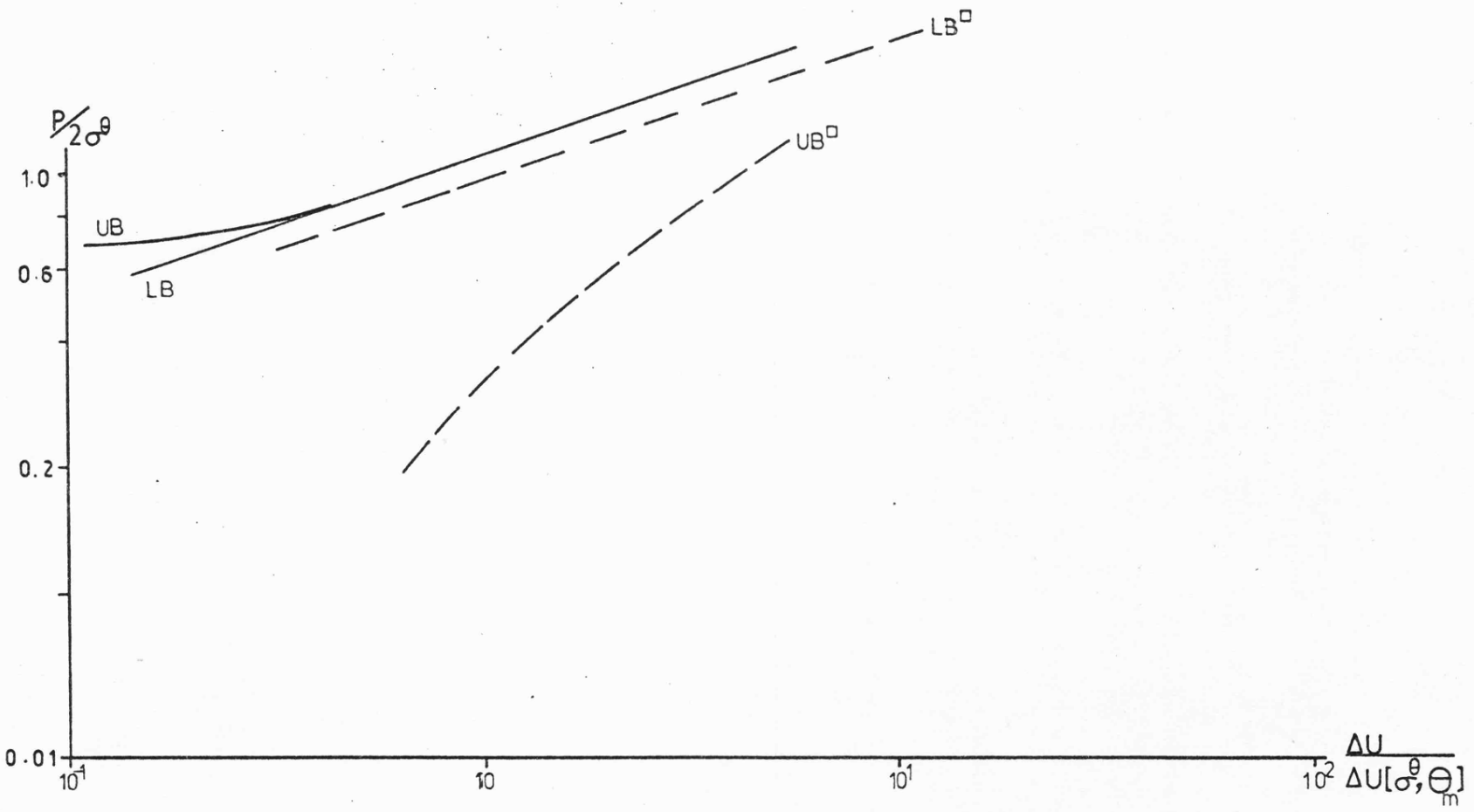

Fig 6.11 Displacements corresponding to the Work Bounds [n = 3]

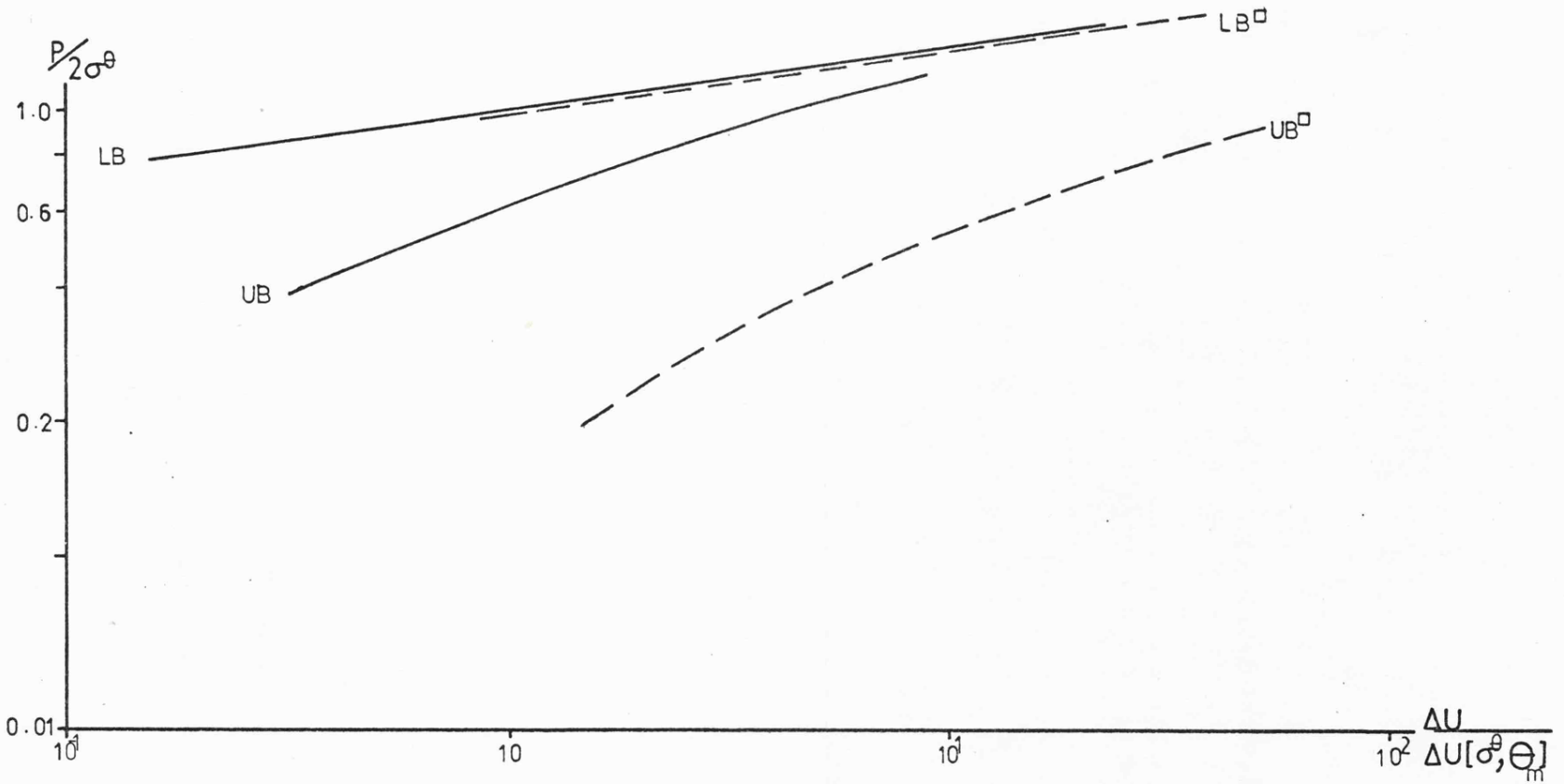

Fig 6.12 Displacements corresponding to the Work Bounds [n=7]

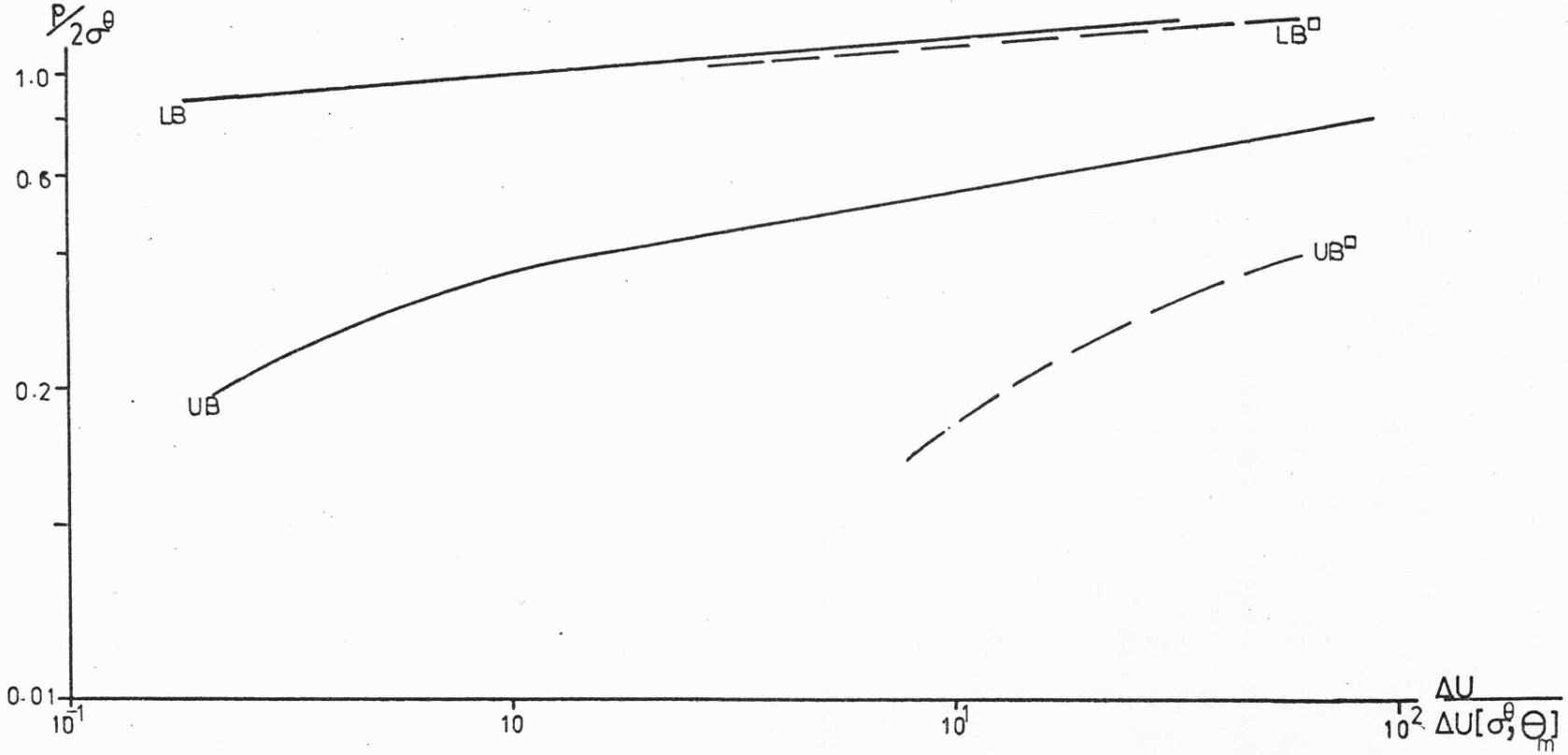

Fig 6.13 Displacements corresponding to the Work Bounds [n=11]

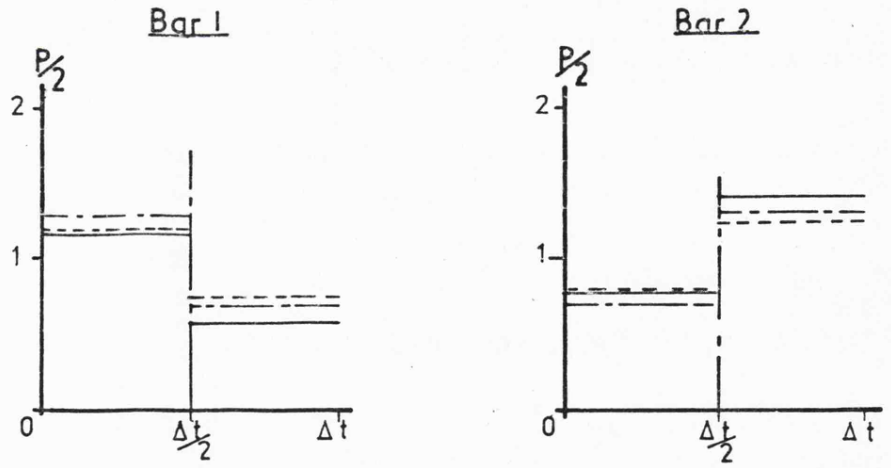

a] $P=1.7\bar{\sigma}_y$, $W^U/W^L=1.03$

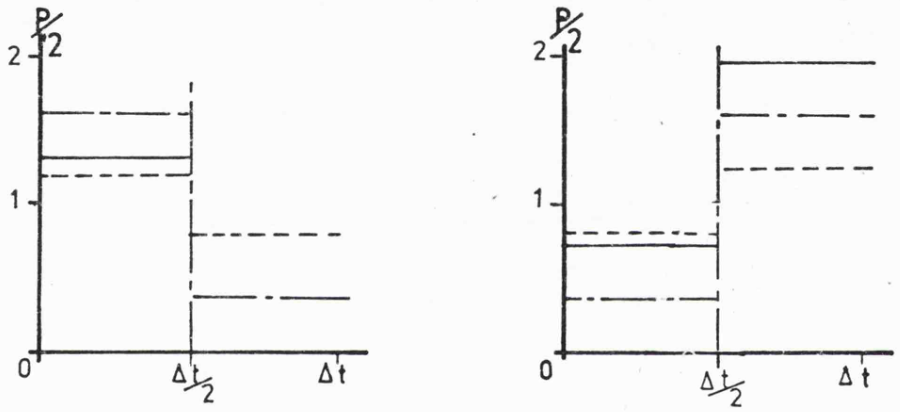

b] $P=0.8\bar{\sigma}_y$, $W^U/W^L=2.26$

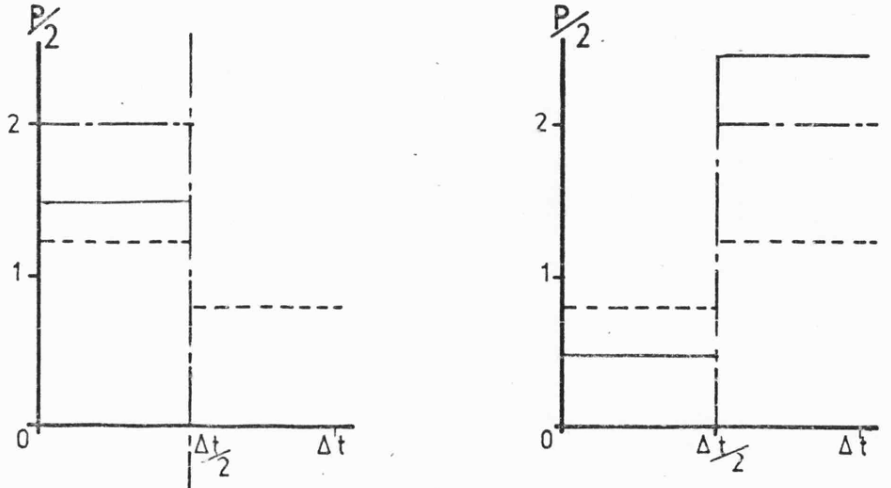

c] $P=0.5\bar{\sigma}_y$, $W^U/W^L=11$

Fig 6.14 Stress histories for $\Delta\Theta$ 47°K, $n=7$

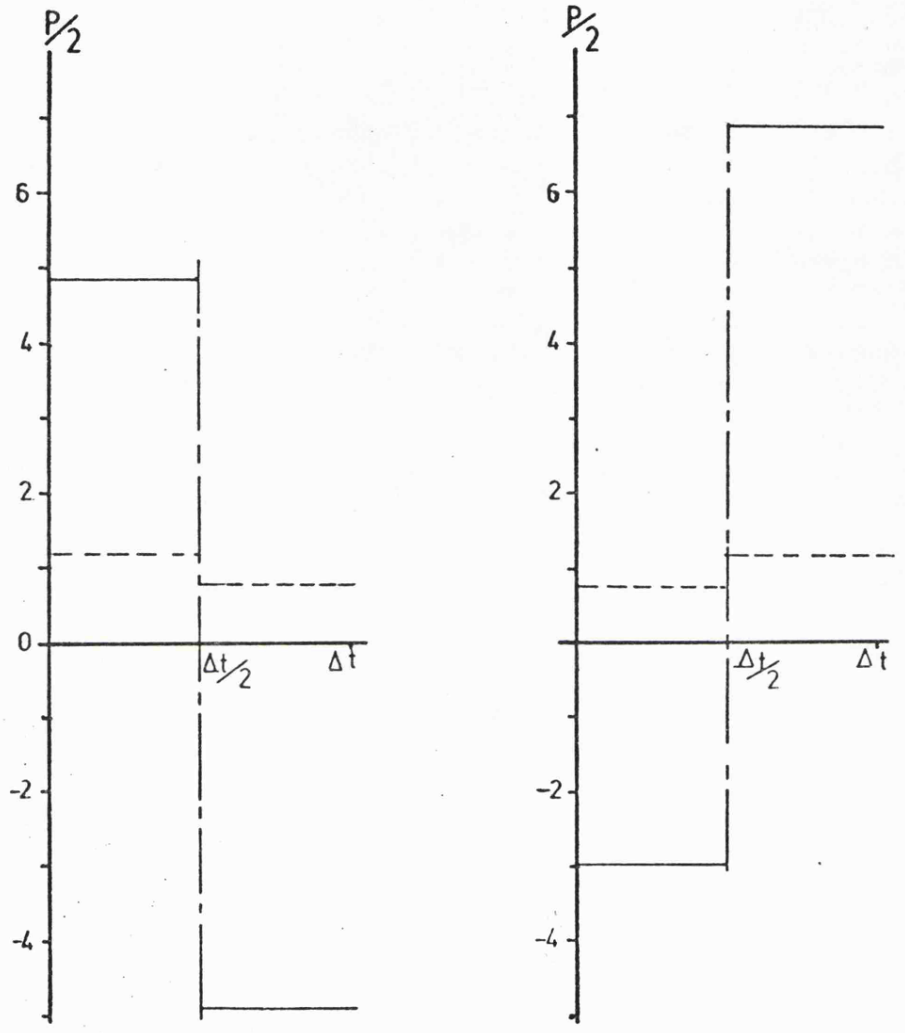

Bar 1 Bar 2

$P = 0.1\bar{\sigma}_y \quad \Delta U = 0$

Fig 6.15 Stress history for $\Delta\Theta = 47°K$, $n = 7$

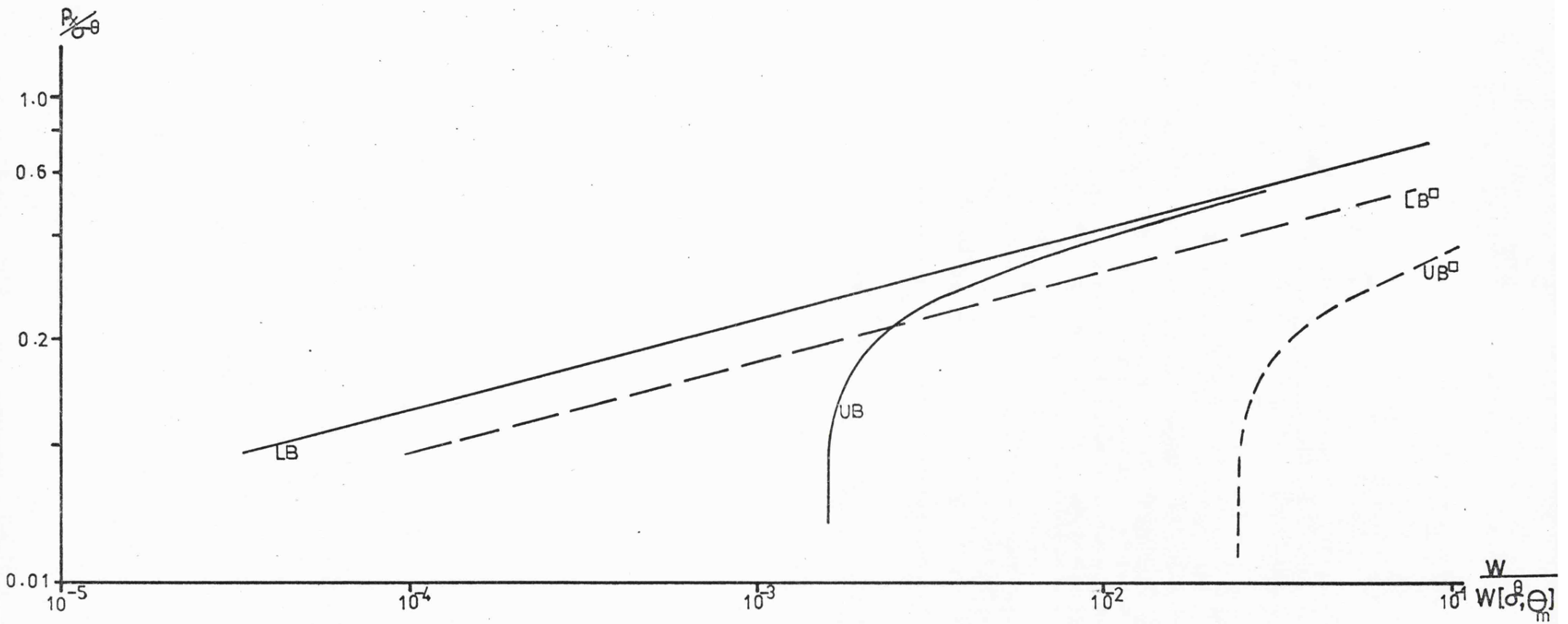

Fig 6.16 Work Bounds [n = 3]

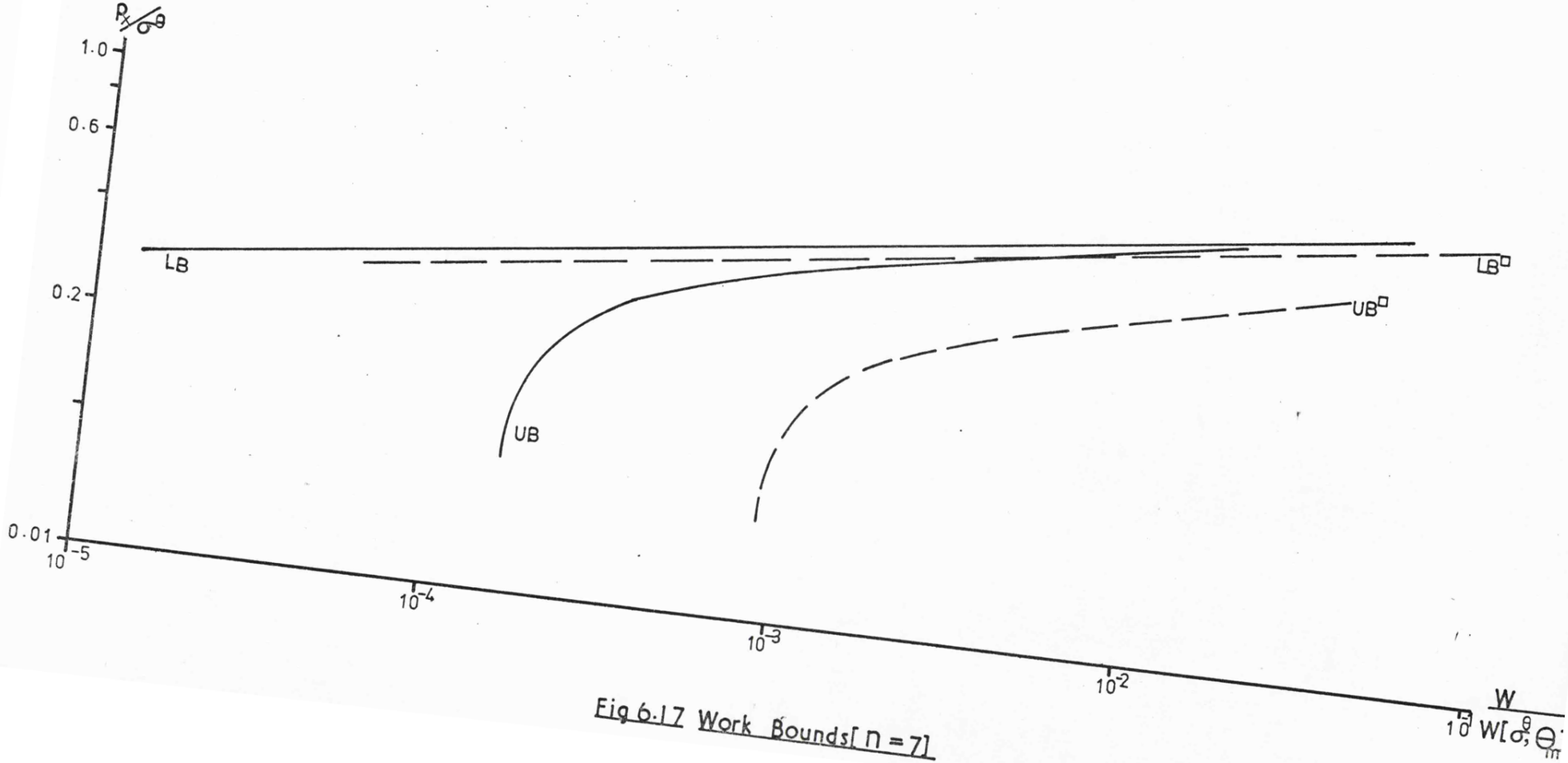

Fig 6.17 Work Bounds[n = 7]

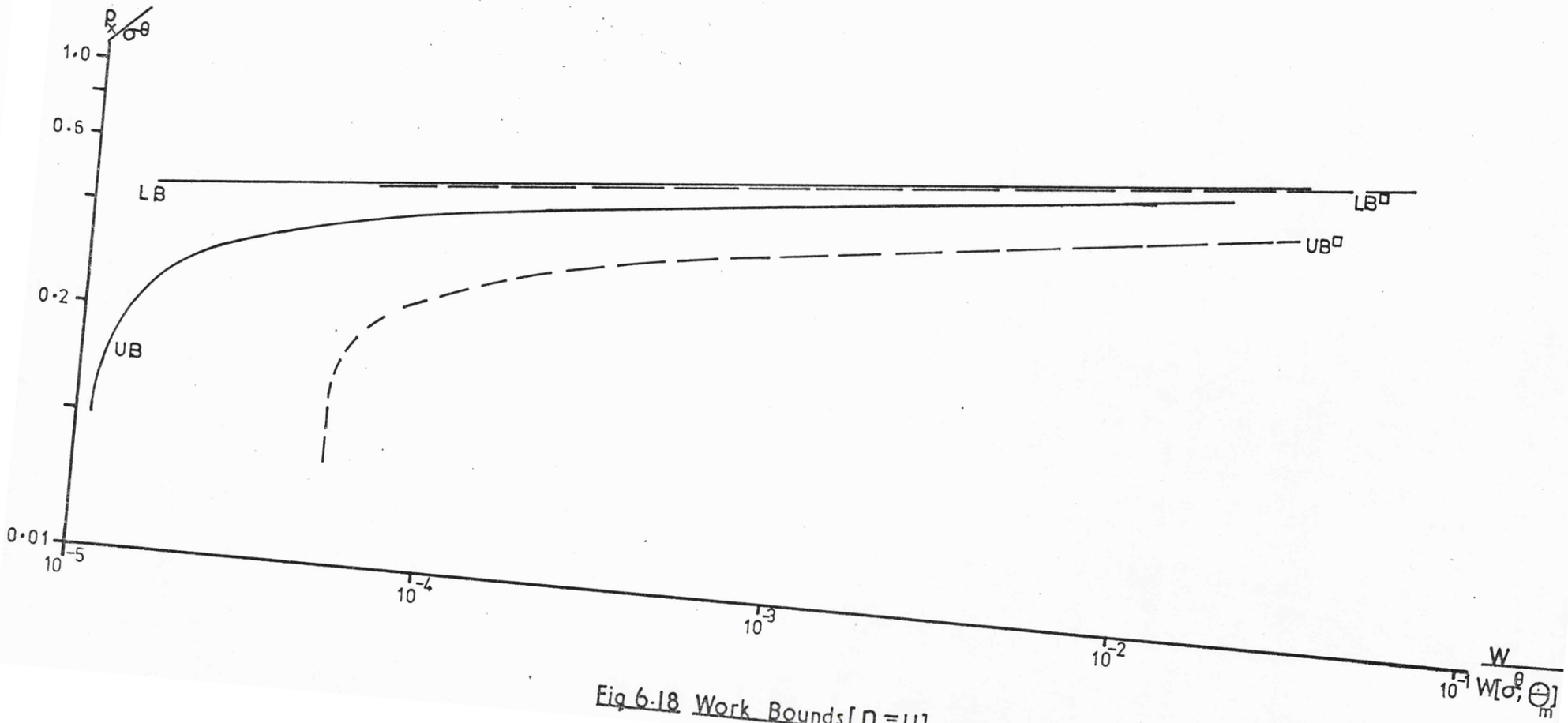

Fig 6.18 Work Bounds [n = 11]

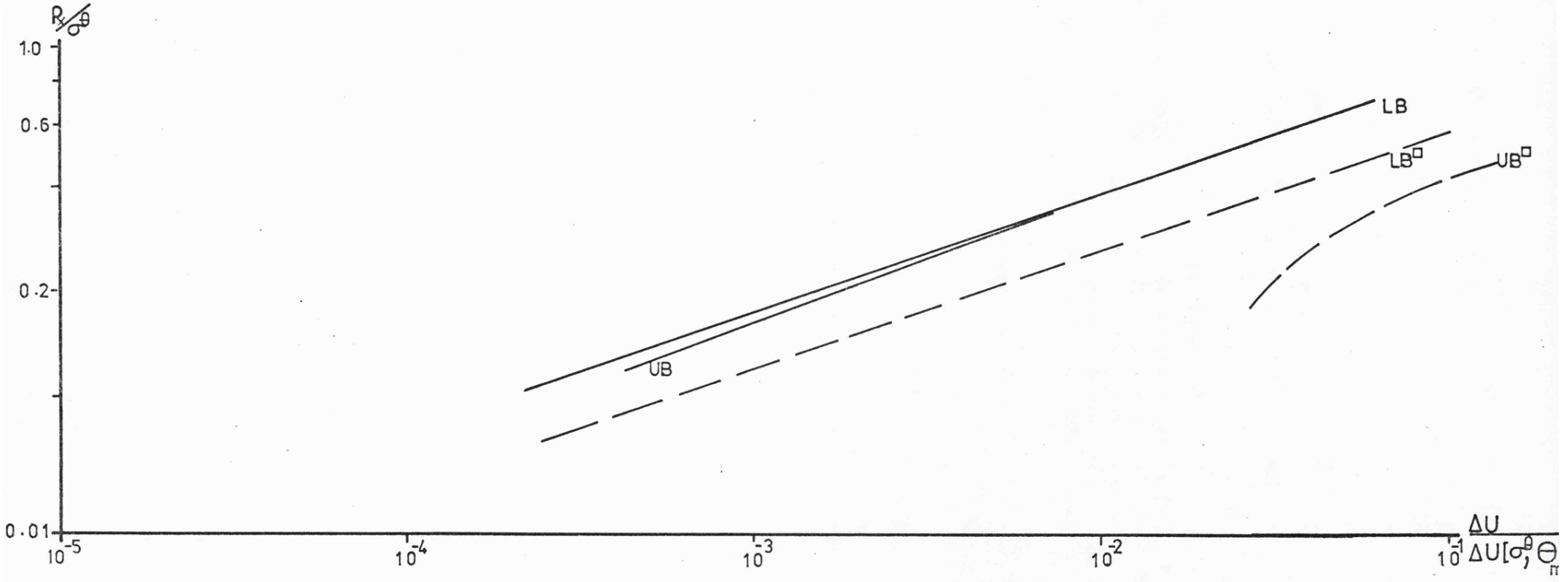

Fig 6.19 Displacents corresponding to the Work Bounds[n=3]

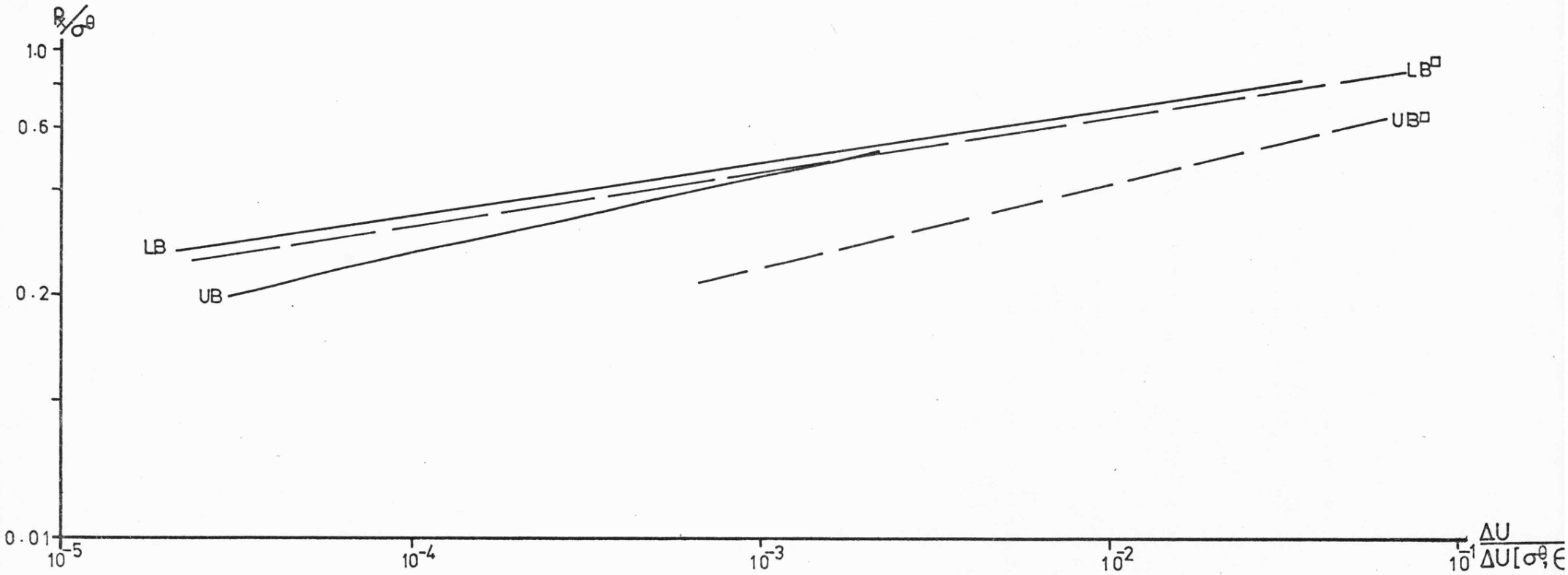

Fig 6.20 Displacements corresponding to the Work Bounds [n=7]

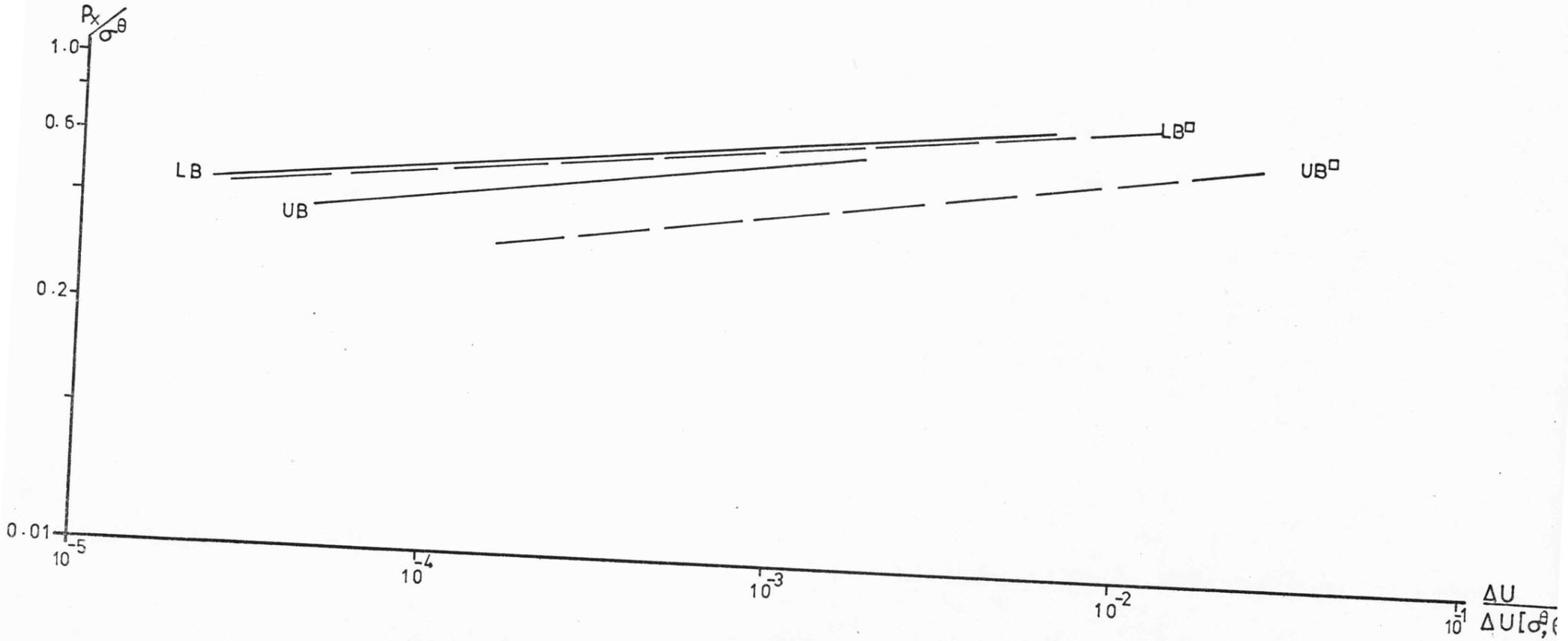

Fig 6.21 Displacements corresponding to the Work Bounds [n=11]

PLATE

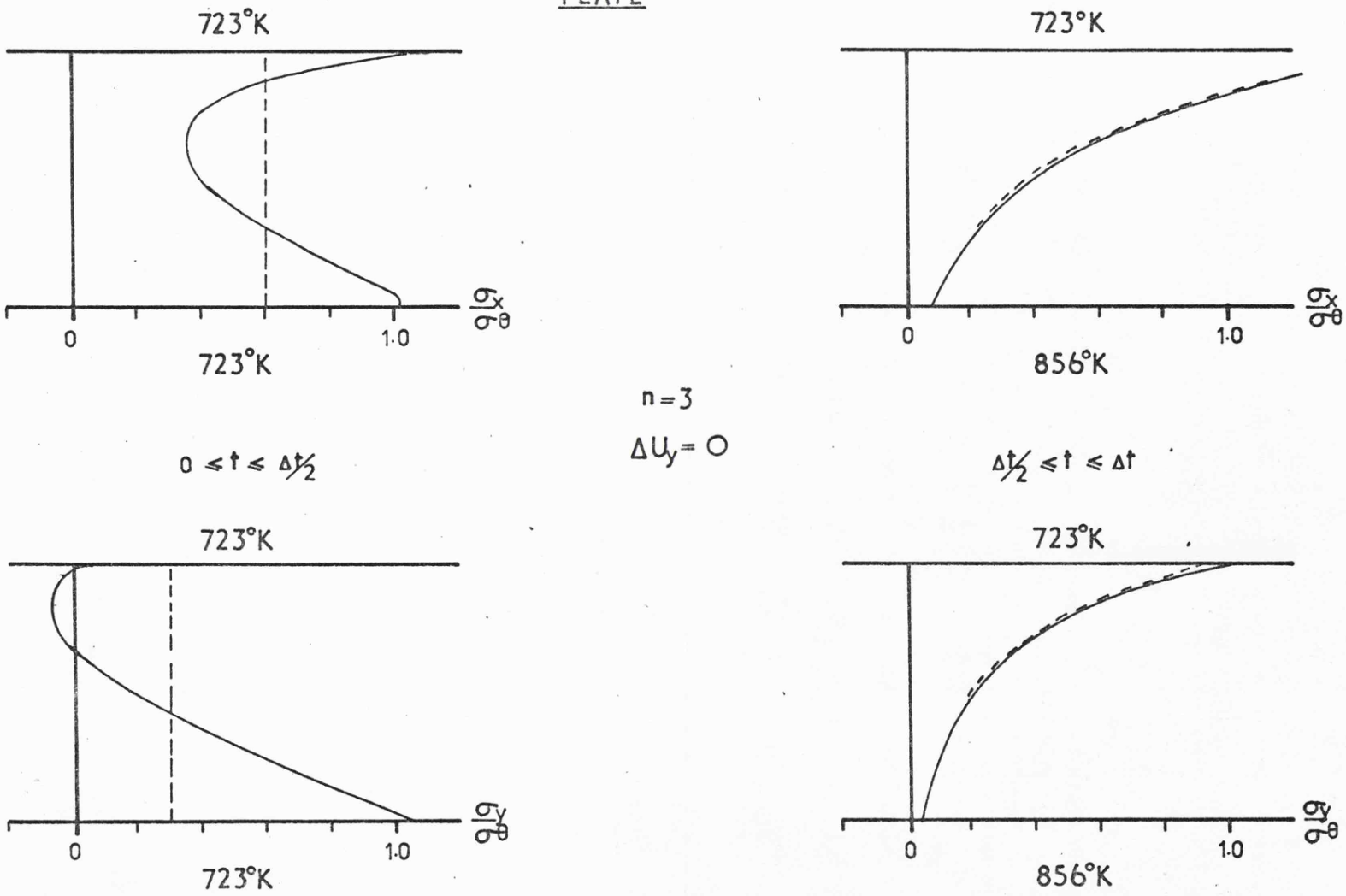

Fig 6·22 Stress distribution for $P_x/\sigma^\theta = 0{\cdot}6$

PLATE

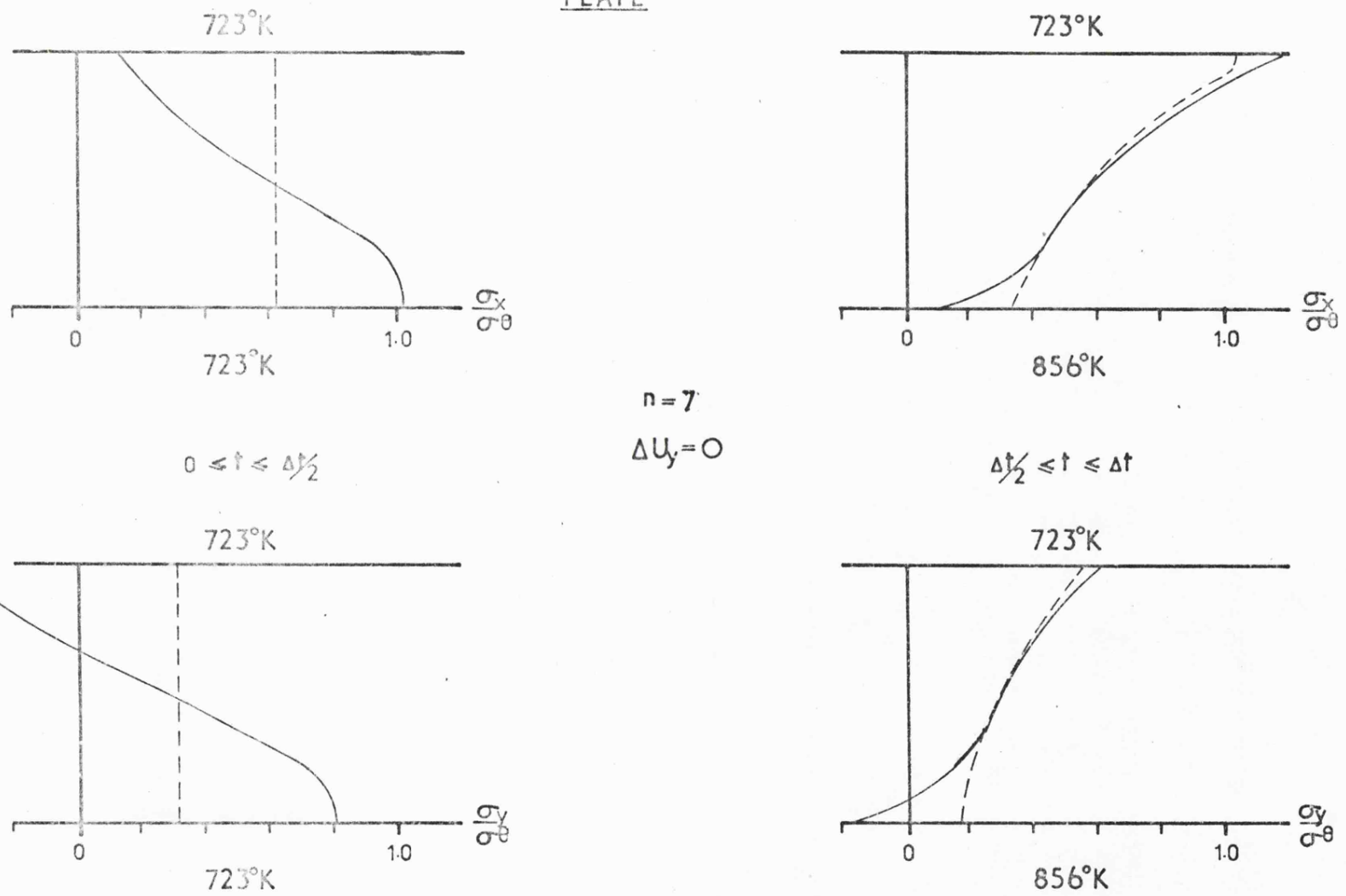

Fig 6·23 Stress distribution for $P_x/\sigma_\theta = 0·6$

PLATE

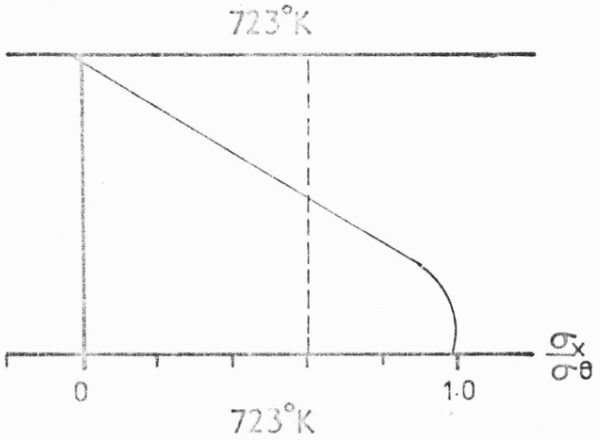

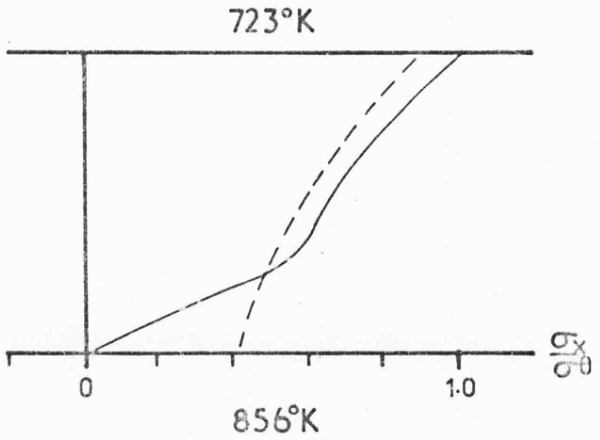

n = 11

$\Delta U_y = 0$

$0 \leq t \leq \Delta t/2$

$\Delta t/2 \leq t \leq \Delta t$

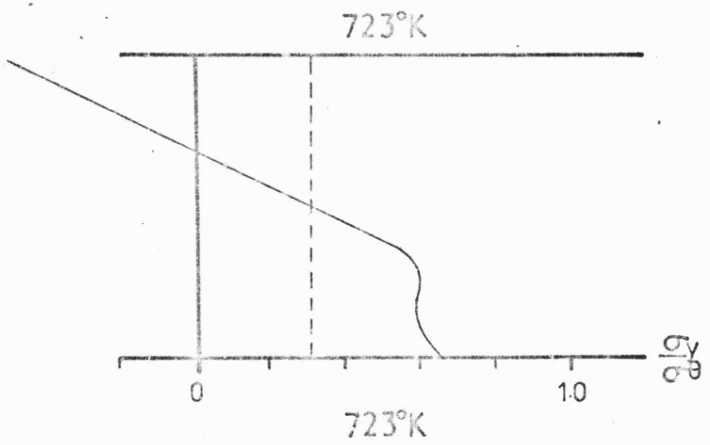

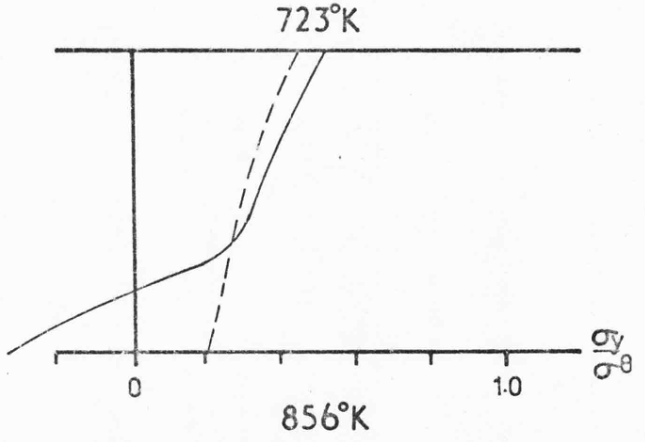

Fig 6.24 Stress distribution for $P_x/\sigma_\theta = 0{\cdot}6$

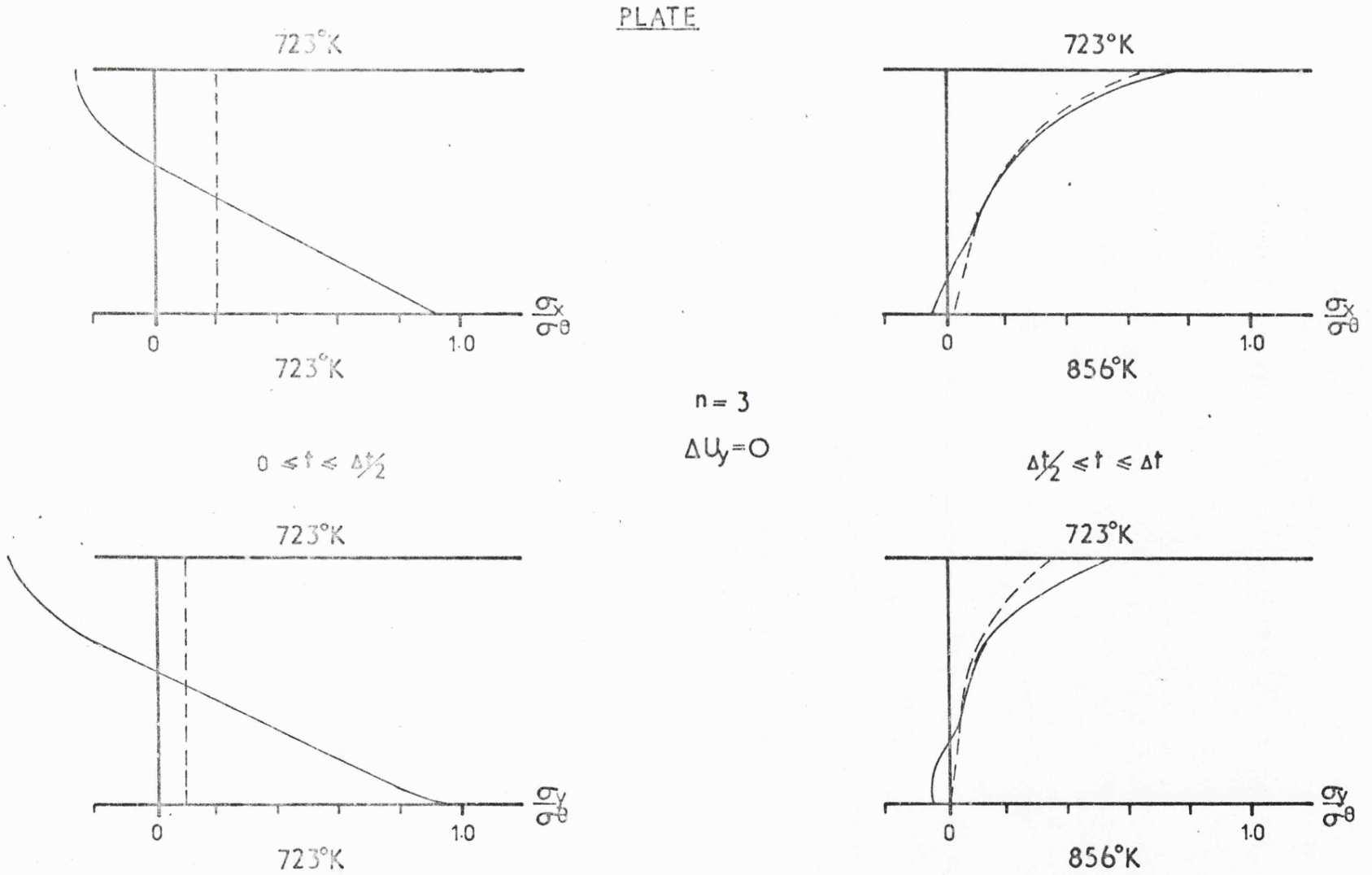

Fig 6·25 Stress distribution for $P_x/\sigma^\theta = 0{\cdot}2$

PLATE

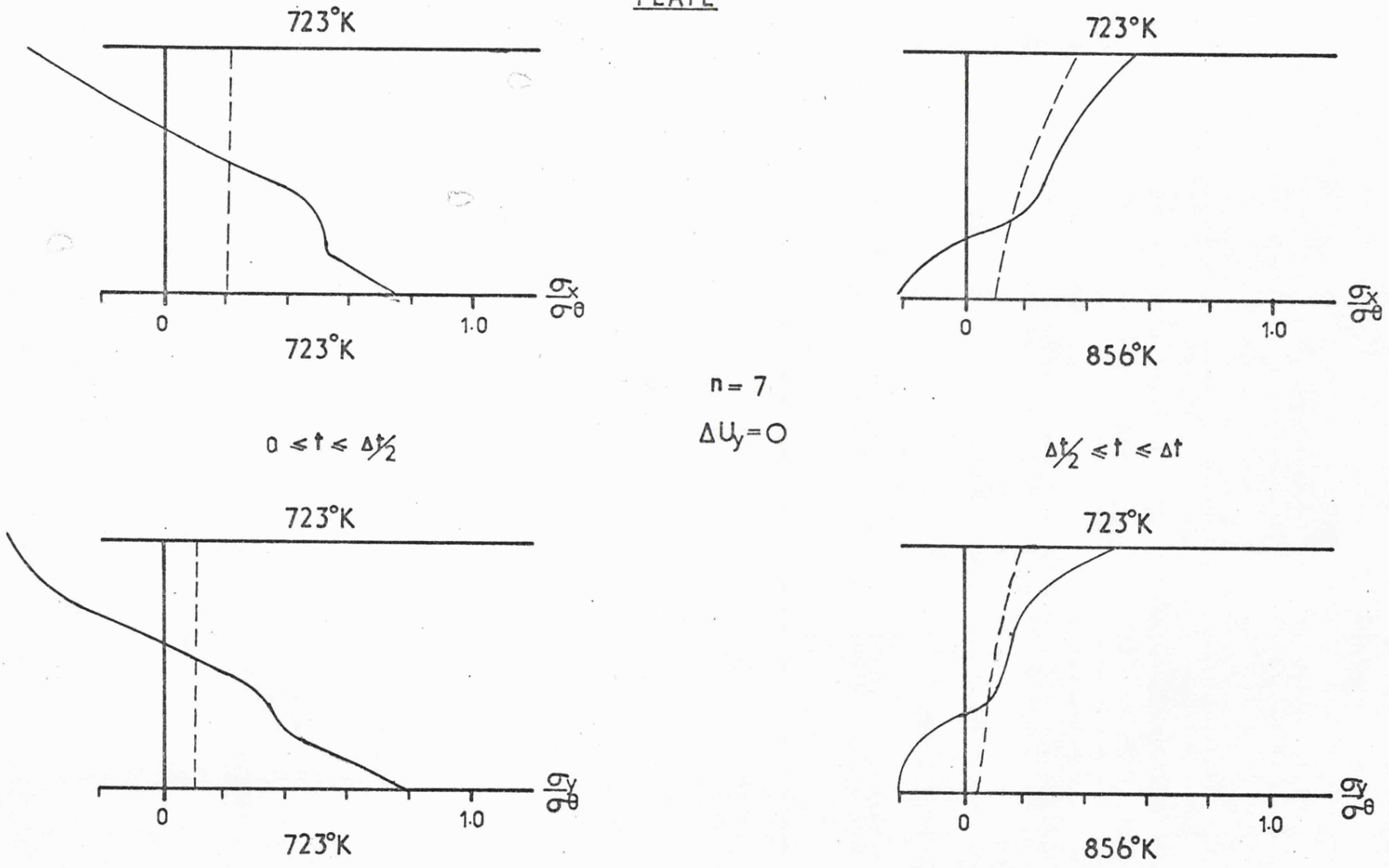

Fig 6·26 Stress distribution for $P_x/\sigma^\theta = 0{\cdot}2$

PLATE

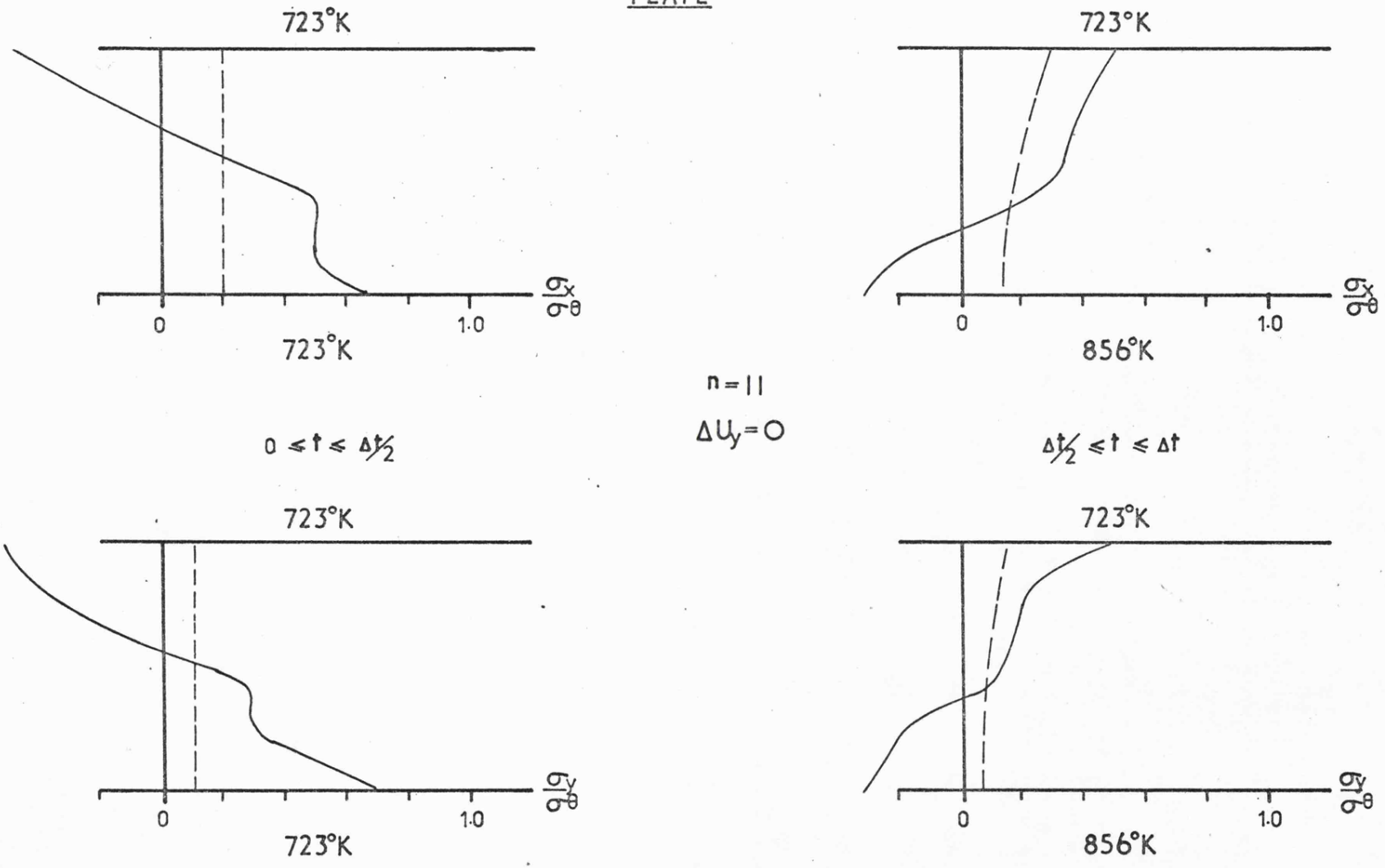

Fig 6·27 Stress distribution for $P_x/\sigma^\theta = 0{\cdot}2$

PLATE

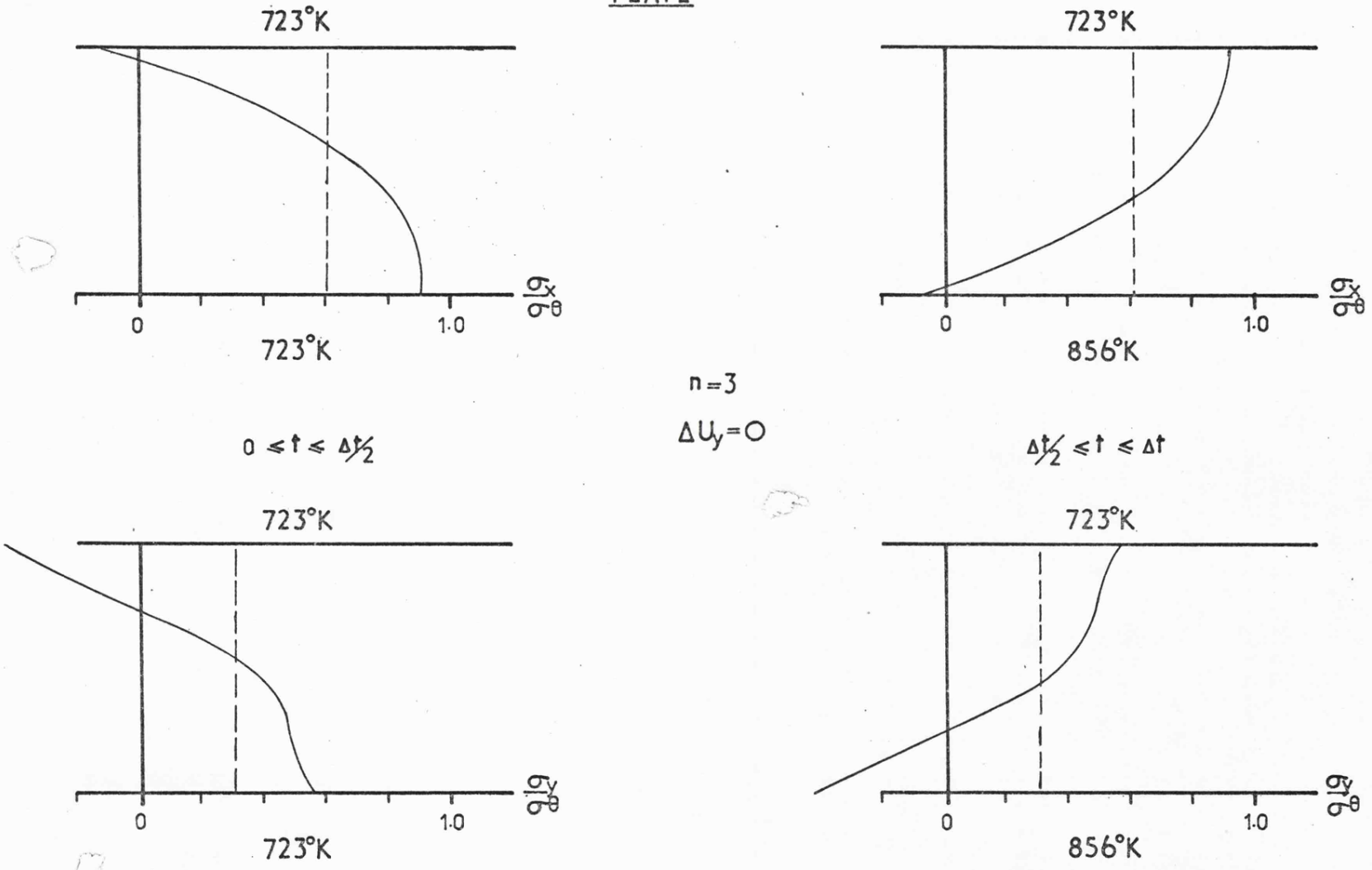

Fig 6·28 Stress distribution for $P_x/\sigma^\theta = 0 \cdot 6$, $\Delta H = O$

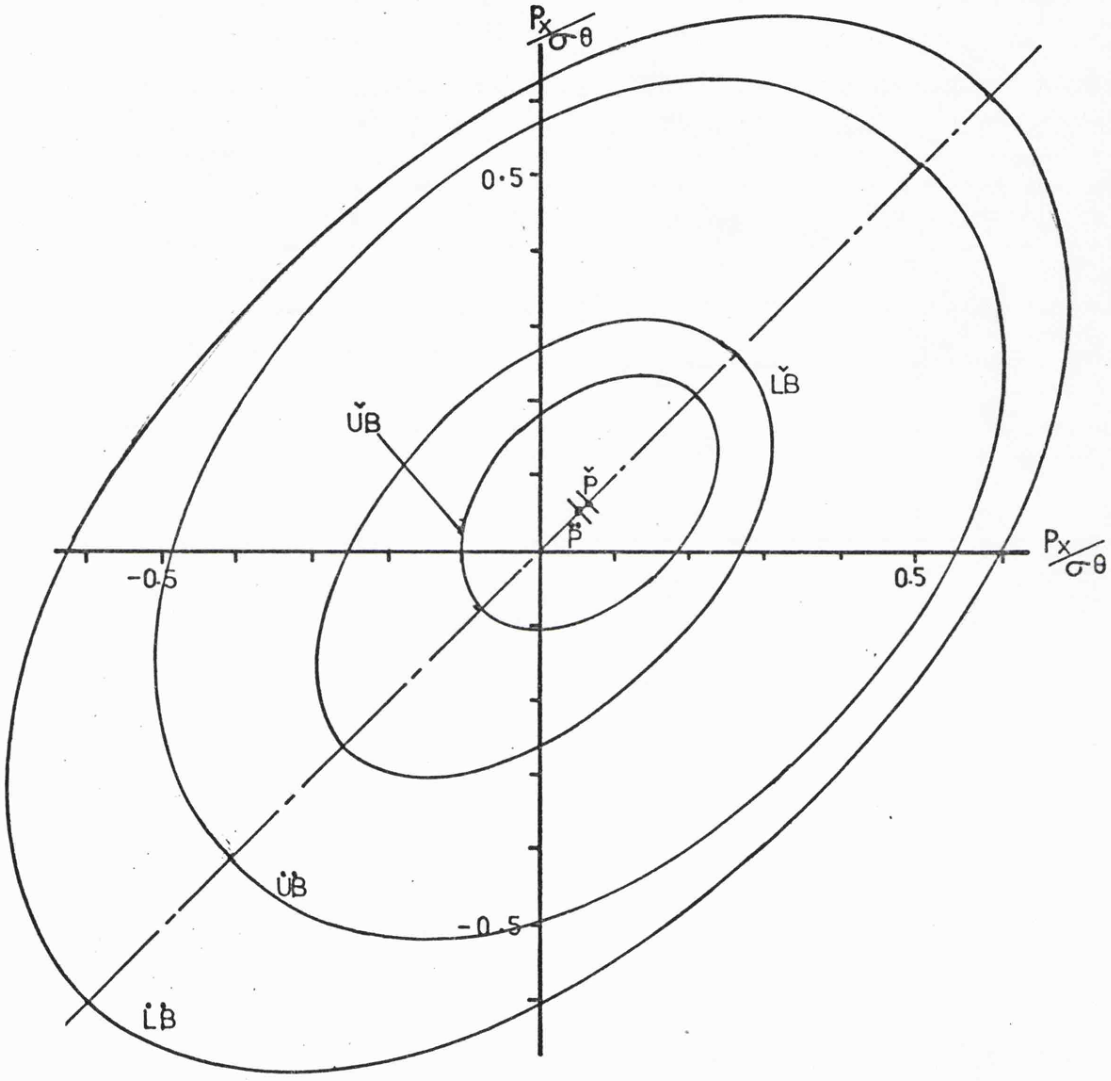

LB – Lower Bound
UB – Upper Bound
•• n=11
ˇ n=3

Fig 6·29 Surfaces of Constant Work

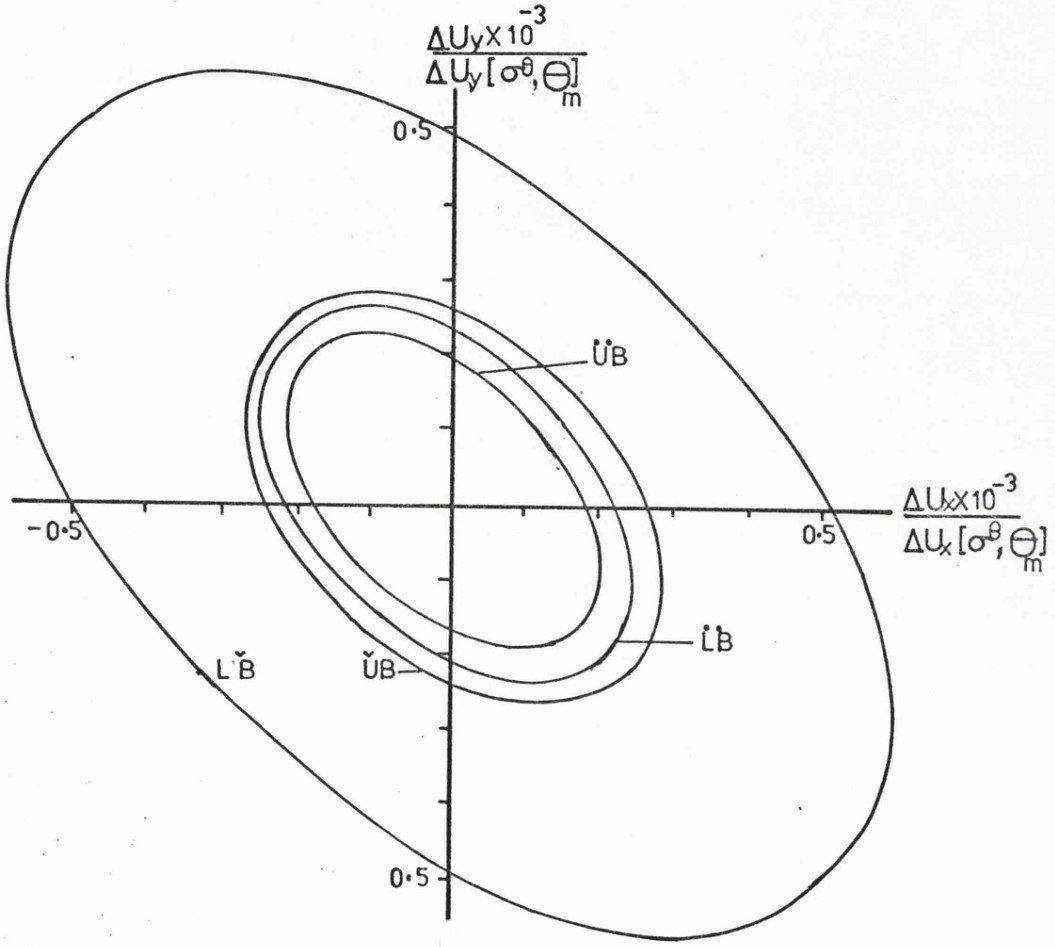

Fig 6·30 Displacements corresponding to the Work Surfaces

Chapter 7

Deformation Maps and a Material Related Parameter for Structures Subjected to Cyclic Temperatures

7.1. Introduction.

Conventional computing methods may be used to evaluate cyclic stationary state solutions. However, such methods usually incur large computing costs and are thus unsuitable for general design purposes. An alternative approach has been discussed in the preceding chapter and, as such, offers a simplified understanding of the complex effects of cyclic temperature histories on structures undergoing creep. The solutions obtained provide an indication that the comparatively simple calculations involved in the bounding theorems may provide a most suitable means of obtaining relevant design information.

In this chapter it will be shown that the solutions obtained from these bounding theorems can be presented in the form of deformation maps. When a non-linear viscous constitutive relationship is used, separate regions of behaviour that coincide with distinct ranges of stress and temperature are clearly distinguishable. These regions may be understood as resulting from the dominance of the stresses which occur during that part of the cycle when either the stress is largest or the highest temperature acts. The degree of severity of stress redistribution may be understood from those regions where the rapid cycling solutions (upper bound) differ from the slow cycling (lower bound) solutions. It is shown that the solutions can be expressed in terms of a material parameter β which allows the structural behaviour to be related to uniaxial behaviour by appropriate choice of reference stresses and reference temperatures. Therefore, a reference stress/temperature approach may be applicable to cyclically varying temperature problems with, however, the relevant reference

values being dependent on the value of β .

Similar bounding calculations have been performed[71] using both the strain-hardening and Bailey-Orowan constitutive equations in order to see if comparable regions of behaviour are discernable. It was found that the solutions using the strain-hardening model exhibit similar patterns of behaviour to those of the non-linear viscous model, but those of the Bailey-Orowan model are distinctly different due to the presence of recovery. This difference occurs because the Bailey-Orowan model predicts a much greater strain rate for a history of loading where a high stress at low temperature is followed by a lower stress at a higher temperature, than do the other models.

The structural examples analysed in this chapter are those previously described in Chapter 6. In both problems the load and temperature histories are of a similar form to those previously employed and the general theoretical approach remains unchanged. However in the plate problem, two load cases are examined: The first case assumes that deformation in the y direction is fully restrained i.e. $\Delta U_y = 0$, whilst in the second case the deformations in both directions are equal i.e. $\Delta U_x = \Delta U_y$. In both cases positive and negative applied loads are considered. As in Chapter 6 the solutions are concerned solely with the interaction between elastic and creep strains. The effects of plasticity and incremental collapse mechanisms are not considered.

In the following section a physical interpretation of the material parameter β is given, and in section 7.3 details of the construction of the displacement maps are described. Sections 7.4 and 7.5 describe the displacement maps for the two examples assuming a non-linear viscous behaviour. In sections 7.6.1 and 7.6.2 the strain-hardening model and the Bailey-Orowan model are briefly discussed in relation to the two-bar structure. The complete theory is well documented in references (72, 73, 74, 75) and the inclusion of these models is necessary as an aid to a more fuller

understanding of the experimental results described in the next chapter.

7.2. Material Parameter β .

In the two-bar structure and plate problem the ratio of the cyclic stationary state deformations, $U = \Delta U^{u}/\Delta U^{L}$, is dependent upon the parameters σ/σ^{θ} , n and β . The quantity σ/σ^{θ} is the ratio of the average applied stress, due to the applied load, to the maximum thermo-elastic stress occurring during a cycle of the loading history.

The material parameter, β , is defined by

$$\beta = \frac{2\gamma\Delta\theta}{n}$$

where $2\Delta\theta$ is the difference between the maximum temperature $(\theta_c + \Delta\theta)$ and the minimum temperature $(\theta_c - \Delta\theta)$ occurring during a cycle of the temperature history. The physical interpretation of β arises from the relationship between the creep rates which occur at $(\theta_c + \Delta\theta)$ and $(\theta_c - \Delta\theta)$. Providing changes in temperature are sufficiently small, the constitutive equation may be written as

$$\dot{\varepsilon} = k\,\sigma^{n} \exp\left(-\frac{\Delta H}{R\theta_c}\right) = k'\sigma^{n} \exp[\gamma(\theta-\theta_c)] , \qquad (7.1)$$

where

$$k' = k \exp\left(-\frac{\Delta H}{R\theta_c}\right) \text{ and } \gamma = -\frac{\Delta H}{R\theta_c^{2}} . \qquad (7.2)$$

If constant stress uniaxial tests are conducted at the two temperatures, then raising the temperature from $(\theta_c-\Delta\theta)$ to $(\theta_c+\Delta\theta)$ will increase the creep rate. Referring to Fig.7.1 suppose the same increase in creep rate is caused by maintaining the temperature at $(\theta_c-\Delta\theta)$ but increasing the stress to $\chi\sigma$, then

$$\dot{\varepsilon} = k'(\chi\sigma)^{n} \exp(-\gamma\Delta\theta) = k'\sigma^{n} \exp(\gamma\Delta\theta) . \qquad (7.3)$$

Rearrangement of equation 7.3 gives $\beta = \log_e \chi$. Therefore, on a

uniaxial plot of log $\dot{\varepsilon}$ against log σ at constant temperature, β corresponds to the distance between the lines representing the creep behaviour at the two temperatures. The parameter β therefore provides a measure of the change in stress required to make the creep rates equal, and reflects the temperature sensitivity of the material behaviour.

7.3. Map Construction.

The construction of the displacement maps involved computing upper and lower bounds on the creep energy dissipation at a sequence of values of σ/σ^{θ} for a range of values of β and n. In practice the calculations were performed at three values of ΔH (114, 250 and 342 KJ/mole) and a range of values of θ_c and $\Delta\theta$ for $n = 3$, 5 and 7. The resulting data was processed by the University computer to produce values of U, σ/σ^{θ}, β, n, $\Delta H, \theta_c$ and $\Delta\theta$. These values when plotted on a two-dimensional space with σ/σ^{θ} as the ordinates and β as the abscissas form contours of constant U.

In both problems the regions of interest are found to lie within the range $0 \leqslant \beta \leqslant 6$ with $-1 \leqslant \sigma/\sigma^{\theta} \leqslant 1$ for the plate and $0 \leqslant \sigma/\sigma^{\theta} \leqslant 2.5$ for the two-bar structure.

7.4. Two-bar Structure: Non-linear Viscous Material

When the cycle time Δt is small in comparison with a characteristic material time the rapid cycling solution (upper bound) is given by equation (6.17). On the other hand when Δt is large the resulting work bound, equation (6.18), is a lower bound on the creep energy dissipation.

Contours of constant $U = \Delta U^{u}/\Delta U^{L}$ are shown in Fig.7.2 for $n = 3$ where it is seen that the deformation map can be subdivided into three distinct regions. In Region 1, $U > 1$ and the difference between the bounds achieves high values for relatively small changes in either σ/σ^{θ}

or β . Therefore the rapid cycling solution predicts a considerable increase in displacement rates for small cycle times. Region 2 corresponds to $U = 1$ where both the rapid cycling solutions and slow cycling solutions provide near identical displacement rates. Since the lower bound solution is independent of the magnitude of the thermal stress then so is the upper bound solution. In Region 3 , $U < 1$ and the rapid cycling solution yields a lower displacement rate than the corresponding slow cycling solution. It is seen that for any value of β , as σ / σ^{θ} decreases, $U << 1$ until a value is attained at which $U = 0$. Although at this value the slow cycling solution remains positive and finite, the rapid cycling solution predicts equal but opposite displacements during the first and second parts of the cycle yielding a net displacement equal to zero. Further decrease in σ/σ^{θ} results in the rapid cycling solution producing a net negative displacement over a cycle; i.e. creep deformation produces shortening of the bars.

The general arrangement of the displacement contours is not entirely unexpected since it was noted in Chapter 6 that the elastic-creep interactions occurring are highly sensitive to both the relative magnitudes of the thermal and applied stresses and to the corresponding temperature history. From consideration of fixed temperature histories (i.e. β = constant) it was shown that as σ/σ^{θ} decreased, the energy dissipation bounds and corresponding displacements diverged with the lower bound solution reducing to zero displacement at zero applied load whilst the upper bound remained finite and negative. Therefore the effect of the temperature history on the rapid cycling solution is to produce a net negative displacement over a cycle. In the limit the β axis corresponds to $U = -\infty$. The manner in which the solutions approach this value was found to be dependent on the value of $\Delta\theta$ (i.e. β) adopted, and this is clearly illustrated by the map. For example at larger values of $\beta > 2.5$ the rapid cycling solution always predicts a displacement rate less than that

predicted by the slow cycling solution and, consequently as σ/σ^{θ} decreases, U also decreases. However, for $\beta < 1.8$ an entirely different regime exists with the difference in the bounds rapidly increasing with decreasing σ/σ^{θ} , This continues until U achieves a maximum at a small value of σ/σ^{θ} and thereafter rapidly decreasing until $U = -\infty$ is attained. For $1.8 < \beta < 2.5$ the two regimes interact and the behaviour becomes less defined.

The loading histories considered in Chapter 6 are shown as the broken lines on Fig.7.2. Line AA' corresponds to the first case considered with $n = 3$, $\Delta H = 342$ KJ/mole and $\Delta\theta = 40$, 50, 60 and 70°K. Line BB' corresponds to the fixed temperature history $\Delta\theta = 47$°K and $\Delta H = 342$ KJ/mole discussed in the second part of section 6.4.2.

The behaviour within the three regions may be understood in terms of simple stress histories, and each region is now discussed in turn.

Region 1, U > 1. In this region, which corresponds to smaller values of β, the most severe increase in displacement rate occurs for small cycle times. Consider the extreme case when $\beta = 0$, i.e. the creep rate independent of temperature. The rapid cycling solution is self-evident and is shown in Fig.7.4. The residual stress ρ , equals zero and effectively all the deformation occurs when the stress is largest and equal to $\sigma + \sigma^{\theta}$. If the creep strain that occurs when the stresses are at the lower values is completely ignored the resulting values of U are shown as the broken lines in Fig.7.2. It is clearly seen that these lines closely approximate the complete solution throughout this region. Hence the deformation is effectively equal to that of the structure subjected to a constant load $P = 2A(\sigma + \sigma^{\theta})$ with half the cycle time and a temperature distribution $\theta_1 = \theta_c$, $\theta_2 = \theta_c - \Delta\theta$ followed by a lower of zero applied load over the remainder of the cycle. This approximation is least accurate near the boundary between Region 1 and Region 3 where extremely rapid changes in ΔU^{u} occur.

Region 2, U = 1. This region corresponds approximately to $\beta > 2$ and $\sigma/\sigma^{\theta} > 1$. Since U is close to unity, the rapid cycling solutions and slow cycling solutions are virtually identical in their evaluation of displacement rate. As β is large, the creep rates during the first part of the cycle when the higher temperature acts provides the major contribution to the total displacement. Even though the temperature on bar 1 remains constant and the stress reduces during the second part of the cycle the large value of β ensures that the stresses during the first part of the cycle provide the larger creep rates. In the rapid cycling solution the stress history is virtually identical to the slow cycling solution and, similarly, the contribution of the creep strains during the second part of the cycle to the total deformation is negligible. Therefore in this region the deformation may be assumed to be equal to one half of that which would occur if the condition of the first part of the cycle remained constant over the complete cycle. Hence the reference stress lies close to σ and the reference temperature lies between θ_c and $\theta_c + \Delta\theta$.

Region 3, U < 1. This region corresponds to $\sigma/\sigma^{\theta} < 1$ with contours of U becoming independent of β for larger values of β. If the case when β is large is considered, the behaviour may be more easily understood. From consideration of the stress history shown in Fig.7.5 it is seen that during the first part of the cycle the stress in bar 2 becomes small and either positive or negative since $\rho = (\sigma^{\theta}-\sigma)$. During the second part of the cycle although $\sigma_2 = 2\sigma^{\theta}$, since the average temperature is much lower the creep rate is again very small. Hence the deformation is governed by the stress on bar 1 which changes from 2σ to $2(\sigma-\sigma^{\theta})$ and as the temperature on this bar remains constant at $\theta_1 = \theta_c$ the displacement rate is independent of β. When $\sigma/\sigma^{\theta} = 0.5$ the net accumulation of strain over a cycle in the rapid cycling solution is zero.

Therefore for $0.5 \leqslant \sigma/\sigma^{\theta} \leqslant 1.0$, $1 > U > 0$ and for $0 \leqslant \sigma/\sigma^{\theta} \leqslant 0.5$, $U < 0$. In this latter case the displacement rate evaluated from the rapid cycling solution is of opposite direction to the applied load P and in order to maintain a zero displacement rate, a load equivalent to $\sigma = 0.5\,\sigma^{\theta}$ is required. The lower bound solutions are also independent of β for large values of β as all the deformation occurs during the first half of the cycle when $\sigma_2 \simeq 0$ and $\sigma_1 = 2\sigma^{\theta}$.

The rapid transition from Region 1 to Region 3 lies close to the origin of Fig.7.2. As ΔU^{L} is a function of σ and β solely, ΔU^{L} changes extremely rapidly for small changes of σ/σ^{θ} . The transition line corresponds to $U = 0$ which arises when σ_1 fluctuates between $\pm\,\sigma^{\theta}$.

It is clearly demonstrated that these simple solution regimes are separated by regions in which fairly rapid transitions from one regime to another occur. For larger values of n a similar picture emerges except that the regions become more distinct with the transitions occupying a smaller area of the diagram. These transition regions are defined by contours of U close to unity and it is seen from Fig.7.3 that when contours of $U = 0.99$ and $U = 1.01$ are plotted for $n = 3$, 5 and 7 they are reasonably close together. For $U = 0$ the contours as expected are identical. Contours of $U = 50$ are also included to demonstrate that within the regions (with the exception of Region 2) the value of U remains dependent on n although the stresses are still governed by the calculations described above.

It is therefore seen that within Regions 1 and 2 the rapid cycling solution may be correlated with the same structure subjected to constant loads at constant temperatures. For Region 1 the relevant applied load is $P = 2\,(\sigma+\sigma^{\theta})$ with $\theta_1 = \theta_c$ and $\theta_2 = \theta_c - \Delta\theta$. In Region 2 , the relevant values are $P = 2\sigma$ with $\theta_1 = \theta_c$ and $\theta_2 = \theta_c + \Delta\theta$. Therefore these loading histories can be correlated with a constant reference stress and reference temperature as described in Chapter 4. In Region 3 a

variable stress history fluctuating between 2σ and $2(\sigma-\sigma^{\theta})$ at temperature $\theta = \theta_c$ defines the displacement rate.

To form a more complete solution to the problem it is necessary to consider the creep energy dissipation. If this quantity is denoted by W^u and W^L for the upper and lower work bounds respectively, then contours of $W = W^u/W^L$ can be plotted on the coordinate axes defined. In Fig.7.6 contours of W that correspond to the displacement map, Fig. 7.2, are presented. In this diagram, unlike contours of U, W shows a monotonic change with σ/σ^{θ}. Since both W^u and W^L are finite and positive, with the exception of the lower bound, W^L, when $\sigma/\sigma^{\theta} = 0$, and W^L is by definition the absolute minimum for any statically admissable stress history, then W may be expected to decrease as σ/σ^{θ} increases, i.e. as σ/σ^{θ} increases the creep energy dissipation associated with thermal ratchetting decreases and hence the corresponding displacements become more equal. Similarly, if σ/σ^{θ} remains constant W decreases with increasing β. i.e. increasing β effectively increases the temperature difference and increased thermal softening therefore offset the thermal ratchetting. For values of $\sigma/\sigma^{\theta} < 1.0$ and $\beta > 3$, W becomes independent of β. Further, by comparison of Figs.7.6 and 7.2, at any W, U in this region is unique whereas for $\beta < 3$, U is dependent on β.

7.5. The Plate Problem: Non-linear Viscous Material.

The displacement map for the stressed plate subjected to a uniform state of positive (tensile) mean stress (p_x,p_y) and creep index $n = 3$ are presented in Figs.7.9 and 7.10 for $\Delta U_y = 0$ and $\Delta U_x = \Delta U_y$ respectively. The vertical stress axis is defined as previously but with the applied stress in both cases equal to p_x. For negative (compressive) mean stress $(-p_x,-p_y)$ the corresponding maps assume the form shown in Figs.7.11 and 7.12.

The contours corresponding to the positive mean stress cases clearly show similar features to those of the two-bar structure. However, when the negative mean stresses act the displacement maps are substantially different with the contours exhibiting a monotonic change with p_x/σ^θ and no distinct regions of behaviour.

For larger n values the contours for the positive states of mean stress are remarkably similar. Since the transitions between the regions, whose notation and general description follows that of section 7.4, are defined by contours close to unity, contours of $U = 0.99$ and $U = 1.01$ are shown for $n = 3$, 5 and 7 in Figs.7.13 and 7.14 for $\Delta U_y = 0$ and $\Delta U_x = \Delta U_y$ respectively. In both cases the contours for the three n values lie close together and for $U = 0$ are indistinguishable. However, within Region 1 contours of $U = 5$ shows that U still retains some sensitivity to n.

To understand the behaviour within each of the four regions, each region with stress histories typical of that region will be discussed in turn. Particular attention is given to the $\Delta U_y = 0$ case which was dealt with in some detail in the previous chapter but the general features described will be seen to be generally admissable to the $\Delta U_x = \Delta U_y$ case.

As in the previous example, Region 1 is confined to smaller values of β where the most severe increases in displacement rate occur for short cycle times. The load cases described in Chapter 6 are contained within this region and are represented on Fig.7.9 as points A, B and C for $\beta = 0$, $\beta = 0.88$ (n=11) and $\beta = 1.26$ (n=7) respectively with $p_x/\sigma^\theta = 0.6$. The $\beta = 2.96$ (n=3) case is represented by point D which is within Region 2 where $U \simeq 1$. These four cases will be used to illustrate typical stress distributions within these regions and also the transition from Region 1 to Region 2. The distributions of stress corresponding to A, B, C and D are presented in Figs.6.28, 6.24, 6.25 and 6.22. These have been individually described previously. However, the parameter

β allows the solutions to be described independently of n and thus the individual behaviour can be studied in terms of the regions of the displacement map.

It is seen that as β increases from zero the distributions of stress change markedly. When $\beta = 0$ the upper and lower bound stresses are distinctly different and do not approach each other during any parts of the cycle. The effect of an increase in β is to cause the stress distributions occurring during the second part of the cycle, when the average temperature is higher, to move closer together on the cooler side of the plate. This progressive change in the stress distribution continues as β changes and culminates in the stress distribution of point D where $U = 1$ and the stresses during the second part of the cycle are virtually indistinguishable, although those occurring during the first part remain totally different.

The $\beta = 0$ and $\beta = 2.95$ cases therefore provide, in a sense, two extreme cases of behaviour. In the latter case, when the creep rate varies with temperature, the dominant period occurs during the second part of the cycle when the average creep rate is higher and thus the total deformation is dominated by the deformation that occurs during this part of the cycle. As β decreases, thermal softening effects also decrease, the stresses diverge and this period becomes less dominant. Similarly as β decreases, U increases and in the extreme case when $\beta = 0$, no dominant period appears to exist.

It may be noted that for any finite β, the stress profiles are always closest together during the second part of the cycle and on the cooler side of the plate; a feature previously noted in Chapter 6.

In the $\Delta U_x = \Delta U_y$ case, similar load cases to the above are denoted by points A′, B′, C′, and D′ on Fig.7.10. The corresponding distributions of stress are shown in Figs.7.15, 7.16, 71.7 and 7.18. The general description given for the $\Delta U_y = 0$ case applies equally well to this example with the exception that the stresses in the x and y directions are identical in either bound.

In Region 3 values of U are less than unity and become independent of β for larger values of β. If p_x/σ^θ is reduced at constant β from the condition of Region 1, U tends to zero. At $U = 0$ the average displacement rate in the rapid cycling solution is zero although the slow cycling solution remains positive and finite for all positive applied loads. Further reduction in p_x/σ^θ produces, in the rapid cycling solution, increasing average displacements in the negative direction, (i.e. the plate contracts) whilst the lower bound slow cycling solution rapidly approaches zero and thus large negative values of U result. In the limit when $p_x/\sigma^\theta = 0$, $\Delta U^L = 0$ and $U = -\infty$.

For negative applied loads $(p_x/\sigma^\theta < 0)$ the contours shown in Figs.7.11 and 7.12 result. These may be described as Region 4 where as $p_x/\sigma^\theta \to -1$, $U \to 1$. Typical distributions of stress that result as p_x/σ^θ reduces from Region 1 to Region 4 at constant β are shown in Figs.7.19, 7.20, 7.21 and 7.22 for $\Delta U_y = 0$ and $\beta = 4.11$. When $\Delta U_x = \Delta U_y$ similar stress distributions occur but as in the positive applied load cases $\sigma_x/\sigma^\theta = \sigma_y/\sigma^\theta$.

It is seen for all of the applied load cases the stress distributions arising from the upper and lower bounds in the first part of the cycle are totally dissimilar although the upper bound stress distributions do not differ too greatly in form. On the other hand the upper bound stress distributions show a distinct variation in form for $p_x/\sigma^\theta < 0$. For small values of p_x/σ^θ, U large and negative, the stresses are closest together during the second part of the cycle on the hotter side of the plate whereas for positive applied loads they lie closest together on the cooler side. However as $U \to 1$, as in the positive applied load cases, the distributions of stress during the second part of the cycle tend to become identical.

In section 7.4 it was demonstrated that the solutions to the cyclic temperature problem could be understood in terms of simple stress and temperature histories. In this problem where highly complex residual stress

fields arise all attempts to express Regions 1 , 3 and 4 in terms of appropriate constant loads and temperatures have been unsuccessful. However since the upper and lower bound stresses in Region 2 are identical during the second part of the cycle when the majority of the creep strains are accumulated, the steady state solution is therefore sufficient to describe the creep behaviour. From these readily obtained solutions representative stresses and temperatures can be obtained and the displacement rates are then equivalent to these values acting for half the cycle time.

In the case when $\beta = 0$ and $\Delta U_x = \Delta U_y$ an appropriate residual stress field has been obtained. This is presented in Fig.7.23 and is a function of the thermoelastic stress only. The resulting stress history for $p_x/\sigma^\theta = 0.6$ is shown in Fig.7.24 and is seen to approximate the distribution of stress shown in Fig.7.15 which was obtained numerically. If it is assumed that creep strains occur only during that region where $\sigma = p_x + \sigma^\theta/4$ then the resulting displacement rate corresponds to a constant stress $p_x + \sigma^\theta/4$ acting over half the original cycle time. From the creep rate equation (6.21)

$$\frac{\Delta U^u}{\Delta t} = \frac{k}{2}\{p_x + \sigma^\theta/4\}^n \left\{\frac{3}{4}\right\}^{\frac{n+1}{2}} \qquad (7.4)$$

and

$$\frac{\Delta U^L}{\Delta t} = \frac{k}{2}(p_x)^n \left\{\frac{3}{4}\right\}^{\frac{n+1}{2}} \qquad (7.5)$$

Therefore contours of constant U intersect the p_x/σ^θ axis according to

$$U = \frac{1}{2}\left\{1 + \frac{\sigma^\theta}{4p_x}\right\}^n .$$

It is found that if this equation is evaluated for $n = 3$, the appropriate values of U virtually coincide with those gained numerically.

In the case when $\Delta U_y = 0$ this residual stress field appears to correspond to the stress history in the x direction and the relevant

applied load is $(p_x + \sigma^{\theta}/4)$ acting for half the cycle time. In the y direction the residual stress field remains unidentified although a tentative investigation suggests that a similar but scaled form exists.

This problem remains to be further investigated.

7.6.1. Two-Bar Structure: Strain-Hardening Model.

Primary creep may be described by the time hardening equation

$$\varepsilon_{ij} = B \frac{\partial}{\partial \sigma_y} \left\{ \frac{\phi^{n+1}}{n+1} \right\} t^m \tag{7.7}$$

where B denotes a constant and m a time constant which in accordance with experiment is often given the value $m = 1/3$. The corresponding creep rate is given by

$$\dot{\varepsilon}_{ij} = B \frac{\partial}{\partial \sigma_y} \left\{ \frac{\phi^{n+1}}{n+1} \right\} m t^{m-1}. \tag{7.8}$$

If it is assumed that the state of the material is described by the accumulated creep strain ε_{ij}, then a strain hardening relationship is formed by eliminating t between the above two equations to yield in the uniaxial case

$$\dot{\varepsilon} = m B^{1/m} \sigma^{n/m} \varepsilon^{(m-1)/m}. \tag{7.9}$$

For constant stress commencing at $t = 0$ when the creep strain $\varepsilon = 0$,

$$\varepsilon(t) = B\sigma^n t^m. \tag{7.10}$$

It is assumed that $B = B' \exp\gamma(\theta - \theta_o)$.

The rapid cycling solution is given in reference (72) by

$$\frac{\Delta U^u}{\Delta t} = \left\{ \frac{1}{\Delta t} \int_o^{\Delta t} B^{1/m} (\hat{\sigma}+\rho)^{n/m} \, dt \right\}^m m t^{m-1} \tag{7.11}$$

where ρ and $\hat{\sigma}$ have the same meaning as before.

As in the non-linear viscous case, ρ becomes determinate

from the compatibility condition $\Delta U_1^u = \Delta U_2^u$ over a cycle. In fact the calculations are identical if n/m is substituted for n and $\Delta H/m$ substituted for ΔH .

There exists no lower bound solution as such but for the purpose of providing a normalization similar to the previous case, the solution was computed so that the integrand of (7.11) remains equal in each bar during $0 \leqslant t \leqslant \Delta t$. This solution corresponds to assuming that the cycle time is sufficiently long for stress redistribution to occur at each instant within the cycle but that the average creep rate is calculated assuming that, from the point of view of the constitutive relationship, the cycling is rapid. This solution has no direct physical meaning but will reduce to the solution arising from equation (7.11) if the conditions of Region 2 occur.

The displacements predicted by these two methods are denoted by ΔU^u and ΔU^L and their ratio by U .

It is found that the solutions so generated have patterns of behaviour very similar to those of the viscous material. The boundaries of the regions are shown in Fig.7.7 and are seen to be similar to those of Fig.7.2. There are however differences in the values of U as the relationship (7.11) provides a higher value of the creep rate under varying stress, when compared with constant stress maintained at the maximum value than does the viscous relationship. The stress histories themselves, however, are very similar and are divided into the same sub-regions.

Therefore the behaviour of the viscous material and the strain hardening material are very similar when described in this way, and the same reference stress histories are relevant.

7.6.2. Two-Bar Structure: Bailey-Orowan Model.

This constitutive relationship includes the effect of thermal recovery. The relevant theory is described in references (73,74).

The state of the material is described by an internal flow stress s which increases due to strain hardening and decreases due to thermal softening.

$$\dot{s} = H(s)|\dot{\varepsilon}| - Q(s) \tag{7.12}$$

where $H(s)$ and $Q(s)$ are coefficients of strain hardening and thermal recovery respectively. The creep rate $\dot{\varepsilon}$ is given by

$$\dot{\varepsilon} = \text{SIGN}(\sigma) f(|\sigma| - s) \tag{7.13}$$

where

$$\begin{aligned} f(|\sigma| - s) &= 0 \quad , \quad |\sigma| < s \\ &> 0 \quad , \quad |\sigma| = s \end{aligned} \tag{7.14}$$

Stationary creep occurs when $|\sigma| = s$ and therefore

$$\dot{\varepsilon} = \text{SIGN}(\sigma)\ Q(|\sigma|)/H(|\sigma|). \tag{7.15}$$

Assuming $Q(s) = k_1 s^{n-\alpha}$ and $H(s) = 1/k_2 s^{\alpha}$ yields Norton flow

$$\dot{\varepsilon} = k_1 k_2 |\sigma|^n \ \text{SIGN}(\sigma) \tag{7.16}$$

with

$$k_1 k_2 = k' \exp\gamma(\theta - \theta_o) \ .$$

This model differs from both the viscous relationship and the strain hardening model by possessing thermal softening. When $|\sigma| < s$, then $\dot{s} = -Q(s)$ and s decreases with time. If the stress is suddenly increased, $\dot{s} = \dot{\sigma}$ and plastic strains occur according to

$$\dot{\sigma} = H(|\sigma|)\dot{\varepsilon} \ . \tag{7.17}$$

Thus for a cycle of stress, both plastic and creep strains occur. In common with the viscous material, an upper bound on the energy dissipation in a structure composed of the material corresponds to assuming that the cycle time is short compared with a characteristic material time. The stress history is given by $\sigma = \hat{\sigma} + \rho$ and the accumulation of strain over a cycle is given by

$$\frac{\Delta U^u}{\Delta t} = \text{SIGN}\,(\sigma(t_o))\,|\sigma(t_o)|^n \frac{1}{\Delta t}\int_o^{\Delta t} k' \exp(\gamma(\theta-\theta_o))dt \qquad (7.18)$$

where t_o is the instant during the cycle when $|\sigma|$ achieves its maximum value. Hence the average strain rate is the same as if $\sigma = \sigma(t_o)$ occurs throughout the cycle. The model predicts the same creep rate as the viscous relationship for constant stress but, due to the presence of recovery, a greater creep rate for any other stress history.

The lower work bound is identical to that described in section 7.4 and the ratio of displacements predicted by these two bounding solutions may be directly compared.

The average displacement rate predicted from the upper work bound is the same as if a constant applied load $P = 2A(\sigma+\sigma^\theta)$ were applied throughout the cycle with one bar maintained at $\theta_1 = \theta_o$ and the other at $\theta_2 = \theta'$ where

$$\exp\gamma(\theta'-\theta_o) = \frac{1}{2}\,(\exp(\gamma\Delta\theta) + \exp(-\gamma\Delta\theta)). \qquad (7.19)$$

In Fig.7.8 contours of constant U are shown for $n = 3$. The above solution is appropriate in Region 1, but in Region 2, $|\sigma_2|$ achieves its maximum value when $\sigma_2 = \pm\,\sigma^\theta$ and $\rho = -\sigma$. The average creep rate in bar 2 thus becomes indeterminate and becomes determined by the stress history σ_1. In bar 1, the stress fluctuates between $2\sigma + \sigma^\theta$ and $2\sigma - \sigma^\theta$ and hence the average displacement rate is the same as if a constant applied load of $P = 2A\,(\sigma+\sigma^\theta)$ were maintained and both bars were at $\theta = \theta_o$.

It is seen that the behaviour shown in Fig.7.8 is entirely different to

that shown in either Fig.7.7 or Fig.7.2. No reverse creep occurs and the ratio U remains at high values for large β as recovery increases. Effectively the Region 1 of Fig.7.2 now dominates a larger area of the diagram.

These calculations demonstrate that when temperatures vary rapidly between two limits, the stress history in the cyclic state fluctuates between a higher stress at a lower temperature and a lower stress at a higher temperature. The rate of deformation is strongly governed by the amount of recovery which occurs during the high temperature period. To the author's knowledge no experiments have been conducted under these conditions.

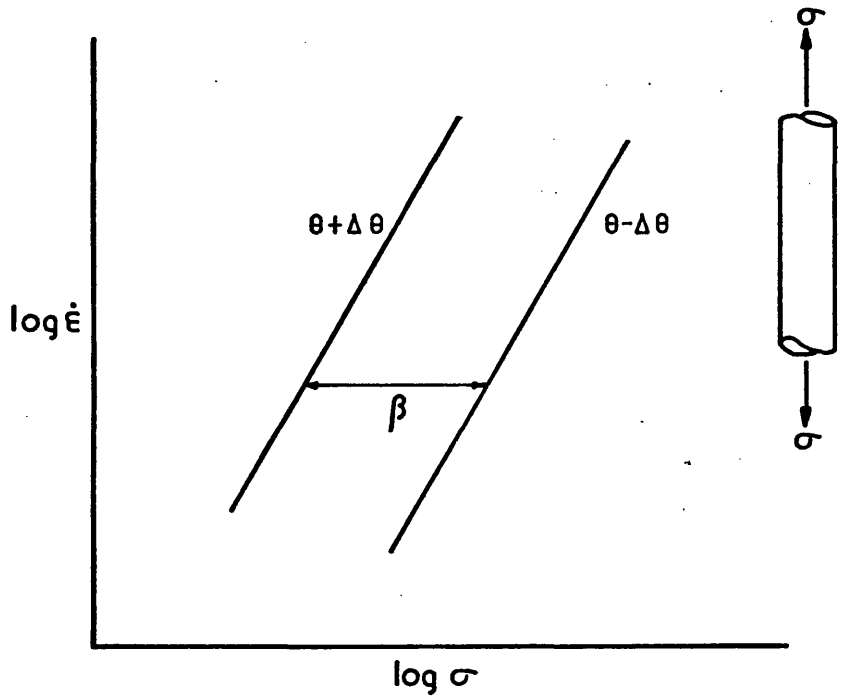

Fig 7.1 Uniaxial behaviour

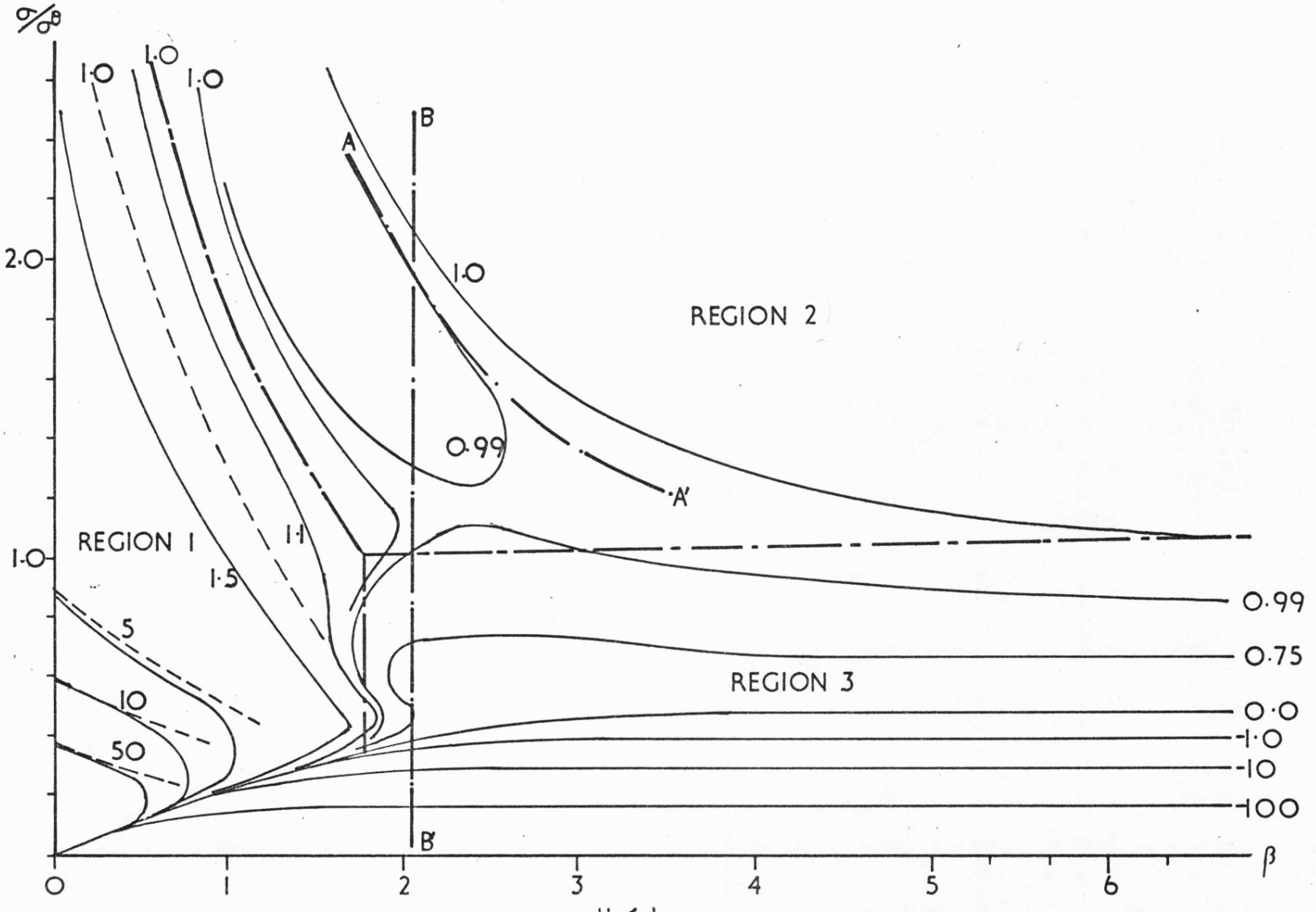

Fig 7·2 Contours of constant $U = \Delta U^U / \Delta U^L$ for a viscous material with n=3

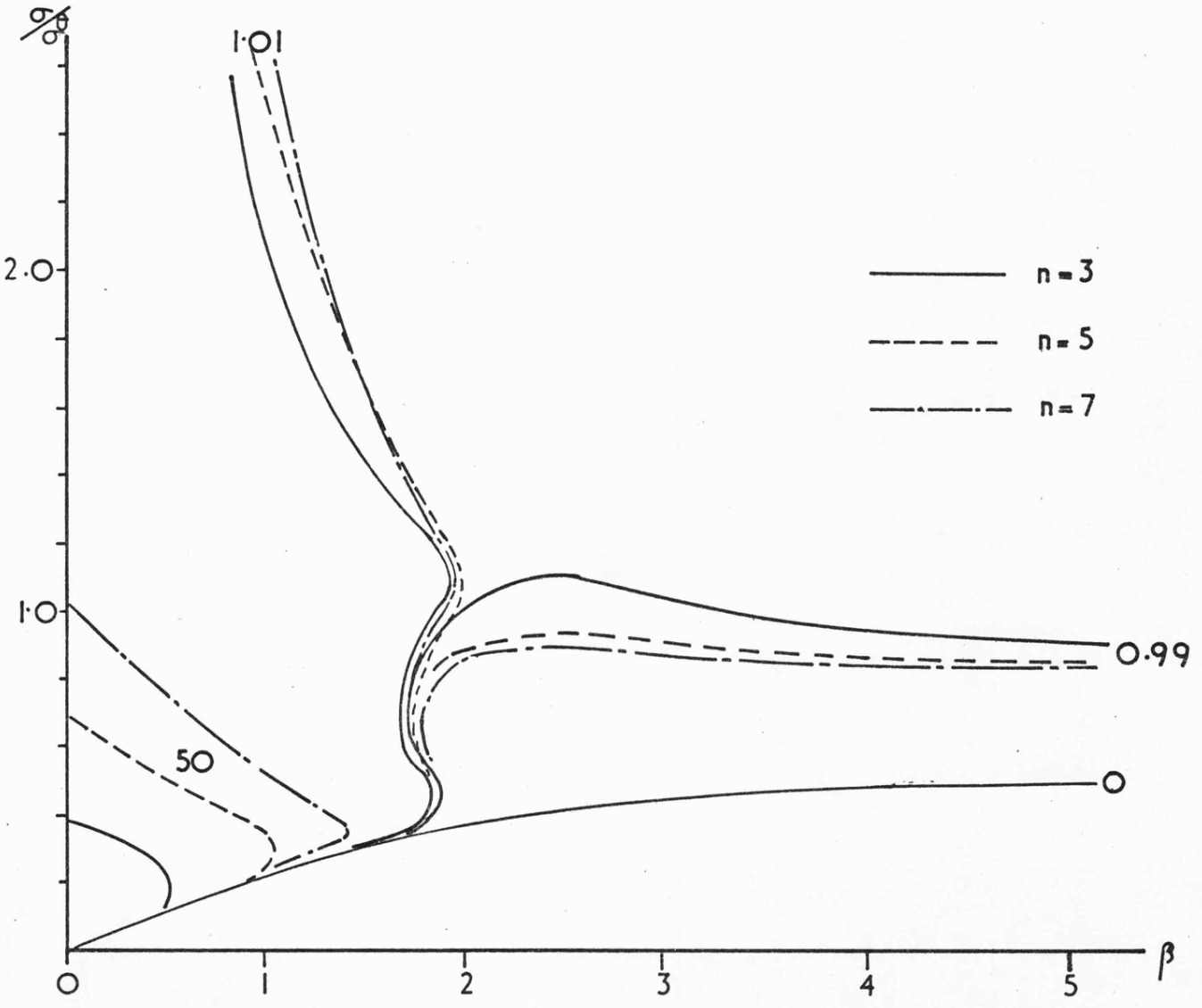

Fig 7·3 Contours of constant U for n=3,5 and 7 for a viscous material

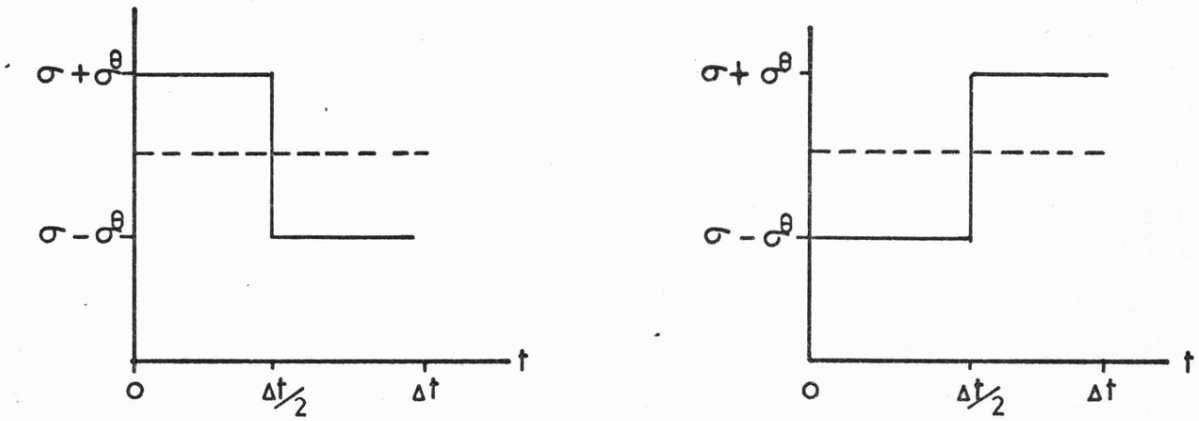

Fig 7.4 Solution for $\beta = 0$, Region 1, $(\rho = 0)$

Bar 1 Bar 2

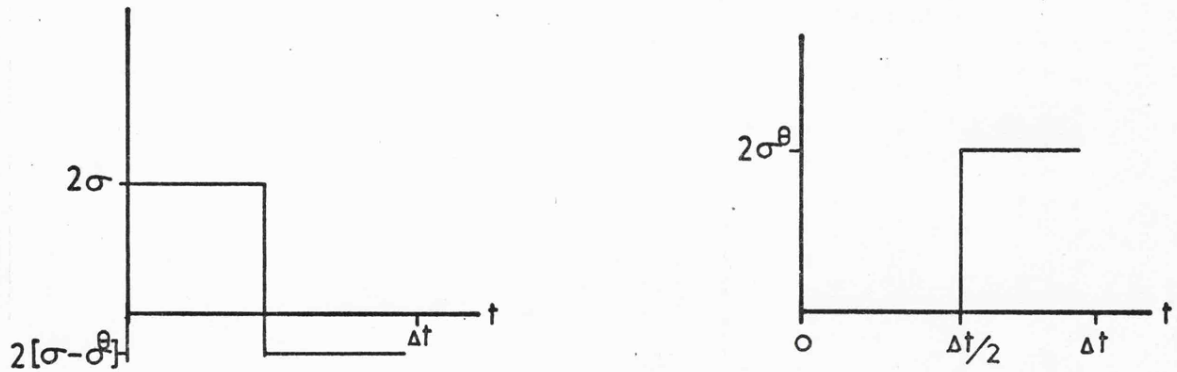

Fig 7.5 Solution for β large, Region 3, $(\rho = \sigma^\theta - \sigma)$

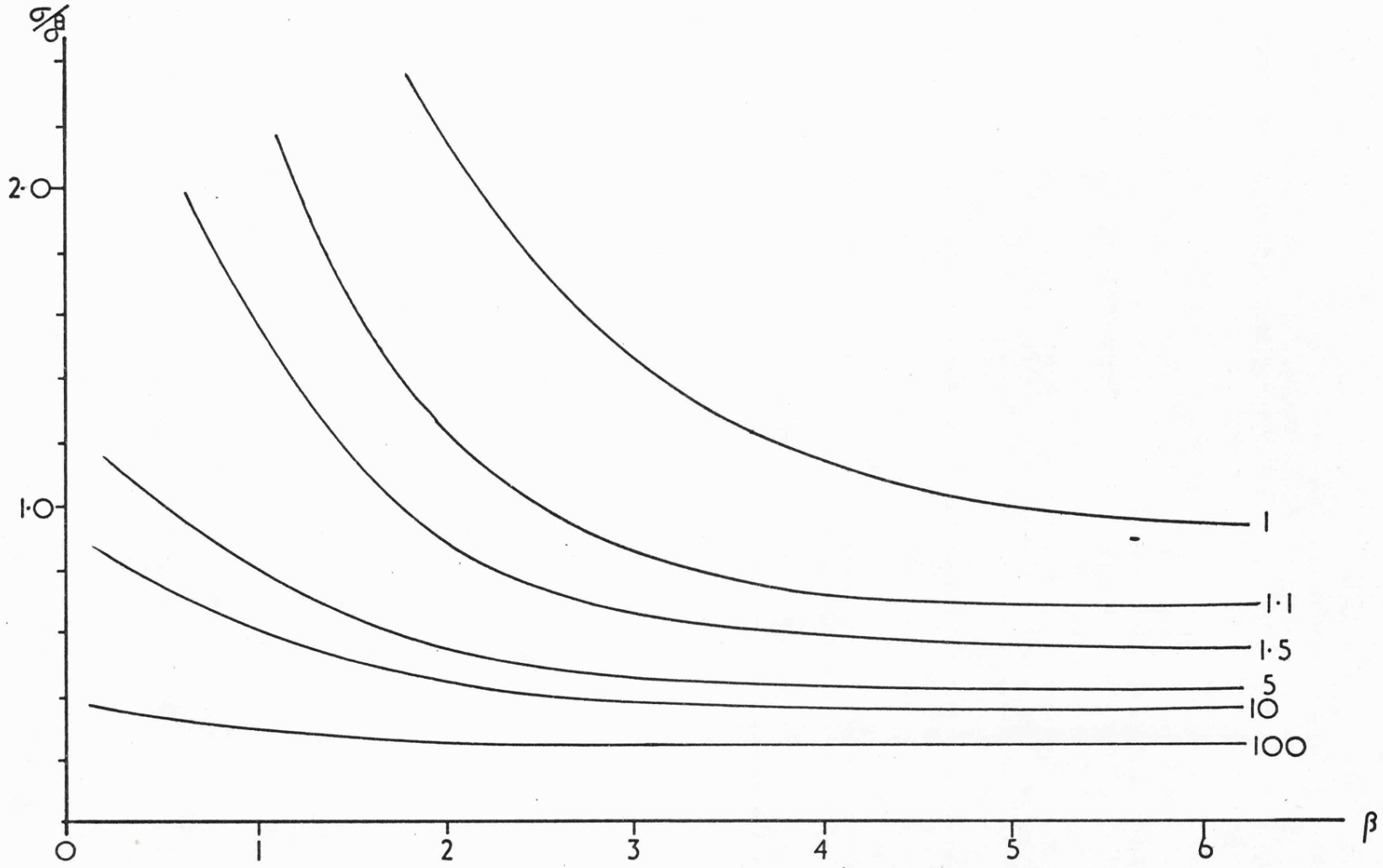

Fig 7·6 Contours of constant work ratio $W = W^U/W^L$ for a viscous material [n=3]

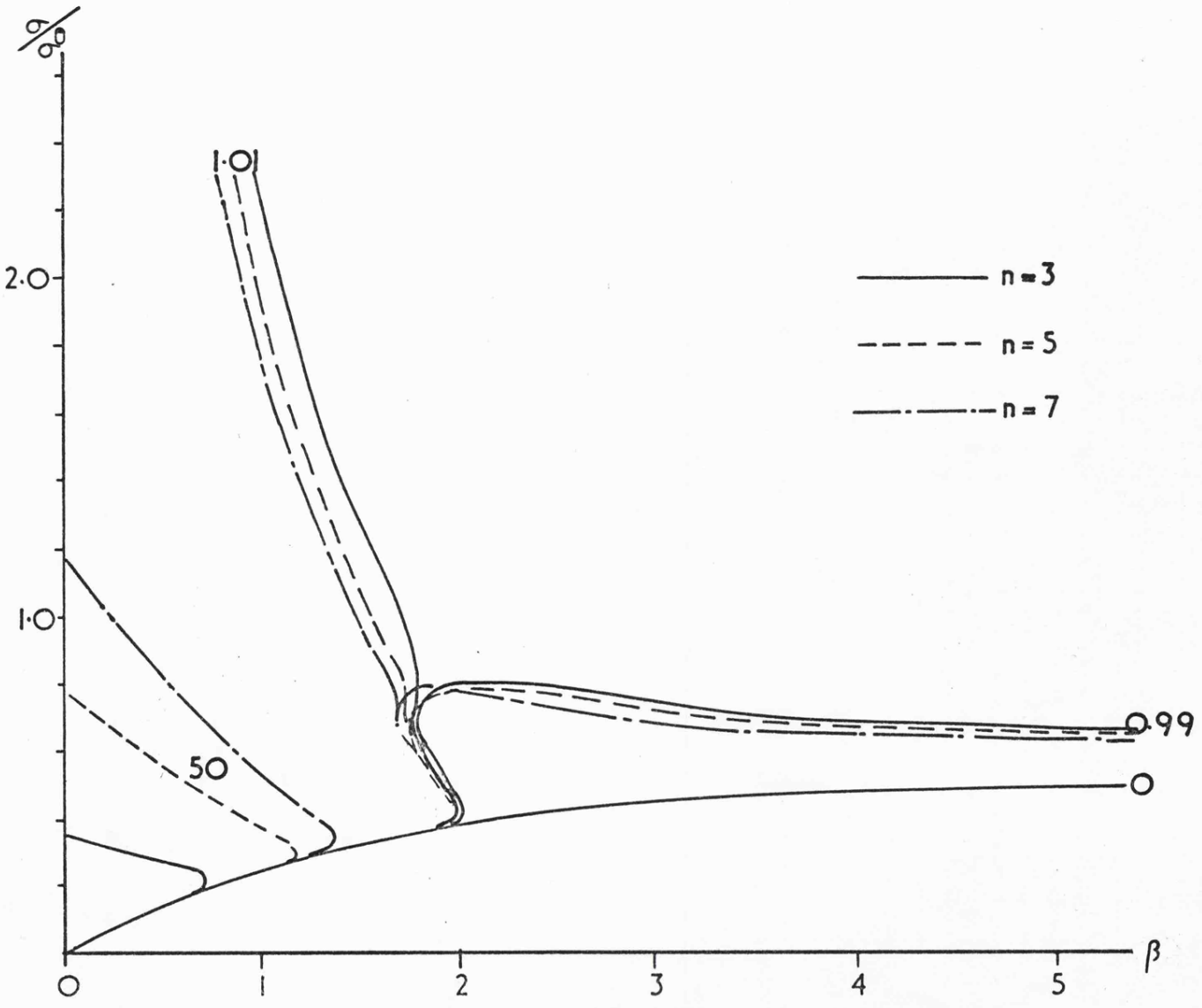

Fig 7·7 Contours of constant U for n=3,5 and 7 for a strain-hardening material

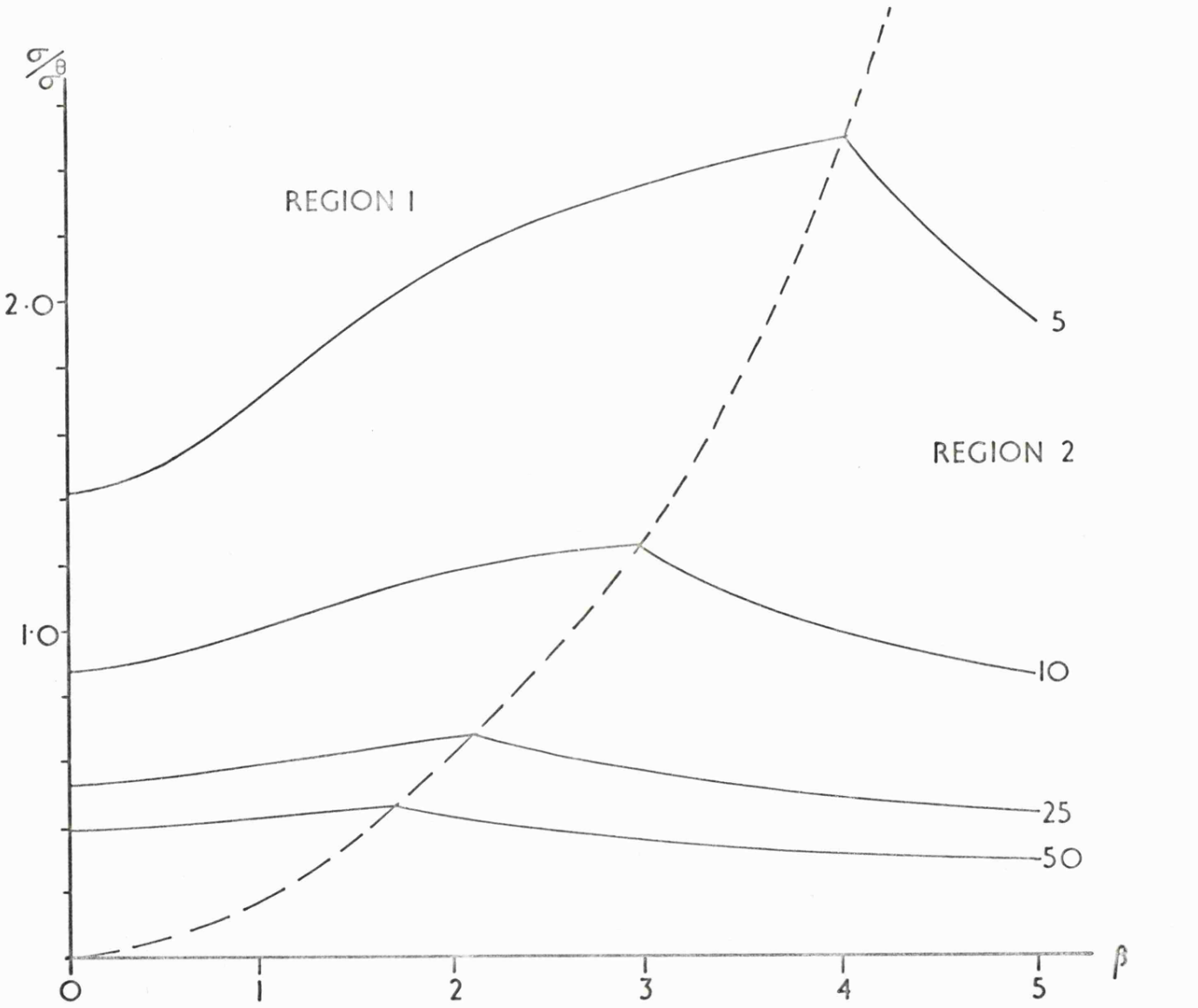

Fig 7.8 Contours of constant U for the Bailey–Orowan model and n = 3

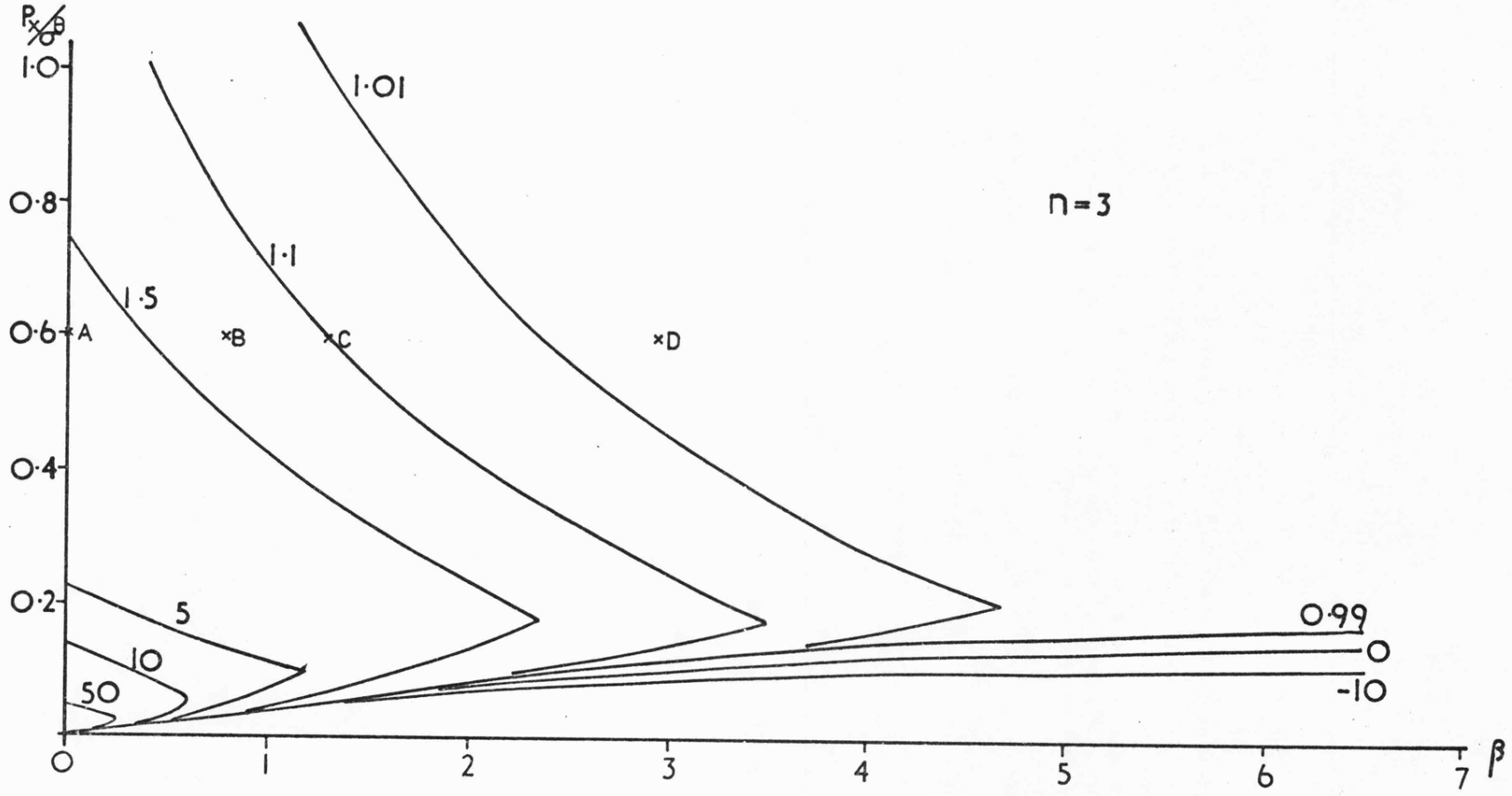

Fig 7·9 Contours of constant U for the plate with $\Delta U_y = 0$

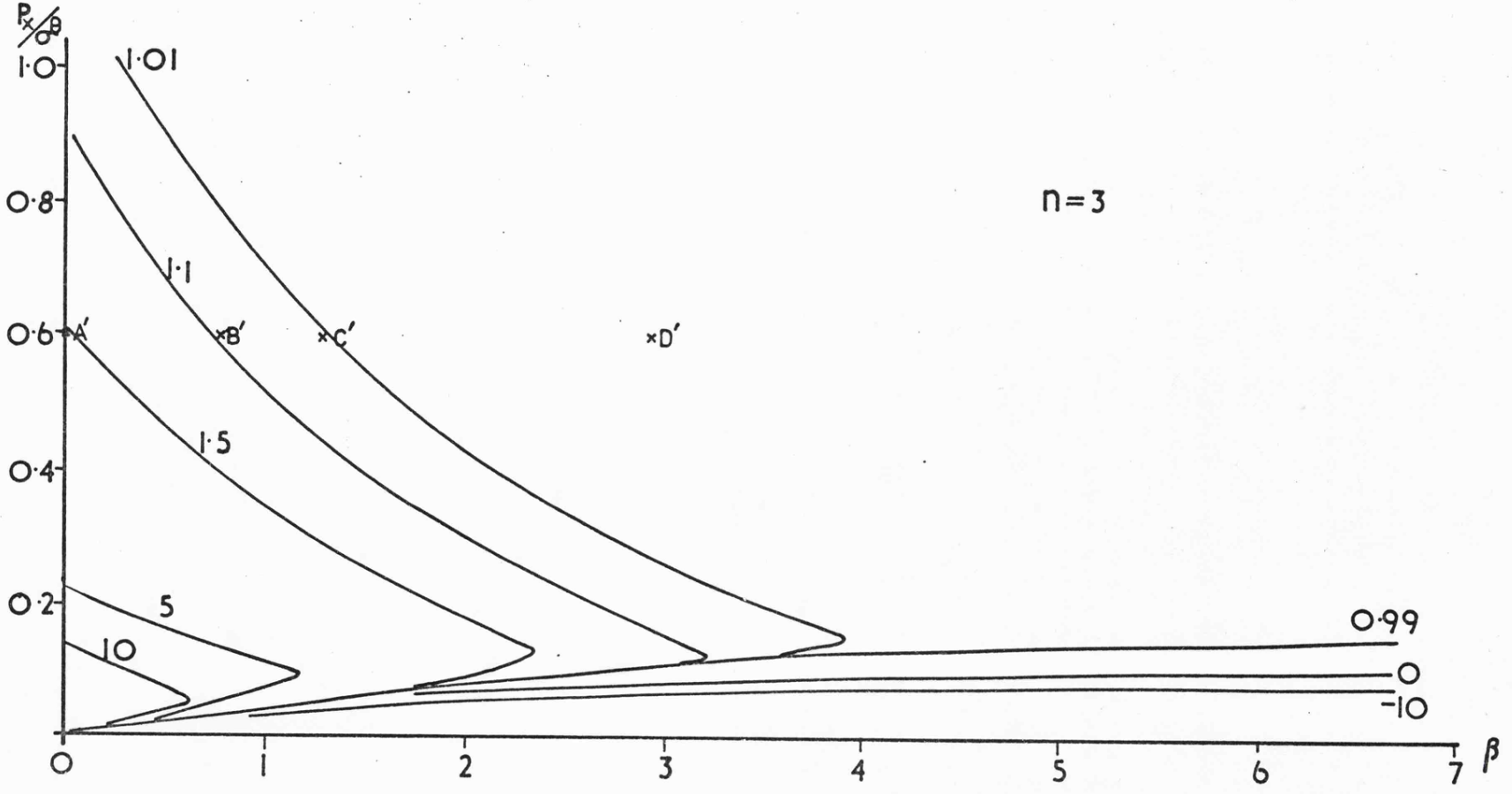

Fig7·10 Contours of constant U for the plate with $\Delta U_x = \Delta U_y$

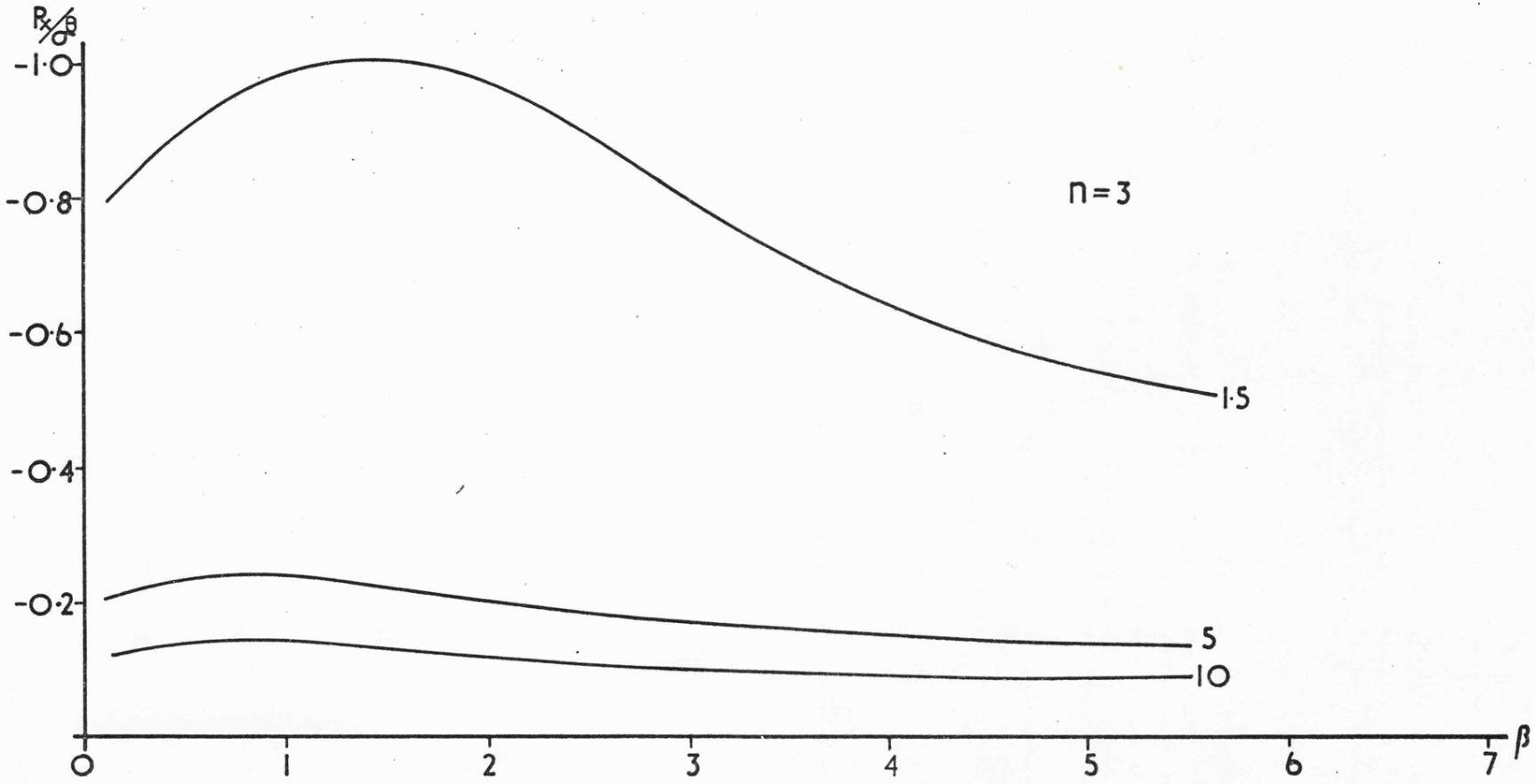

Fig 7·11 Contours of constant U for the plate with $\Delta U_y = 0$ [Comp. stress]

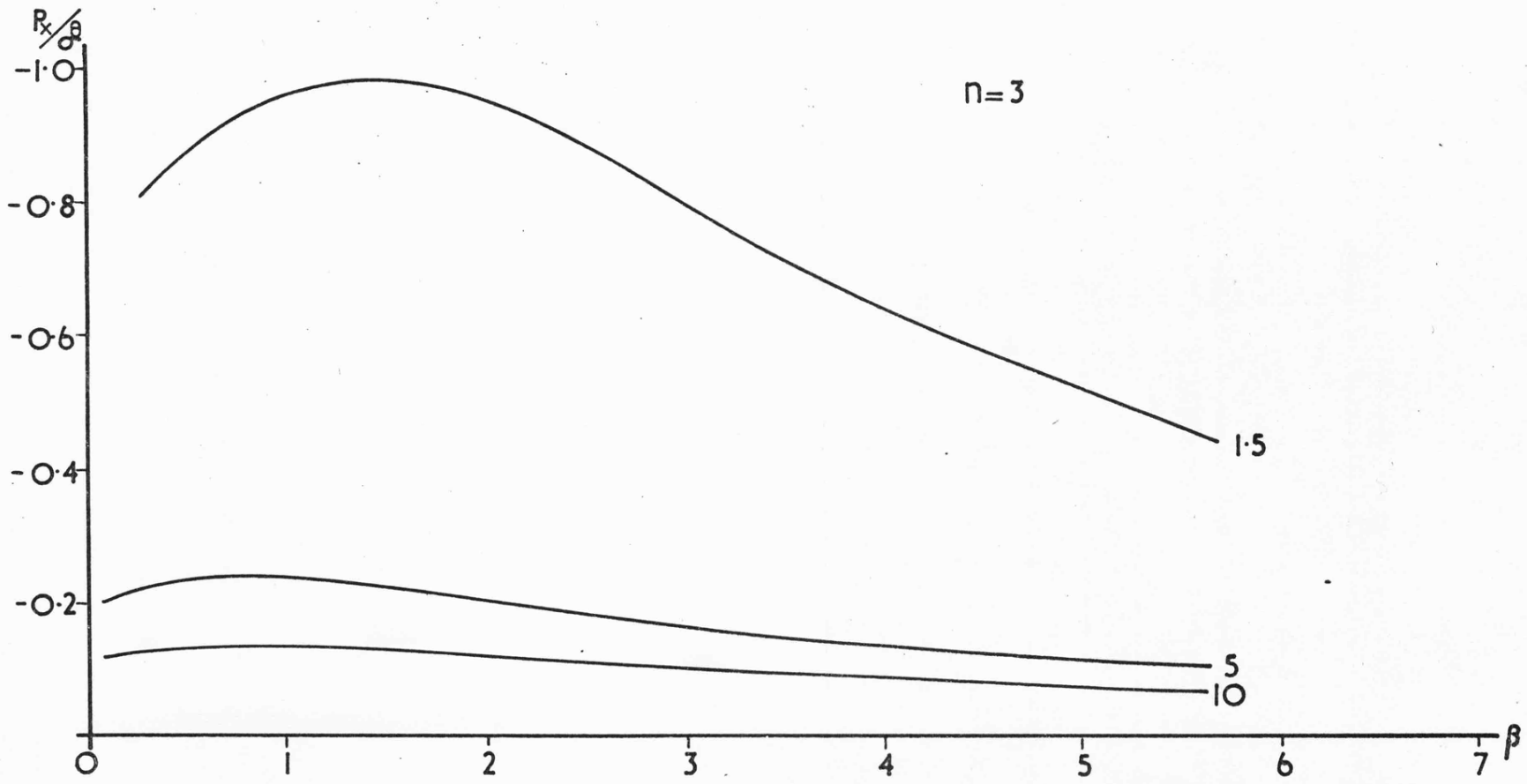

Fig 7·12 Contours of constant U for the plate with $\Delta U_x = \Delta U_y$ [Comp. stress]

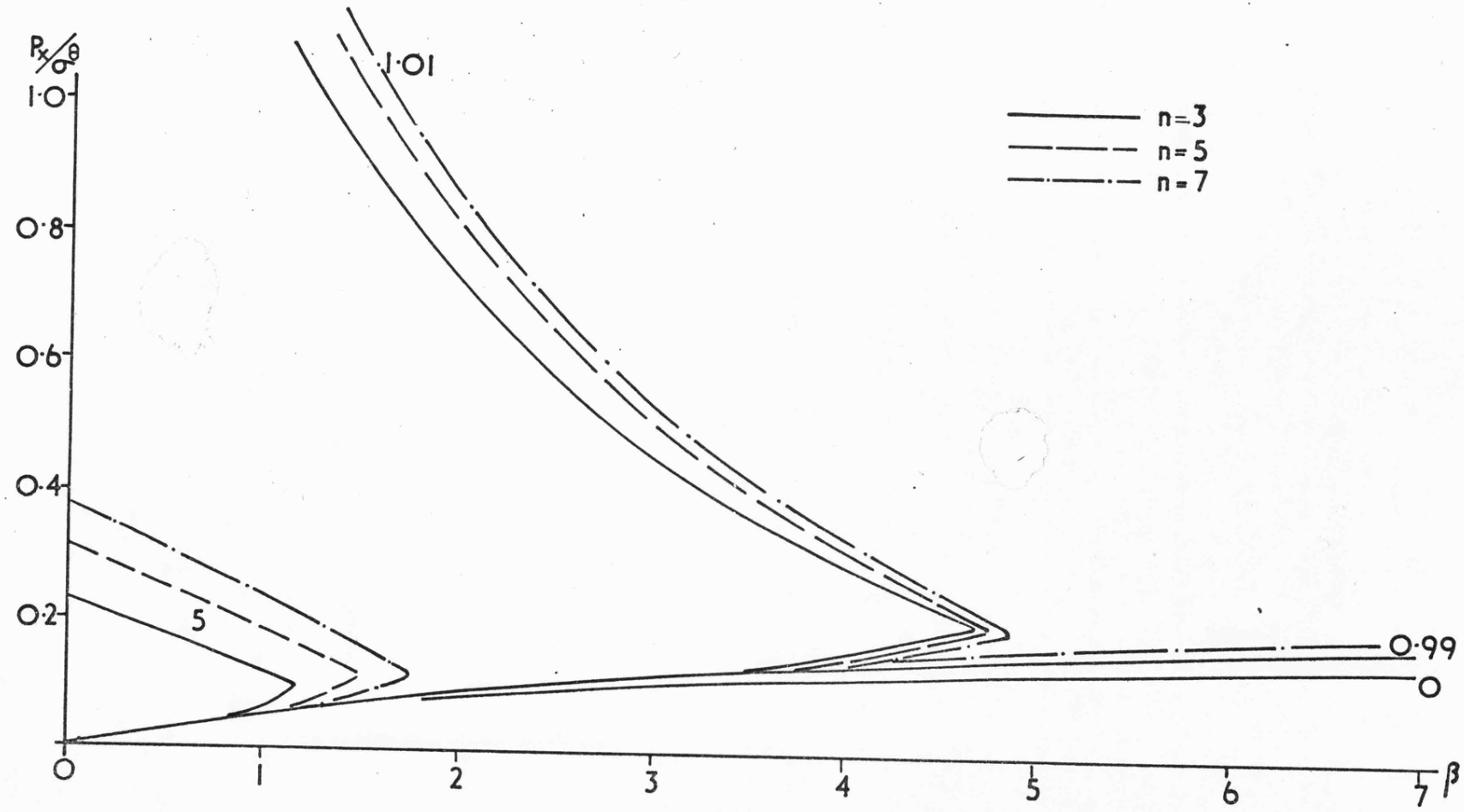

Fig 7·13 Contours of constant U for n = 3, 5 and 7 with $\Delta U_f = 0$

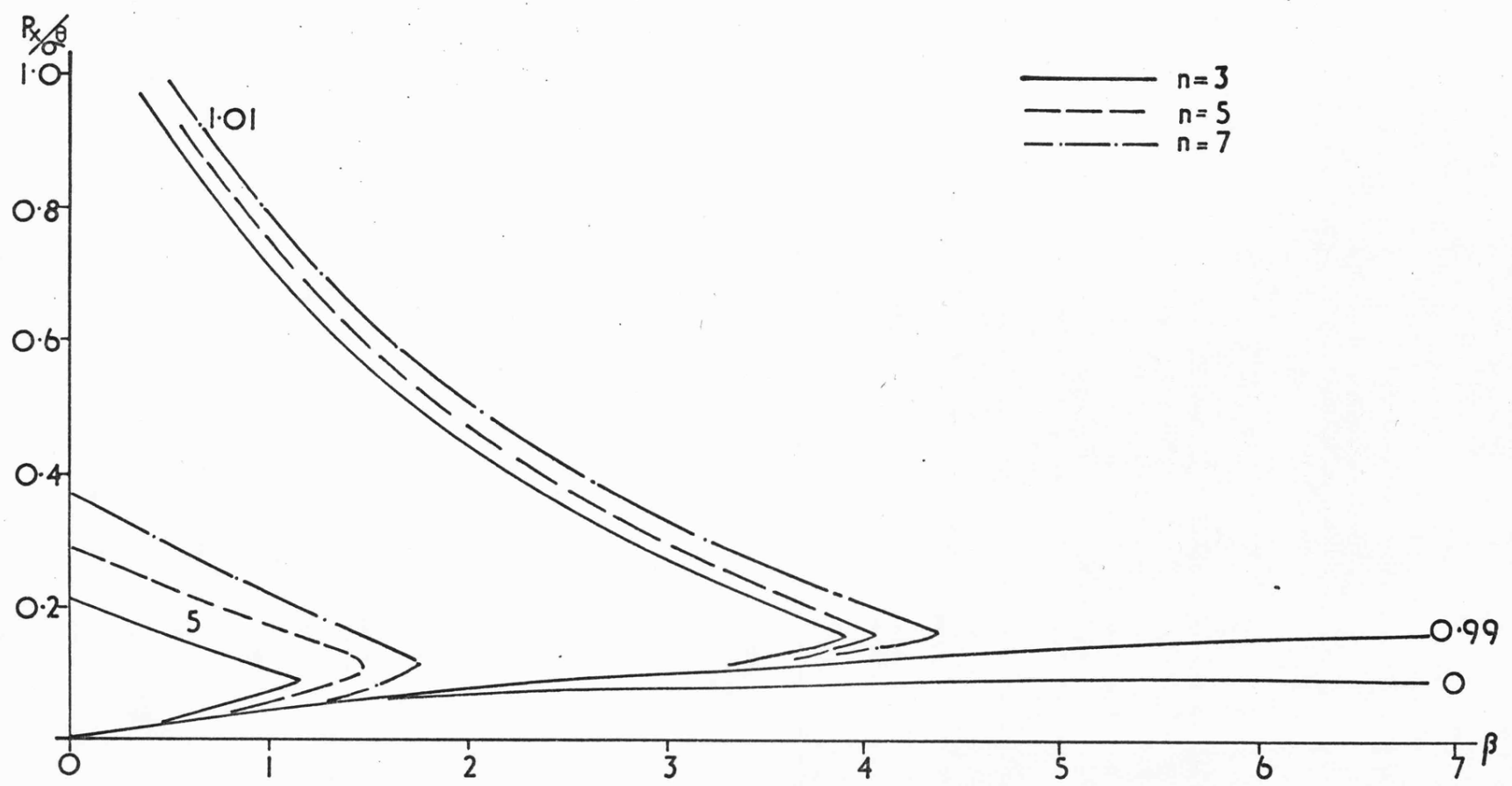

Fig 7·14 Contours of constant U for n=3, 5 and 7 with $\Delta U_x = \Delta U_y$

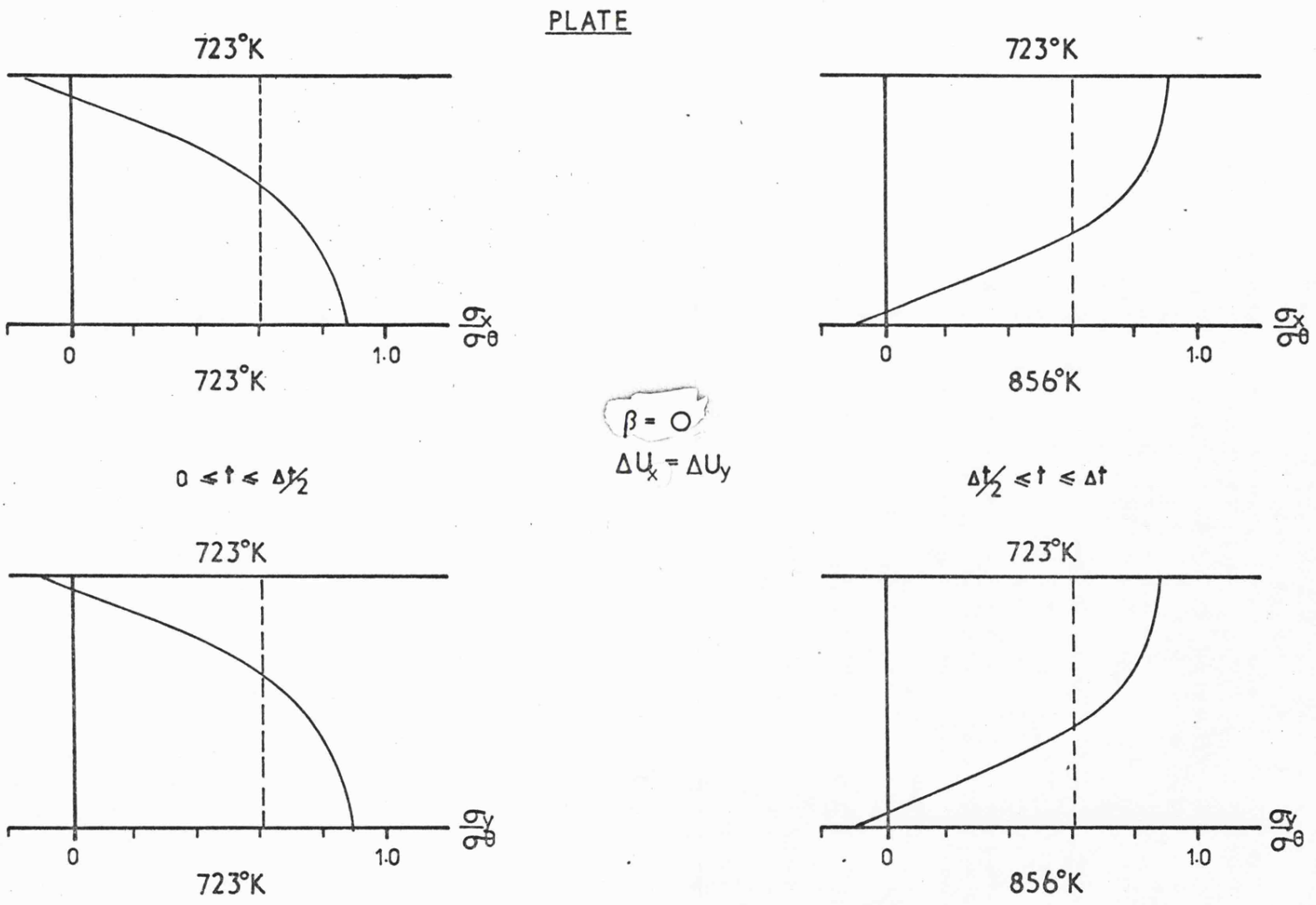

Fig 7·15 Stress distribution for $P_x/\sigma^\theta = 0·6$

PLATE

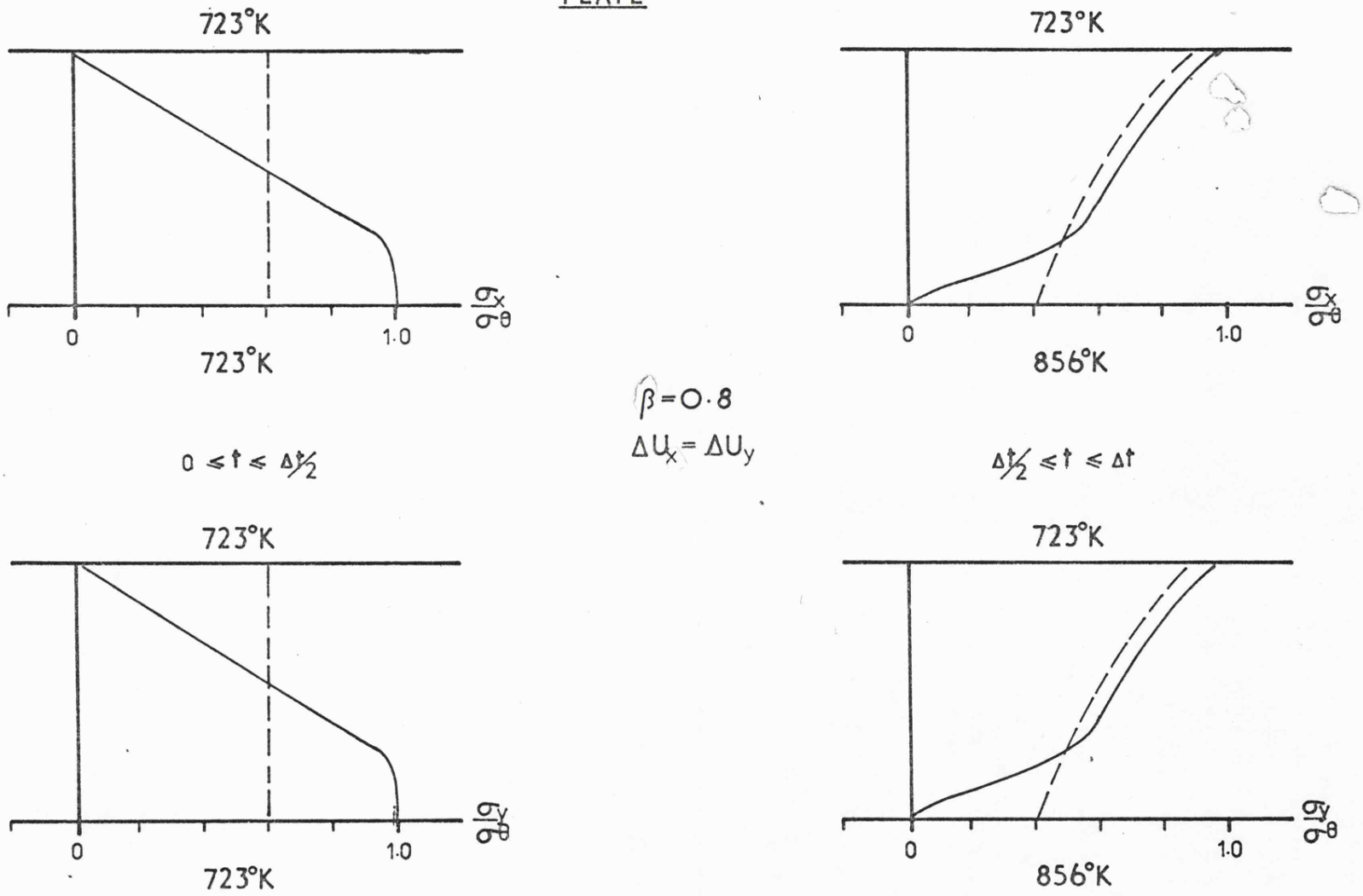

Fig 7·16 Stress distribution for $P_x/\sigma_\theta = 0 \cdot 6$

PLATE

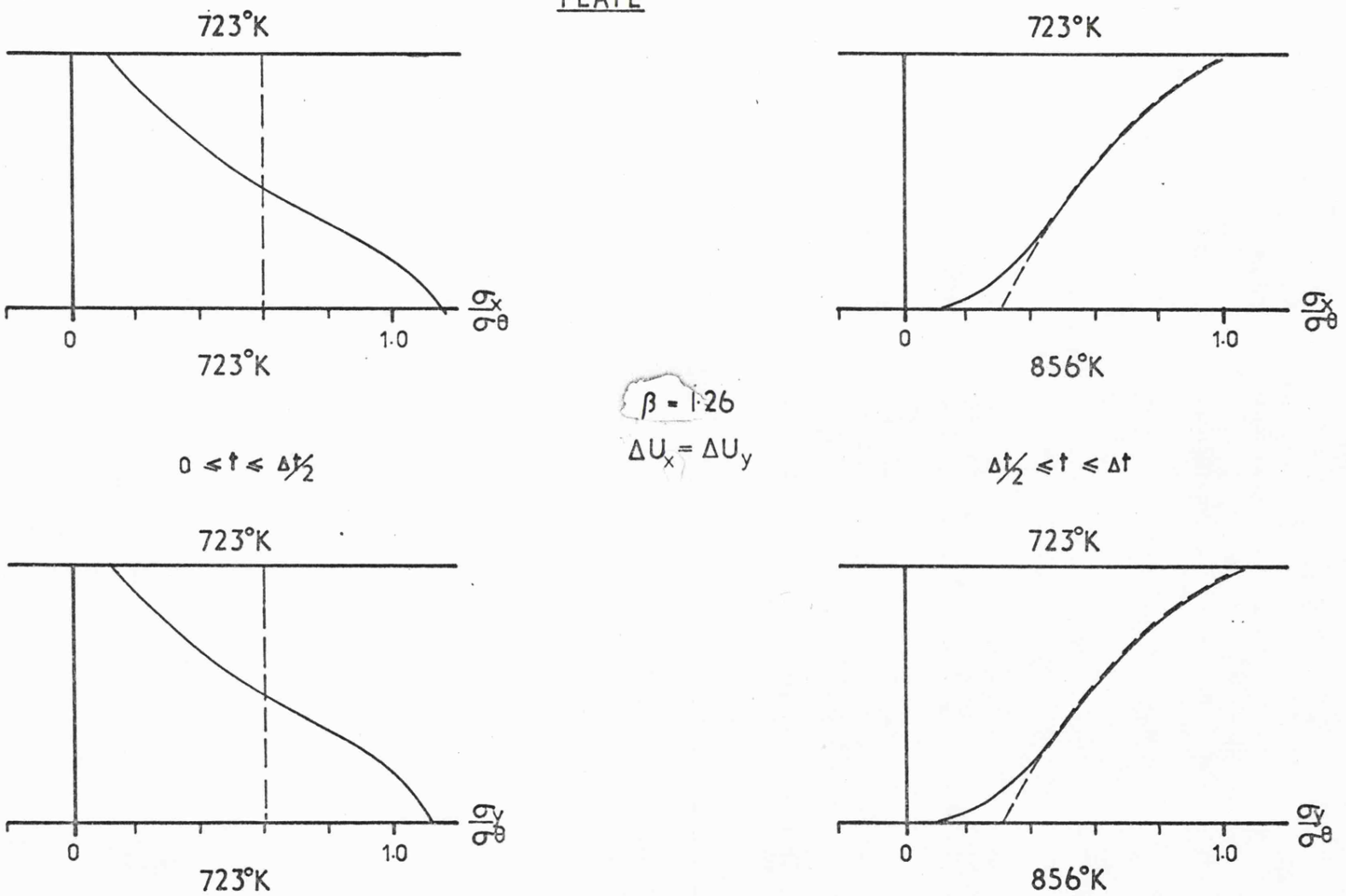

Fig 7·17 Stress distribution for $P_x/\sigma^\theta = 0{\cdot}6$

PLATE

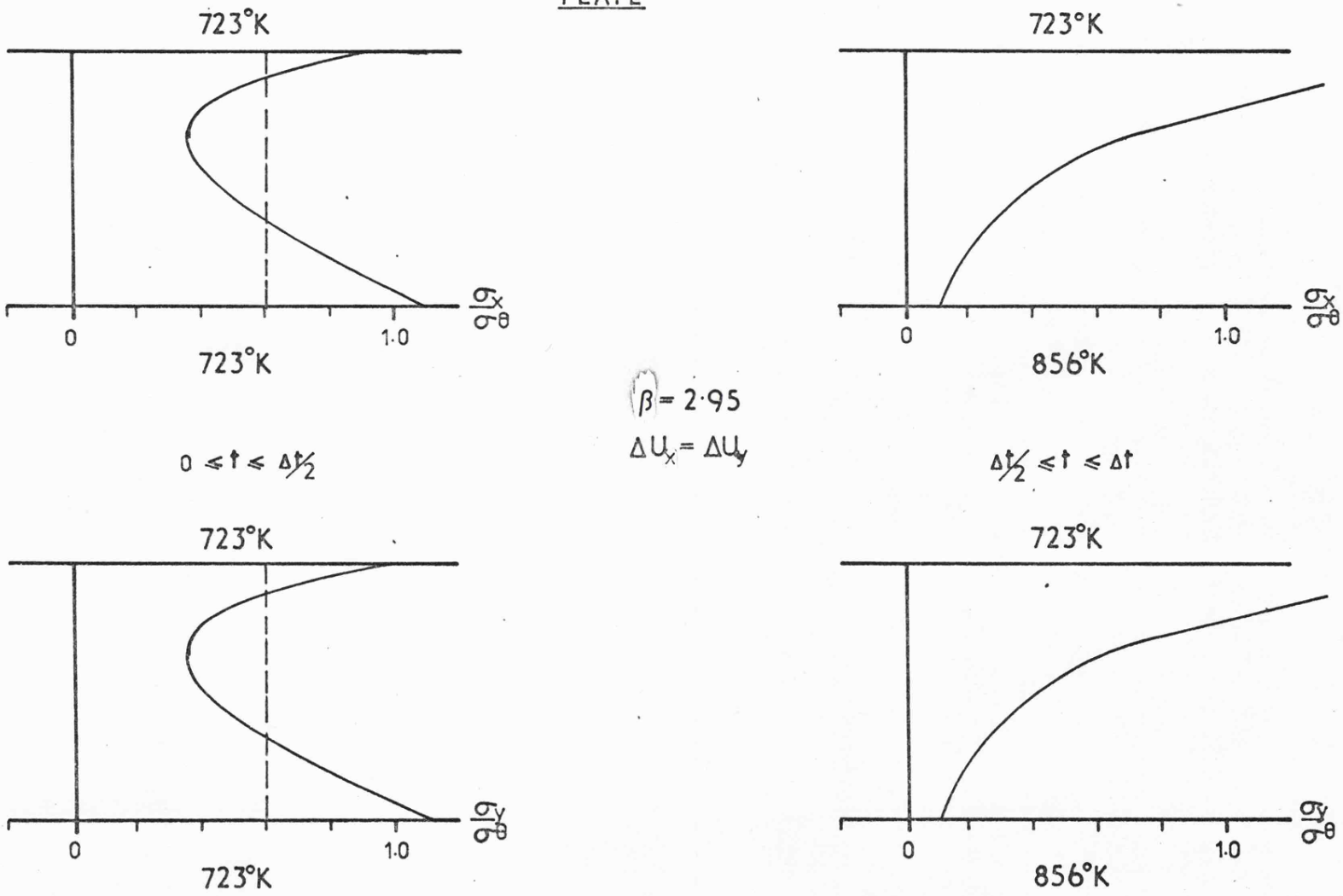

Fig 7·18 Stress distribution for $P_x/\sigma_\theta = 0{\cdot}6$

PLATE

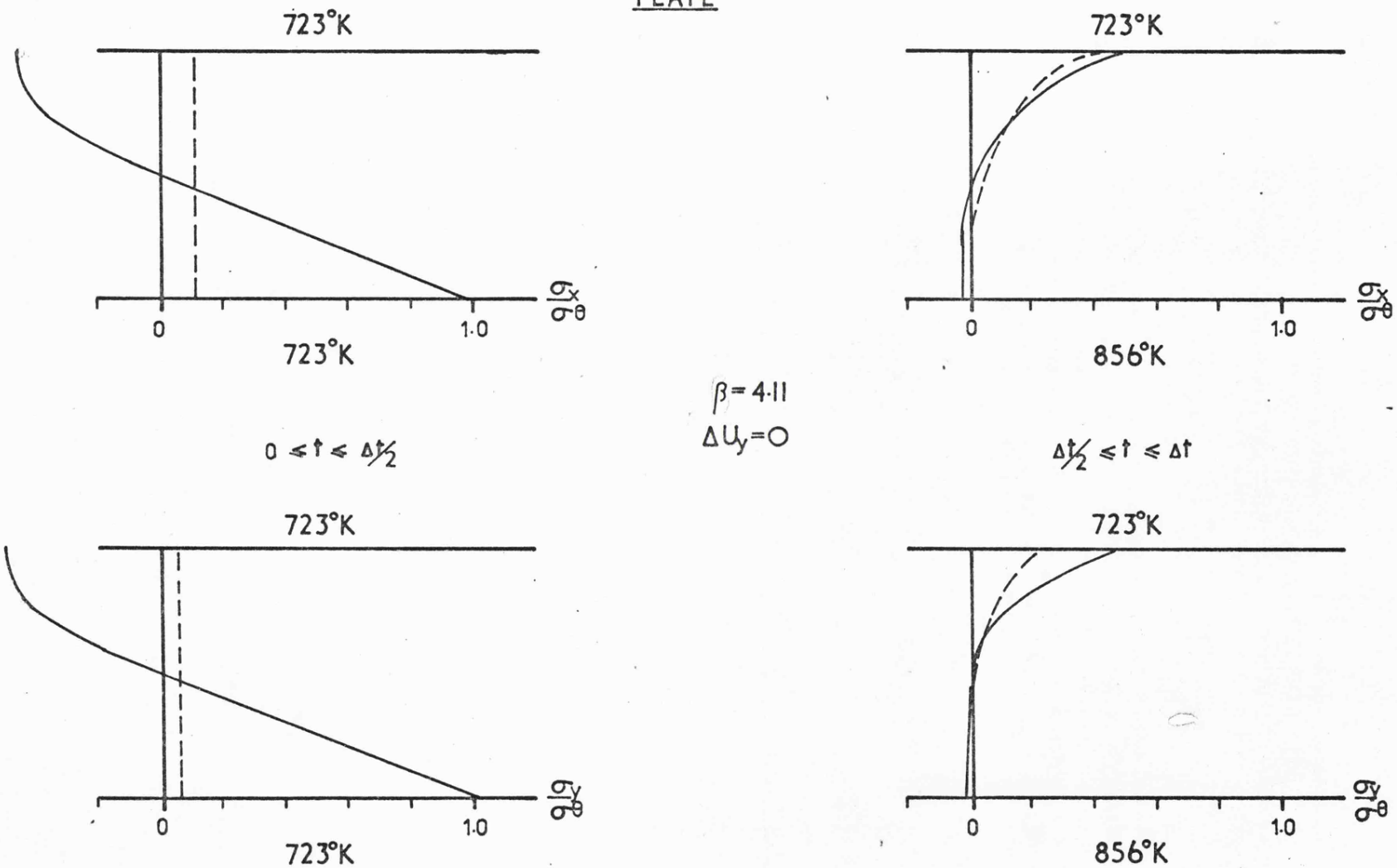

Fig 7·19 Stress distribution for $P_x/\sigma^\theta = 0{\cdot}1$

PLATE

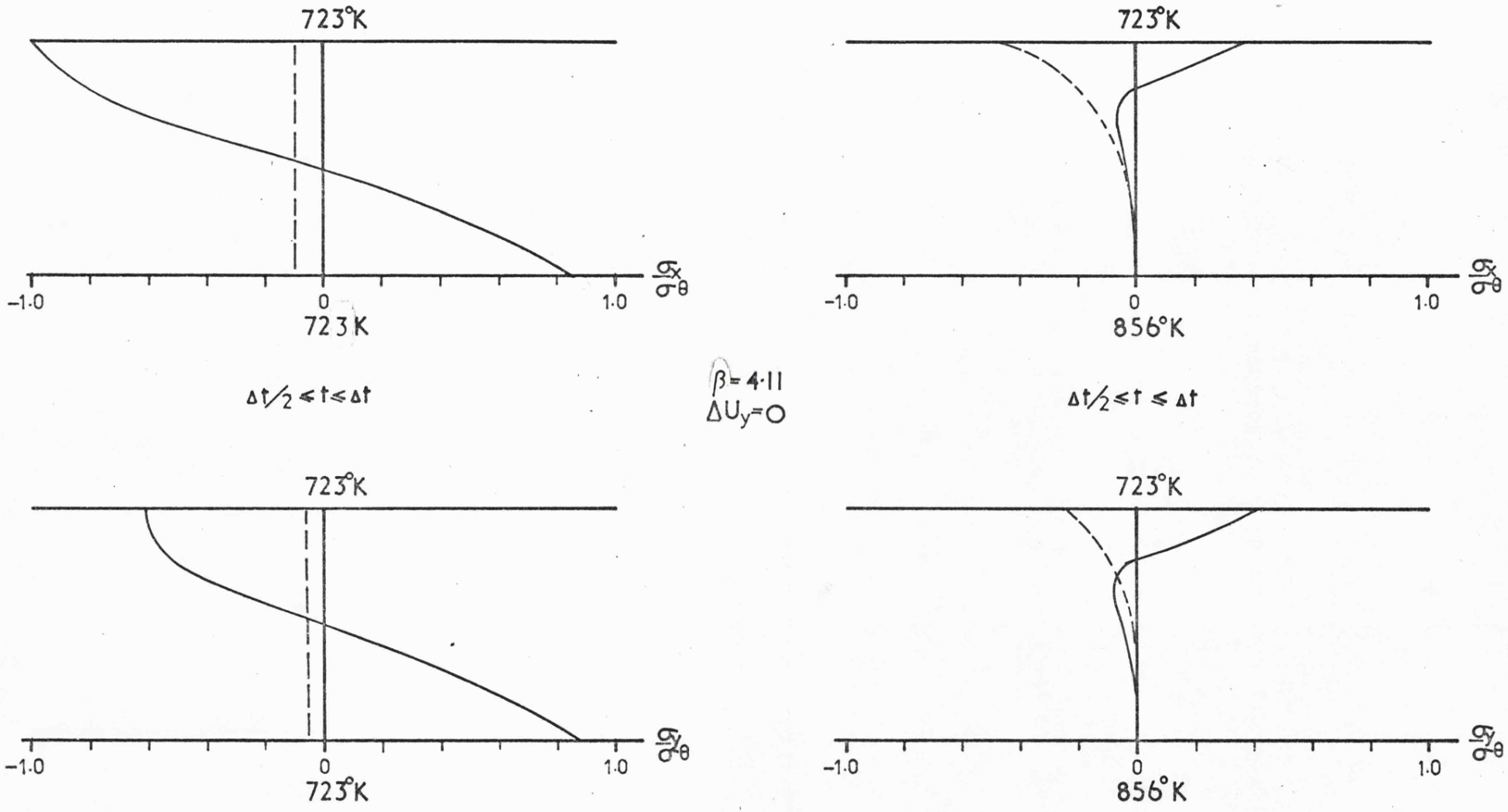

Fig 7·20 Stress distribution for $P_x/\sigma_\theta = -0{\cdot}1$

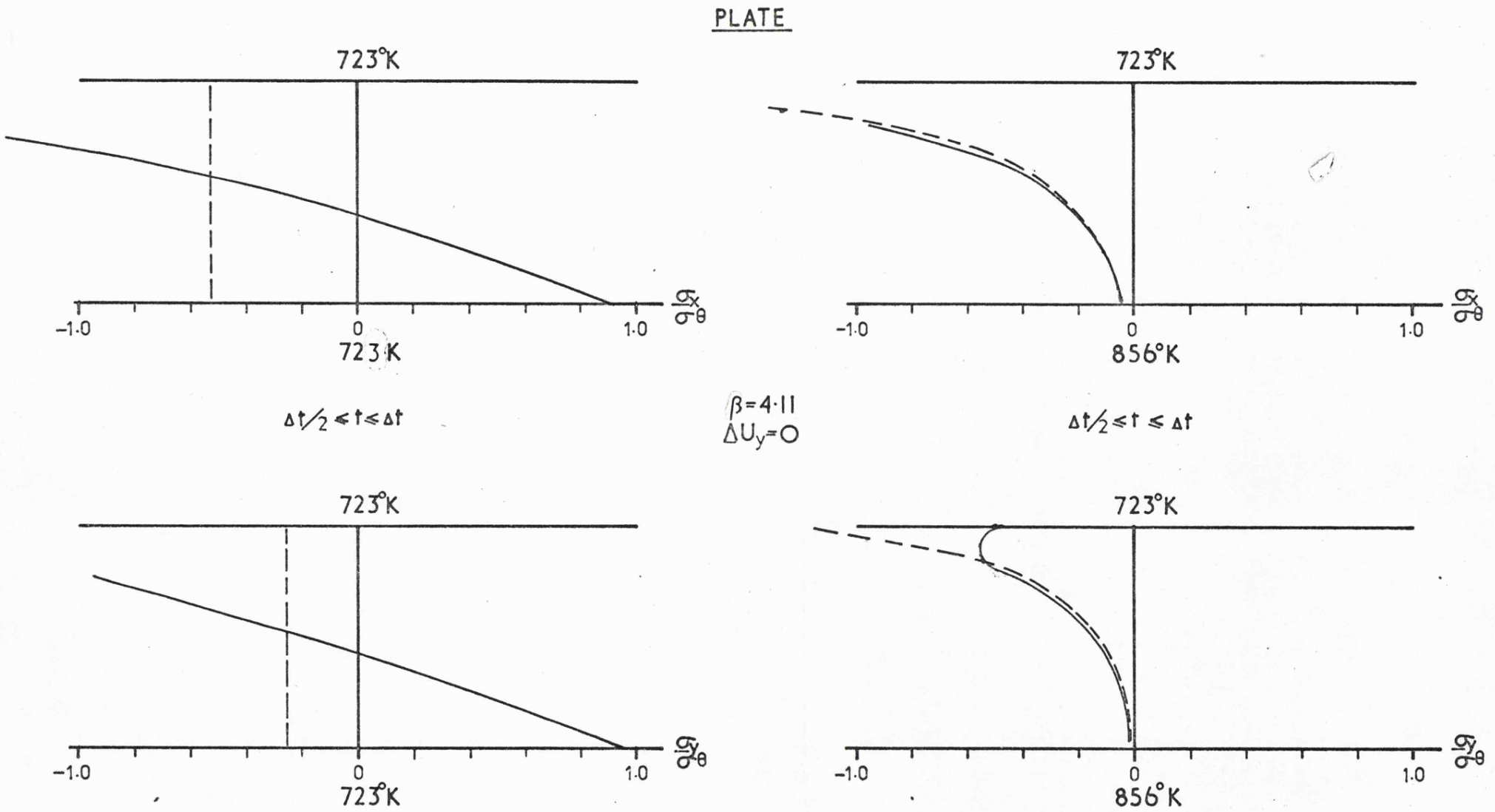

Fig7·21 Stress distribution for $P_x/\sigma^\theta = -0.5$

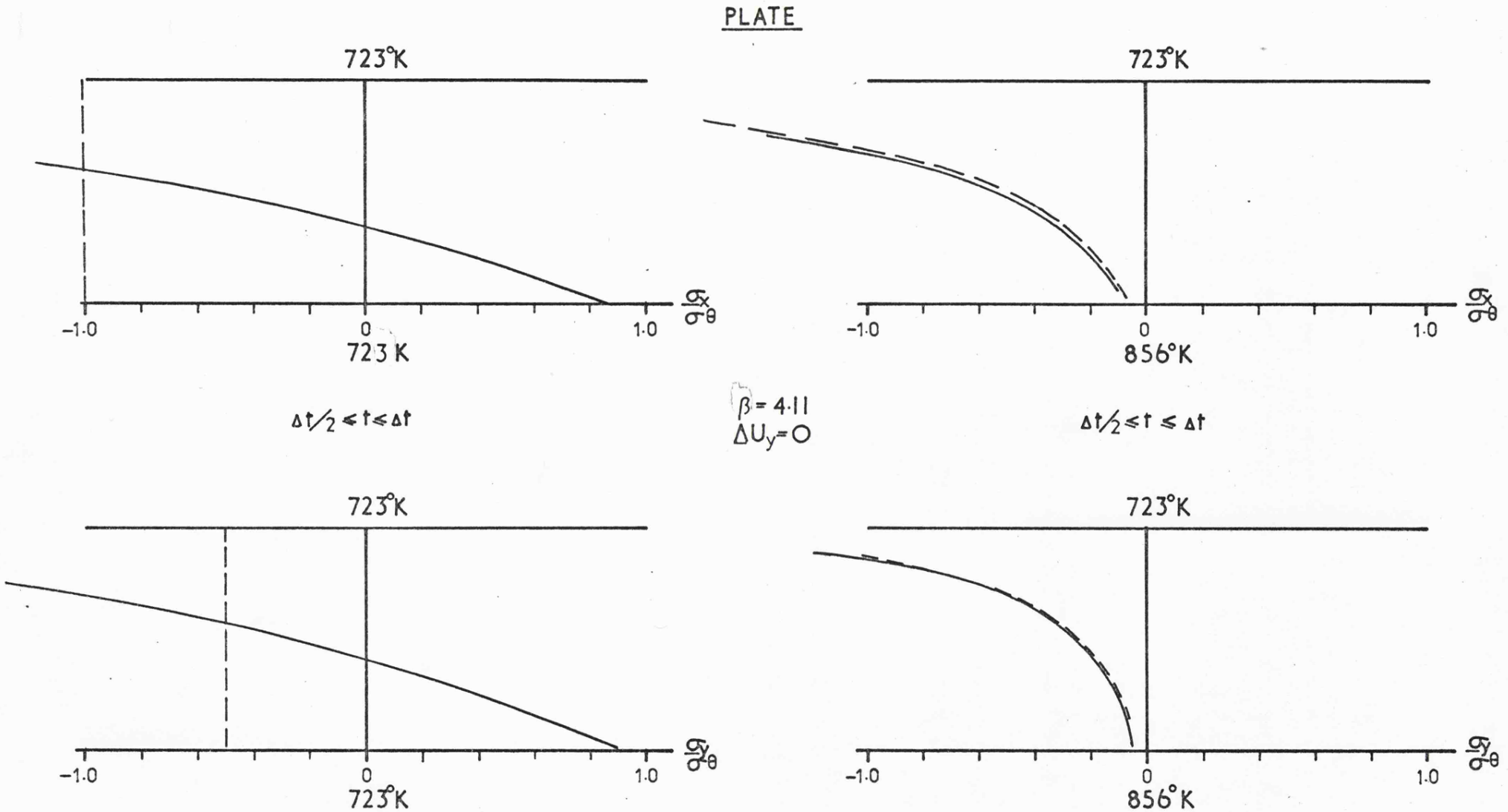

Fig7·22 Stress distribution for $P_x/\sigma^\theta = -1{\cdot}0$

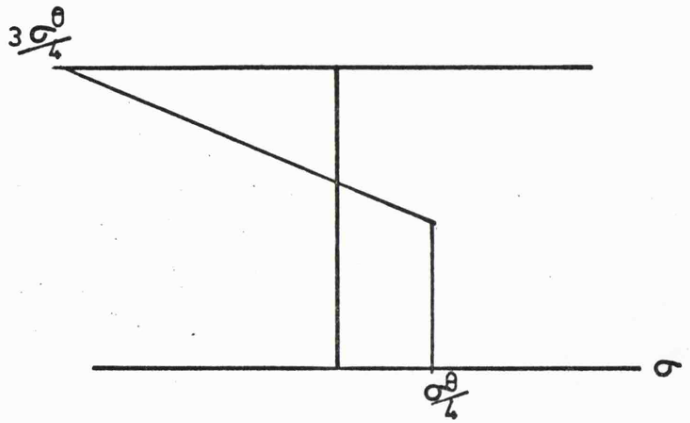

Fig 7·23 Residual stress field

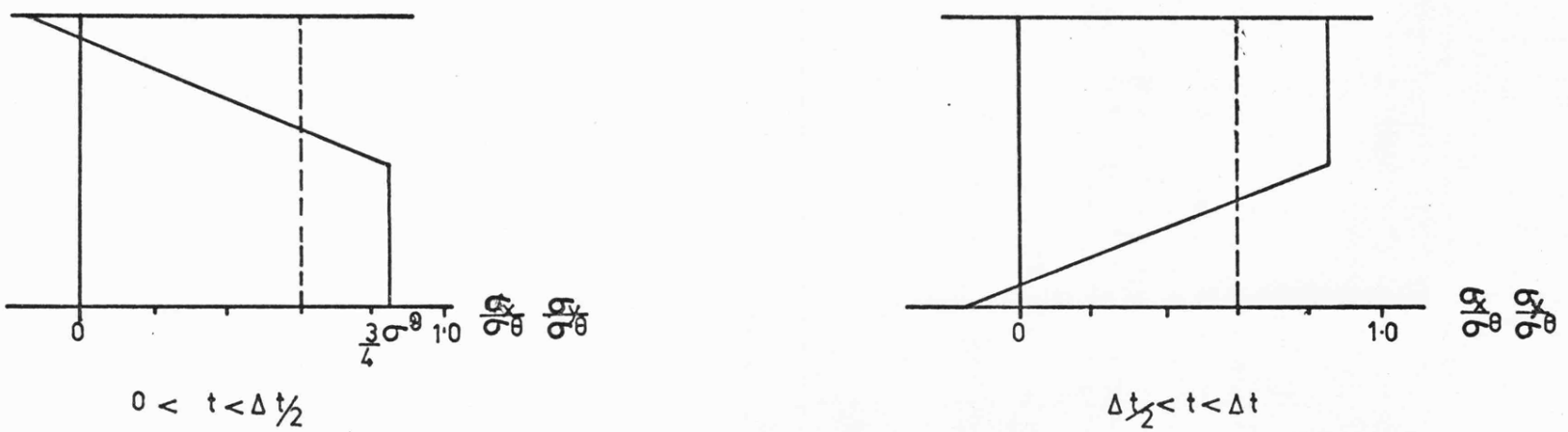

Fig 7·24 Stress distribution for $\beta=0$ and $p/\sigma^\theta=0·6$

Chapter 8

An Experimental Study on the Two-Bar Structure Subjected to Cyclic Histories of Temperature

8.1. Introduction.

An important aspect of the response of a metallic structure subjected to cyclic loading and a superimposed mean load is its capacity for progressive strain accumulation. The concept of a cyclic stationary state and the phenomenon of cyclic dependent creep has aroused interest in recent years.

In the preceding chapters the concept of the cyclic stationary state has been examined theoretically and the solutions to two examples related to a material parameter β. These studies have also shown that under cyclic histories of temperature the directions in which the creep strains are accumulated in relation to the steady applied loads are a function of the parameters, σ/σ^{θ}, β and n. Since the behaviour of many real materials are so complex that the physical and metallurgical processes involved are not fully understood: the theoretical deformation processes are, at best, only approximations. So, although computer codes manipulate and deliver numbers, the models on which they are based may differ in their behaviour from the real materials to such an extent that, for certain loading histories, the results may be erroneous and misleading.

The main objective in this chapter is to describe a series of experimental tests that were conducted to provide an assessment of the various assumptions made in the analyses of Chapters 6 and 7 and also to compare the predictions of displacement rate with those observed. The tests were conducted on a simulated two-bar model subjected to cyclic histories of temperature and steady applied loads. This structure was chosen as a model for two simple reasons: in the first instance it is probably the simplest

redundant structure imaginable and secondly, it is also one of the few redundant structures available in which it is possible to measure, experimentally, not only the deformation during creep but also the stress sharing conditions.

Previously, Barnes et al[48] simulated the two bar structure experimentally by means of two linked uniaxial tensile creep test machines holding specimens of Nimonic Alloy 90. They observed the redistribution of load that occurred for several initial stress conditions at different temperatures within the range 800-900°C, and in each case the results were compared with calculations based on creep strain data obtained from constant stress tests. These short term tests were extended further by Bullard and Clifton[76] to variable conditions of total load and temperature. However, to the author's knowledge the behaviour of the two-bar model under cyclic histories of temperature has not been investigated.

In the following sections details of the experiments are given and the results compared with previously obtained uniaxial data.

8.2. Experimental Equipment.

The details of the experimental apparatus are reviewed only briefly, as a more complete description is given in Chapter 10, section 10.1.

Basically, the apparatus consisted of two identical modified uniaxial tensile test machine load strings, with their individual extensometers and furnaces, arranged in parallel and mounted in a frame of welded construction. The total load on the test specimens was provided by two fluid filled drums connected by plastic tubing through a reversible peristaltic pump, thus forming a closed system. This allowed the individual load on each specimen to be varied although the total load remained constant. A schematic diagram of the apparatus is shown in Fig.8.1.

The peristaltic pump used for fluid transfer was controlled by the difference between the readings of sensitive extensometers mounted on each specimen. In this way the extension of each test specimen was maintained as nearly as possible equal to that of the other, thereby satisfying conditions of compatibility. Therefore if the extension of bar 1 increased above that of bar 2 , the pump was activated to transfer fluid from the drum loading bar 1 to that of bar 2 and vice-versa, thereby restoring 'equilibrium' of the system. The sensitivity of the control device was such that the strains differed by at most 10^{-4} % strain.

Specimen loads were measured by high output strain gauged load cells.

A cyclic temperature history was achieved by enclosing one specimen, bar 1 , within a furnace, of low thermal inertia, which was controlled to remain constant at different temperatures for periods of 12 hours, i.e. a cycle time of 24 hours. The other specimen, bar 2 , was maintained at constant temperature.

For technical reasons it was found more convenient to operate with the temperature histories;

$$\theta_1 = \theta_c + \Delta\theta \quad , \quad 0 \leqslant t \leqslant \Delta t/2$$
$$\theta_1 = \theta_c \quad , \quad \Delta t/2 \leqslant t \leqslant \Delta t \qquad (8.1)$$

$$\theta_2 = \theta_c \qquad 0 \leqslant t \leqslant \Delta t$$

and $\Delta t = 24$ hrs.

A facility in the control device allowed simulation of thermal expansions electronically so that the case $\beta = 0$ could be achieved, i.e. thermal expansion occurs but there is no resulting change in temperature dependent properties.

8.3. Test Conditions.

All the tests were conducted on specimens machined from the same commercially pure aluminium as used in the constant load tests described in Chapter 5. Since the steady state uniaxial creep data obtained at a series of constant stresses and constant temperatures (section 10.2), indicates that this material exhibits consistent creep behaviour it was considered well suited for an initial experimental investigation.

The test specimens were manufactured following the procedure given in section 10.2.4. and the rigid setting-up procedure described was strictly followed.

The experiments were conducted between room temperature, 20°C, and 150°C with several different combinations of θ_c and $\Delta\theta$. Over this temperature range the creep behaviour of aluminium is thought to correlate most closely with the strain-hardening hypothesis and this was, to a large extent, borne out by the experiments. As recovery creep, which forms the basis of the Bailey-Orowan model, is associated with temperatures in excess of 0.4 of the melting temperature, in degrees Kelvin, the creep acceleration observed in the theoretical study was not expected.

Before describing the tests themselves, the strain-hardening theoretical conclusions which are relevant to the temperature history 8.1 is first reviewed.

8.4. Strain-Hardening Model.

For a history of stress and temperature (σ_1,θ_1) followed by (σ_2,θ_2) for equal time intervals, the rapid cycling strain-hardening average creep rate is given by equation 7.11 which may be written in the form

$$\frac{\Delta\varepsilon}{\Delta t} = \{(\dot{\varepsilon}_1)^{1/m} + (\dot{\varepsilon}_2)^{1/m}\}^m \, 0.5^m \qquad (8.2)$$

where

$$\dot{\varepsilon}_1 = B\sigma_1^n \, mt^{m-1},$$

and

$$\dot{\varepsilon}_2 = B\sigma_2^n \, mt^{m-1}.$$

Hence $\dot{\varepsilon}_1$ and $\dot{\varepsilon}_2$ are the creep rates at time t for constant stress and temperature tests at (σ_1,θ_1) and (σ_2,θ_2) respectively. The most important feature of equation 8.2 is that the value of $\Delta\varepsilon/\Delta t$ is nearly equal to the larger of $\dot{\varepsilon}_1$ and $\dot{\varepsilon}_2$. For example, if $\dot{\varepsilon}_2 = 0.5\,\dot{\varepsilon}_1$ and $m = 1/3$, then $\Delta\varepsilon/\Delta t = 1.04\,\dot{\varepsilon}_1\,0.5^m$, and $\dot{\varepsilon}_2$ may be effectively ignored. As a result the regions in Fig.7.7 are very distinct from each other and the solutions corresponding to region 1 and region 2 (see Fig.7.2) may be described in simple terms.

In region 1 the dominant strain rates occur when the stresses are largest which, in both bars for the temperature history of equation 8.1, occurs when the temperatures are $\theta = \theta_c$. Assuming the strain rates during the other halves of the cycle are negligible (i.e. when $\theta_1 = \theta_c + \Delta\theta$, $0 \leqslant t \leqslant \Delta t/2$ and $\theta_2 = \theta_c$, $\Delta t/2 \leqslant t \leqslant \Delta t$) then the stress histories are

$$\sigma_1 = \sigma - \sigma^\theta/2 \quad , \quad 0 \leqslant t \leqslant \Delta t/2$$

$$\sigma_1 = \sigma + \sigma^\theta/2 \quad , \quad \Delta t/2 \leqslant t \leqslant \Delta t \qquad (8.3)$$

and

$$\sigma_2 = \sigma + \sigma^\theta/2 \quad , \quad 0 \leqslant t \leqslant \Delta t/2$$

$$\sigma_2 = \sigma - \sigma^\theta/2 \quad , \quad \Delta t/2 \leqslant t \leqslant \Delta t \qquad (8.4)$$

where σ is the average applied stress.

The theory therefore predicts that the two specimens will creep, at a given time, at a rate which is 0.5^m of the creep rate of a specimen held at a constant temperature θ_c and subjected to a constant stress $\sigma + \sigma^\theta/2$ from time $t = 0$. This assumes that the creep rates at $\sigma - \sigma^\theta/2$ at θ_c and $\theta_c + \Delta\theta$ make negligible contribution. Therefore if appropriate

values are taken from the experimental results, this may be confirmed by the creep rates obtained from the uniaxial data.

With the exception of two tests, which were unsuccessful attempts to simulate the conditions of region 2 , all the tests conform to the conditions of region 1 , therefore the strain-hardening theory will not be extended to cover region 2 .

8.5. Experimental Tests and Comparison of Results with Theory.

The two-bar test machine has been used for approximately twenty tests that included several combinations of temperature difference and mean stress. Several of these tests were conducted while the standard of the apparatus was being improved and consequently a number of results have proved unsatisfactory. As a result of experience during these tests several modifications were carried out and these are given in the section on apparatus development in section 10.1. Some tests were also abandoned due to mechanical and electrical failures of various components. However ten experiments have provided acceptable results and six of these tests will be described here. Some tests were repeated to check the reproducibility of results and these were found to be acceptable and well within the experimental error usually associated with creep testing.

In Table 8.I experimental conditions of six tests are given. The thermal stresses quoted were evaluated on the assumption that $E = 9 \times 10^6$ lb/in^2 and the coefficient of thermal expansion = 26×10^{-6}/°C. In test 5 the thermal expansions were induced electronically and both specimens remained at 20°C throughout the test.

The values of the material parameter β were calculated from the constant load uniaxial creep data (section 10.2). It is clear from this data that β is a stress dependent quantity, yielding smaller values at higher stresses and, therefore, the values quoted are average values over the range of stresses which occur in the test.

The initial stress difference on the bars was theoretically zero. However, in practice due to the slight differences in the measured amount of liquid in each drum, stress differences of the order of 20 lb/in^2 were detected on load-up. These differences were, however, quickly rectified by the control system satisfying the compatibility condition.

All tests were conducted with a cyclic temperature history of period 24 hrs. and were allowed to continue for 400-500 hrs.

Tests 1, 2, 3 and 5.

In Fig.8.2 a typical temperature-time graph is shown. This plot is the temperature history of test 2 and illustrates the long term stability of the furnace and temperature control system. In all tests the maximum temperature occurring in a cycle was applied approximately twenty minutes from the application of load after any small stress redistribution had ceased (i.e. both bars were creeping at the same rate and no transfer of load was occurring). In tests where the temperature θ_c was above room temperature (20°C) both specimens were allowed to attain their steady temperature for approximately 12 hrs. before the commencement of the test.

Some transient phenomena occurred due to thermal lag of the furnace and the steady temperatures were achieved within $1\frac{1}{2}$ - 2 hours after the temperature change was signalled. Although the transient may appear to be of short duration, it will be shown to have a significant effect upon the interpretation of the results.

The plot of temperature against time, Fig.8.2, was obtained from data collected at hourly intervals by the laboratory data logger system, and whilst it clearly shows the long term stability of the heating system it does not show any short term instabilities. Chart recorders were used to continuously monitor thermocouple as well as load cell outputs to provide a record of any short term fluctuations. In the lower portion of Fig.8.3

the Chromel/Alumel thermocouple output corresponding to the fifth cycle of Fig.8.2 is shown. It is clearly seen that when the temperature change is signalled the furnace system provides a progressive smooth rise in temperature with no discernable overshoot. Likewise, the fan assisted cooling curve shows no undershoot and reaches the lower equilibrium temperature in approximately $2\frac{1}{2}$ hrs. During this test no large short term fluctuations in temperature are observed, although from inspection of digital data, fluctuations of the order $\pm \frac{1}{2}$°C occurred.

In Figs.8.4 and 8.5 the variation of stress with time for the 'hotter' bar are shown for tests 1 and 3 respectively. From these stress histories it appears that the stresses during the constant temperature periods are far from constant. However, the behaviour displayed is not that which actually occurred but is an undesirable feature of the switching devices employed in the data logger system interfering with the load cell output. In practice the stresses remain stable as can be judged from the chart recorder output shown in Fig.8.7. (This corresponds to the fifth cycle of Test 3). The large 'spikes' on this plot and that of Fig.8.3, occurring hourly, are interference from the data logger system as it scans through its selected channels, the high frequency signals are due to the pump control system and also to other electronic equipment located in the laboratory. These unwanted interferences still persist even after much of the equipment was extensively shielded and is an obvious problem when such sensitive instrumentation is used.

The stress histories of Figs.8.4 and 8.5 do, however, appear to closely conform to the concept of a constant residual stress field. After the first few cycles the stress histories remain stable and cyclic, oscillating between two fixed limits. The strain-time graph, Fig.8.6, on the other hand, does not achieve a constant stationary state displacement rate until far more cycles have been accumulated. The general form of the curve still

follows the form of the constant stress behaviour with a preliminary primary portion prior to a steady creep rate being achieved. The difference between stress limits in Figs.8.4 and 8.5 is theoretically equal to the thermal stress σ^{θ}, but experimentally these values are found to be much smaller. In Table 8.2 the experimental values, row (a) are compared with the theoretical values, row (b), and their ratio is given in row (c). It is seen that the experimental thermal stress is only 64% to 77% of that expected theoretically. The reason for this is difficult to discern from tests 1, 2 and 3 but can be more clearly seen from Test 5 .

In Test 5 the thermal expansion was simulated electronically by applying an additional voltage equivalent to the thermal expansion to the extensometer output of one bar. The control system interprets this voltage as an extension of the bar and immediately signals the pump to transfer liquid to the other drum i.e. increasing the creep rate of this bar, until compatibility is again restored. In this test the thermal expansion is therefore induced instantaneously whereas in the preceding tests it occurred over the period of the temperature transient. However, there still remains a transient load as the pump required a finite time in which to transfer load. The stress history corresponding to this test is shown in Fig.8.8 and again conforms to the concept of a cyclic state. Immediately after the simulated temperature change a peak in stress is observed which rapidly declines to a lower value which then, in the cyclic state, changes slowly. This phenomenon is caused by a creep strain which occurs over a short time interval. Further, over a complete cycle of the temperature history it appears to provide no net accumulation of strain and is apparently an anelastic strain which acts rather in the manner of a delayed elastic strain. If the stress histories of Figs.8.3 and 8.7 are examined closely it is seen to occur to a less marked effect. The stresses appear to 'overshoot' their equilibrium values and then slowly reach equilibrium. It appears that this 'delayed' strain is relatively insensitive to temperature, giving

a similar magnitude of effect in both tests 1 and 2 .

In rows (d) and (e) of Table 8.2 the average experimental stresses are given and in rows (f) and (g) the predicted values from equations 8.3 and 8.4 are given. The theoretical values satisfactorily bracket the observed values and despite the discrepancy in the thermal stresses give a good prediction of observed behaviour. In row (h), the predicted experimental creep rates are compared with the observed values, and are within the range of expected experimental error. The experimental creep rates were taken as the average creep rates within the time interval 300-500 hrs. and the constant stress rates over the same time interval were used in calculating the theoretical values. It is worth noting that tests 1 and 5 yielded the same value of the creep rate, which in accordance with the theory, shows that the effect of temperature on the material has had no effect on the creep rate. Further, the creep rates predicted and recorded tend to be greater than those which are required in design.

The remaining two experiments (4a) and (4b) were conducted under more severe conditions and were intended to simulate the conditions of region 2, where the deformation is dominated by creep strains occurring during the first part of the cycle. The tests were identical and gave near identical creep rates but although the cyclic stress histories were similar, appreciable differences are apparent. The strain-time and σ_1 stress histories are shown in Figs.8.9 and 8.10 and details of the experimental results given in Table 8.3.

In Fig.8.9 it is seen that the creep rates during the first part of the cycle are far greater than during the second part, and thus conforms to the condition of Region 2 . For σ = 9000 lb/in^2 the stationary state solution corresponding to the first part of the cycle was evaluated directly from the material data, yielding σ_1 = 6000 lb/in^2 and σ_2 = 12000 lb/in^2. (Due to scatter in the data values were rounded off

to the nearest 1000 lb/in^2.) The theoretical stress history for Region 2 type behaviour is given in column (a), rows (f) and (g) of Table 8.3. Due to the theoretical value of σ^θ being 14,660 lb/in^2, the stresses predicted for the second half of the cycle, σ_1 = 20,280 lb/in^2 and σ_2 = - 2660 lb/in^2 are unreasonable since the yield stress at room temperature is in the vicinity of 16000 lb/in^2. Therefore, plastic strains must be occurring during each cycle and this aspect of these tests take them outside the range of applicability of the theory.

The experimental thermal stress lies close to 8000 lb/in^2 in both tests and the ratios of experimental to theoretical σ^θ are 0.56 and 0.52, (row (c) of Table 8.3). If the experimental σ^θ is adopted in the theory then the resultant stress history is that given in column (b), row (f) and (g). This closely follows the observed history. The creep strain rate predicted from this stress history (row (h)) yields 9.10^{-4}% strain/hr. which is appreciably below the observed value of 3×10^{-3}% strain/hr. However if it is assumed that Region 1 type behaviour is occurring then the stress history given in column (c), rows (f) and (g) is obtained. This history gives an excessively high creep rate in excess of 10^{-2}% strain/hr. as the maximum stresses are again above yield.

The results of these two tests may be explained thus: the condition normally corresponds to that of Region 1 , but plastic straining occurs at the beginning of the second part of the cycle introducing a high strain rate. The history of σ_1 is shown in Fig.8.10 for test 4a and possesses some interesting features. During the first part of the cycle appreciable stress redistribution occurs and the apparent σ^θ increases over a number of cycles presumably due to plastic strain hardening. Although the tests are outside the applicability of the theory, it is clear that the rapid cycling solution indicates that plastic straining occurs. Further, the creep strain rates which occurred and were predicted would, in design

terms, be considered excessive and hopefully avoided since a creep strain rate of 3×10^{-3}% strain/hr. corresponds to 26% strain/year. Normal design work would be in the region of 1% strain/year.

8.6. Discussion.

The experiments described have simulated the two bar structure in which redistribution of stress can be caused by creep. It has been established that for constant applied loads and cyclic histories of temperature there exists, as predicted by the theory, a constant residual stress field and further, the strain histories presented show that cyclic stationary states are achieved after relatively few cycles. From the theory postulated in Chapters 6 and 7 a useful description of the stress and strain histories can be obtained from calculations applying constant stress creep data according to the strain hardening hypothesis providing the appropriate stress regime in which the structure is operating is known.

Test No.	θ_c (°C)	$\Delta\theta$ (°C)	σ (lb/in^2)	$\sigma^{\theta*}$ (theoretical)	$\sigma/\sigma^{\theta*}$	β
1	20	40	5733	4510	1.27	0.5
2	100	50	6300	5640	1.12	0.7
3	100	50	5100	5640	0.90	0.7
4a	20	130	9000	14,660	0.61	1.4
4b	20	130	9000	14,660	0.61	1.4
5+	20	40	5850	4510	1.27	0.0

$\sigma^{\theta*}$ calculated assuming $E = 9.10^6$ psi and $\alpha = 23 \times 10^{-6}/°C$.

+ In Test 5 the thermal expansions were induced electronically.

Table 8.1 Test Conditions

	Test Number	1	2	3	5	
	Experimental σ^{θ}	3140	4240	3590	3480	a
	Theoretical $\sigma^{\theta *}$	4510	5640	5640	4510	b
	Ratio $\frac{\sigma^{\theta}}{\sigma^{\theta *}}$	0.70	0.70	0.64	0.77	c
EXPERIMENTAL	$0 \leqslant t \leqslant \Delta t/2$	3660	4180	2410	4550	d
	$\frac{\Delta t}{2} \leqslant t \leqslant \Delta t$ $\frac{\sigma_1}{}$	6860	8410	6012	8024	
	$0 \leqslant t \leqslant \Delta t/2$	8000	8460	7830	7155	e
	$\frac{\Delta t}{2} \leqslant t \leqslant \Delta t$ $\frac{\sigma_2}{}$	4570	4210	4270	3680	
THEORETICAL	$0 \leqslant t \leqslant \Delta t/2$	2380	3480	2280	3595	f
	$\frac{\Delta t}{2} \leqslant t \leqslant \Delta t$ $\frac{\sigma_1}{}$	7980	9120	7920	8105	
	$0 \leqslant t \leqslant \Delta t/2$	7980	9120	7920	8105	g
	$\frac{\Delta t}{2} \leqslant t \leqslant t$ $\frac{\sigma_2}{}$	2380	3480	2280	3595	
	Exp. Creep Rate % Strain/hr.	$3.2\ 10^{-5}$	$2.4\ 10^{-4}$	$1.1\ 10^{-4}$	$3.5\ 10^{-5}$	h
	Theory	$2.\ 10^{-5}$	$2.5\ 10^{-4}$	$1.3\ 10^{-4}$	$2.\ 10^{-5}$	

† In Test 5 , thermal expansion was simulated electronically.

All stress are in lb/in^2.

Table 8.2

Stress Histories and Creep Rates for Tests 1, 2, 3 and 5

	Test Number	4a		4b	
	Experimental σ^{θ}	8300		7580	a
	Theoretical $\sigma^{\theta*}$	14660		14660	b
	Ratio $\frac{\sigma^{\theta}}{\sigma^{\theta*}}$	0.56		0.52	c
EXPERIMENTAL	$0 \leq t \leq \Delta t/2$	3540		6130	d
	$\frac{\sigma_1}{\frac{\Delta t}{2} \leq t \leq \Delta t}$	11790		13720	
	$0 \leq t \leq \Delta t/2$	14280		11960	e
	$\frac{\sigma_2}{\frac{\Delta t}{2} \leq t \leq \Delta t}$	5940		4390	
THEORETICAL		(a)	(b)	(c)	
	$0 \leq t \leq \Delta t/2$	6000	6000	1670	f
	$\frac{\sigma_1}{\frac{\Delta t}{2} \leq t \leq \Delta t}$	20660	12000	16330	
	$0 \leq t \leq \Delta t/2$	12000	12000	16330	g
	$\frac{\sigma_2}{\frac{\Delta t}{2} \leq t \leq \Delta t}$	-2660	4000	1670	
	Exp.	$3.04 \quad 10^{-3}$		$3. \quad 10^{-3}$	h
	Creep Rate / % Strain/hr.	(b) $9. \quad 10^{-4}$			
	Theory	(c) $> 10^{-2}$			

Table 8.3

Stress Histories and Creep Rates for Tests 4a and 4b

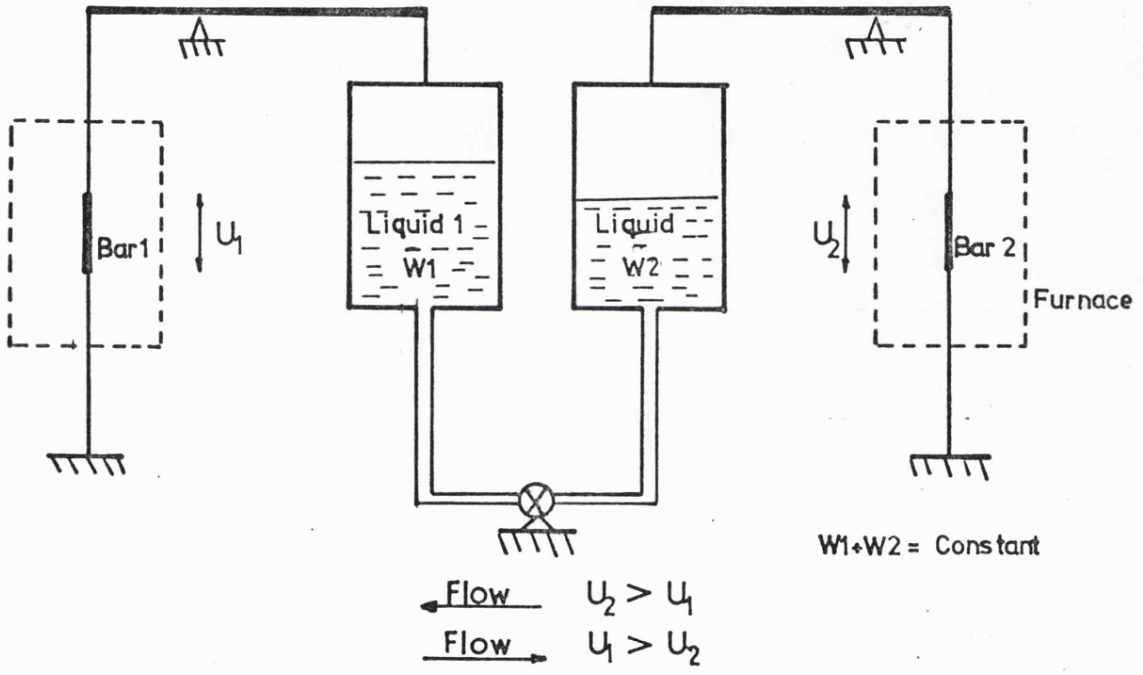

Fig 8.1 Schematic diagram of two-bar structure

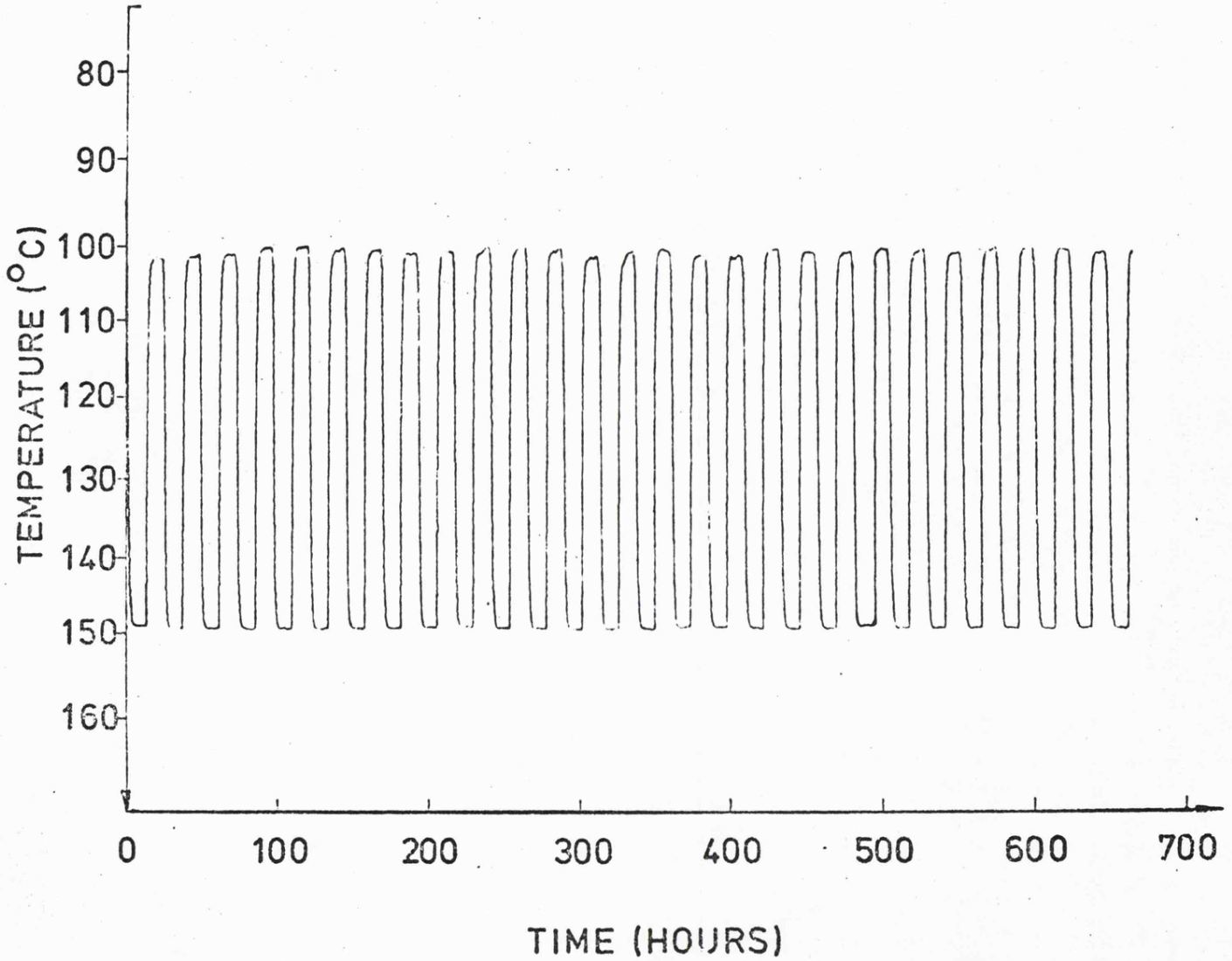

Fig 8.2 Temperature history of bar 1 during test 2

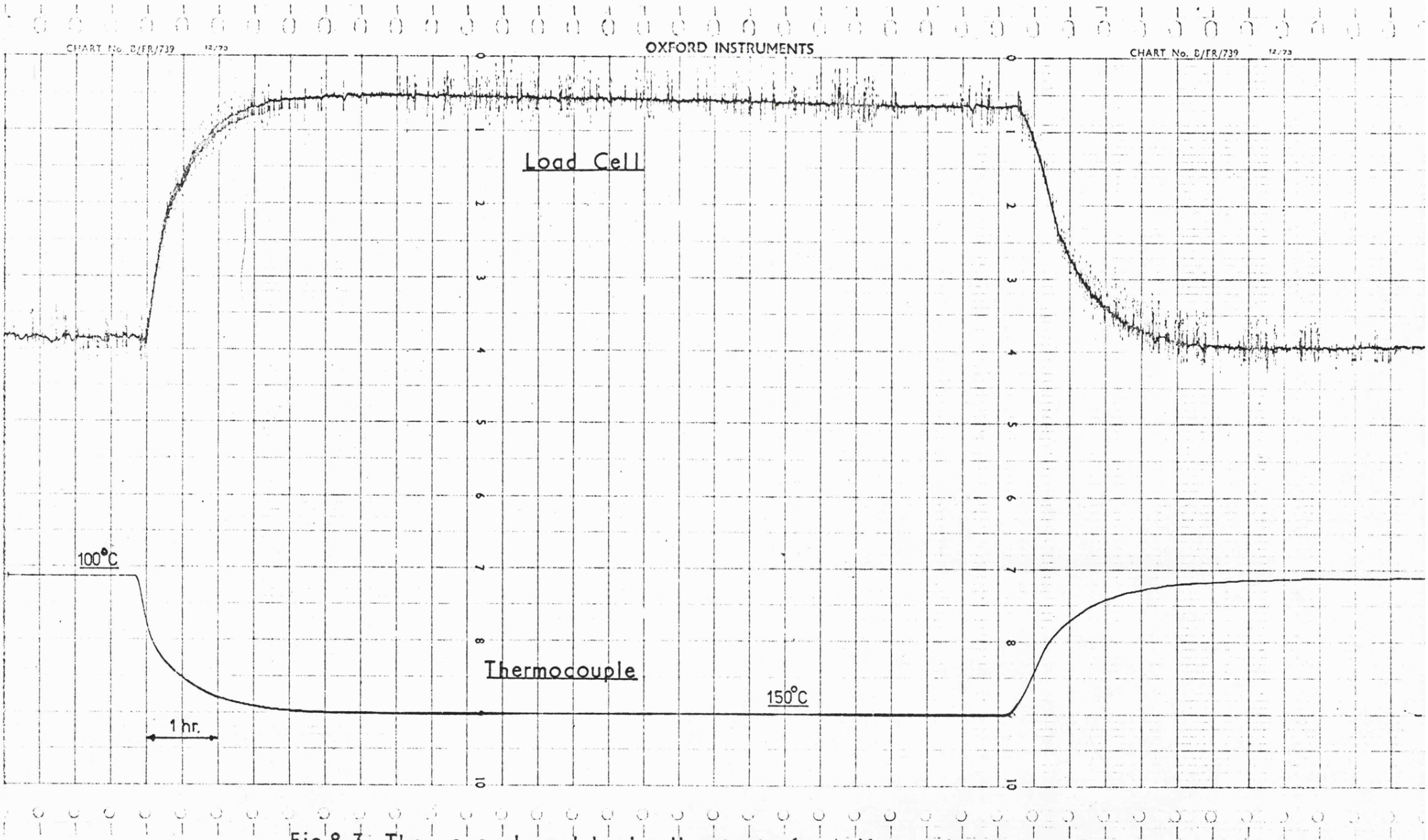

Fig 8.3 Thermocouple and load cell outputs for half a cycle of test 2

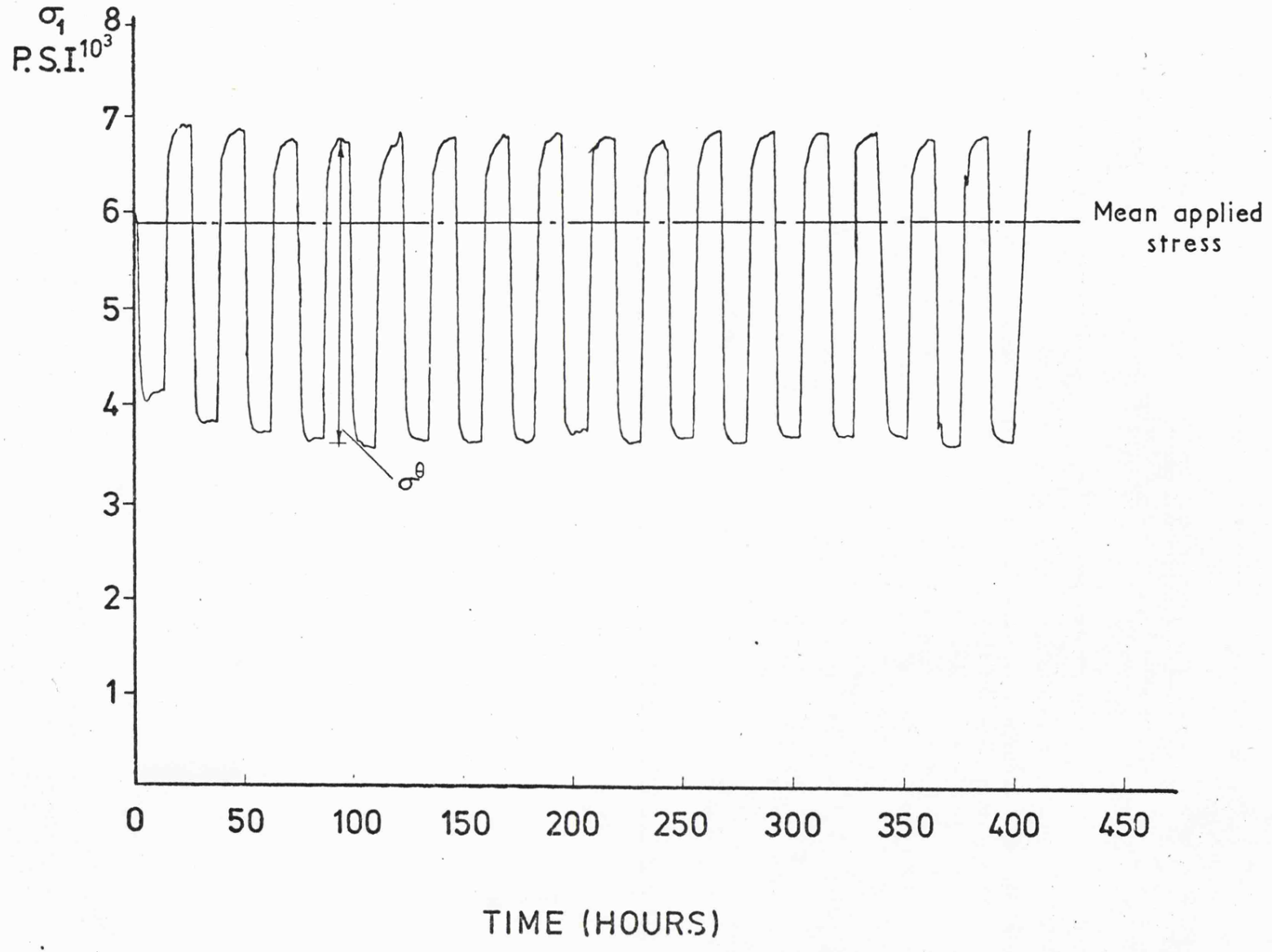

Fig 8.4 Stress history on bar 1 for test 1

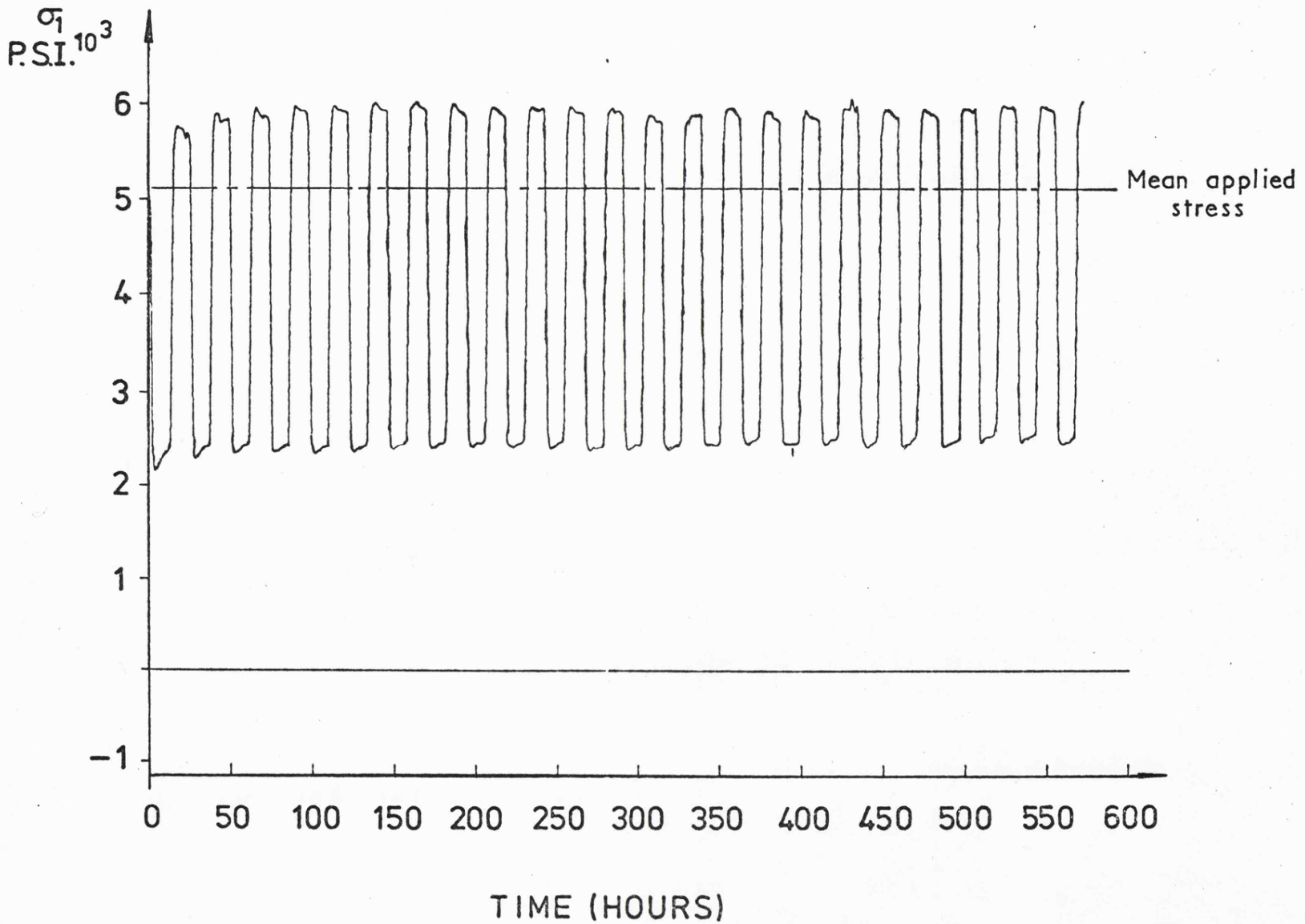

Fig 8.5 Stress history on bar 1 for test 3

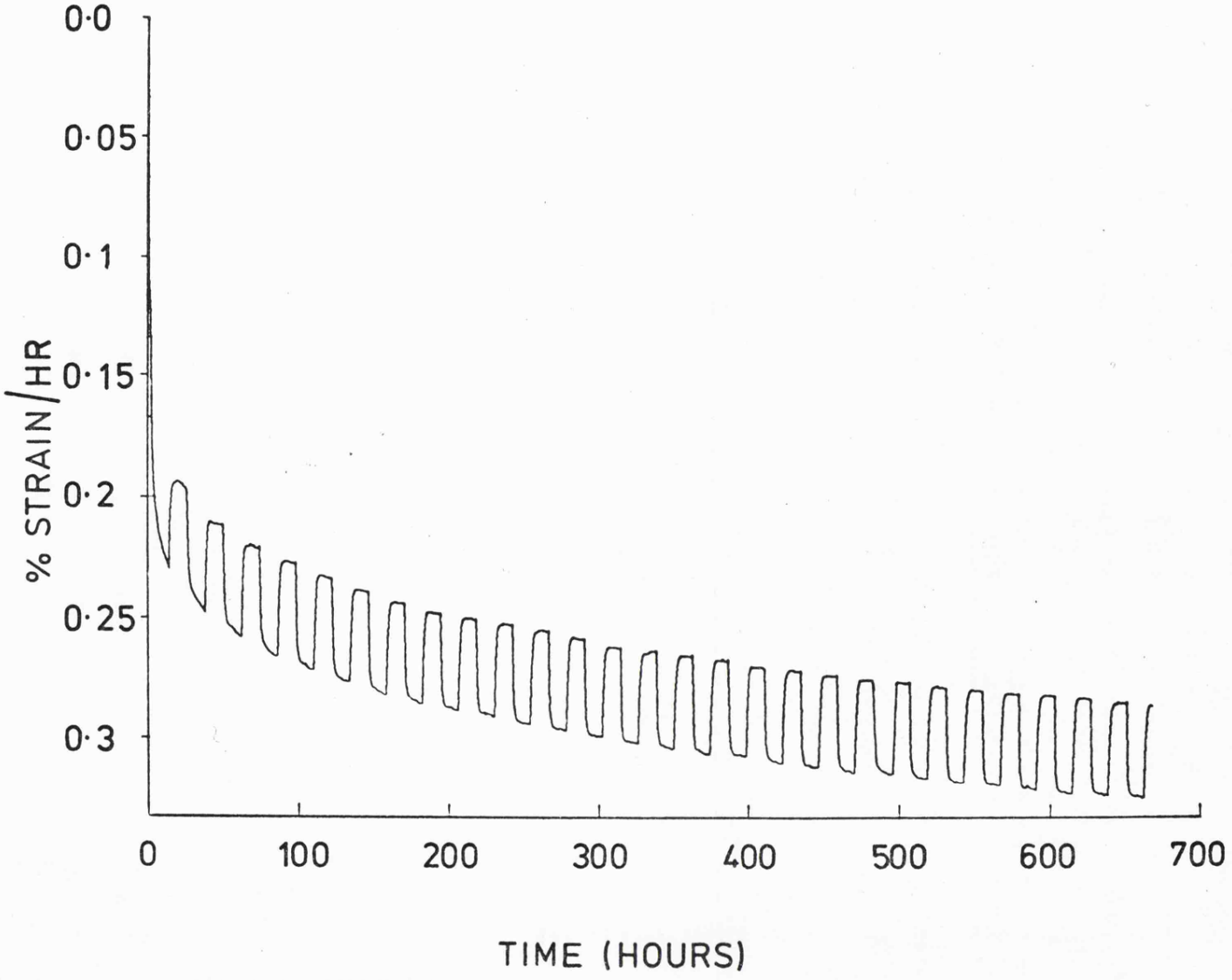

Fig 8.6 Strain–time output for test 3

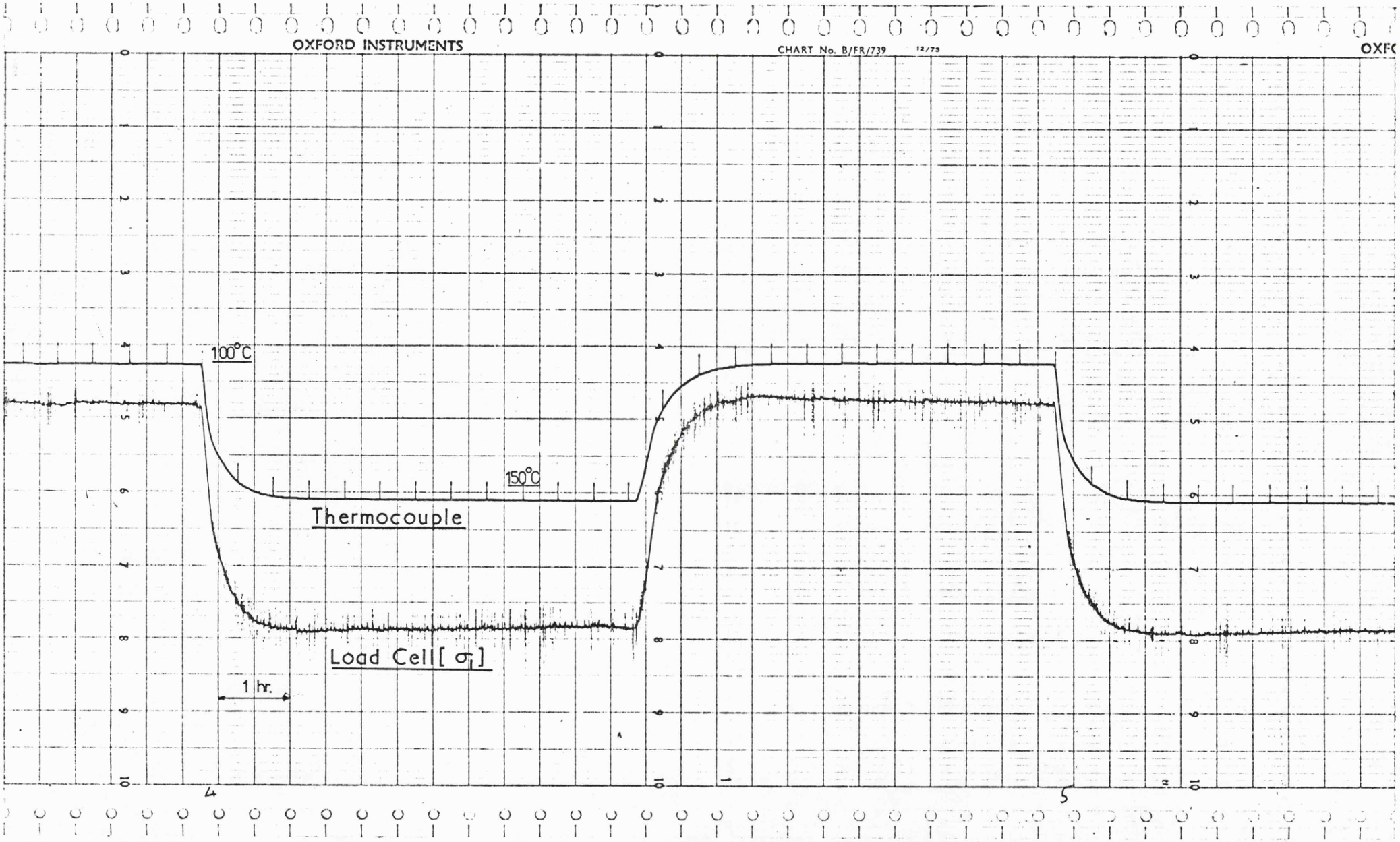

Fig 8·7 Stress and temperature history of test 3

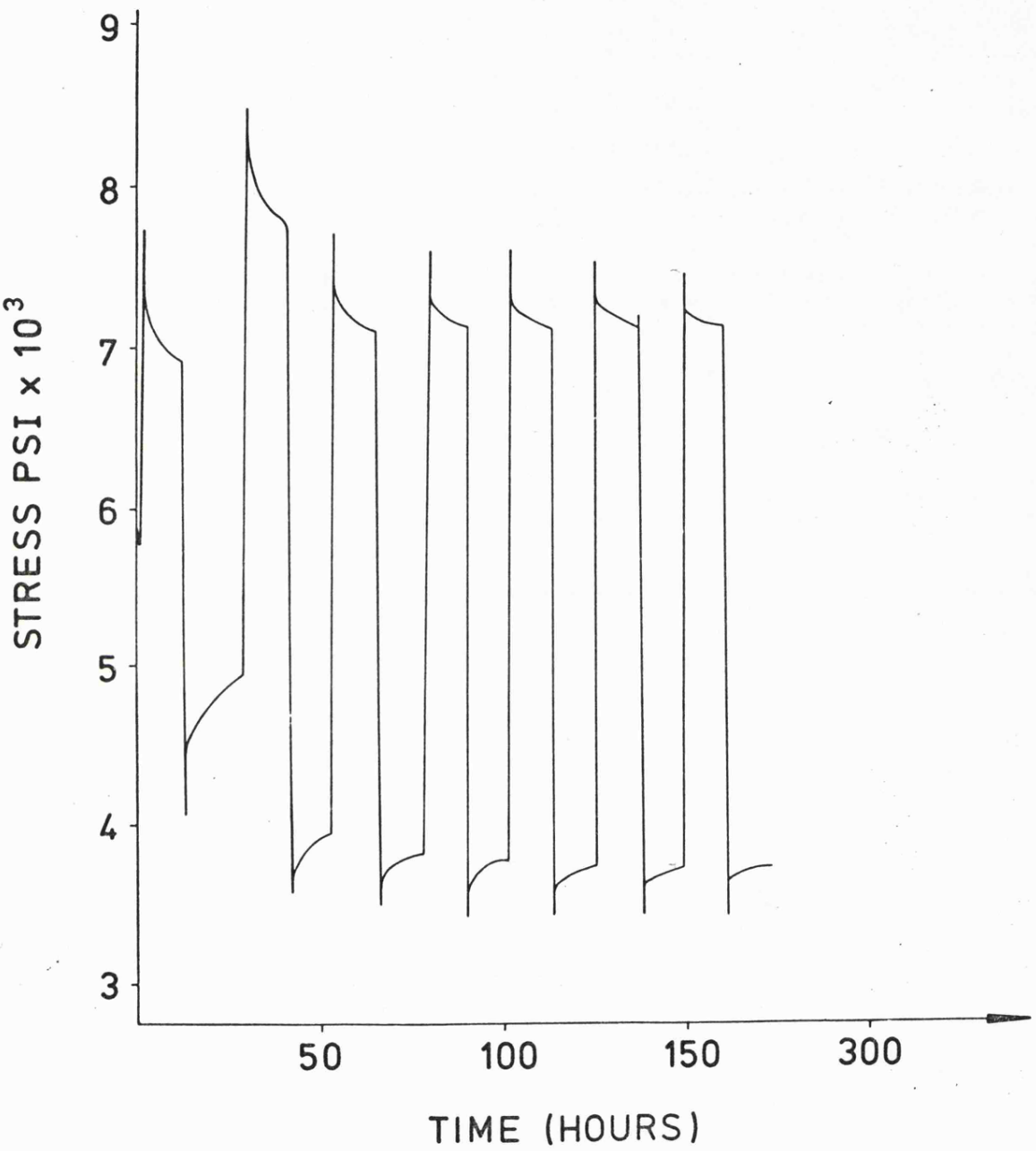

Fig 8·8 Stress history for simulated thermal cycling

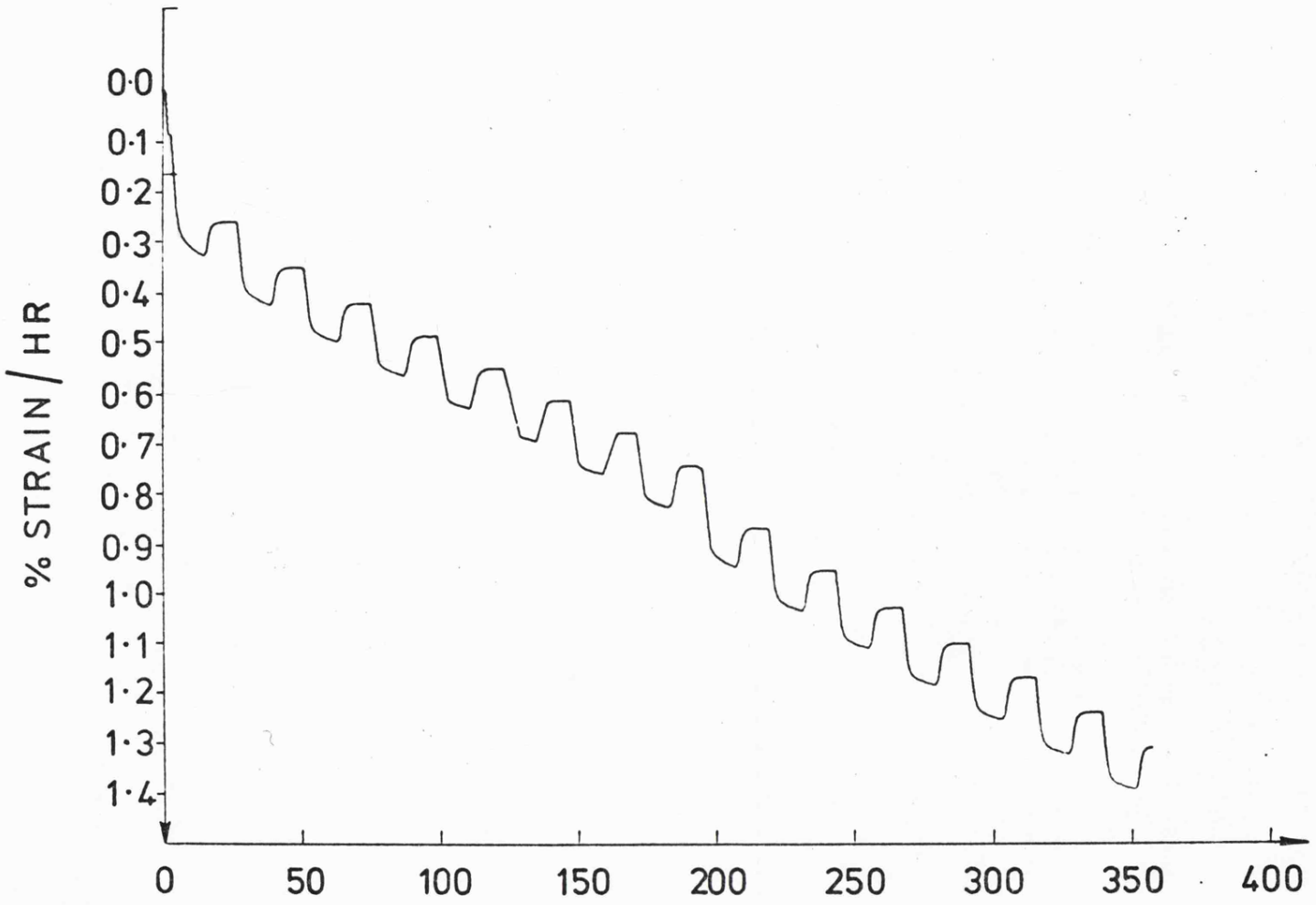

Fig 8.9 Strain–time output for test 4a

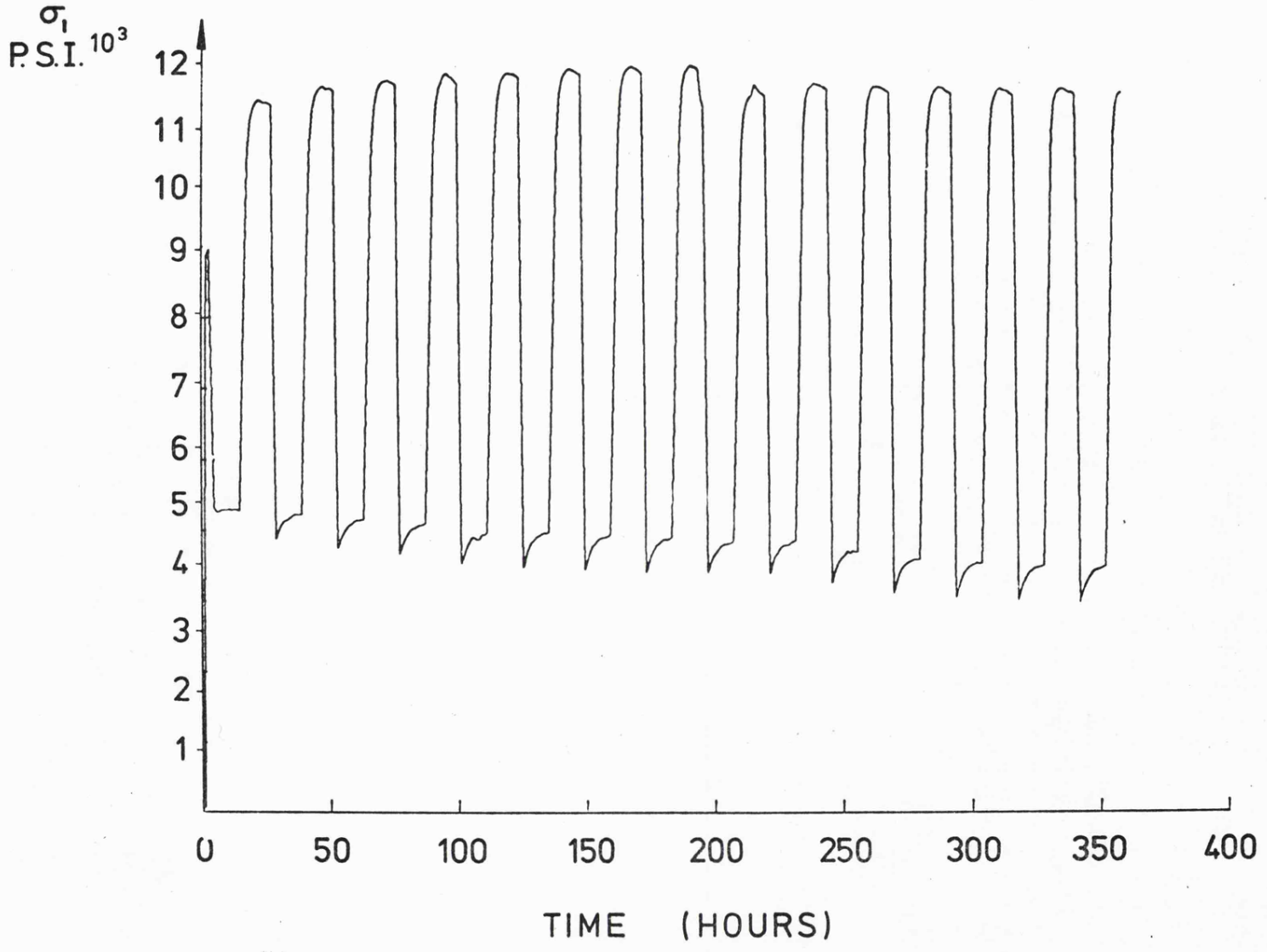

Fig 8·10 Stress history on bar 1 for test 4a

Chapter 9

Discussion and Conclusions

The calculations described provide a first step towards an understanding of the complex effects of variable temperature on creeping structures. An attempt has been made to describe the principal features of structural creep behaviour and to identify the material test parameters which are likely to be most useful in providing an estimate of creep deformation. It is found that reference stress technqiues coupled with bounding methods based on idealized material models provide a rapid means of assessing structural performance.

A technique is established for predicting stationary state deformation rates of a creeping structure, subjected to time constant temperature gradients, from a single uniaxial test conducted at a reference stress and a reference temperature. By relating the prediction of structural behaviour directly to test data the uncertainties involved in the mathematical definition of material creep behaviour are avoided. The potentially most useful application of the reference stress/reference temperature technique is for structures subjected to variable loads and variable temperatures. When cyclic histories of temperature occur the bounding solutions may be expressed in terms of a material parameter β which effectively couples structural behaviour to material behaviour. It is found that distinct regions of behaviour displaying the effects of stress redistribution processes can be described in terms of β together with the appropriate reference stress and reference temperature. Using this method the stationary state deformation rate of a structure subjected to a cyclic history of temperature can be obtained from a constant load uniaxial test conducted at the reference stress and reference temperature.

The results of the experiments conducted on aluminium beam structures subject to constant load and thermal gradient correlate with uniaxial data obtained at the reference temperature and lend support to the reference stress/reference temperature technique. Experiments on a simulated two-bar structure were designed so that an assessment of the behaviour of structures under cyclic histories of temperature could be made. Although the temperature histories differ in detail from those assumed in the theory it is clearly shown that there exists time constant residual stress fields. Furthermore the stress histories used in upper bound calculation are achieved within the first few cycles for a wide range of average strain rates. Recovery does occur but appears to be somewhat less than predicted by the Bailey-Orowan model. A useful description of the cyclic stress and strain histories can be obtained by applying constant stress creep data according to the strain-hardening model providing the value of the material constant p is known.

Chapter 10

Appendices

10.1. Two-Bar Uniaxial Tensile Testing Machine

One of the main problems in the field of engineering structures in which creep occurs is that of extending basic (constant stress) creep data to situations in which the stresses are known to vary owing to the mutual constraint (compatibility) between components or regions. The two-bar model system is probably the simplest redundant structure available and is one of the few redundant structures in which it is possible to measure experimentally, not only the deformation during creep, but also the stress sharing conditions. The two conditions to be satisfied in the experimental simulation of the two-bar system are:

(i) The total load in the 'parallel creep' system must remain constant, although the proportions borne by the two components may vary with time.

(ii) The extensions of the two components must remain equal with time.

It was clearly impracticable to set up the physical equivalent of the two-bar system and to expect to control their individual temperatures over the whole of their lengths if truly rigid end members were to be used. Nor would it be possible to measure individual stresses in such an arrangement. The solution was to build a machine on the lines suggested by Barnes et al[48] and Lomax[77]. Both workers have used coupled standard uniaxial creep testing machines to provide simulation of the two-bar system but in view of the 'inherent' difficulties usually encountered in creep testing this idea was dismissed and a multi-specimen machine designed.

Excessive variation in certain independent test parameters (e.g.

temperature) may alone be sufficient to lead to serious loss in precision and provide creep data having a large scatter band but additionally, cross interference between apparently minor variations among dependent variables (e.g. heat flow and stress distribution as functions of specimen geometry) may produce equally significant discrepancies. Penny and Leckie [78], for instance, have drawn attention to the fact that material data scatter can arise from two quite distinct sources, viz. intrinsic variations in material properties and inadequate control of test conditions. They suggest that, given the high precision control of temperature, etc. (normally better than the limits required by B.S.3500) and with careful design to reduce non-axiality of loading, the second source of scatter is virtually eliminated. An extensive investigation into the effects of bending on the tensile test has been presented recently by Schmieder[79]. This includes assessments of earlier contributions made by Jones and Brown [80], and Penny [81]. Where appropriate, the recommendations made by Schmieder are incorporated into the machine.

The general arrangement of the machine is shown in Figures 10.1 and 10.2. It comprises of a welded construction main frame, two individual load trains with specimens and extensometers, and an electronically controlled loading system with the facility for continuously varying the loads on each specimen. Two tubular electrical resistance furnaces of low thermal inertia provide heating of the specimens.

Subsequent sections describe each part of the machine in turn.

10.1.1. Main Frame and Components

The general requirements of a creep testing machine having desirable squat and massive proportions are to some extent compromised by the requirements of specimen heating, extensometry, load cell provision and accessibility. In this machine the two individual load trains are incorporated into a rigid main frame that is both compact and economical to build, but more importantly allows all location faces to be precision

machined in one operation. The machine follows conventional uniaxial machine manufacturing practice with 3in. steel tubes for the columns and lin. steel plate for the base and top and bottom location plates.

As the tests to be conducted in the machine were to include variable temperature tests, the overall lengths of the load trains are kept as short as possible in order that thermal expansion effects on lever beam rotation are small but not too short that the condition of constant load is violated.

The relationships between the basic dimensions of the loading system were determined from consideration of the simplified system shown in Figure 10.3. It can be shown by taking moments about O that the specimen load, P , and the applied load, W , are related by

$$P = \frac{Wb \cos \xi}{a \cos (\xi - \eta)}$$

If η is small relative to ξ then the lever ratio b/a is independent of the angular rotation ξ of the beam. It may also be shown that the rotation, η , of the specimen load train is given by

$$\eta = \text{Tan}^{-1} \left[\frac{(1 - \cos \xi)}{(h/a + \sin \xi)} \right].$$

Therefore, providing h/a is maintained large relative to unity and the angular rotation ξ , does not exceed about five degrees, η is maintained small relative to ξ . In addition it was desired that for a temperature change of 400°C on the load train, a lever beam rotation of the order of one degree was tolerable. The final dimensions of h = 33in. and a = 2in. adequately satisfy these requirements.

With the load trains being shorter than in conventional uniaxial machines and load levels considerably smaller than in conventional uniaxial creep tests great emphasis has been put on the elimination of non-axial strains on the specimens. Non-axiality of loading distorts the strain field and results in bending stresses being superimposed on the required mean axial stress. Under such conditions, a randomness in measured strains and rupture lives can be expected.

The lever beams are supported on pinned knife bearings bolted in the top plate. The main reactions act along the longitudinal axes of the columns and thus sensibly prevent rotation about the fixed base centre line.

The elements of the universal block system can be seen in the photograph of the assembled load train shown in Figure 10.4. All components including the external joints and pull rods are precision machined to better than $\pm$ 0.0005in.

Specimen load measurement is accomplished through measured deflection of stiff proof rings incorporated in the base of each load string. By boring pin link holes at right angles to each other, the proof rings also act as the base universal joint. These are connected by manually adjustable collars mounted on thrust bearings to the load train reaction base and thereby allow levelling of the lever beams during tests.

10.1.2. Specimens.

Standard circular section uniaxial tensile test specimens are of the type recommended by Penny et al machined to the dimensions of Figure 10.5. The protrusions machined at each end of the gauge length accurately define the gauge length and provide location for the extensometer clamps.

Repeatability of specimen manufacture is assured by closely following the metal cutting techniques detailed in section 10.2.4. on uniaxial tensile testing.

10.1.3. Extensometer.

The measurement of displacements under cyclic temperature conditions is difficult because of expansion and contraction of the extensometer system during temperature changes. The system adopted on the two-bar machine, Figure 10.4, is similar to that used for normal uniaxial tensile machines, except that the four vertical rods are machined from Invar 36 which has a coefficient of expansion of $< 10^{-6}$ / deg.C. and enables displacements of the aluminium specimens to be measured within 6 per cent of the actual

values without resorting to costly equipment.

The output from each L.V.D.T. (Linear Variable Differential Transformer) is 100 mV/thou and in order to increase the sensitivity of the system and provide a check on axiality of loading, two L.V.D.T's are incorporated in each extensometer. The combined sensitivity of the system is 5×10^{-6}in. over a linear range of 0.2in. The transducers are series coupled and the voltage output connected to the load control system. Tappings are provided to allow individual L.V.D.T. voltages to be recorded.

Micrometer heads incorporated in the extensometer base clamps allows the initial voltage output from each pair of L.V.D.T's to be equalized. This is a requirement of the control system.

10.1.4. Specimen Heating and Temperature Control.

Each specimen is heated by a tubular three-zone electrical resistance furnace of low thermal inertia which allows both rapid heat-up and cool-down. Overall temperature control is affected by means of a Eurotherm Proportional Temperature Controller firing an independent thyristor unit in the power supply to the furnace. Controlled heating rates and a certain amount of overshoot suppression are provided by derivative and integral control facilities built into the controller. The sensing device is a welded Chromel/Alumel thermo-couple strapped to the centre section of the specimen gauge length.

To eliminate any temperature gradient along the specimen, the furnace windings are connected as three distinct zones. It is possible to 'trim' the proportions of the total power to each zone by variable autotransformers, the settings being indicated on the separate controls on the side panels. Two reference thermocouples embedded in the specimen protrusions allow monitoring of the temperature gradient.

A fan bolted to a central port hole in the furnace side forces air at ambient temperature over the furnace windings and test specimen to give rapid reductions in temperature. The duration of fan operation is adjustable

and controlled by an electronic timer.

Thermal cycling with period of four to fifty hours is achieved by a programmable master timer system operating a set of relays to which are connected the temperature control unit, the fan-timer system, the control thermocouple and an adjustable constant voltage source. At all times the temperature control unit is set to the maximum desired temperature. During the hotter part of the thermal cycle, the control thermocouple is directly linked, via a relay, to the temperature control unit and the set temperature is held. During the change from the hotter to the cooler part of the cycle, the timer system switches the constant voltage source in series with the control thermocouple and provides power to the fan which rapidly reduces the temperature. The constant voltage is equivalent to the difference in thermocouple output at the desired higher and lower temperatures of the cycle and therefore increases the control voltage to the temperature controller. The controller then switches off the supply to the furnace and as the specimen cools the control signal decreases until the combined signal equals the original control signal. At this point the fan is switched off and the temperature is controlled at this lower value. During heat-up the constant voltage source is taken out of circuit and the control thermocouple is again directly linked to the temperature controller, which then switches full power to the furnace until the control thermocouple output equals the set value. In this manner controlled thermal cycling is achieved.

At all temperatures up to a maximum of 400°C the temperature gradient along the specimen is less than $\frac{1}{2}$°C, the maximum overshoot is approximately 5°C , and undershoot is negligible. It would be possible to remove the temperature overshoot by lowering the thermal inertia of the system, but doing so would produce long term temperature instability.

10.1.5. Loading System

The load acting on each creep test specimen is provided by a drum capable of holding up to 10 gal. of liquid. The actual weight of the drum is counter-balanced, so that with a lever ratio of 10:1 , a full drum exerts a pull on the specimen of approximately 1000 lb. Provision is made for adding additional tare weights if needed. Flexible pipes connected via a reversible peristaltic pump allows liquid to be transferred from one drum to the other. The direction and rate of flow of liquid is controlled by the control system and is a function of the L.V.T.D's output.

Measurement of the loads acting at any instant of time is achieved by calibrated load cells in the load train base and additionally by sensitive load cells connected between the lever arms and drums. These high resolution load cells have a linear response over the range 0-200 lb. with a change of 0.01 lb. being detected.

The liquid is an undiluted anti-freeze solution (glycol) chosen because it is readily available and to counteract any possibility of corrosion in the system. As the machine is in a laboratory environment where large changes in humidity cannot be catered for, glycol offers a cheap alternative to water.

Cyclic loading is achieved by attaching dead weights and load hangers to the base of the drum and bolting motorized jacks, controlled from the programmable timer, to the loading platform.

10.1.6. The Control System.

The primary function of the control system is to compare the voltage outputs from the two L.V.D.T. extensometer systems and to arrange for the pump to provide flow of liquid in the desired direction so that compatibility conditions remain satisfied.

A block wiring diagram of the control system is shown in Figure 10.6.

Since the voltage output from each extensometer system varies from

-10V to +10V d.c. and in order to avoid control instability about the null point, the control system provides a 10V d.c. offset effectively transferring the linear range to 0-20V d.c. To provide impedance matching each output is connected in series with a matching amplifier (IC1 and IC2).

The compatibility condition is satisfied by reversing the sign of one pair of L.V.D.T's output and then feeding the two signals (one positive, one negative) into a differential amplifier (IC3). The output of IC3 drives two comparators (IC4 and IC5) which are triggered by positive or negative demand. If the magnitudes of each extensometer system signals are equal, there is no demand. The comparators drive reed relays which in turn drive heavier relays which energise the pump motor to provide flow of liquid in the appropriate direction.

The band level at which the reed relays are triggered is adjusted to a differential of $\pm$ 1mV which corresponds to a specimen displacement of $\pm$ 5 x 10^{-6} in. At such small voltage levels, large random voltage spikes can be detected and in order to prevent simultaneous energization of the two heavy output relays an interlock device is fitted.

As a result of experience during the first few tests it was found that as the apparatus was so sensitive to very small changes in displacement, pump 'hunting' occurred. This is overcome by incorporating small electronic timers with a time delay of two seconds into the system. Thus the system only operates if the demand signal occurs for longer than two seconds. This produces a highly sensitive stable system that operates the pump continuously when either total load or temperatures are changing and intermittently at other times.

Additional provision is made in the control system to simulate thermal expansions electronically by switching in the appropriate voltage steps in series with the L.V.D.T. outputs.

10.1.7. Recording Equipment.

Chart recorders provide a visual display of voltages corresponding to extensometer displacements, specimen loads and temperatures. In addition, this information is also recorded, at hourly intervals, by a Solartron D.T.U. Data Logger system on punched paper tape. The information from these tapes is processed by I.B.M. computer with graph plotting facilities. Appropriate voltage-time graphs can then be obtained as desired.

10.1.8. Bending Tests.

A proving set of time-independent bending tests were conducted in the machine using standard mild steel uniaxial specimens and dead weight loads. Bending is defined as the difference of two diametrically opposite surface strains divided by their sum and was measured at a sequence of temperatures up to 250°C by electrical resistance strain gauges bonded to the specimen sides at the centre of the gauge length.

The bend test results obtained at room temperature, shown in Figure 10.7, are significantly better, especially at low load levels, than those reported by Penny and Leckie[78]. Similar results were obtained at the higher temperatures and are due primarily to the accurately machined and assembled load train components and also great care in the setting-up procedure.

10.2. Uniaxial Tensile Tests.

The collection of fundamental creep data for a single engineering material is a time consuming and expensive operation. Exploration of creep behaviour at successive temperature levels requires evaluation of both thermal and stress fields within the specimen geometry, selection of appropriate heating methods and assessment of precision of measurement under thermal and mechanical transients.

In the following sections the experimental testing techniques used in the evaluation of the uniaxial creep behaviour of commercially pure aluminium will be described.

10.2.1. Uniaxial Testing Machine.

The creep tests were conducted in standard uniaxial creep testing machines similar to that shown in Figure 10.8 incorporating knife edge pivots and a lever system with a 10:1 ratio. The machines were mounted on anti-vibration pads to minimise vibration effects and the use of accurately machined universal joints in the loading train ensured axiality of loading. Great care in centering the specimens to within 0.0005 ins. in the universal blocks minimised any bending effects.

Specimen load was measured using a strain gauged load cell connected in series with the loading train. The loads provided by tare weights, were applied at a constant rate by a screw jack system driven by an electric motor through a reduction gearbox.

For tests carried out at temperature the specimen and loading train was surrounded by a three zone electrical resistance tubular furnace. Individual control of the power input to the three zones allowed temperature gradients of less than $\frac{1^\circ}{2}$C over the entire specimen gauge length to be obtained. The overall temperature, controlled by a C.N.S. proportional controller, using, as a sensor, a platinum resistance thermometer embedded in the furnace windings, was maintained to within $\pm \frac{1^\circ}{2}$C of the desired

value. Chromel/Alumel thermocouples embedded in the specimens allowed monitoring of specimen temperature.

Wherever possible experimental measurements were represented by electrical signals. These included outputs from displacement transducers, load cells, and strain gauges. In all cases, d.c. systems were used because of their convenience.

The main recording system was a Solatron Digital Logging system capable of recording changes of 1×10^{-5} volts. In addition to this system several chart recorders were also used.

10.2.2. Material.

The material selected for testing was a half-hard commercially pure aluminium in sheet form 0.25ins. thick. All the specimens were obtained from one sheet thereby providing material repeatability that is otherwise difficult to obtain with a commercial purity material.

The degree of anisotropy exhibited by the material in the longitudinal (rolling) and transverse (non-rolling) direction has been shown[43] to be approximately five per cent on steady state creep strain rates. This has been supported by a limited number of creep tests performed at room temperature by the author.

10.2.3. Specimens.

Two types of specimens were used to investigate the uniaxial creep behaviour of the material. As the material was only available in sheet form, both types of specimen were machined with their longitudinal axes parallel to the rolling direction in order to reduce the effects of anistropy.

The first type was a rectangular section sheet specimen. This standard specimen, shown in Figure 10.9 has a two inch gauge length, 0.25ins. x 0.375 ins. in section. Strains were measured with either electrical resistance strain gauges bonded to the centre of the gauge length sides or alternatively by an extensometer system. Basically the extensometer consists

of four relatively rigid rods clamped to the specimen by machined heads and attached to a sensing linear variable differential transformer, (L.V.D.T.), Figure 10.11. Each head, cruciform in plan view, is in two parts and is clamped to the specimen by tightening connecting bolts, contact with the specimen being made by hardened points. Relative movement of the heads transfers a relative displacement to the L.V.D.T.. With a gauge length of 1.50ins., 6×10^{-6} per cent strain could be detected. This system was employed for tests conducted at temperatures where the reliability of available strain gauges was in doubt and also for room temperature tests whilst the second type of specimen was being developed. Additionally, this system has the advantage that measurements can be made by the L.V.D.T. at a position suitably removed from the furnace.

The second type of specimen was designed to make the task of creep data collection less time consuming. Much energy was devoted to the design and development of a specimen capable of yielding in one creep test the equivalent information gained from three tests conducted at different stress levels. This idea was feasible since only steady state creep rates were of interest. The triple-section specimen shown in Figure 10.10 is the result of an exhaustive program of photoelastic analyses. The original design criteria were that in order to ease the process of manufacture, overall dimensions and locating holes should be the same as in the standard sheet specimen; stress concentration arising from the transition between gauge lengths should not cause premature failure, and finally a region of pure tension extending to 0.2ins. either side of the centre of the gauge length to accommodate 0.25ins. electrical resistance strain gauges was required. The triple section sheet specimen which satisfies these criteria has three 0.75ins. parallel sided gauge lengths of widths 0.375, 0.300 and 0.250 inches giving stress levels in the ratio 1:1.25 : 1.5 respectively.

10.2.4. Specimen Manufacture

In order to reduce the amount of scatter in results obtained from creep tests, the repeatibility of specimen machining is important. In all of the specimens machined, metal cutting techniques which take small rapid cuts were employed. By using these techniques the regions of material adjacent to the machining cuts which were influenced by plastic straining were contained within a localised region. The specimens were first marked out and then cut 0.1 in. oversize. The circular gripping holes were then accurately drilled and bored to size on a jig boring machine. These holes also provided the specimen location on a purpose built machining jig. The overall length and width of the specimen was then machined to size. Finally the gauge lengths were accurately milled using a side cutter either side of the centre line to final size.

10.2.5. Isothermal Uniaxial Tests and Results.

In all the tests performed the specimens received a twenty-four hour temperature 'soak' before commencement of the test.

Short Term Tests.

A series of uniaxial limit load tests were performed to evaluate the variation of the time-independent material properties with temperature. The tests were carried out on the standard single gauge length specimens at a sequence of temperatures between room temperature and 250°C . As the strains to be measured were outside the range applicable to the available strain gauges the L.V.D.T. extensometer system was used. During the eighteen limit load tests performed this system has proved utterly reliable. Each test was completed within a few minutes thereby ensuring that the material behaviour was sensibly time-independent.

Typical examples of the stress strain plots obtained are presented in Figure 10.12. Three tests were conducted at each temperature level and variation of less than 0.5 per cent on 0.2 per cent proof stress was

observed. Over the temperature range at which the tests were conducted the variation of 0.2 per cent proof stress with temperature appears approximately linear, Figure 10.13 . The elastic moduli on the other hand remained approximately constant at 9×10^6 lb/in^2 within the temperature range RT-150 °C . Above 150°C the value decreased rapidly being 6×10^6 lb/in^2 at 250°C .

Creep Tests.

A series of creep tests at constant load were performed for various values of the applied loads at a sequence of temperature levels (20,100,125, 150 and 200°C). The normal test duration was 600 hours.

With regard to the experimental technique it is worth recording that approximately 95 per cent of the tests performed using both types of specimen provided useful results. This was due primarily to a rigid setting up procedure being adhered to during the testing program. Most failures were attributable to malfunctions of strain gauges and recording equipment. Some problems with temperature control were also experienced.

At temperatures above 150°C and for the stress levels (> 4000 lb/in^2) of interest when this testing program was carried out no clearly defined steady-state behaviour was observed, the material exhibiting only regions of primary and tertiary creep. This behaviour is outside the context of this thesis and was not considered further.

The results of the tests conducted at room temperature (20°C) showed that the material exhibits logarithmic creep. As there was no steady-state region average creep strain rates were taken over the time period 300 - 550 hours and the plot of log °/₀ strain rate against log stress obtained is shown in Figure 10.14.

As a check on the strain measurement devices three tests were conducted using the standard sheet specimens to which both the L.V.D.T. extensometry and strain gauges were attached. No marked difference between the resulting average creep strain - time curves was detected. In addition the results

obtained using the triple section specimens were repeatable and well within the scatter band usually associated with creep testing. The plots of log °/₀ strain rate against log stress obtained from the tests conducted at 100, 125, and 150°C are shown in Figures 10.15, 10.16 and 10.17. It was found that at these temperatures the material attained steady-state creep rates approximately 200 hours after the application of load.

10.2.6. Discussion of Results.

The room temperature results, Figure 10.14, show that the value of the stress index n remains constant at 3.9 up to a stress of 12,800 lb/in^2 and thereafter increases rapidly becoming infinitely large at the yield stress (16,000 lb/in^2). This is in accordance with the results of Leckie et al [24] who applied the structural theorem of Ponter[37] to a polycrystalline aggregate considered as a multi-component structure. They concluded that the plastic contribution to the total deformation is unlikely to be significant until the applied stress is n/(n + 1) of the yield stress. Therefore the strain rate should not increase significantly until the stress $n/(n+1)\bar{\sigma}y \simeq 12{,}800$ lb/in^2 is reached. This stress level is in agreement with the experimental results. The steeply rising portion of the curve between 12 - 14,000 lb/in^2 may be approximated by a straight line corresponding to a stress index equal to 18 . Thus it is seen that at room temperature the material behaviour is sensitive to the value of the applied stress and the benefits of a reference stress approach to structural deformation can be appreciated.

It was found that in the creep tests performed above approximately 13,500 lb/in^2 quite large instantaneous plastic strains relative to the creep strains occurred. Below 7000 lb/in^2 the creep strains were of the order 0·02°/₀ for 200 hours testing and it was difficult to maintain standards of accuracy when dealing with such small strains.

The results of the tests conducted at temperature show that as the temperature increases the transition between the two previous approximately

linear regions becomes less easily defined, and the creep rates at any given stress are correspondingly higher. Between 5000 and 10,000 lb/in^2 the steeply rising portion of the curves become approximately linear with a stress index that increases appropriately. It was found that above approximately $0.8\bar{\sigma}y$ creep rupture occurred within the first 100 hours and no discernable steady-state behaviour was observed. Even at these relatively high stresses it was found that the instantaneous plastic strains were small in comparison with the elastic strains.

At low values of the applied stress the gradient of the curves show a rapid change and tend towards unity when linear viscous creep becomes operative. Some support of this is provided by the deformation-mechanism maps of Ashby[82]. He presents a map for pure aluminium from which it is evident that for temperatures above 60°C and stress levels below approximately 4000 lb/in^2 , $n \to 1$.

It is seen from the results that the material behaviour is highly dependent upon both stress and temperature and that the simple constitutive relationship given by a Norton-type law is clearly deficient. However for these reasons it provides an extreme test for the reference stress, reference temperature approach to the creep deformation of structures.

10.3. Derivation of Stationary State Deformation Rates.

10.3.1. Beam under Flexure.

Beam of rectangular section, width b and depth d, subjected to end moments M and a temperature gradient $\theta(y)$, through the thickness.

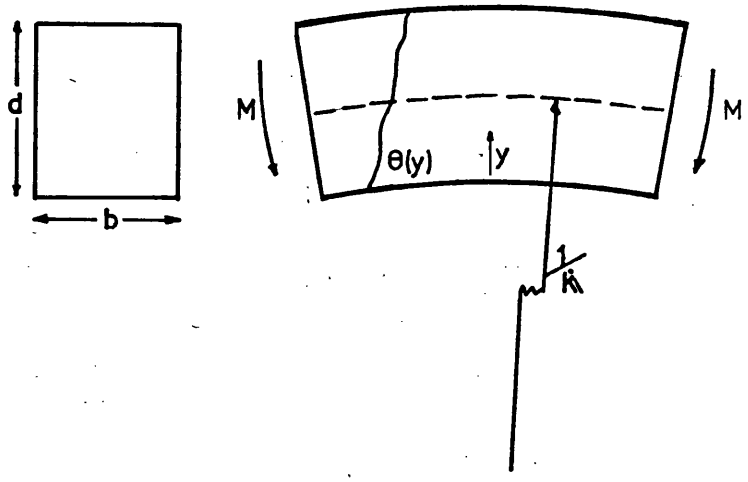

Exact Solution.

The creep strain rate at distance y from the lower edge is given by

$$\dot{\varepsilon}(y) = \dot{\kappa}(y + \phi d) \qquad 10.3.1.$$

where $|\phi d|$ denotes the position of the neutral axis from the lower edge, $\dot{\kappa}$ the curvature rate and

$$\dot{\varepsilon} = k\sigma^n \exp(-\Delta H/R\theta).$$

From equilibrium conditions with zero axial loads

$$\int_0^1 (\phi + x)^{1/n} \exp(\Delta H/nR\theta(x))dx = 0 , \qquad 10.3.2.$$

and the moment of the stresses must equal the applied moment

$$M = \int_0^1 \sigma.x \, dx , \qquad 10.3.3.$$

where $x = y/d$.

Equality 10.3.2. yields the value of ϕ and equation 10.3.1. substituted into equation 10.3.3. gives

$$\dot{\kappa} = \frac{k}{d}\left[\frac{2M}{bd^2}\right]^n I_B \qquad 10.3.4.$$

where

$$I_B = \left[2 \int_o^1 (\phi + x)^{1/n} \, x \exp \Delta H/nR\theta(x) dx \right]^{-n} . \qquad 10.3.5.$$

A value of I_B was obtained by solving equation 10.3.2. for ϕ using a Newton-Raphson method and thence by evaluating equation 10.3.5.

For isothermal conditions $\phi = -5$ and I_B reduces to

$$I_B = 2 \left\{ \frac{2n+1}{n} \right\} / \exp(\Delta H/R\theta_i).$$

The stress field is given by

$$\sigma(x) = [(\phi+x) I_B \exp(\Delta H/R\theta(x))]^{1/n} \left(\frac{2M}{bd^2} \right) . \qquad 10.3.6.$$

Approximate Solution

Assume a stress function of the form

$$\sigma(x) = \sigma_o \exp \{\Delta H/nR\theta(x)\}.$$

From equilibrium conditions with zero axial loads gives

$$\int_o^{\phi} \exp[\Delta H/nR\theta(x)]dx - \int_{\phi}^1 \exp[\Delta H/nR\theta(x)]dx = 0 \qquad 10.3.7$$

and

$$\frac{M}{bd^2\sigma_o} = \int_{\phi}^1 x \exp[\Delta H/nR\theta(x)]dx - \int_o^{\phi} x \exp[\Delta H/nR\theta(x)]dx \qquad 10.3.8.$$

The bound on curvature rate is given by

$$\dot{\kappa} \leq \frac{k}{d} \left[\frac{2M}{bd^2} \right]^n I_B^u ,$$

where

$$I_B^u = \frac{\int_o^1 \exp[\Delta H/nR\theta(x)]dx}{\left[\int_{\phi}^1 x \exp[\Delta H/nR\theta(x)dx - \int_o^{\phi} x \exp[\Delta H/nR\theta(x)dx \right]^{n+1}} \qquad 10.3.9.$$

10.3.2. Tube under Flexure

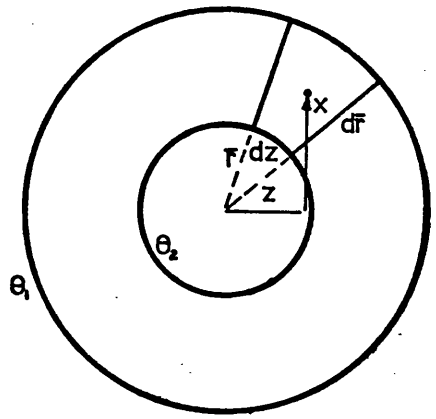

For a tube of circular section internal and external radii, r_i and r_o respectively, the temperature at any point in the section is given by

$$\theta(\bar{r}) = \theta_2 + \frac{\log(\bar{r}\, r_o/r_i)}{\log(r_o/r_i)} \quad (\theta_1 - \theta_2)$$

where θ_2 and θ_1 are the internal and external temperatures.

Area of element $dA = \bar{r}d\bar{r}dz$ and distance of centroid of element from the neutral axis $x = \bar{r}\sin z$.

Creep strain rate $\dot{\varepsilon} = k\sigma^n/\exp[\Delta H/nR\theta]$ and since $\dot{\varepsilon}(x) = \dot{\kappa}x$

$$\sigma(x) = \frac{\dot{\kappa}}{k}\, x^{1/n} \exp\, \Delta H/nR\theta(x) \qquad 10.3.10$$

Then equating internal and external moments

$$M = \int^{A} x\sigma dA = 4\, r_o^{\frac{3n+1}{n}} \left(\frac{\dot{\kappa}}{k}\right)^{1/n} \int^{A} \bar{r}^{\frac{2n+1}{n}} (\sin z)^{\frac{n+1}{n}} \exp[\Delta H/nR\theta(\bar{r})]d\bar{r}dz \qquad 10.3.11$$

$$M = 4\, r_o^{\frac{3n+1}{n}} \left(\frac{\dot{\kappa}}{k}\right)^{1/n} \int_{z=o}^{z=\pi/2} \int_{r_1/r_o}^{1} \bar{r}^{\frac{2n+1}{n}} (\sin z)^{\frac{n+1}{n}} \exp[\Delta H/nR\theta(\bar{r})]d\bar{r}dz \qquad 10.3.12$$

Therefore $$\dot{\kappa} = \frac{k}{r_o} \left[\frac{M}{4r_o^3}\right]^n \cdot I_T \cdot$$

where $$I_T = \left[\int_{z=o}^{z=\pi/2} \int_{r_i/r_o}^{1} \bar{r}^{\frac{2n+1}{n}} (\sin z)^{\frac{n+1}{n}} \exp[\Delta H/nR\theta(\bar{r})]drdz\right]^{-n} \qquad 10.3.13.$$

10.3.3. Two-bar Structure

From conditions of equilibrium and compatibility of displacements the stress in each bar is given by

$$\sigma_1 = \left[\frac{P}{A}\right] I_{TB}^{1/n} / \exp(\Delta H/nR\theta_1)$$

and

$$\sigma_2 = \left[\frac{P}{A}\right] \left[\frac{I_{TB}}{4}\right]^{1/n} \exp(\Delta H/nR\theta_2)$$

for the shorter and longer bar respectively.

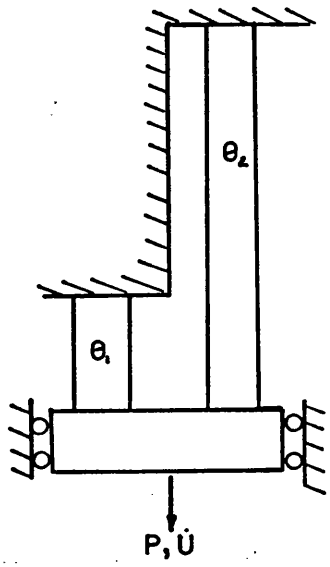

The quantity I_{TB} is given by

$$I_{TB} = \frac{4/\exp(\Delta H/R\theta_2)}{\left[1 + 4^{1/n} \exp \frac{\Delta H}{nR}\left[\frac{1}{\theta_1} - \frac{1}{\theta_2}\right]\right]^n} \qquad 10.3.14$$

The displacement rate $\dot{U} = k\ell \left[\frac{P}{A}\right]^n I_{TB}$. 10.3.15

10.3.4. Propped Cantilever Beam.

A uniform rectangular beam of length ℓ is simply supported at one end and encastre at the other. (Figure 3.3). A point load acts laterally at the centre of span and a temperature field $\theta(x)$ occurs along the beam's length. It is assumed that the temperature through any section remains constant.

Exact Solution

The example involves a single redundancy and has a moment distribution of the form,

$$M = Pm_1 + Fm_2$$

where m_1 denotes a moment distribution due to a unit load acting at the centre of a simply supported beam and m_2 a reactive moment distribution due to a unit load acting at the tip of a cantilever of length ℓ .

From consideration of the creep energy dissipation rate expression

$$\dot{D}_c = \int_{\ell} M\dot{\kappa}\,dx \ , \qquad 10.3.16$$

a moment curvature rate relationship of the form

$$\dot{\kappa} = kM^n/\exp(\Delta H/R\theta) \ , \qquad 10.3.17$$

and assuming a dummy load acting at $\bar{x} = \frac{x}{\ell} = 1$, the reactive component F can be evaluated from

$$\int_0^{\frac{1}{2}} (1-\bar{x}) \left[\frac{\bar{x}}{2} + \frac{F}{P}\ (1-\bar{x})\right]^n / \exp(\Delta H/R\theta(\bar{x}))d\bar{x}$$

$$+ \int_{\frac{1}{2}}^{1} (1-\bar{x})^{n+1} \left(\frac{1}{2} + \frac{F}{P}\right)^n / \exp(\Delta H/R\theta(\bar{x}))d\bar{x} = 0 \ . \qquad 10.3.18$$

The moment distribution is then fully described and the displacement rate at $x = \ell/2$ evaluated using equation 10.3.16 in the form

$$P\dot{U} = k \int_0^2 M^{n+1}/\exp[\Delta H/R\theta(x)]dx \qquad 10.3.19$$

Approximate Solution.

Assume a temperature dependent plastic bending moment is given by

$$|M| = M_o \exp\left[\frac{\Delta H}{nR}\left(\frac{1}{\theta} - \frac{1}{\theta_o}\right)\right] \qquad 10.3.20$$

The plastic limit state solution for this yield condition involves the values of the bending moment, M , at $x = 0$ and $x = \ell/2$ where plastic hinges

occur. By assuming such a hinge mechanism and equating internal and external work rates the plastic collapse load is given by

$$P_L = \frac{2}{\ell}\left\{M_{x=o} + 2M_{x=\ell/2}\right\} \qquad 10.3.21$$

where

$$M_{x=o} = M_o \exp\left[\frac{\Delta H}{nR}\left\{\frac{1}{\theta_{x=o}} - \frac{1}{\theta_o}\right\}\right]$$

and

$$M_{x=\ell/2} = M_o \exp\left[\frac{\Delta H}{nR}\left\{\frac{1}{\theta_{x=\ell/2}} - \frac{1}{\theta_o}\right\}\right]$$

Taking moments about $x = 0$ yields a value of the reaction F as

$$F_L = \frac{M_{x=\ell/2}\, P_L}{M_{x=o} + M_{x=\ell/2}} = \frac{P_L}{2 + \exp\left[\frac{\Delta H}{nR}\left\{\frac{1}{\theta_{x=o}} - \frac{1}{\theta_{x=\ell/2}}\right\}\right]} \qquad 10.3.22$$

Hence the limit state solution is given in terms of the temperatures at $x = 0$ and $x = \ell/2$ and is independent of the temperature elsewhere in the beam. The bound however depends upon the temperature distribution and achieves the form

$$\dot{P}\dot{U} \leq \int_o^{\ell} k\, M^*(x)^{n+1}/\exp[\Delta H/R\theta(x)]dx \qquad 10.3.23$$

where $k = \kappa_o/M_o^n \exp(-\Delta H/R\theta_o)$ and $\dot{U}$ is the displacement at $x = \ell/2$. The moment distribution $M^*(x)$ is formed by the super-position of the moment distribution due to P and F assuming no support at $x = \ell$ where these quantities are given by dropping the suffix L in equations 10.3.21 and 10.3.22.

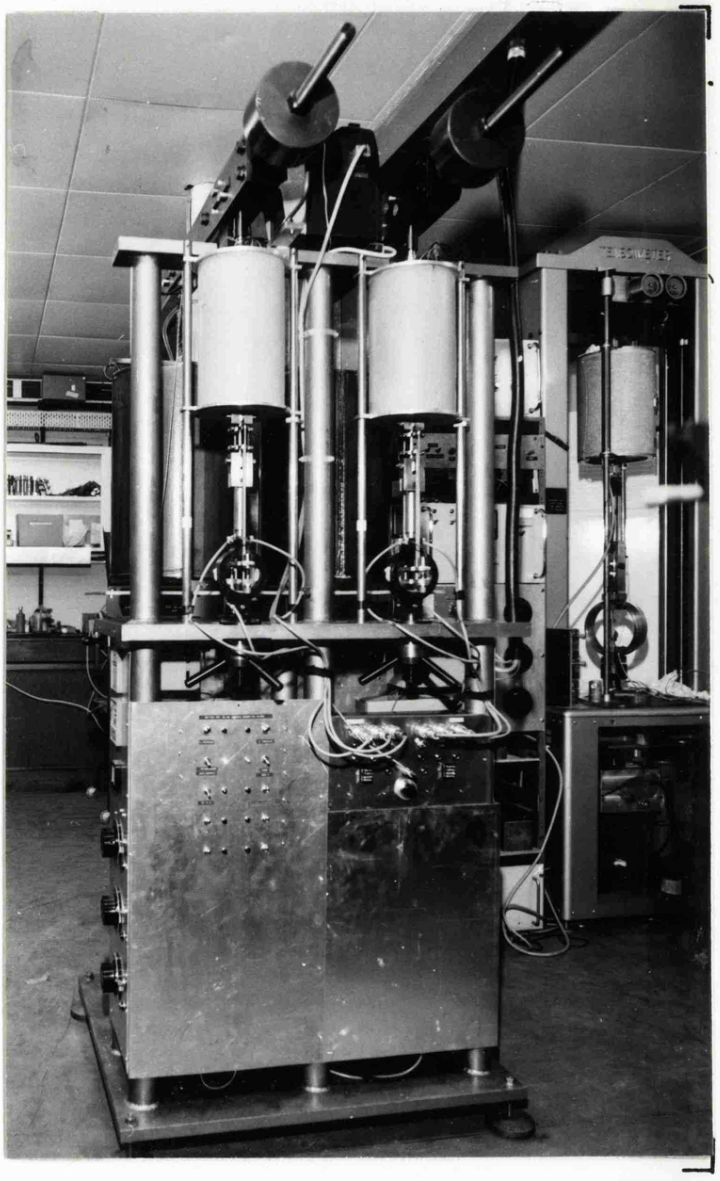

Fig 10.1 Front view of two-bar machine

Fig 10.2 Side view of two-bar machine

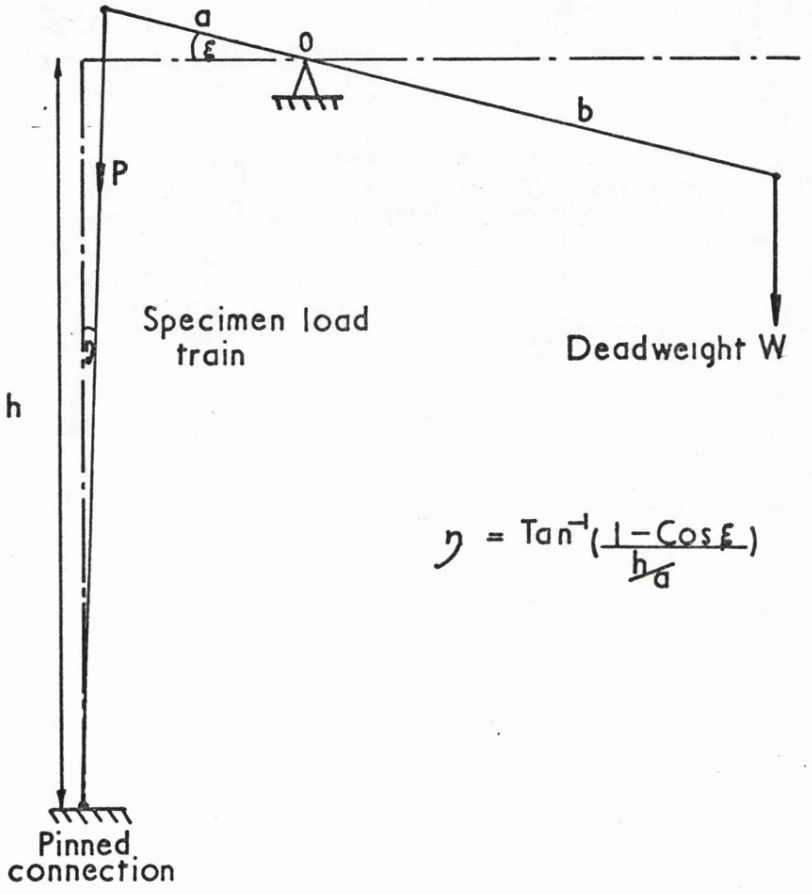

Fig 10.3 Simplified loading system

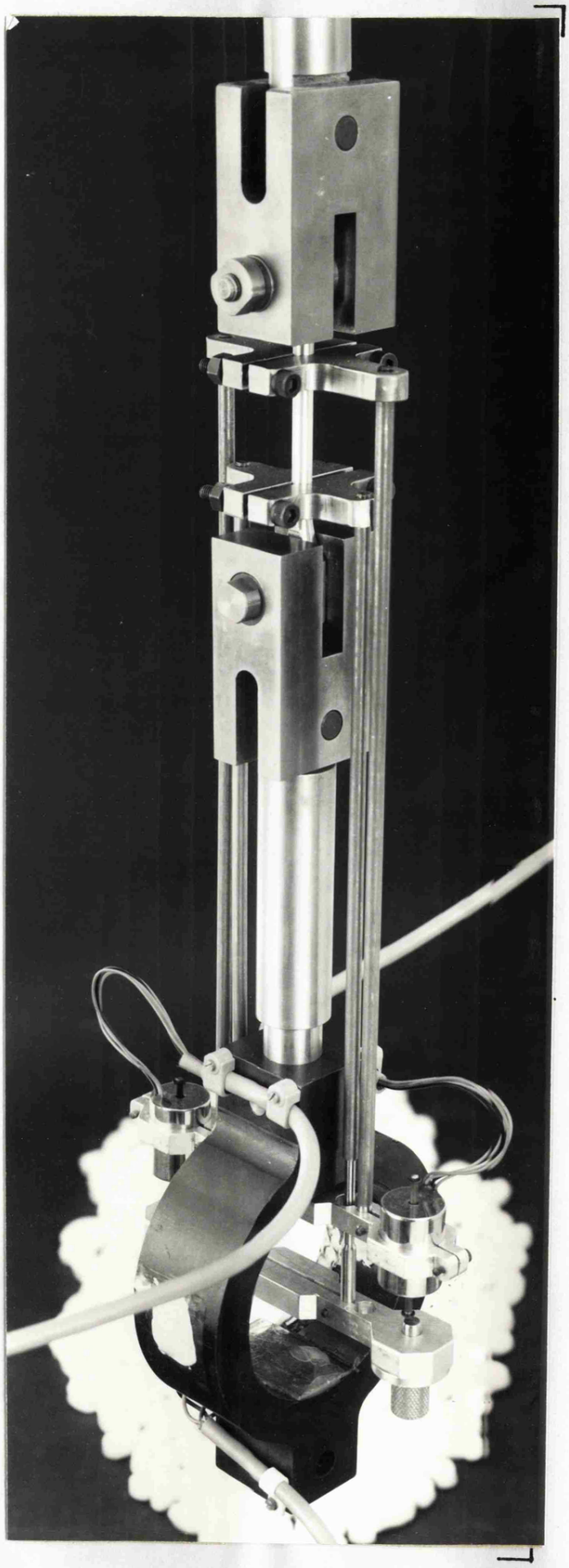

Fig 10·4 Assembled load train showing major components

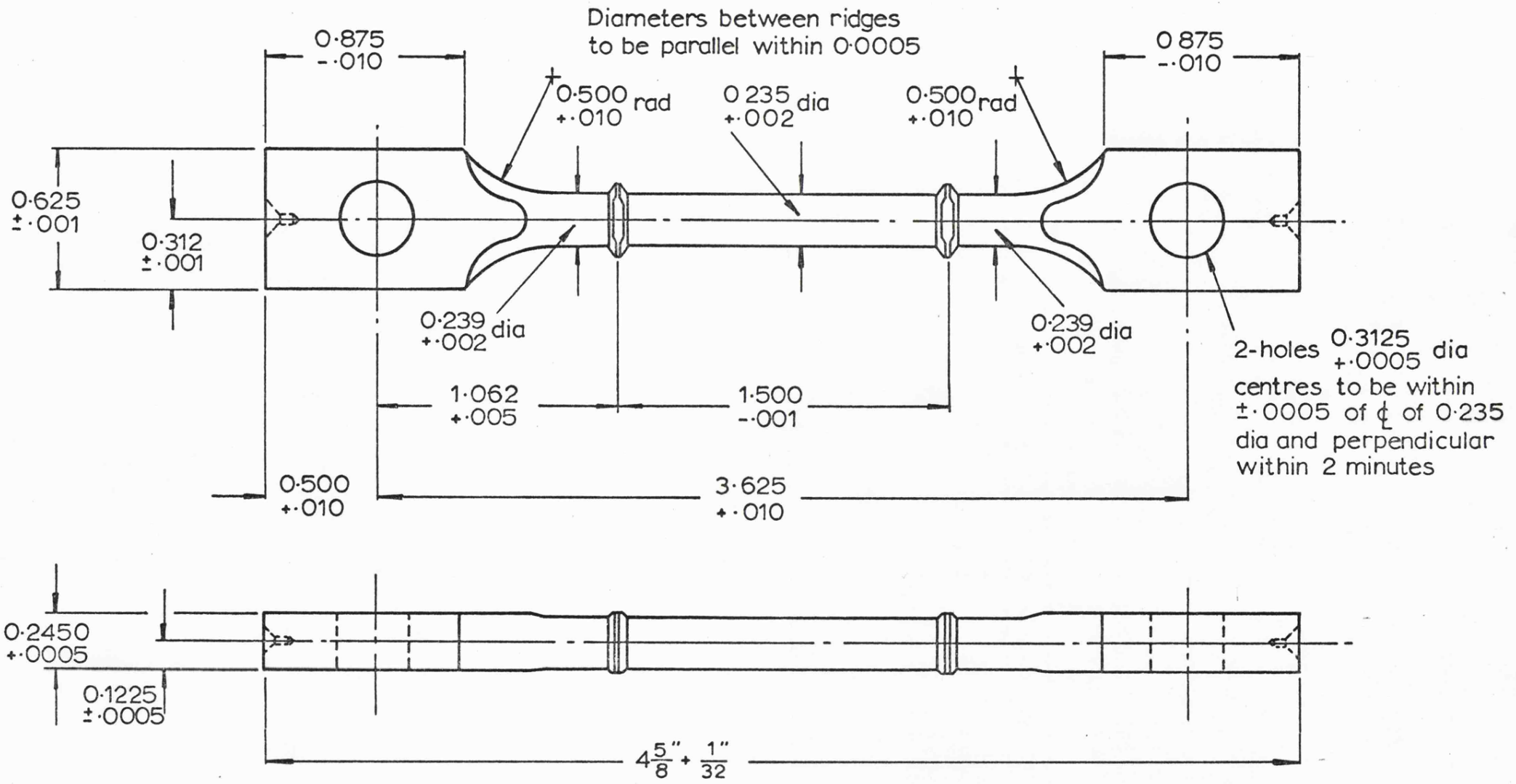

Fig 10·5 Dimensions of test specimens

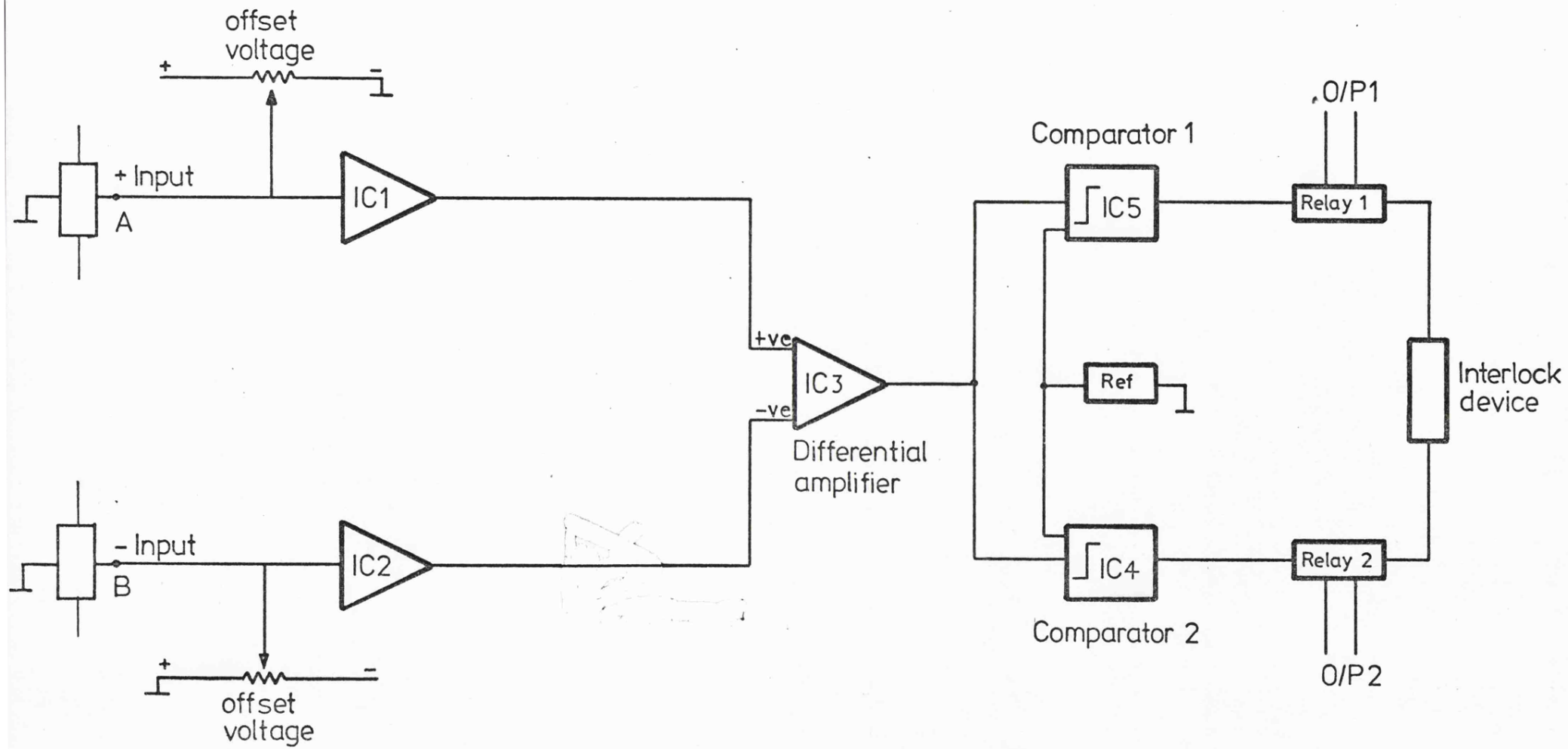

Fig 10.6 Block diagram of load control system

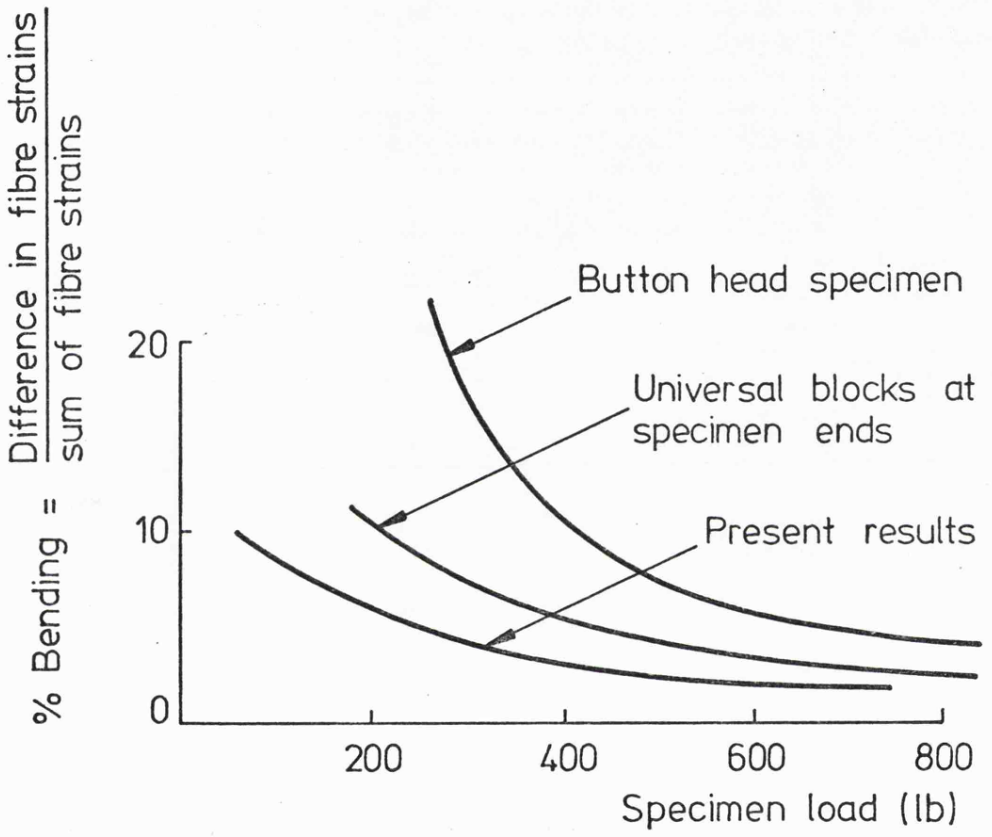

Fig 10.7 Results of bending tests

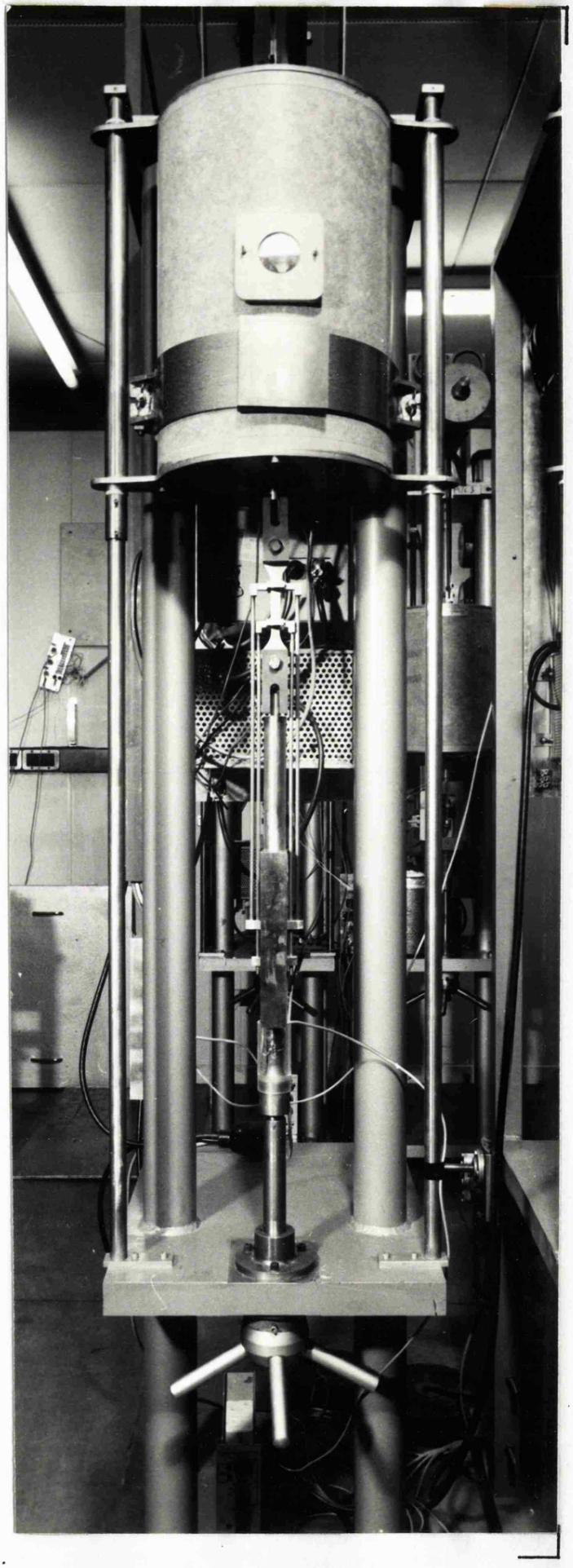

Fig 10·8 Uniaxial creep machine

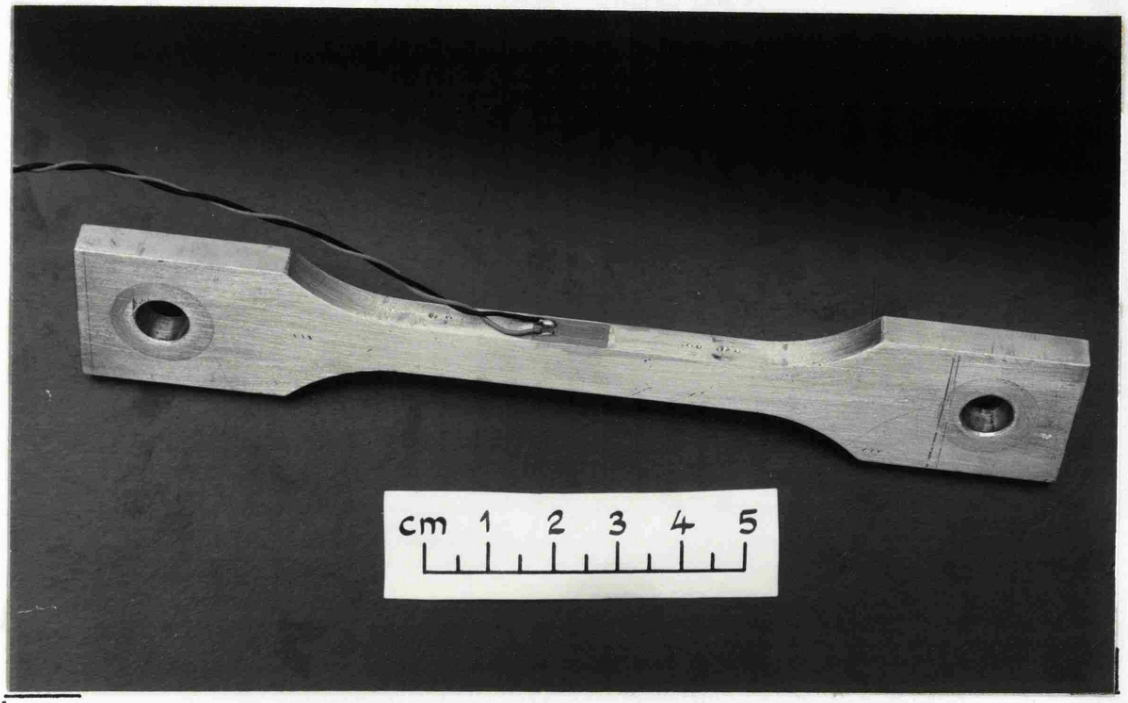

Fig 10.9 Standard rectangular uniaxial tensile specimen

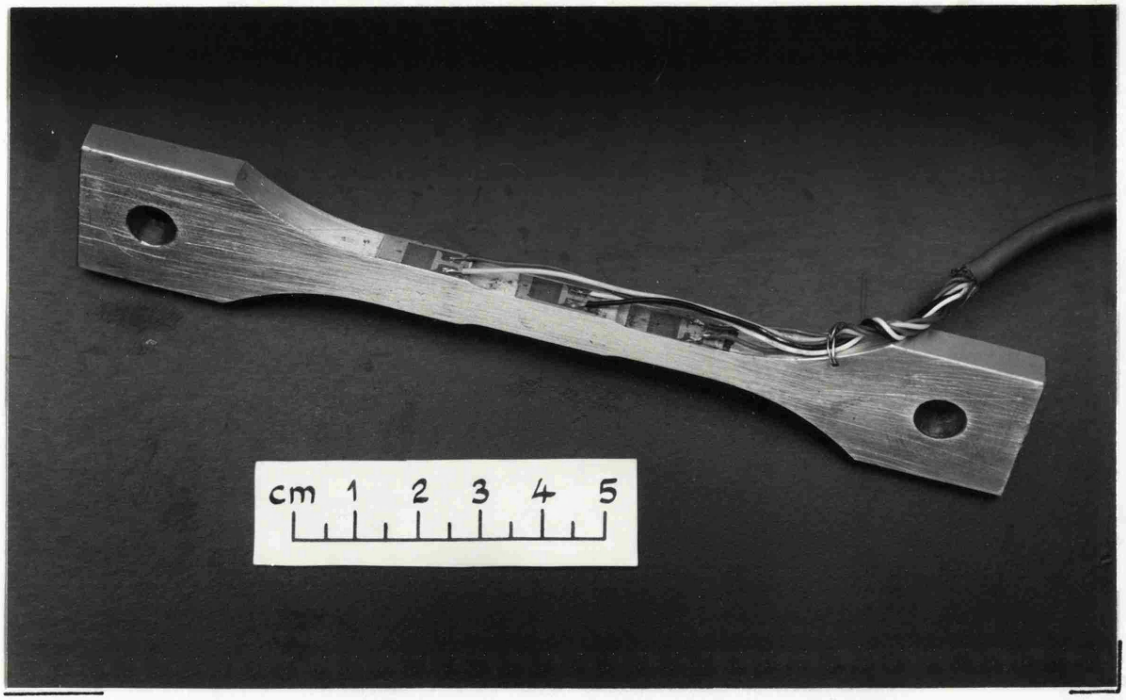

Fig 10.10 Triple-section uniaxial tensile specimen

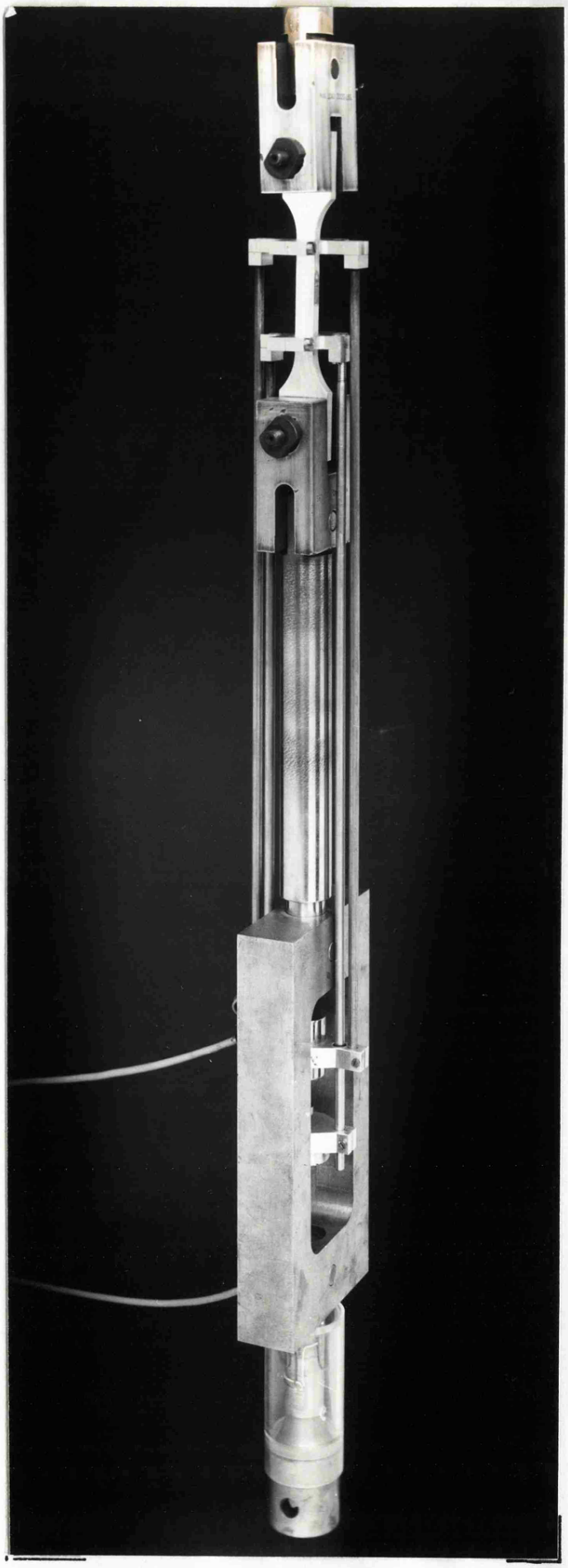

Fig 10·11 Uniaxial load train

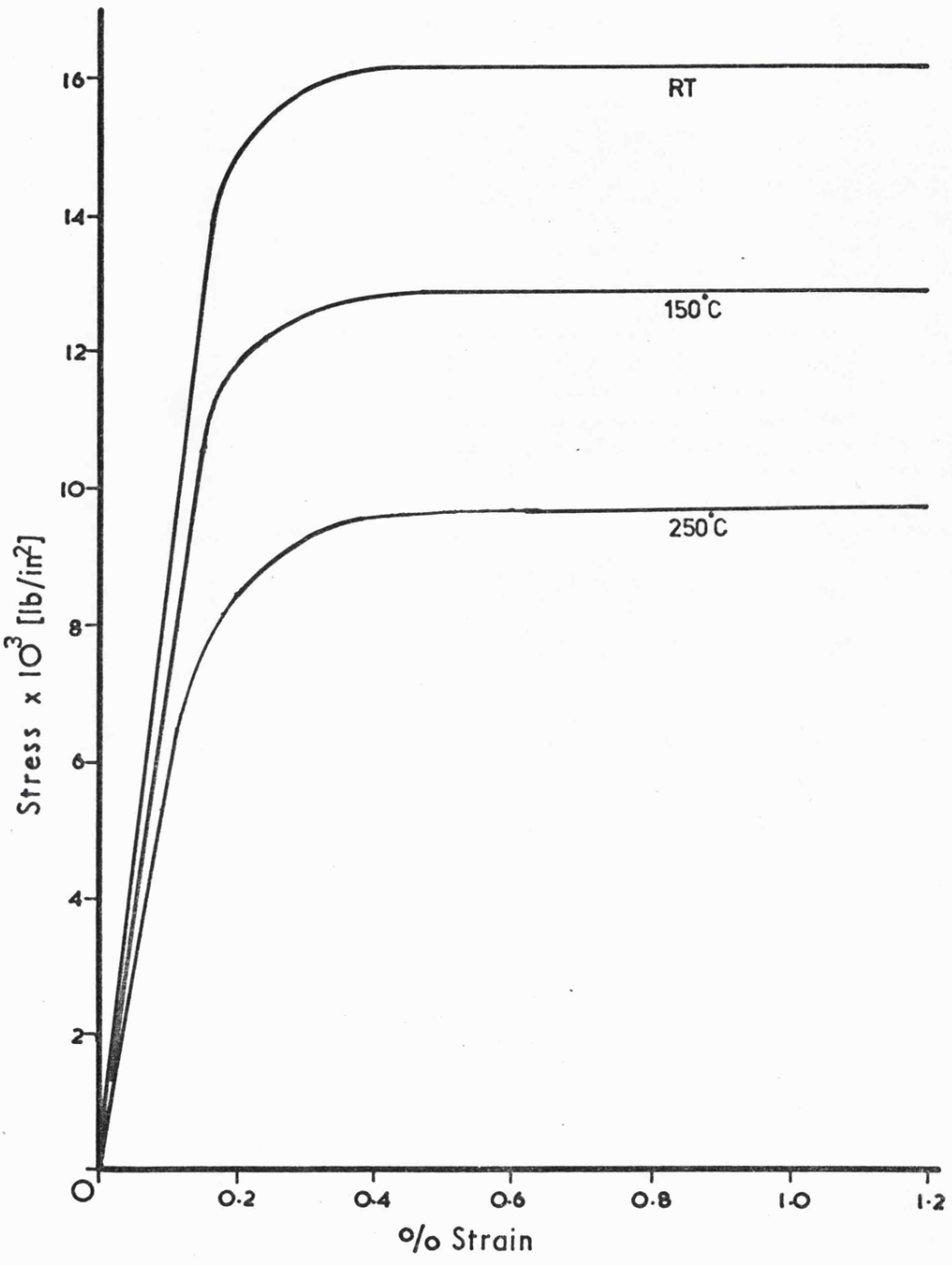

Fig 10·12 Stress-strain curves for ½ hard commercially pure aluminium

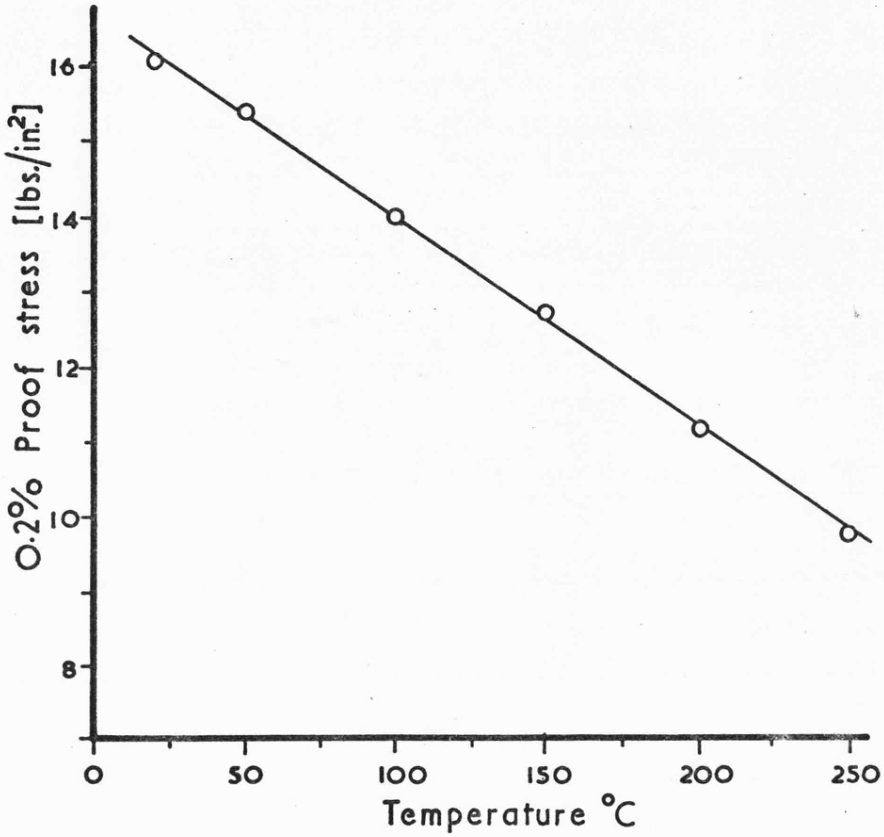

Fig 10·13 Variation of 0·2% Proof stress with temperature

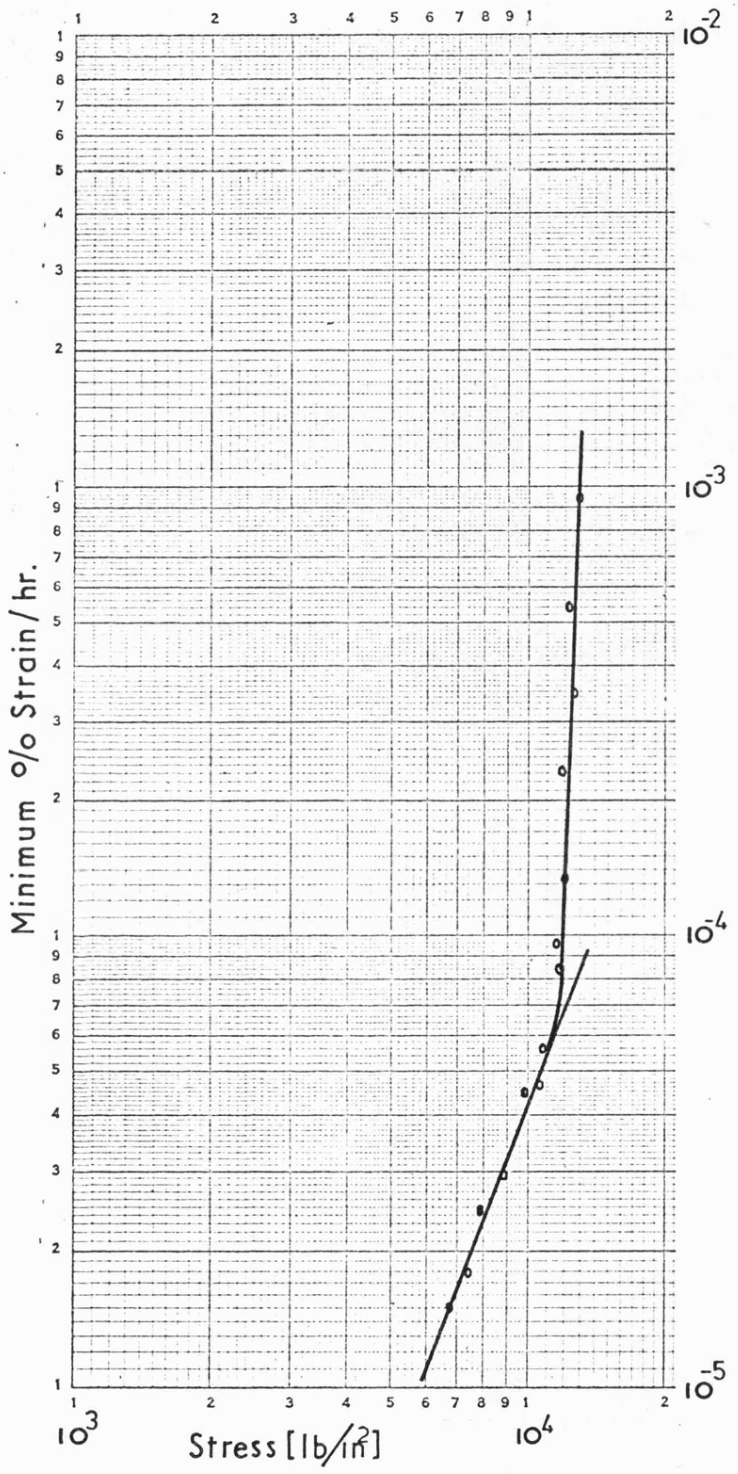

Fig 10·14 Uniaxial data [RT]

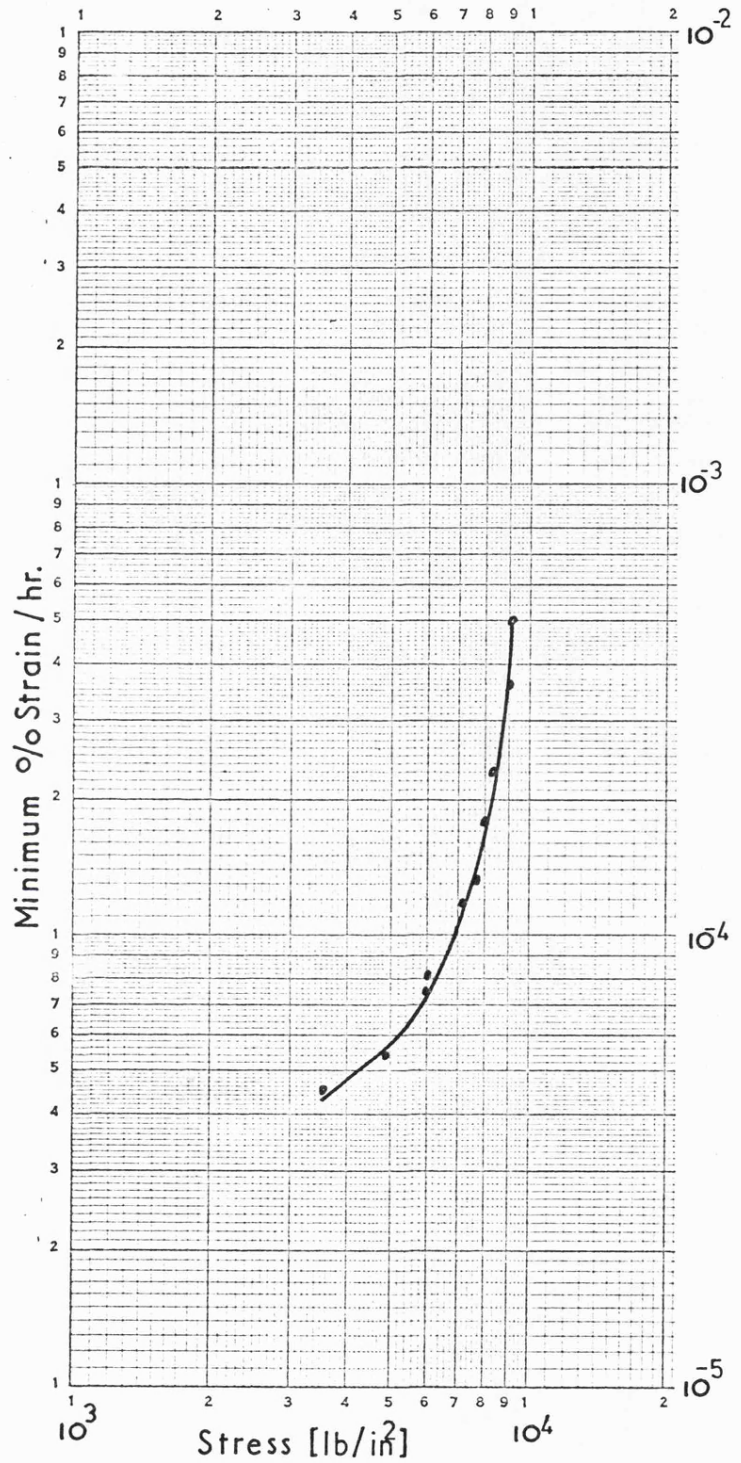

Fig 10·15 Uniaxial data [100°C]

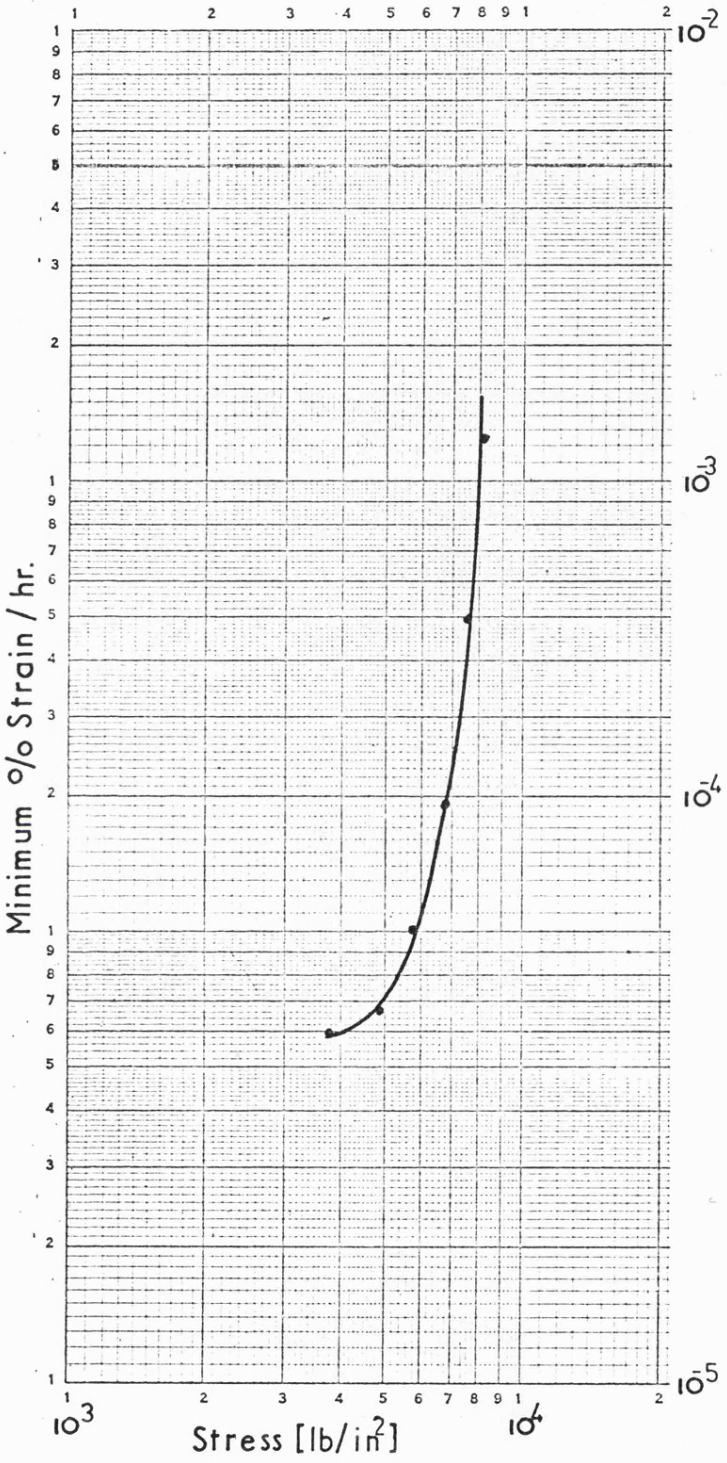

Fig 10·16 Uniaxial data [125°C]

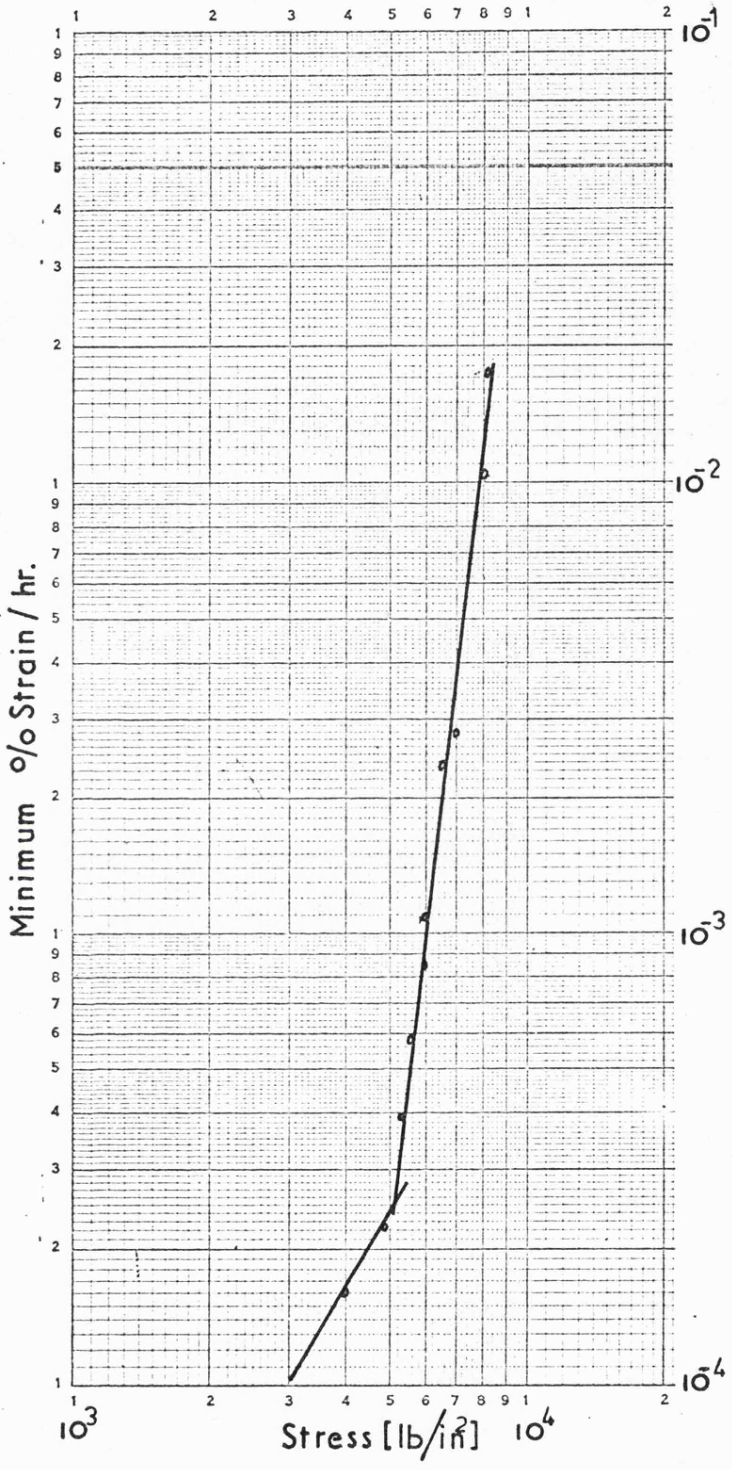

Fig 10·17 Uniaxial data [150°C]

References

1. Ponter, A.R.S., 'On the Stress Analysis of Creeping Structures Subject to Variable Loading". J. Appl. Mech., Trans. ASME, Vol. 95, Series E, 1973.

2. Ponter, A.R.S. & Williams, J.J., 'Work Bounds and Associated Deformations of Cyclically Loaded Creeping Structures'. J. Appl. Mech., Trans. ASME, Vol. 95, Series E, 1973.

3. Ponter, A.R.S. & Leckie, F.A., 'Bounding Solutions to a Plate Subjected to Variable Surface Temperature". J. Appl. Mech., Trans. ASME, Vol. 95, Series E, 1974.

4. Nemy, A.S. & Rhines, F.N., 'On the Origin of Tertiary Creep in Aluminium Alloy'. Metall. Soc., Trans. ASME, Vol. 215, 1959.

5. Hoff, N.J., 'The Necking and Rupture of Rods Subjected to Constant Tensile Loads'. J. Appl. Mech., Trans. ASME Vol. 20, 1953.

6. Andrade, E.N. da C., 'Flow in Metals Under Large Constant Stresses'. Proc. Roy. Soc., Vol. 90A, 1914.

7. Mott, N.F. & Nabarro, F.R.N., 'Dislocation Theory and Transient Creep'. Rep. Conf. Strength of Solids, Phys. Soc., 1948.

8. Cottrell, A.H., 'Time Laws of Creep'. J. Mech. Phys. Solids, Vol. 1, 1952.

9. McLean, D., 'The Physics of High Temperature Creep in Metals'. Inst. Physics & Physics Soc. Report on Progress in Physics. Vol. 29, 1966.

10. Kauzman, W., 'Flow of Solid Metals from the Standpoint of Chemical Rate Theory'. Am. Inst. Min. & Metall. Eng., Trans. ASME, Vol. 143, 1941.

11. Bailey, R.W., 'Note on the Softening of Strain-Hardened Metals and its Relation to Creep'. J. Inst. Metals, Vol. 35, 1926.

12. Orowan, E., 'The Creep of Metals'. J. West of Scotland Iron and Steel Inst., 1946-47.

13. Mitra, S.K. & McLean, D., 'Work Hardening and Recovery in Creep'. Proc. Roy. Soc. Vol. 295, 1967.

14. Herring, C., 'Diffusional Viscosity of a Polycrystalline Solid'. J. Appl. Phys., Vol. 21, 1950.

15. Van Leuuwen, H.P., 'Predicting Material Behaviour under Load, Time and Temperature Conditions'. NATO AGARD Report 513, 1965.

16. Finnie, I. & Heller, W.R., 'Creep of Engineering Materials'. McGraw Hill 1959.

17. Marriott, D.L., 'Creep of Structures'. Ph.D. Thesis, Univ. Cambridge, 1965.

18. Kennedy, A.J., 'Creep and Fatigue of Metals'. Oliver and Boyd, 1962.

19. Norton, F.H., 'The Creep of Steel at High Temperatures'. McGraw Hill, 1929.

20. McVetty, P.G., 'Working Stresses for High Temperature Service'. Mech. Eng. Vol. 56, 1934.

21. Soderberg, C.R., 'Interpretation of Creep Tests for Machine Design'. Trans. ASME, Vol. 58, 1936.

22. Dorn, J.E., 'Some Fundamental Experiments on High Temperature Creep'. J. Mech. Phys. Solids, Vol. 3, 1954.

23. Garofalo, F., 'Fundamentals of Creep and Creep-Rupture in Metals'. MacMillan Co., 1965.

24. Leckie, F.A. Ponter, A.R.S. & Sim, R.G., 'On Creep Rates in Metals'. Leicester University Engineering Dept. Report 68-12, 1968.

25. Bailey, R.W., 'Utilization of Creep Test Data in Engineering Design'. Proc. Inst. Mech. Eng., Vol. 131, 1935.

26. Sherby, O.D. Lytton, J.L. & Dorn, J.E., 'Activation Energies for Creep of High Purity Aluminium'. Acta. Metall., Vol. 5, 1957.

27. Mendelson, A. Hirschberg, M.H. & Manson, S.S., 'General Approach to the Practical Solution of Creep Problems'. J. Basic Eng. Trans. ASME, Vol. 81, Series D, 1959.

28. Goodey, W.J., 'Creep Deflection and Stress Distribution in a Beam'. Aircraft Eng., Vol. 30, 1958.

29. Johnson, A.E. Henderson, J. & Kahn, B., 'Multiaxial Creep Strain/Complex Stress/Time Relations for Metallic Alloys with some Applications to Structures'. Joint. Int. Conf. on Creep, ASME, ASIM, I. Mech. E., New York and London, 1963.

30. Anderson, R.G. Gardiner, L.R.T. & Hodgekins, W.R., 'Deformation of Uniformly Loaded Beams Obeying Complex Creep Laws'. J. Mech. Eng., Sci., Vol. 5, 1963.

31. Marriott, D.L. & Leckie, F.A., 'Some Observations on the Deflections of Structures During Creep'. Conf. on Thermal Loading and Creep in Structures and Components, Proc. Inst. Mech. Eng., Vol. 178, 1964.

32. Williams, J.J. & Leckie, F.A., 'A Method for Estimating Creep Deformation of Structures Subjected to Cyclic Loading'. J. Appl. Mech., Trans. ASME, Vol. 95, Series E, 1973.

33. Calladine, C.R. & Drucker, D.C., 'Nesting Surfaces of Constant Energy Dissipation'. Quart. Appl. Math., Vol. 20, 1962.

34. Leckie, F.A. & Martin, J.B., 'Deformation Bounds for Bodies in a State of Creep'. J. Appl. Mech. Trans. ASME, Vol. 89, Series E, 1967.

35. Leckie, F.A. & Ponter, A.R.S., 'Deformation Bounds for Bodies which Creep in the Plastic Range'. J. Appl. Mech., Trans. ASME, Vol. 92, Series E, 1970.

36. Ponter, A.R.S., 'On the Relationship between Plastic Shakedown and the Repeated Loading of Creeping Structures'. J. Appl. Mech., Trans. ASME, Vol. 93, Series E, 1971.

37. Ponter, A.R.S., 'Deformation, Displacement and Work Bounds for Structures in a State of Creep and Subject to Variable Loading'. J. Appl. Mech., Trans. ASME, Vol. 94, Series E, 1972.

38. Hill, R., 'New Horizons in the Mechanics of Solids'. J. Mech. Phys. Solids, Vol. 5, 1966.

39. Hoff, N.J., 'Approximate Analysis of Structures in the Presence of Moderately Large Creep Deformations'. Quart. Appl. Math., Vol. 12, 1954.

40. Calladine, C.R. & Drucker, D.C., 'A Bound Method for Creep Analysis of Structures: Direct Use of Solutions in Elasticity and Plasticity'. J. Mech. Eng., Vol. 4, 1962.

41. Calladine, C.R., 'Stress Concentration in Steady Creep: Interpolation between Solutions in Elasticity and Plasticity'. Joint Int. Conf. on Creep, Proc. Inst. Mech. Eng., Vol. 178, 1964.

42. Mackenzie, A.C., 'On the Use of a Single Uniaxial Test to Estimate Deformation Rates in Some Structures Undergoing Creep'. Int. J. Mech. Eng. Sci., Vol. 10, 1968.

43. Sim, R.G., 'Creep of Structures'. Ph.D. Thesis, Univ. Cambridge, 1968.

44. Leckie, F.A., 'Some Structural Theorems of Creep and their Implications'. Advances in Creep Design, Applied Science Publishers, 1971.

45. Williams, J.J., 'Creep of Structures Subjected to Cyclic Loading'. Ph.D. Thesis, Univ. Leicester, 1972.

46. Martin, J.B., 'A Note on the Determination of an Upper Bound on Displacement Rates for Steady Creep Problems'. J. Appl. Mech., Trans. ASME, Vol. 88, Series E, 1967.

47. Hult, J., 'On the Stationarity of Stress and Strain Distribution in Creep'. Proc. of Int. Symp. on Second Order Effects in Elasticity, Plasticity and Fluid Mechanics, Haifa, Israel, Pergamon Press, 1962.

48. Barnes, J.F. Clarke, M.J. & Clifton, T.E., 'An Experiment in Stress Redistribution caused by Creep'. J. Strain Analysis, Vol. 2, 1967.

49. Leckie, F.A. & Ponter, A.R.S., 'Theoretical and Experimental Investigation of the Relationship between Plastic and Creep Deformation of Structures'. Int. Symp. on Foundations of Plasticity, Warsaw, 1972.

50. Calladine, C.R., 'Time Scales for Redistribution of Stress in Creep of Structures'. Proc. Roy. Soc., Vol. 309, Series A, 1969.

51. Bill, I.M. & Mackenzie, A.C., 'Reference Stress for Redistribution Time in Creep of Structures'. J. Mech. Eng. Sci., Vol. 11, 1969.

52. Megahed, M., Private Communication, Univ. of Leicester.

53. Calladine, C.R., 'A Rapid Method for Investigating the Greatest Stress in a Structure Subject to Creep'. Proc. Inst. Mech. Eng., Vol. 178, 1964.

54. Ponter, A.R.S. & Leckie, F.A., 'The Application of Energy Theorems to Bodies which Creep in the Plastic Range'. J. Appl. Mech., Trans. ASME, Vol. 92, Series E, 1970.

55. Marriott, D.L., 'A Review of Reference Stress Methods for Estimating Creep Deformation'. Creep in Structures, (Edited by J. Hult) Springer-Verlag, 1972.

56. Schulte, C.A., 'Predicting Creep Deflection of Plastic Beams'. Proc. ASTM , Vol. 60, 1960.

57. Sim, R.G. & Penny, R.K., 'Some Results of Testing Simple Structures under Constant and Variable Loading during Creep'. Exp. Mech., Vol. 10, 1970.

58. Fairbairn, J., 'A Reference Stress Approach to Creep Bending of Straight Tubes'. J. Mech. Eng. Sci., Vol. 16, 1974.

59. Johnsson, A., 'Reference Stress for Structures Obeying the Prandtl and Dorn Creep Laws'. J. Mech. Eng. Sci., Vol. 16, 1974.

60. Sim, R.G., 'Reference Stresses and Temperatures for Cylinders and Spheres under Internal Pressure with a Steady Heat Flow in the Radial Direction'. Int. J. Mech. Sci., Vol. 15, 1973.

61. Spence, J., 'Creep of a Straight Pipe under Combined Bending and Internal Pressure'. Nuclear Eng. and Design, Vol. 24, 1973.

62. Fairbairn, J., 'Some Effects of Differences in Tension and Compression on the Creep Bending of Tubes'. N.E.L. Report 558.

63. Spence, J., 'Creep Behaviour of Smooth Curved Pipes under Bending'. Proc. First Int. Conf. on Pressure Vessel Technology, ASME, 1969.

64. Spence, J., 'An Upper Bound Analysis for the Deformation of Smooth Pipe Bends in Creep'. Creep in Structures (Edited by J. Hult) Springer-Verlag, 1972.

65. Frederick, C.O., Chubb, E.J. & Bromley, W.P., 'Cyclic Loading of a Tube with Creep, Plasticity, and Thermal Effects'. Proc. Inst. Mech. Eng., Vol. 180, 1966.

66. Ponter, A.R.S., 'General Bounding Theorems for the Quasi-Static Deformation of a Body of Inelastic Material with Applications to Metallic Creep'. J. Appl. Mech., Trans. ASME, Vol. 96, Series E, 1974.

67. Frederick, C.O. & Armstrong, P.J., 'Convergent Internal Stresses and Steady Cyclic States of Stress'. J. Strain Analysis, Vol. 1, 1966.

68. Martin, J.B. & Williams, J.J., 'On the Existence of an Extremum Principle for Creeping Structures Subjected to Cyclic Loading'. Int. J. Mech. Eng. Sci., Vol. 13, 1971.

69. Bree, J., 'Elastic-Plastic Behaviour of Thin-Tubes Subjected to Internal Pressure, and Intermittent High Heat Fluxes with Application to Fast-Nuclear Reactor Fuel Elements'. J. Strain Analysis, Vol. 2, 1967.

70. Bree, J., 'Incremental Growth due to Creep and Plastic Yielding of Thin-Tubes Subjected to Internal Pressure and Cyclic Thermal Stresses'. J. Strain Analysis, Vol. 3, 1968.

71. Ponter, A.R.S. & Walter, M.H., 'A Theoretical and Experimental Investigation of Creep Problems with Variable Temperature'. Proc. 3rd Int. SMiRT Conf. Vol. 5, 1975.

72. Ponter, A.R.S., 'Finite Element Solution of Creep Problems Involving Rapid Cycling Loading'. Proc. 3rd Inst. SMiRT Conf., Vol. 5, 1975.

73. Ponter, A.R.S., 'Deformation Bounds for Bailey-Orowan Creep'. J. Appl. Mech., Trans. ASME, Vol. 97, Series E, 1973.

74. Ponter, A.R.S., 'Some Properties of the Bailey-Orowan Theory of Creep'. L.U.E.D. Report 73-16, 1973.

75. Ponter, A.R.S., 'The Analysis of Cyclically Loaded Creeping Structures'. L.U.E.D. Report 75-12, 1975.

76. Bullard, J.B. & Clifton, T.E., 'Further Experiments in Stress Redistribution Caused by Creep'. J. Strain Analysis, Vol. 5, 1970.

77. Lomax, A.B., 'A Model System to Simulate Creep of Composites'. Metals and Materials, Vol. 5, 1967.

78. Penny, R.K. & Leckie, F.A., 'The Mechanics of Tensile Testing'. Int. J. Mech. Sci., Vol. 10, 1968.

79. Schmieder, A.K., 'Measuring the Apparatus Contribution to Bending in Tension Specimens'. ASTM Bulletin STP488, 1971.

80. Jones, M.H. & Brown, W.F., 'An Axial Loading Creep Machine'. ASTM Bulletin 1956.

81. Penny, R.K. Ellison, E.G. & Webster, G.A., 'Specimen Alignment and Strain Measurements in Axial Creep Tests'. Materials Research and Standards, MTRSA, Vol. 6.

82. Ashby, M.F., 'A First Report on Deformation - Mechanism Maps'. Acta Metall. Vol. 20, 1972.

A THEORETICAL AND EXPERIMENTAL INVESTIGATION OF CREEP PROBLEMS WITH VARIABLE TEMPERATURE

A.R.S. PONTER and M.H. WALTER

Department of Engineering,
University of Leicester, Leicester LE1 7RH, United Kingdom

SUMMARY

Although there has been extensive investigation of the creep behaviour of structures which are subject to isothermal conditions and constant load, the behaviour when temperatures vary spatially and both load and temperature vary with time has received relatively little attention. Numerical solutions are extremely difficult to produce under these circumstances and appropriate constitutive relationships have yet to be evolved.

This paper attempts to delineate the principal features of the behaviour when load level are maintained at those appropriate to many design situations and when the temperature and loading histories are cyclic with relatively short cycle times. We are concerned with structures which accumulate creep strains of less than 1% per year and have cycle times of the order of a few days at most.

In the first section the behaviour of a few simple structures are investigated for spatially varying temperature fields which remain constant in time. Adopting an appropriate form of Norton's Law we show that the deformation of the structure may be related to a single reference material test conducted at a reference stress and a reference temperature, which is independent of material constants, thereby providing a generalization of the reference stress method for isothermal structures. A sequence of experiments on a simple beam structure indicates that the co-relation between structural behaviour and material tests provides an acceptably accurate design method. In all cases considered the reference temperature remains close to the lowest temperature in the structure indicating that locally high temperature may sometimes be tolerated without excessive structural deformation.

The last section discussed a preliminary experimental investigation of a two-bar structure subject to variable temperature. It is shown that the residual stress field varies quite slowly in time and remains effectively constant after a few cycles. The theoretical consequences of the result are discussed and it is shown that constitutive relationships with differing physical assumptions can yield quite sharply contrasting deformation rates.

The results of the paper show that the behaviour of structures subject to a time constant temperature distribution may be related to material behaviour without difficulty. When temperature and load vary with time, the more important feature of the structural behaviour may be understood, although certain features of the material behaviour remain ill-defined.

1. Introduction

The analysis of the creep deformation behaviour of structures subject to variable loading and temperature remains amongst the least tractable problems of structural mechanics. A number of phenomena interact with each other. Changes in temperature induce thermal expansion and have an ill-defined effect upon the material behaviour. The continuum problem requires the evaluation of a continuously varying stress history. Even when computed to an acceptable accuracy such solutions remains only as accurate as that of the constitutive relationship.

This paper attempts to shed some light on the importance of these various effects by the analysis of a very simple two bar structure, by means of a method of structural analysis which arises from certain bounding theorems. In a number of previous papers [1,2,3] a theory was derived for a non-linear viscous material which allows the evaluation of upper and lower bounds on the energy dissipated in a cyclically loaded structure. These solutions correspond to the exact solution when the cycle time is either very short (upper bound) or very long (lower bound) compared with a characteristic time scale of the average deformation rate. This reference time scale may be taken as the time for the creep strain, in the steady state, to be equal to the elastic strain at either an average or maximum stress in the structure [1]. Consideration of typical time scales indicates that in most applications cycle time may be considered to be very short and hence the upper bound solution may be expected to provide a relevant solution which should closely approximate the exact solution. A full description of these arguments may be found in the references cited above.

If we accept the relevance of the upper bound solution, we may compute corresponding solutions for any constitutive relationship, and this theory is described in reference [4]. Here we compute these rapid cycling solutions for three constitutive relationships, non-linear viscous, strain hardening and the Bailey-Orowan model. The objective is to see if any general modes of behaviour are discernable. We find that the solution for the viscous and strain hardening materials exhibit similar behaviour. For distant ranges of stress and temperature the solution may be understood as resulting from the dominance of the strains occurring during either that part of the cycle when the stress is greatest or when the temperature is greatest. A material parameter β is introduced in terms of which regions may be defined where a reference stress may be defined which is independent of other material parameters. This result indicates that a reference stress approach is applicable to variable temperature problems, but that the relevant reference stress depends upon the range of values of this quantity β.

However when the solution for the Bailey-Orowan model is investigated, no such regions occur and a distinctly different pattern of deformation is exhibited due to the presence of recovery. This difference occurs as the model predicts a much greater strain rate for a history of stress and temperature which involves a high stress at a lower temperature followed by a low stress at a high temperature.

Experiments on the simulation of a two-bar model involving a coupled pair of uniaxial testing machines are described in the full paper. Tests on aluminium indicate that the rapid cycle solution is achieved within a few cycles, and that recovery is present, but of a magnitude which is much less than that predicted by the Bailey-Orowan model.

2. The Two-Bar Structure

Consider the model exhibited in Fig. 1. Two bars of equal initial length are restrained to remain of equal length under the action of a constant load $P = 2\sigma_p A$, where A denotes the cross-sectional area of each bar. One bar remains at a constant temperature $\theta_2 = \theta_0$ whereas the second bar is subject to a temperature history

$$\theta_1 = \theta_0 + \Delta\theta \quad , \quad 0 \le t \le \Delta t/2$$

$$\theta_1 = \theta_0 - \Delta\theta \quad , \quad \Delta t/2 \le t \le \Delta t$$

The thermo-elastic solution is given by

$$\left.\begin{aligned} \hat{\sigma}_1 &= \sigma_p - \sigma_t \\ \hat{\sigma}_2 &= \sigma_p + \sigma_t \end{aligned}\right\} \quad 0 \le t < \Delta t/2$$

$$\left.\begin{aligned} \hat{\sigma}_1 &= \sigma_p + \sigma_t \\ \hat{\sigma}_2 &= \sigma_p - \sigma_t \end{aligned}\right\} \quad \Delta t/2 \le t < \Delta t$$

where $\sigma_t = E\alpha\Delta\theta/2$ and α and E denotes the coefficient of linear expansion and Youngs modulus respectively.

Consider a non-linear viscous material,

$$\dot{\epsilon} = \frac{\dot{\sigma}}{E} + \dot{v} \quad , \quad \dot{v}(\sigma, \theta) = k\,\sigma^n \exp\left(-\Delta H/R\theta\right) \qquad (1)$$

where k denotes a material constant, n an odd integer, ΔH an activation energy and R the universal gas constant. For sufficiently small changes in θ we may write

$$\dot{v} = k'\,\sigma^n \exp\left(\gamma(\theta - \theta_0)\right) \qquad (2)$$

where $k' = k \exp(\Delta H/R\theta_0)$ and $\gamma = \Delta H/R\theta_0^2$

When the cycle time Δt is small, the cyclic solution is given by

$$\sigma_1 = \hat{\sigma}_1 + \rho \quad , \quad \sigma_2 = \hat{\sigma}_2 - \rho \qquad (3)$$

where ρ denotes a constant residual stress which is determinate from the compatibility condition over a cycle

$$\Delta v = \frac{\Delta u}{\ell} = \int_0^{\Delta t} \dot{v}_1\, dt = \int_0^{\Delta t} \dot{v}_2\, dt, \qquad (4)$$

where ℓ denotes the length of the bars, and ΔU^u the displacement accumulated over a cycle.

When Δt is very large, the instantaneous solution becomes the steady state solution given by

$$\dot{v}_1 = \dot{v}_2$$

i.e. $\sigma_1^n \exp\gamma(\theta_1 - \theta_c) = \sigma_2^n \exp n\gamma(\theta_2 - \theta_0)$

The accumulated displacement over a cycle is given by,

$$\Delta v = \frac{\Delta^L u}{\ell} = \int_0^{\Delta t} \dot{v}_1\, dt = \int_0^{\Delta t} \dot{v}_2\, dt.$$

It may easily be shown that the ratio $U=\Delta U^u/\Delta U^L$ is dependent upon three parameters, σ^p/σ^t, n and

$$\beta = \frac{2\gamma\Delta\theta}{n} \qquad (5)$$

The physical meaning of β arises from the relationship between the creep rates which occur at $\theta_o - \Delta\theta$ and $\theta_o + \Delta\theta$. Consider tests conducted at these two temperatures. Raising the temperature from $\theta_o - \Delta\theta$ to $\theta_o + \Delta\theta$ will increase the creep rate. Suppose the same increase in creep rate is caused by maintaining the temperature at $\theta_o - \Delta\theta$ but increasing the stress to λσ. Then

$$\dot{v} = k'(\lambda\sigma)^n \exp(-\gamma\Delta\theta) = k'\sigma^n \exp(\gamma\Delta\theta).$$

Hence $\beta = \ln\lambda$. In a graph of $\ln\dot{v}$ against $\ln\sigma$ at constant θ then β becomes the distance between the lines corresponding to the two temperatures, as shown in Fig. 2.

In Fig. 3 contours of constant $U=\Delta U^u/\Delta U^L$ are exhibited for n = 3 and a range of values of σ^p/σ^t and β. It can be seen that the contours exhibit four distinct regions which we will discuss in turn.

Region 1. U > 1. In this region, which corresponds to smaller values of β, the most severe increase in displacement rate is shown for small cycle times. Consider the extreme case when β = 0, i.e. the creep rate independent of temperature. The rapid cycling solution is self-evident and is shown in Fig. 4(a). Effectively all the deformation occurs when the stress is largest and equal to $\sigma_p + \sigma_t$ and ρ = 0. If we completely ignore the creep strain which occurs when the stresses have their lower values and evaluate U we obtain the dashed line shown in Fig. 3. It clearly can be seen that these lines closely approximate the exact solution throughout this region. Hence the deformation is effectively equal to that of the structure subject to a constant load $P = 2A(\sigma^p + \sigma^t)$ with half the cycle time and temperature $\theta_1 = \theta_o - \Delta\theta$, $\theta_2 = \theta_o$, followed by a lower or zero applied load over the remainder of the cycle. This approximation is least accurate near the boundary between Region 1 and Region 3.

Region 2. U ≈ 1. This region corresponds approximately to β > 2 and $\sigma_p/\sigma_t > 1$. As u is near unity then the slow and rapid cycling solutions are nearly identical in their prediction of displacement rate. As β is large then the creep rates during the first part of the cycle when the highest temperature occurs provides the major contribution to the displacement. In bar 1, although the temperature remains constant the stress reduces during $\Delta t/2 < t < \Delta t$. In bar 2 the stress increases but the temperature reduces and the large value of β ensures that the creep rates in $0 < t < \Delta T/2$ dominates. In fact, in the rapid cycling solution the stresses are virtually identical to those of the slow cycling solution during $0 < t < \Delta t/2$ and the contribution from the second half of the cycle is negligible, resulting in a value of U close to unity. In this region the deformation may be assumed to be equal to one half of that which would occur if the condition of the first part of the cycle remained constant in time.

Region 3. U < 1. This region corresponds to $\sigma_p/\sigma_t < 1$ and lines of constant U become independent of β for large β. If we consider the case when β is very large the behaviour may easily be understood. During $0 < t < \Delta t/2$, σ_1 becomes very small ($\rho = \sigma_p + \sigma_t$) and either negative or positive, and during $\Delta t/2 < t < \Delta t$ although $\sigma_1 = 2\sigma_t$ as $\theta = \theta_o - \Delta\theta$

the creep rate is small. Hence the deformation is governed by σ_2 which changes from $2\sigma_p$ to $2(\sigma_p-\sigma_t)$. As $\theta = \theta_o$ in this bar the displacement rate is independent of β. When $\sigma_p/\sigma_t=0.5$ the net accumulation of strain is zero. Hence for $1 < \sigma\, p/\sigma_t < 0.5$, $1 > U > 0$ and for $0.5 < \sigma_p/\sigma_t < 0$ then $U < 0$. In this latter case the displacement rate in the rapid cycle solution is of opposite sign to the applied load σ_p, and a load of $\sigma_p = 0.5\sigma_t$ is required to maintain zero displacement rate.

It can clearly be seen that these simple solution regions are quite distinct and are separated by regions in which fairly rapid transition occurs. The most marked transition occurs near the origin of Fig. 3 where large changes in U occur for small changes in σ_p/σ_t. For larger values of n a similar picture emerges except that the regions become more distinct, the transitions occupying a smaller area of the diagram. These transitional regions are defined by the contours of U of values close to unity. In Fig. 5 contours of $U = 0.99$ and 1.01 are shown for n = 3, 5 and 7, and they are seen to be very close to each other. For $U = 0.00$ the contours are indistinguishable. Contours for $U = 50$ are also included to demonstrate that within the regions (with the exception of Region 2) the value of U is dependent of n, but the stresses are governed by the calculation described above. We see therefore that within Regions 1 and 2 the rapid cycling solution may be co-related with the behaviour of the same structure subject to constant load and constant temperature. For Region 1 the relevant applied load is $P = 2A(\sigma_p + \sigma_t)$ with $\theta_1 = \theta_o-\Delta\theta$ and $\theta_2=\theta_o$. In Region 2, $P = 2A\sigma_p$ and $\theta_1= \theta_o+\Delta\theta$ and $\theta_2=\theta_o$. These situations may themselves be co-related with a constant reference and temperature history, as described by Ponter and Walter [5]. In Region 3, a variable stress history, fluctuating between $2\sigma_p$ and $2(\sigma_p-\sigma_t)$ at temperature $\theta=\theta_o$, defines the displacement rate.

3. Strain Hardening

In this section we describe a similar analysis for a strain hardening material. Consider the uniaxial strain hardening model

$$\dot{v} = m\,\beta^{1/m}\,\sigma^{n/m}\,v^{(m-1)/m} \tag{6}$$

For constant stress commencing at t=0 when v=0

$$v(t) = \beta\sigma^n t^m \qquad , \beta = \beta' \exp\gamma(\theta-\theta_o)$$

In accordance with experiment we take m = 1/3. The rapid cycling solution is given by [4]

$$\frac{\Delta v}{\Delta t} = \left\{ \frac{1}{\Delta t}\int_o^{\Delta t} \beta^{1/m}\,(\hat{\sigma}+\rho)^{n/m} \right\}^m m\,t^{m-1} \tag{7}$$

where $\hat{\sigma}$ and ρ have the same meaning as in the time hardening case. Again ρ becomes determinate from the condition that $\Delta v/\Delta t$ shall be equal in the two bars. In fact the calculation for ρ becomes identical to the time hardening case with n/m substituted for n and $\Delta H/m$ substituted for ΔH.

There exist no lower bound solution, but for purposes of providing a normalization comparable with the time hardening case, the solution was computed so that the integrand of (7) remains equal in each bar during $0 < t < \Delta t$. This solution corresponds to assuming that the cycle time is sufficiently long for redistribution to occur at each instant

within the cycle but that the average creep rate is calculated assuming that, from the point of view of the constitutive relationship, the cycling is rapid. This solution has no direct physical meaning but will reduce to the solution arising from equation (7) if the conditions of Region 2 occur.

The displacements predicted by these two methods are denoted by ΔU^u and ΔU^L and their ratio by U.

We find that the solutions so generated have a behaviour which is very similar to that of viscous material and corresponds to the conditions described above. The boundary lines of the regions are shown in Fig. 6, and are seen to be very similar to these in the viscous case Fig. 5. There are however differences in the values of U as the relationship (6) provides a higher value of the creep rate under varying stress, when compared with constant stress maintained at the maximum value than does the viscous relationship. The stress histories themselves are however very similar and are divided into the same sub-regions.

We conclude therefore that the behaviour of a viscous material and a strain hardening material are very similar when described in this way, and the same reference stress histories are relevant.

4. Bailey-Orowan Theory

This theory is described in references [6]. The state of the material is described by an internal flow stress s which increases due to strain hardening and decreases due to thermal softening,

$$\dot{s} = h(s)\,|\dot{v}| - r(s) \qquad (8)$$

where h(s) and r(s) are coefficients of strain hardening and thermal softening respectively. The creep rate $\dot{v}$ is given by,

$$\dot{v} = \mathrm{sign}(\sigma)\; f(|\sigma| - s) \qquad (9)$$

where $f(|\sigma|-s) = 0$, $|\sigma| < s$

≥ 0, $|\sigma| = s$.

Stationary state creep occurs when $|\sigma| = s$ and hence

$$\dot{v} = \mathrm{sign}(\sigma)\; r(|\sigma|)/h(|\sigma|).$$

Assuming $r(s) = k_1 s^{n-\alpha}$ and $h(s) = 1/k_2 s^{\alpha}$ yields Norton's flow

$$\dot{v} = \mathrm{sign}(\sigma)\; k_1 k_2 |\sigma|^n \quad , \quad k_1 k_2 = k' \exp(\gamma(\theta - \theta_c)).$$

This model differs from both the viscous relationship, equation (1) and strain hardening, equation (6), by possessing thermal softening. When $|\sigma| < s$, then $\dot{s} = -r(s)$ and s decreases in time. If the stress is now suddenly increased, $\dot{s} = \dot{\sigma}$ and plastic strains occur according to

$$\dot{\sigma} = h(|\sigma|)\,\dot{v}$$

For a cycle of stress, both plastic and creep strains occur. But in common with the viscous

relationship, an upper bound on the energy dissipation in a body of the material corresponds to assuming that the cycle time is very short compared with characteristic material times [6]. The stress history is given by $\sigma = \hat{\sigma} + \rho$, and the accumulation of strain over a cycle is given by

$$\frac{\Delta v}{\Delta t} = \mathrm{sign}(\sigma(t_o)) \; |\sigma(t_o)|^n \; \frac{1}{\Delta t} \int_0^{\Delta t} k' \exp(\gamma(\theta-\theta_o))\, dt.$$

where t_o is the instant during the cycle when $|\sigma|$ achieves its maximum value. Hence the average strain rate is the same as if $\sigma = \sigma(t_o)$ throughout the cycle. The model predicts the same creep rate as the viscous relationship (1) for constant stress and a greater creep rate for any other stress history, the increase being due to the presence of recovery in the model.

The lower work bound is identical to that of viscous relationship, equation (1), described in Section (2), and the ratio of the displacements predicted by these two bounding solutions, U, may therefore be directly compared with the results in Section (2).

It can easily be shown that the upper bound average displacement rate of the two bar model is the same as if a constant applied load $P = 2A(\sigma_p+\sigma_t)$ were applied throughout the cycle, with one bar maintained at $\theta_2=\theta_o$ and the other at $\theta_1=\bar{\theta}$ where

$$\exp(\gamma(\bar{\theta}-\theta_o)) = \frac{1}{2}\left(\exp(\gamma\Delta\theta) + \exp(-\gamma\Delta\theta)\right)$$

In Fig. 7 contours of constant U are shown for n = 3. This solution is appropriate in Region 1, but in Region 2 $|\sigma_1|$ achieves its maximum value when $\sigma_1 = \pm\sigma_t$ and $\rho=-\sigma_p$. The average creep rate in bar 1 becomes indeterminate and becomes determined by the stress history σ_2. In bar 2, the stress fluctuates between $2\sigma_p+\sigma_t$ and $2\sigma_p-\sigma_t$ and hence the displacement rate is the same as if a constant applied load of $P = 2A(\sigma_p + \sigma_t)$ were maintained and both bars were at temperature $\theta = \theta_o$.

The behaviour shown in Fig. 7 is entirely different to that shown in either Figs. 3, 5 or 6. No reverse creep occurs and the ratio U remains at high values for large β, as recovery increases. Effectively the Region 1 of Fig. 3 now dominates a larger area of the diagram.

These calculations demonstrate a central problem of this type of calculation. When temperatures vary rapidly between two limits, the stress history, in the cyclic state, fluctuates between a higher stress at a lower temperature and a lower stress at a higher temperature. The rate of deformation is strongly governed by the amount of recovery which occurs during the high temperature period. To the authors knowledge no experiments have been conducted under these conditions.

In the full paper, experiments on a simulated two bar structure are described which allows some assessment of the behaviour of aluminium under these conditions. The temperature histories differ in detail from those assumed in Section 2 and the experiments were conducted in Region 1 of both Fig. 3 and Fig. 7. These experiments indicate the following:

1) The stress histories of the upper bound solution are achieved within a few cycles of 24 hours duration over a range of average strain rates.

2) Recovery does occur, but it appears to be somewhat less than that predicted by the Bailey-Orowan model.

Acknowledgment

The assistance of the Science Research Council is acknowledged for both the numerical calculations and the experimental work. Many of the calculations were carried out by Phillip Brown and his assistance is gratefully acknowledged.

References

[1] PONTER, A.R.S. "On the stress analysis of creeping structures subjected to variable loading". Jnl. App. Mech., Trans. ASME, Vol. 40, Series E, 1973, p. 589-594.

[2] PONTER, A.R.S. and WILLIAMS, J.J. "Work bounds and associated deformations of cyclically loaded creeping structures". Jnl. App. Mech., Trans. ASME, Vol. 40, Series E, p. 921-927.

[3] PONTER, A.R.S. and LECKIE, F.A. "Bounding solutions for a plate subjected to variable surface temperature". Jnl. App. Mech. Trans. ASME, Vol. 41, Series E, p. 941-946.

[4] PONTER, A.R.S. "Finite element solution of creep problems involving rapid cyclic loading". Paper L6/3, 3rd SMiRT Conference.

[5] PONTER, A.R.S. and WALTER, M.H. "Some properties of the creep of structures subjected to non-uniform temperatures". University of Leicester, Department of Engineering, Report 73-17, August 1973.

[6] PONTER, A.R.S. "Deformation bounds for the Bailey-Orowan Theory of Creep". To appear, Jnl. App. Mech., Trans. ASME.

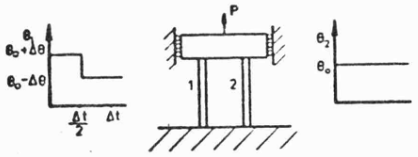

Fig 1

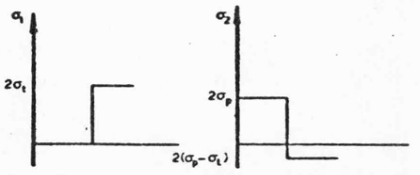

Fig(4 b) Solution for β large, Region 3, ($P = -\sigma_p + \sigma_1$)

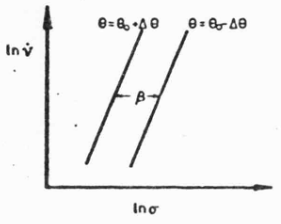

Fig 2

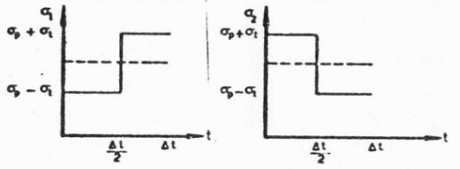

Fig(4 a) Solution for β = 0, Region 1, ($P = 0$)

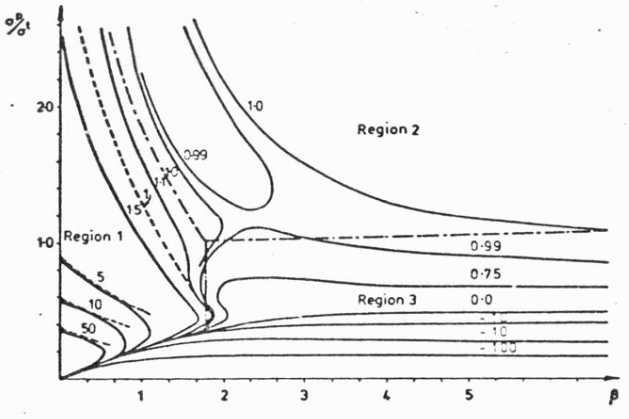

Fig 3 Contours of constant, $U = \Delta u^b / \Delta u^t$ for a viscous material with n = 3.

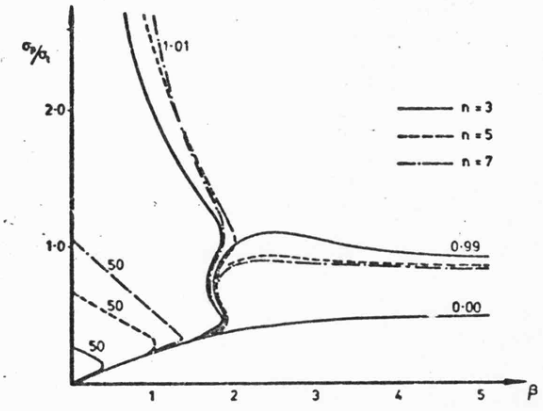

Fig 5 Contours of constant U for n = 3, 5 and 7, for viscous material.

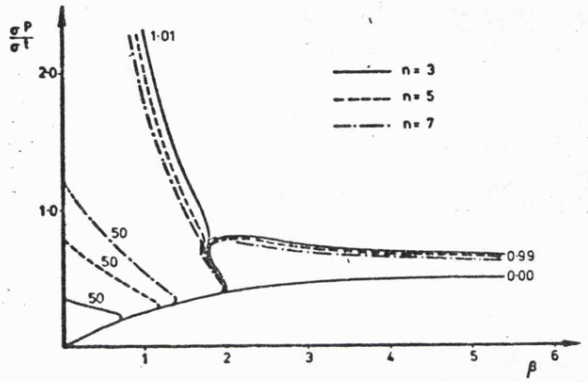

Fig 6 Contours of constant U for n = 3, 5 and 7, for strain hardening material.

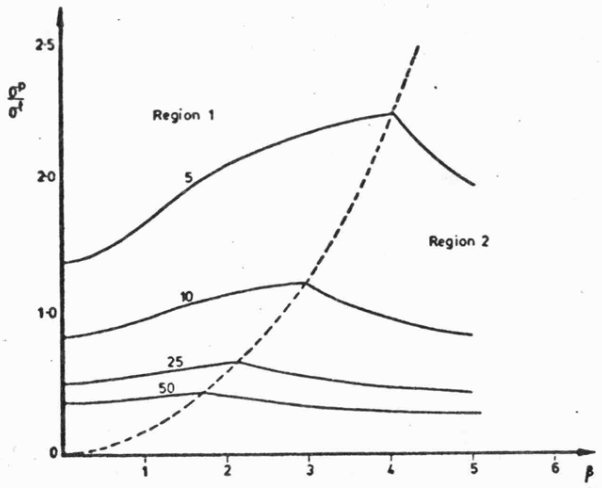

Fig 7 Contours of constant U for the Bailey-Orowan model and n = 3.